Identification of small molecule inhibitors
of clinically relevant human polyomavirus infections

Dissertation

zur Erlangung des Doktorgrades (Dr. rer. nat.)

an der Fakultät für Mathematik, Informatik und Naturwissenschaften

Fachbereich Chemie

der Universität Hamburg

vorgelegt von

Emma Kraus

Hamburg, 2019

Gutachter: Prof. Dr. Nicole Fischer

                    Prof. Dr. Wolfram Brune

Tag der Disputation: 28.06.2019

Die vorliegende Arbeit wurde in der Zeit vom Januar 2016 bis April 2019 im Heinrich-Pette-Institut – Leibniz-Institut für Experimentelle Virologie unter Anleitung von Prof. Dr. Adam Grundhoff in der Arbeitsgruppe Virus Genomik und im Universitätsklinikum Hamburg Eppendorf (UKE) im Institut für Medizinische Mikrobiologie, Virologie und Hygiene unter Anleitung von Prof. Dr. Nicole Fischer angefertigt.

Zusammenfassung

Humane Polyomaviren sind in der gesunden Bevölkerung weit verbreitet. Die Primärinfektion erfolgt früh im Kindesalter und verläuft klinisch unauffällig im immunkompetenten Wirt. Von den 13 bislang bekannten humanen Polyomaviren können vier, MCPyV, TSPyV, JCV und BKV, unter Immunsuppression zu schweren Erkrankungen führen. Insbesondere die Reaktivierung von JC und BK Virus führt zu erheblichen klinischen Komplikationen in Transplantationspatienten und Patienten, die Immunsuppressiva erhalten. Insbesondere stellt die Anzahl der BKV-Reaktivierungen in nierentransplantierten und knochenmarktransplantierten Patienten ein großes klinisches Problem dar. In 5 – 15% aller Knochenmarktransplantierten kann BKV-Replikation zu einer hämorrhagischen Zystitis beitragen und bis zu 10% aller nierentransplantierten Patienten weisen in Folge der BKV-Reaktivierung eine schwere Nephritis auf, welche ein erhöhtes Risiko einer Abstoßungsreaktion verursacht. Ungeachtet der Entdeckung von BKV vor Jahrzehnten, gibt es bislang keine spezifischen antiviralen Therapien und die Behandlung von BKV-assoziierten Erkrankungen beschränkt sich auf die Reduktion der Immunsuppression, welche jedoch in Organtransplantierten eine Abstoßungsreaktion sowie den Verlust des Spenderorgans auslösen kann. Das Ziel dieser Doktorarbeit war es daher, neue niedermolekulare Verbindungen zu identifizieren, die effizient und spezifisch BKV-Infektionen inhibieren, und diese hinsichtlich ihrer antiviralen Aktivität zu charakterisieren, um diese in weiteren Verfahren in Richtung präklinische Testung zu optimieren.

Da die *in vitro* Kultivierung von BKV erheblich limitiert ist, wurde das nah-verwandte Affen-Polyomavirus SV40 als Surrogat-Virus verwendet, um in einem phänotypischen Hochdurchsatzscreen ca. 28.000 niedermolekularen Verbindungen auf ihre Aktivität gegen SV40 und nahverwandte Polyomaviren zu testen. Im Zuge des primären Hochdurchsatzscreens wurden 33 neue Inhibitoren gegen SV40 identifiziert. In einem BKV-spezifischen sekundären Screen wurden 16 von den insgesamt 33 Inhibitoren in ihrer inhibierenden Aktivität gegen BKV bestätigt. Hierbei inhibierten neun Inhibitoren eine BKV-Infektion in primären renalen proximalen Tubuluszellen um mehr als 90%. Ausgewählte Inhibitoren wurden in Abhängigkeit ihrer *in silico* abgeschätzten pharmakokinetischen Eigenschaften auf ihre Aktivität gegen eine Infektion mit JCV oder dem Maus-Polyomavirus untersucht. Während die Mehrheit der BKV-Inhibitoren auch eine Infektion mit JCV zu mehr als 90% inhibierten, hemmten im gleichen Maße nur etwa vier der 16 Inhibitoren auch eine Infektion mit Maus-Polyomavirus.

Basierend auf Analysen der chemischen Struktur wurden fünf der insgesamt 16 Inhibitoren hinsichtlich ihrer IC50- und CC50-Werte in primären Zellen getestet. Dabei wiesen vier dieser Inhibitoren erhebliche BKV-inhibierende Aktivität auf, welche sich in einem IC50-Wert im nanomolaren Bereich und einem Selektivitätsindex über 10 äußerte. Insbesondere ein Inhibitor, bezeichnet als Verbindung

C1, hob sich erheblich hervor, da dieser höchst signifikant eine Infektion mit BKV bereits bei einer sehr niedrigen Konzentration hemmte, ohne Zelltoxizität zu verursachen, und einen Selektivitätsindex von über 100 aufwies.

Um die BKV-inhibierende Aktivität von Verbindung C1 genauer zu charakterisieren, wurde der Einfluss von C1 auf die einzelnen Schritte des viralen Lebenszyklus im Detail untersucht. Die Ergebnisse in dieser Doktorarbeit deuten darauf hin, dass die Verbindung C1 die ersten Schritte der BKV-Infektion, d.h. den Prozess der Interaktion von BKV mit der Wirtszelle und/oder die Internalisierung beeinträchtigt, indem C1 entweder mit viralen Proteinen von BKV oder mit zellulären Faktoren, die durch BKV reguliert werden, interagiert. Der genaue Wirkmechanismus der Verbindung C1 inklusive der Identifizierung der Zielstruktur muss jedoch in weiteren Studien untersucht werden.

In der vorliegenden Arbeit wurden 16 neue niedermolekulare Verbindungen identifiziert, die hoch signifikant im nanomolaren Bereich eine BKV-Infektion inhibieren. Darüber hinaus wurden in dieser Arbeit erste Versuche durchgeführt, die in ihrer Gesamtheit darauf hindeuten, dass C1 die initialen Schritte der BKV-Infektion hemmt. Basierend auf diesen Ergebnissen wurde die Verbindung C1 als ein vielversprechender Kandidat für die klinische Weiterentwicklung einer sogenannten pre-lead Struktur identifiziert. In Kollaboration mit industriellen Partnern wird derzeit die Weiterentwicklung vorangetrieben, um präklinischen Testungen dieses neuen BKV/JCV Inhibitors anstoßen zu können.

Abstract

While infections with human polyomaviruses are highly prevalent in the healthy population, only four of the 13 so far known human polyomaviruses, MCPyV, TSPyV, JCV and BKV, are associated with severe diseases in immunosuppressed patients. In particular, reactivation of JCV and BKV leads to major complications in transplant patients and other patients receiving immunosuppressive agents. Uncontrolled BKV replication causes two major diseases, hemorrhagic cystitis in 5 – 15% of allogenic transplant patients and polyomavirus associated nephropathy in up to 10% of kidney transplant recipients, resulting in subsequent graft loss. Despite the identification of BKV decades ago, hitherto no specific antiviral drugs are available and treatment of BKV associated diseases is limited to reduction of immunosuppression at the expense of an increased risk of graft rejection.

To alleviate the urgent need for novel antiviral therapies, the aim of this study was to identify and subsequently improve novel inhibitors active against BKV infection. Due to limitations concerning efficient *in vitro* propagation of BKV and highly restricted cell culture systems, the primate polyomavirus SV40 was used as a surrogate virus in a phenotypic high throuput screen of a library comprising approximately 28,000 small molecule compounds, to identify novel inhibitors active against the closely related human polyomaviruses JCV and BKV.

In the primary high throuput screen, 33 novel inhibitors active against SV40 infection were identified of which 16 were confirmed in a secondary BKV specific screen in renal proximal tubule epithelial cells. Nine of these inhibitors reduced BKV infection more than 90%. Inhibitors, selected by their *in silico* predicted physical chemical properties, were tested for broad range activity against JCV and murine polyomavirus infection. While the majority of inhibitors identified as active against BKV show also high inhibitory activity against JCV infection, only four of the 16 compounds inhibit murine polyomavirus infection by 90%.

Based on analysis of the chemical structure, five inhibitors of the identified 16 inhibitors were tested for their IC50 and CC50. Four of these compounds demonstrated high inhibitory activity with IC50 values in nanomolar range and a selectivity index of over 10. In particular, one inhibitor, compound C1, exhibited a highly significant inhibitory activity against BKV infection at low concentrations, without inducing host cell toxicity, and displayed a selectivity index of over 100.

The inhibitory activity of compound C1 against BKV in renal proximal tubule epithelial cells was extensively investigated for each step during viral life cycle. While the findings in this study indicate that compound C1 blocks entry of BKV infection by interacting either with a viral protein of BKV or a host cell protein regulated upon BKV infection, the precise mechanism that underlies compound C1 induced inhibition of BKV infection requires further analysis in order to identify the cellular or viral target of compound C1.

This study presents the identification of 16 small molecule compounds with novel chemical structures that inhibit human polyomavirus infections at low concentrations. Additionally, this study provides strong evidence that compound C1 inhibits BKV entry during infection and identifies compound C1 as a promising candidate for clinical development of drugs against BKV infection.

Table of Contents

1. Introduction

1.1 Family of polyomaviruses

The family *Polyomaviridae* comprises a rising number of avian and mammal viruses [1]. In 1953, the characterization of a transmissible agent causing multiple tumors in newborn mice, led to the discovery of the first polyomavirus (PyV), murine polyomavirus (MuPyV), thus providing the name (greek: *poly* = many; *-oma* = tumors) [2]. In 1960, the first primate PyV, simian virus 40 (SV40), was identified as a contaminant in poliovirus vaccines produced in African green monkey kidney cells [3]. Similar to MuPyV, SV40 exhibits a high transforming potential in foreign hosts, mice and rodents [4], but not in its natural host [5]. These PyVs were crucial models to study DNA and RNA metabolism, and paradigmatic research on them has noticeable contributed to the current knowledge about cellular processes such as DNA replication, transcription, mRNA splicing and transformation [6].

The first two human PyVs, BK virus (BKV) and JC virus (JCV), were discovered in 1971 and named after the initials of the patients from which they were isolated. BKV was primarily detected in the urine of kidney transplant patient, while JCV was found in brain tissue from a patient with progressive leukoencephalopathy [7, 8]. To date, more than 70 PyVs have been identified in animals, but for decades, no further PyVs have been detected in humans. Since 2007, innovations in sequence technology have led to the identification of 11 novel human PyVs [9], called New Jersey polyomavirus (NJPyV) [10], St Louis polyomavirus (STLPyV) [11] and Malawi polyomavirus (MWPyV) [12], which were named regarding the source of the original virus isolate, KIPyV [13] and WUPyV [14], which carry the name of the institutions where they were first described, HPyV6, 7, 9, 10, 12 [15–18], which were named according the order of their discovery, and the disease associated Merkel cell polyomavirus (MCPyV) [19] and Trichodysplasia Spinulosa associated polyomavirus (TSPyV) [20]. Recently, a novel PyV, Lyon IARC polyomavirus (LIPyV), has been identified, but further confirmation of LIPyV as a human PyV, e.g. serology in humans, is still remaining [21].

Hitherto, the family of human PyVs consists of 13 members, characterized by small, non-enveloped, icosahedral virions with a double stranded (ds) DNA genome [22]. Despite the variety of known PyVs, they share a common morphology and similar genome organization. The genome can be divided into three regions: the non-coding control region (NCCR) containing the origin of replication (ori), the early region encoding early proteins such as the small Tumor-Antigen (sT-Ag) and the large Tumor-Antigen (LT-Ag), which are crucial for regulating viral replication, and the late region encoding structural capsid proteins such as VP1 – 3 and the non-structural Agnoprotein [9].

Figure 1 illustrates a phylogenetic tree of human PyVs and their closest animal relatives. Generally, PyVs share high sequence homology at DNA and amino acid levels ranging from 50% to more than 80% [4]. Human PyVs exhibit a 69 to 75% DNA sequence homology and a 76 to 90% protein sequence

homology with SV40 [23]. Thus, SV40, JCV and BKV are closely related members of the PyVs. In respect of the entire viral genome, JCV and BKV share a DNA sequence homology of 75% and both exhibit 70% DNA sequence homology with SV40. The amino acid homology of proteins encoded in the early region is 88% between BKV and JCV, 81% between BKV or JCV and SV40, whereas the amino acid homology of proteins encoded in the late region is 86% between BKV and JCV or SV40 and 82% between JCV and SV40. However, among these viruses homology is low in the NCCR [24]. Additionally, the human PyVs WUPyV and KIPyV share high homology to JCV and BKV genomes [25].
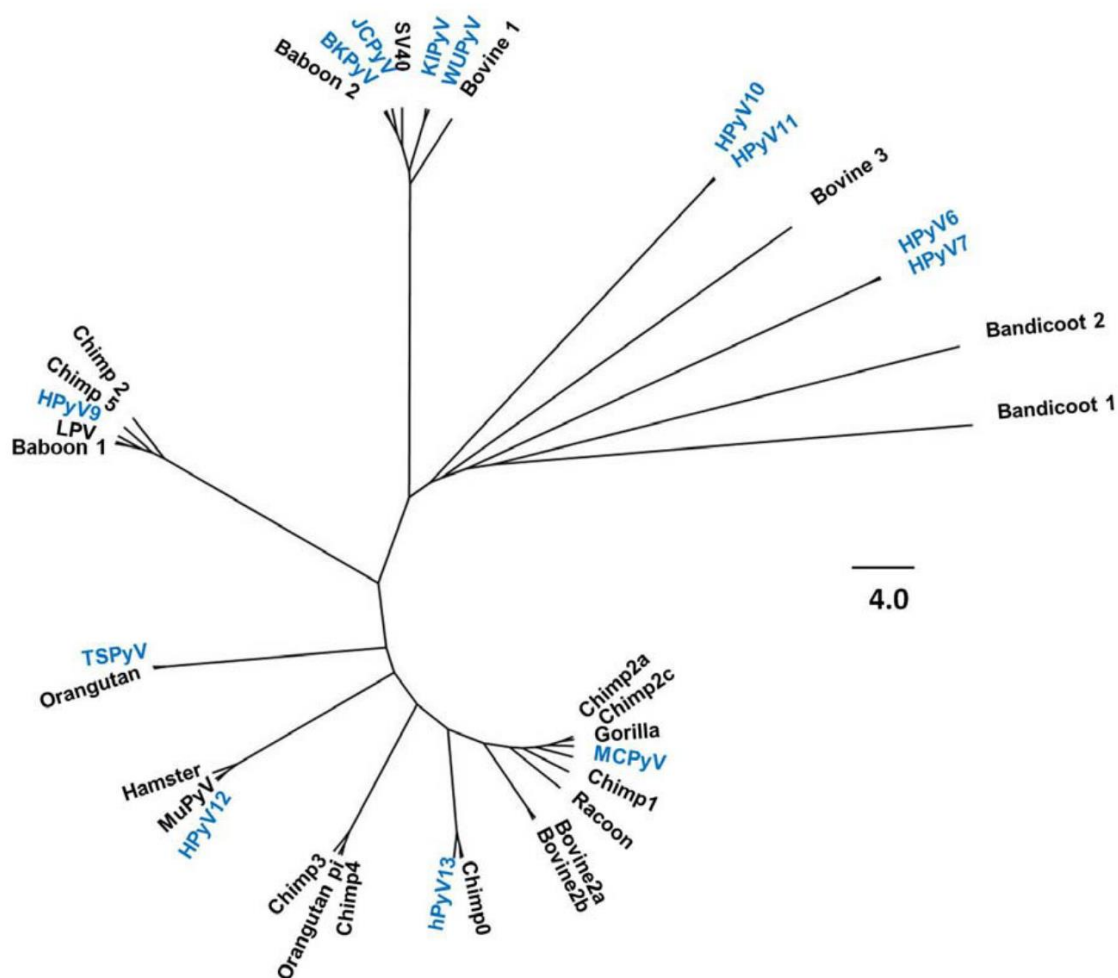
Figure 1: Phylogenetic tree of human PyVs and their closest animal relatives
Depicted is the relation between human PyVs, which are highlighted in blue, and their closest animal relatives based on their LT-Ag amino acid sequences. Adapted from Grundhoff A. and Fischer N. [26].

Although PyV are ubiquitous with a highly conserved structural organization, they are characterized by a restricted host range of infection [9]. Furthermore, PyV display narrow host cell tropism due to host cell surface receptor availability, an important determinant for viral entry. In addition, the absence or presence of specific host cell factors influences the regulation of viral gene expression and thus successful completion of the viral life cycle [4].

In general, seroprevalence of human PyVs is high in adults (40 – 100%). After a primary mostly asymptomatic infection in the early childhood, most human PyVs establish a lifelong persistence accompanied by low-level replication [9, 22]. Despite their highly prevalence in the human population, PyVs associated diseases are rare, predominantly occurring in immunocompromised individuals. In fact, merely four of the known 13 human PyVs are associated to causes severe diseases in humans: JCV, BKV, MCPyV and TSPyV [9, 25]. TSPyV induces a rare skin disease in allograft transplant patients [20], while MCPyV is associated with Merkel cell carcinoma, a rare skin cancer in elderly and transplant patients [19]. In particular, BKV and JCV reactivation causes major complications in transplant patients and other patients receiving immunosuppressive agents [9]. JCV causes progressive multifocal leukoencephalopathy (PML) in immunosuppressed transplantation patients, multiple sclerosis patients under natalizumab treatment or HIV infected AIDS patients [27]. Besides, uncontrolled BKV replication causes two major diseases, hemorrhagic cystitis after bone marrow transplantation and PyV associated nephropathy after kidney transplantation [22].

1.2 Clinical diseases associated with BKV reactivation

Worldwide over 80% of adults are seropositive for BKV infection [28]. After initial infection with BKV in the early childhood, BKV infection proceeds asymptomatically in the urinary tract with periodic shedding into the urine at low level viruria without leading to any clinical diseases in healthy, immunocompetent individuals [29]. However, in immunocompromised individuals BKV reactivates from its persistent subclinical state to a lytic infection resulting in viruria and viremia at high level [30]. In transplant patients with compromised immune system, reactivation of BKV causes two major diseases, polyomavirus associated nephropathy and hemorrhagic cystitis [31]. With the lack of antiviral therapy, treatment options are limited. So far, the only treatment is to reduce immunosuppression, thereby highly increasing the feasibility of graft rejection [28].

1.2.1 Polyomavirus associated nephropathy

Polyomavirus associated nephropathy (PVAN) remains one of the leading causes of graft failure after kidney transplantation, affecting 1 – 10% of recipients and leading to graft rejection in approximately 50% of the cases [32]. Although, the development of better immunosuppressive agents reduced the rate of acute graft rejections in renal transplant patients, the incidence rate of PVAN highly increased [33].

PVAN is primary caused by BKV reactivation in the urinary tract leading to inflammatory interstitial nephropathy approximately 10 – 13 months post renal transplant. Hitherto, no risk factors are strongly associated with the development of PVAN in renal transplant patients, but a variety of weakly associated risk factors for BKV reactivation have been reported [32]. Pre-transplantation risk factors

are distinguished in recipient and graft characteristics. Recipient specific risk factors are male gender, older age, seronegative recipient and previous graft loss induced by PVAN. Graft specific risk factors include the degree of human leukocyte antigen (HLA) mismatch, seropositivity of the donor and pre-existing ischemic or immunological injury [32]. The major post-transplantation risk factor is the immunosuppressive regimen, at which the degree of immunosuppression highly contributes to PVAN development [32]. Additionally, viral factors like mutations within the VP1 capsid protein of BKV have been associated to increase the risk of BKV reactivation [34]. Furthermore, killer cell immunoglobulin-like receptors (KIRs), which are important for controlling the natural killer (NK) cell activity against viral infection, are reported to be activated upon BKV infection and development of PVAN [35].

In PVAN, reactivation of BKV is characterized by intranuclear viral inclusion in epithelial cells of renal tubules, glomeruli and collecting ducts [36]. In the initial stages, PVAN is characterized by increased levels of serum creatinine followed by BKV viruria, which can be determined in 35 − 57% of kidney transplant patients [32]. In 13 − 22% of PVAN patients viruria evolve in BKV viremia, leading to tubular atrophy, interstitial fibrosis, inflammation, and ultimately resulting in graft loss [37].

PVAN can be diagnosed by quantification of viral load in the plasma and urine by PCR detecting viral DNA [32], or by detecting decoy cells in the urine, which originated from infected renal tubular cells, containing altered nuclei [38]. Decoy cells are characterized by nuclear enlargement, viral inclusion bodies, chromatin margination and abnormal chromatin pattern, which can be detected by phase contrast microscopy [39]. Although the use of urine cytology, to detect the presence of decoy cells in the urine, exhibits 100% sensitivity for BKV infection, only a low predictive value for the diagnosis of PVAN of 29% is achieved [40], since decoy cells represent an asymptomatic viral reactivation rather than indications for BKV associated diseases [41]. Generally, a tissue biopsy of the affected kidney remains the gold standard for diagnosing PVAN, although a negative biopsy result cannot rule out persistent diagnosis of PVAN, since lesions caused by BKV reactivation can arise sporadically throughout the graft [32]. In patients with biopsy-proven BKV associated PVAN, BKV viremia of 10^4 genome equivalents per milliliter (Geq/mL) in plasma, or BKV viruria of greater than 10^7 Geq/mL in urine are generally observed [29].

1.2.2 Hemorrhagic cystitis

Hemorrhagic cystitis (HC) is a serious and common complication after hematopoietic stem cell transplantation, associated with high morbidity [42]. Clinical symptoms of HC include suprapubic pain, dysuria and different degrees of hematuria [43]. The severity of HC is ranked based on a grading system, which defines microscopic hematuria as grade 1, visible hematuria as grade 2, visible hematuria with small clots as grade 3, and gross hematuria with urinary tract obstruction, the most

serious deterioration, as grade 4 [44]. The latter instance is caused by clot formation resulting in severe pain, uncontrollable bleeding, acute renal failure and, in rare cases, fatality [32]. However, high-level of BKV replication in urothelial cells represents a hallmark of PyV associated HC affecting bone marrow transplant (BMT) recipients [29].

HC can emerge pre- and post- engraftment and many factors contribute to the cause of HC, e.g. toxic effects of the chemotherapeutic regiments and/or viral infection. As pre-disposing factors transplant type, age at transplantation, presence of graft-versus-host disease (GVHD), donor source, conditioning regimen components and intensity are reported [42]. Different viruses, e.g. cytomegalovirus (CMV), adenovirus and BKV, can initiate HC in the post-engraftment phase with BKV infection being the leading cause. High levels of BKV viruria have been proposed to increase the risk of HC development [32]. HC induced by BKV emerges in 10 – 25% of BMTs, typically occurring two weeks post-transplantation, with BKV viruria detectable in 50% of BMT patients [43].

HC associated with BKV can be diagnosed by cytological examination of the urine or by PCR amplification of viral DNA in urine or serum [32] with BKV viral loads in the urine of HC patients peaking at 10^{14} Geq/mL [45]. The standard treatment for BKV associated HC is supportive care including hyperhydration, pain management, bladder irrigation and forced diuresis [32].

1.3 Host cell immune response to BKV reactivation

BKV infection in the immune competent host is mainly controlled by T cell response [41, 46]. Reactivation of BKV has been linked to a failure of T cell response in kidney transplant patients and may cause PVAN and graft rejection [46]. One study verified that transplant patients exhibiting self-limited BKV reactivation were able to develop BKV specific T cells [47]. Likewise, weak T cell responses have been associated with recurrent BKV viremia and inhibition of BKV replication [32, 48]. In addition, reports indicated that CD4+ T cells dominate BKV specific immunity in kidney transplant patients [46, 48, 49]. Controversially, some studies report that high levels of BKV specific T cells enhance immunopathogenic diseases and accumulation of BKV specific T cells can result in graft loss in PVAN patients, suggesting that T cells play a beneficial role early in BKV infection but an immunopathogenic role in late infection [50].

On the other hand, in general, the first antiviral defense of host cells, prior to increase of T cell populations, is regulated by the innate immune system and unspecific cytotoxic cells like NK cells [48]. Several studies reported that KIRs play an important role in controlling BKV infection [35, 48, 51]. PVAN patients are found to carry significantly low numbers of activated KIRs, suggesting a protective effect of these receptors during BKV infection [35]. Furthermore, dendritic cells have been reported to play a role in BKV specific immune response [32]. A study linked reduced dendritic cell numbers to increased risk of developing BKV viremia in pre-transplant patients [50]. Moreover, different studies have shown

that BKV interacts with promyelocytic leukemia nuclear bodies (PML-NBs), suggesting that intrinsic antiviral immunity response is triggered upon BKV infection [32, 52]. Furthermore, BKV reactivation was linked to induce an additional intrinsic antiviral defense, the DNA damage response (DDR) pathway, in order to prevent genomic damage of infected host cells [53].

The humoral immunity response plays a controversial role in controlling BKV reactivity. In more than 80% of individuals BKV specific antibodies are present [48]. Some reports have shown that in kidney transplant recipients BKV seronegativity correlates with a higher risk of BKV replication and onset of PVAN [54, 55], [32]. However, clinical observations indicate that a humoral immunity response fails to prevent post-transplant BKV reactivation and development of BKV associated diseases [37, 56].

1.4 Treatment options of BKV associated diseases

Implementation of more effective immunosuppressive regiments and decreased rates of acute graft rejection resulted in viral infections being a dominant cause of allograft loss after renal transplantation. Especially, infection with BKV affects approximately 15% of renal transplant recipients [57]. The most common diseases associated with BKV reactivation and lytic infection in renal transplant and BMT patients, respectively, are PVAN and HC [32]. Although BKV was first isolated more than 45 years ago, treatment options of BKV reaction are still restricted [58]. Hitherto, the common approach to regulate BKV reactivation in HC patients is palliative care or in PVAN patients reduction of the dosage of immunosuppressive regiment, thereby highly increasing the risk of acute rejection and graft failure [53]. However, drugs showing *in vitro* activity against BKV such as Cidofovir, Leflunomide or Fluoroquinolones have been used in combination with immunosuppression reduction with some reported success [25], but the benefit of combining these drugs with reduction of immunosuppressants is controversial and has not been evaluated adequately in randomized studies [58].

So far, evidence for the antiviral efficacy of these drugs *in vivo* is sparse and strong side effects have been described [25]. Since currently no FDA approved, specific anti BKV drug is available, reactivation of BKV in transplant patients persists as a crucial risk factor for causing graft loss [53]. However, in the following paragraph the drugs Cidofovir, Leflunomide and Fluoroquinolones as wells as the mammalian target of rapamycin (mTOR) or calcineurin inhibitors and intravenous immunoglobulin (IVIG) will be presented as options for treatment of BKV associated diseases.

1.4.1 Cidofovir and its derivative Brincidofovir

The nucleoside analog Cidofovir is effective against a wide variety of viruses by inhibiting viral DNA polymerase [59]. Cidofovir is approved for the treatment of CMV induced retinitis in HIV infected patients [32]. Although Cidofovir shows *in vitro* activity against BKV, the mechanism of its inhibitory

activity remains unclear as BKV hijacks the cellular DNA polymerases for its replication [60]. Reports validating the *in vivo* activity of Cidofovir against BKV are controversial. In BKV associated HC with coincident CMV infection Cidofovir was observed to decrease both CMV replication and level of BKV viruria leading to clinical improvements. Furthermore, in BMT patients low-dose Cidofovir treatment was found to decrease viruria by 85% and viremia by 47% [61]. In contrast, others reported that Cidofovir treatment resulted in reduced renal function and increased viral load in PVAN patients, demonstrating that Cidofovir evince limited treatment potential in renal transplant patients, due to nephrotoxicity and restricted oral bioavailability. The controversial outcomes of Cidofovir treatment in BKV associated diseases reveal the urgent need for randomized trials [32].

However, Brincidofovir, a bioavailable lipid-ester conjugated prodrug of Cidofovir, bears some benefits compared to Cidofovir. Brincidofovir is orally delivered instead of intravenously and showed decreased nephrotoxicity [62]. Moreover, Brincidofovir was reported to inhibit BKV replication in human primary renal proximal tubule epithelial (RPTE) cells to a higher degree and with a longer lasting effect than Cidofovir [63]. Clinical studies testing its *in vivo* activity in renal transplant and BMT recipients are ongoing [32]. Chimerix presented evidence for the efficacy of Brincidofovir against MuPyV in mice recently [64].

1.4.2 Leflunomide

The prodrug Leflunomide, which combines antiviral and immunosuppressant activity, is approved for the treatment of rheumatoid arthritis and displays *in vivo* activity against DNA viruses like CMV and HSV. Additionally, this drug was used in combination with immunosuppressive regiments to treat BKV associated diseases [32]. Leflunomide is reported to inhibit tyrosine kinase, dihydroorotate dehydrogenase and pyrimidine synthesis leading to diminished cellular proliferation, and presents moderate activity in inhibiting BKV replication *in vitro* [65]. Similar to Cidofovir, the effectivity of Leflunomide treatment is controversial regarding its *in vitro* activity against BKV replication in RPTEC [66]. However, a retrospect study of 26 kidney transplant recipients showed that treatment with Leflunomide decreased viral loads in the plasma and urine compared to untreated controls [32]. Furthermore, a recent randomized phase II trial with a derivative of an active metabolite of Leflunomide, FK778, revealed a significant decrease of BKV viremia, but without improving graft function and with higher incidence of acute rejection, in comparison to those not treated with Leflunomide [67].

1.4.3 Fluoroquinolones

Fluoroquinolones such as Ciprofloxacin, Levofloxacin and Gatifloxacin are antibiotics that block bacterial DNA replication by inhibiting type II topoisomerase. These antibiotics have been described to

inhibit BKV *in vitro* [68], presumably by affecting helicase activity of LT-Ag [69]. In the treatment of BKV associated diseases Fluoroquinolones have been used in combination with a reduction of immunosuppression. A retrospective study demonstrated that the usage of Fluoroquinolones as prophylactic therapy for PVAN in kidney transplant patients decreased the rate of BKV viremia [70]. Additionally, prophylactical treatment with Ciprofloxacin in BMT patients was found to reduce HC incidence compared to immunosuppression reduction alone [71]. Furthermore, treatment with Gatifloxacin resulted in an 80% decrease of viremia or alleviation of decoy cells in the urine in seven of ten renal transplant patients. Beside the inhibitory activity of Fluoroquinolones against BKV *in vivo*, this drug class induces severe adverse effects such as liver damage [32].

1.4.4 Intravenous immunoglobulins

Intravenous immunoglobulins (IVIG) are pooled immunoglobulin G (IgG) isolated from plasma of more than thousand blood donors. IVIG are described to exhibit immunomodulatory effects and bear the potential to bind immunoglobulins and abolish bacterial and viral toxins [72].

The seroprevalence of BKV is very high in the heathy population with > 80% of individuals producing antibodies against BKV infection [41]. Isolation of antibodies from all peripheral B cell subsets revealed a high frequency of monoclonal antibodies able to neutralize BKV [73]. IVIG containing BKV neutralizing antibodies were used in combination with reduction of immunosuppression to treat BKV associated diseases due to its presumed anti-inflammatory properties and BKV neutralizing activities [74, 75]. The outcomes in patients treated with IVIG are controversial. In some cases IVIG therapy seems to suppress BKV reactivation, but other studies report an increase of BKV viral load in the plasma of PVAN patients [32]. So far, no correlation between high antibody titers in the recipient and prevention of PVAN has been found [76], but development of viruria is more likely in transplant patients receiving kidneys from donors exhibiting high BKV titers [77]. Novartis Pharmaceuticals initiated a phase II placebo controlled interventional study (NCT03456999) recently to test a neutralizing antibody (MAU868) in PVAN patients [78].

1.4.5 Immunosuppressive drugs

Immunosuppressive regiments for renal recipients are diverse but usually include mTOR or calcineurin inhibitors [37]. Besides their suppression of host immune response to evade graft rejection, these drugs highly contribute to viral reactivation [32].

Calcineurin inhibitors such as Tacrolimus or Cyclosporin A reduce activation of T cells by inhibiting immunophilins and impairing transcription of Interleukin-2 (IL-2). *In vitro* studies show that Cyclosporine A inhibited BKV replication, while Tacrolimus activated BKV replication [79]. Additionally, mTOR inhibitors like Sirolimus decrease translation and cell cycle progression [32]. Sirolimus has been

found to highly decrease BKV replication *in vitro* by interfering with mTOR-SP6-kinase activation [79]. A retrospective study in transplant patients reported that treatment with mTOR inhibitors reduced BKV viruria and viremia faster than reduction of immunosuppression, resulting in greater recovery of allograft function [80]. Further studies suggested that mTOR inhibitors enhance CD8+ T cell memory, leading to clearance of BKV [81]. Contrarily, one study reported that Sirolimus treatment in pediatric renal patients causes BKV viremia as one adverse effect [82]. An additional study showed that BKV clearance in PVAN patients is detected, after treatment with Sirolimus was terminated [83].

However, Sirolimus and Tacrolimus exhibit opposite effects of BKV replication *in vitro*, suggesting that immunosuppressive drugs directly contribute to the risk of increased BKV replication and nephropathy in addition to suppressing T cell activity [79]. Therefore, randomized studies, determining the effect of immunosuppressive drugs such as mTOR or calcineurin inhibitors, are required to validate their benefits regarding the treatment of BKV associated diseases [32].

1.5 Epidemiology of BKV

Similar to other human PyVs, BKV is highly prevalent in the healthy population with more than 90% of adults being seropositive for BKV [22, 84]. Primary infection with BKV occurs asymptomatically in the early childhood followed by dissemination to the kidney and urinary tract, in particular to kidney tubule epithelial cells and urinary tract epithelial cells, where the virus establishes a lifelong persistence in most individuals [85]. Sporadic virus replication and asymptomatic shedding of BKV in the urine during the persistent state of BKV was observed in a small percentage of healthy individuals, and asymptomatic viruria was found in 3% of pregnant patients during the second and third trimester [25]. However, under conditions of immunosuppression BKV reactivation followed by viral shedding into the urine can lead to severe diseases, such as PVAN in renal transplant patients and HC in BMT recipients [86].

The site and entry route of initial BKV infection and transmission as well as the mode of transmission remains unclear [87]. The early age of seroconversion together with detection of BKV in tonsillar tissue suggested a respiratory transmission route [88]. Other potential modes of transmission include urine, semen, transplacental or blood transfusion [89–91].

Different cell types such as urogenital cells, brain cells and peripheral blood mononuclear cells may be involved in dissemination and persistence of BKV [92]. However, the cells of kidney and urinary tract are suggested to be the major sites of persistence for BKV. In 30 – 50% of conventional kidney tissues, BKV DNA was detected with dissemination patterns of small foci all over the medulla and cortex, and in 40% of ureters. Furthermore, in accordance to BKV specific immunostaining analysis, epithelial cells of the kidney, ureter and bladder seem to be the predominant cell types for persistent infections [30].

1.6 Genomic organization of BKV

Like all PyVs, BKV is a small, non-enveloped DNA virus with a diameter of 45 nm comprising a circular ds genome of approximately 5 kb [90]. The viral genome was found to associated with host cell histone proteins H2A, H2B, H3 and H4 forming minichromosomes [93]. The genome is divided into three major regions, the NCCR, the early coding region and late coding region [85], as depicted in Figure 2.
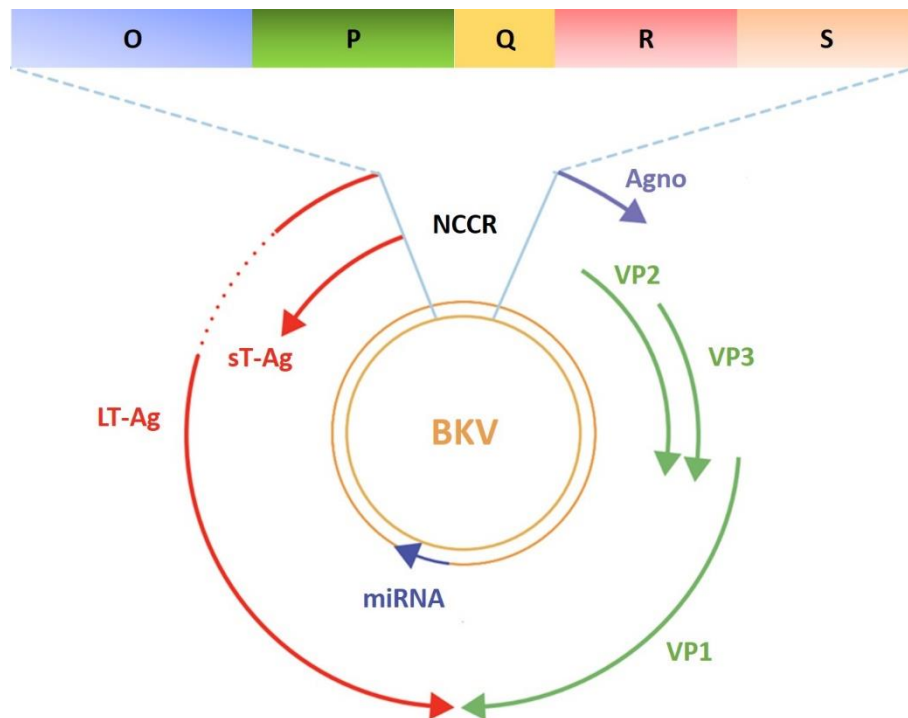
Figure 2: Schematic illustration of the BKV genome
The viral genome of BKV is a small, circular, ds DNA molecule consisting of 5153 bp and is classified into three regions: NCCR, early coding and late coding region. Transcription of the early and late genes proceeds in opposite directions controlled by specific early and late promotors situated in the NCCR. The solid arrows indicate open reading frames and the dashed lines depict early region introns. Viral miRNA is encoded complementary to the early region and transcribed from the late strands. The NCCR is divided into sequence blocks O, P, Q, R and S. Modified from Mazalrey et al. [93].

The NCCR contains the origin of DNA replication and promotor/enhancer elements with DNA binding sites for transcription factors, mediating secondary host cell specificity [94], as well as directing the expression of both early and late genes, which are transcribed from divergent strands of the genome [95]. The genome of BKV contains sequence information for six viral proteins, two encoded from the early coding region, LT-Ag and sT-Ag, and four from the late coding region, VP1 – 3 and Agnoprotein (Agno) [92]. The NCCR is characterized as the sequence between the initiation codon of the LT-Ag in the early region and the initiation codon of Agno in the late region [93] and is categorized into five sequence blocks: O, P, Q, R and S [95]. The O sequence block is a highly conserved region of the NCCR harboring the ori and the transcription initiation site for early genes, which are recognized by LT-Ag, and an NFκB-binding site [93]. The P, Q and R blocks contain enhancer regions and consensus motifs

for the binding of transcription factors such as CRE, NF-1, SP1 and ETS-1, with the latter ones being suggested to regulate viral gene transcription [95]. The S sequence block comprises an estrogen response element and the initiation sites for late gene transcription [93].

The early coding region contains the regulatory proteins LT-Ag and sT-Ag [96]. The T-Ags were named after the initial assumption of them being tumorigenic, although the majority of PyVs including BKV do not cause transformation of their natural host cells. The transforming potential of T-Ags is based on their interaction with cellular targets controlling cell cycle regulation and tumor suppression [97]. The different T-Ag isoforms are produced by alternative splicing of the same early gene transcript and share 81 N-terminal amino acids [92]. The T-Ags are multifunctional proteins important for regulating viral replication and late gene expression [32].

The late coding region encodes for structural viral proteins VP1, VP2 and VP3, which are produced by alternative splicing of the viral late gene transcript. VP1 as the major capsid protein constitutes the outer surface of BKV capsid and is responsible for receptor binding to host cells [98], while the minor capsid proteins VP2 and VP3 are located on the internal side [93]. The icosahedral capsid consists of 72 pentamers of mayor capsid protein VP1 and each pentamer interacts with a single molecule of the minor capsid proteins VP2 or VP3 [30], leading to a linkage of the viral genome to the outer shell [92]. In addition, the late coding region encodes for the non-structural Agno, which is expressed during later stages of infection and is assumed to play a crucial role in virus assembly and egress. Agno is found only in two other PyVs, namely JCV and SV40 [99].

Furthermore, studies have shown that a number of human and animal PyVs, including BKV, encode microRNAs (miRNAs), which are expressed from sequences located in antisense orientation to the early T-Ag encoding transcripts on the genome, although their precise genomic location varies between different PyVs [100–106]. Several studies suggest that all hitherto known PyV miRNAs have the ability to negatively regulate expression of the early proteins due to the perfect sequence complementary of mature miRNA to early gene transcripts [100, 101, 103, 104, 107–109].

1.7 BKV genotypes and serotypes

The genome of BKV is characterized by genetic diversity. Especially the NCCR, the most variable region, contains various deletions, insertions, duplications and complex rearrangements including enhancer/promotor sequences [110]. Based on the NCCR sequence, there are two naturally transmitting forms of viral genomes, designated archetype and rearranged [111]. Since the archetype BKV is the predominantly form identified in the urine of healthy adults and also in the urine of patients with BKV associated diseases, it is suggested to be the transmissible form of BKV [28]. Hence, in immunosuppressed patients associated with BKV diseases, rearranged variants of BKV emerged as a species [94]. The archetype is assumed to be the persistent form, while the rearranged variants are

derived from the archetype strain during reactivation in immunocompromised patients [111], as illustrated in Figure 3.
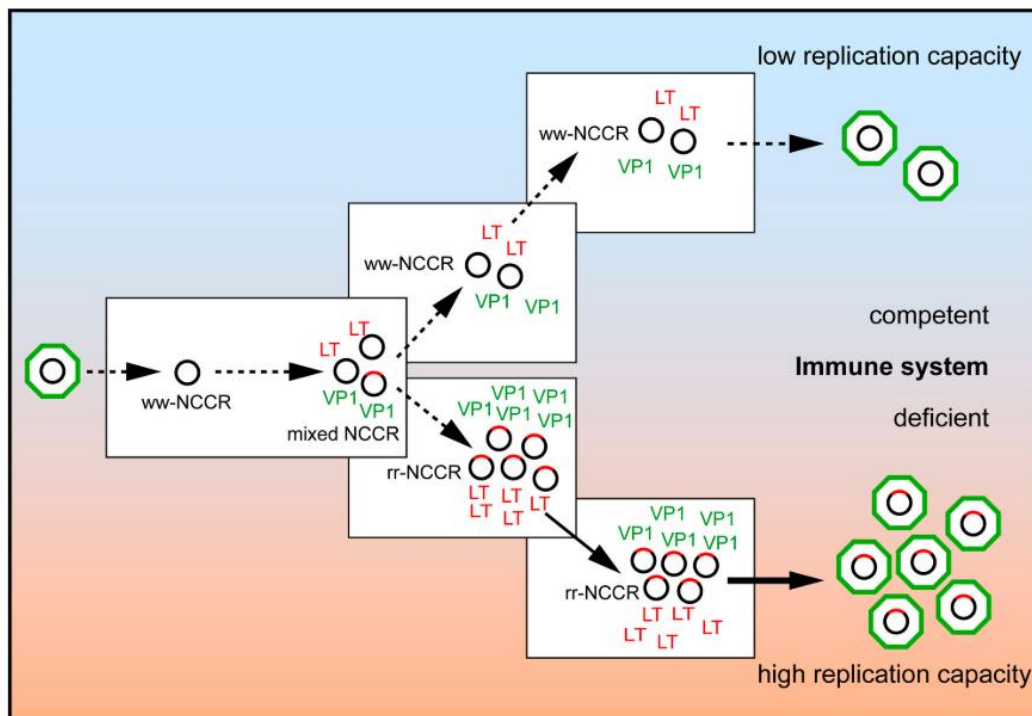
Figure 3: Schematic illustration of the BKV genome
The naturally occurring BKV form with archetype NCCR genome (black circles) is altered by insertion and deletion during replication generating rearranged NCCR genomes (red-tagged circles). In immunocompetent individuals, only the archetype form is present, while in immunodeficient hosts detection of rearranged BKV strains emerges, resulting in increased expression of early genes and higher replication capacity than the archetype form. Adapted from Gosert et al. [112].

The rearranged BKV forms are distinguished by duplications and deletion within the NCCR compared to archetype, while other areas of the BKV genome remain unchanged [112]. Those rearrangements in the NCCR alter the number and environment of transcription factor binding sites [90]. Contrary to archetype BKV, which shows very low viral replication, the rearranged strains produce infectious progeny *in vitro* and demonstrate increased early gene expression with concomitantly higher replication capacity and cytopathology [109]. In addition, the rearranged forms are associated with higher viral loads in plasma and more severe histological lesions compared to archetype virus [112]. Moreover, a study reported that the archetype virus exhibits higher viral miRNA expression levels *in vitro* than the rearranged BKV strains in order to establish persistence [109].

Furthermore, significant variations were detected in the VP1 gene, which encodes for the major structural protein VP1 comprising approximately 80% of the total viral capsid protein. A single change of the amino acid in VP1 protein seems to impair pathogenicity [113]. All existing BKV isolates, identified in healthy individuals and immunosuppressed patients, are categorized into four distinct

subtypes based on their VP1 sequence and seroprevalence, designated by the Roman numerals I, II, III and IV [114]. The subtype I presents the most frequent form found in the normal human population (80%) and comprises the rearranged BKV strains named Prototype, Dunlop, Gardner and MM, while subtype IV is the second most frequent form found (15%) and includes the strains IV and MG. The subtypes II and III are rarely detected in normal adults, with subtype II comprising the strain SB and subtype III the strain AS [90]. Despite subtype I being the most prevalent form, also rare subtypes of BKV are viable and frequently detected in renal transplant patients with PVAN [93]. Additionally, these different BKV genotypes comprise different cellular tropisms and pathogenic potentials *in vivo* [115].

1.8 BKV miRNA

miRNAs are small non-coding RNAs of approximately 22 nucleotides (nt), which posttranscriptionally regulate gene expression by impairing translation or guiding degradation of target mRNAs [116]. In mammalian cells, miRNAs bind target mRNAs with imperfect complementarity implicating the ability of recognizing hundreds of different targets. However, in plants or viruses, miRNAs enable binding of target mRNA with perfect complementary resulting in direct degradation of the target transcription product [109]. Hitherto, functions and biogenesis of PyV miRNAs are poorly understood. Generally, miRNAs are processed from introns of RNA polymerase (pol) II primary transcripts, resulting in the loading of one of the two arms of the precursor hairpin, termed the 5p and 3p arms, into the RNA-induced silencing complex (RISC) with subsequent directing of the miRNA to its target mRNA. Instances of perfect complementary lead to target degradation, while imperfect binding results in translational repression, as shown in Figure 4 [107].

Among other PyVs, SV40, MuPyV, MCPyV, JCV and also BKV encode a miRNA on the late strand with perfect complementary to early transcripts, suggesting the potential to negatively regulate expression of early genes such as LT-Ag [111]. Interestingly, the miRNAs of PyVs are unique since both, the 5p and 3p, arms are functional. Among these PyVs, the genetic location of the miRNA gene and target sequence differ. In the case of BKV, JCV and SV40, the miRNA binds to the 3`end of the LT open reading frame (ORF), whereas for MuPyV and MCPyV the target is located at the 5`end [107]. Since the miRNA is located on the late strand, it is assumed that miRNA may be expressed from the late promotor, although a unique promotor located within or outside the NCCR is possible [109].
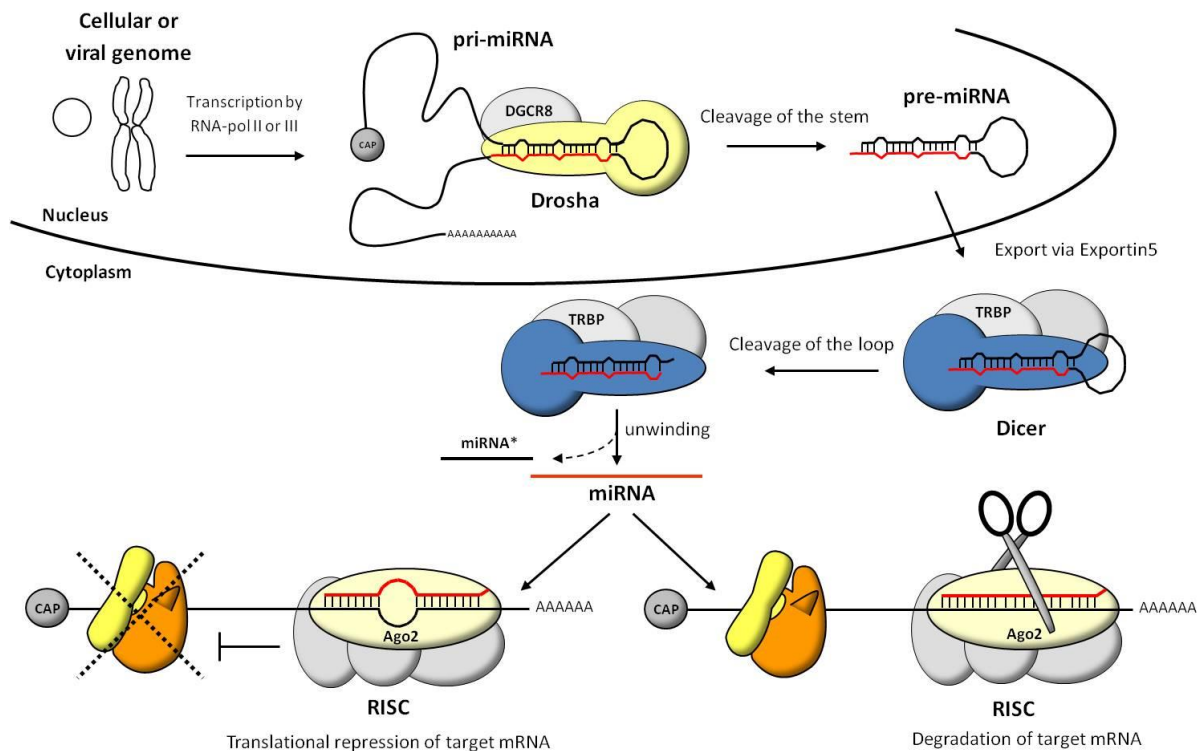
Figure 4: Canonical biogenesis pathway and functional principle of miRNAs
miRNAs, encoded in viral or cellular genomes, are transcribed into a pri-miRNA by RNA-pol II or in uncommon instances by RNA-pol III. After subsequent modelling of the pri-miRNA into a stem-loop structure, the endonuclease RNase III-enzyme Drosha cleaves the stem portion generating a pre-miRNA. Exportin5 transports the pre-miRNA into the cytoplasm, where it undergoes further processing by RNase III-enzyme Dicer, which eliminates the loop region. After unwinding, two single stranded miRNAs of approximately 22 nt are manumitted. Perfect complementarity between miRNA and its target mRNA sequence results in Ago2-dependent degradation of target mRNA, while imperfect base-paring induce translational repression. Adapted from Adam Grundhoff.

In addition to the NCCR, for BKV a further mechanism has been proposed to regulate early gene expression at posttranscriptional level directed by miRNAs of BKV, designated miRB1-3p and miRB1-5p, by targeting LT-Ag transcripts and thereby down-regulating viral replication [94]. This posttranscriptional mechanism have been suggested to play a role in the escape from LT-Ag specific cytotoxic T cells [100], which recently have been connected to the effective impairment of BKV replication in renal transplant patients [94]. Furthermore, a mutant of BKV with archetype NCCR, which does not express BKV miRNAs, was described to result in higher expression levels of LT-Ag and revealed a correspondingly higher replication capacity compared to wildtype, indicating that low level replication is required for establishment and maintenance of persistence [109]. Hence, the miRNA of BKV is considered to direct viral replication by down-regulating early gene expression through its binding to LT-Ag and thereby be involved in the establishment of persistence [111].

1.9 BKV life cycle

In general, PyVs exhibit a narrow host cell tropism concerning their species and cell type, which hinders the establishment of *in vitro* and *in vivo* model systems to investigate the different steps of the viral life cycle [117]. Since PyVs infection is highly prevalent in the normal human population after primary infection in early childhood, PyVs must have contrived strategies to manage a persistent state without triggering an antiviral immune response of the host. The details of these underlying mechanisms are poorly understood. Most of the common knowledge of the different steps of PyVs life cycle are derived from studies on SV40 or MuPyV [111]. Although PyVs can attach to cell surface receptors and enter cells of multiple different species, the outcome of the infection is species specific. For instance, in non-permissive hosts viral replication is hampered resulting in abortive infection or cell transformation, while in permissive hosts initial infection leads to viral DNA replication, production of progeny virions and cell lysis [23, 92]. For BKV, the main site of reactivation and replication is within the urinary tract and kidney, thus primary renal epithelial cells present the natural host cells [32].

As mentioned before, BKV is a non-enveloped virus consisting of only a protein capsid and DNA but is lacking a surrounding lipid bilayer. The structure of the viral capsid is formed by the major structural capsid protein VP1 and the less abundant minor capsid proteins VP2 and VP3. The ds circular DNA genome, which is littered with histones in the form of minichromosomes, is surrounded by the capsid [32]. The capsid of BKV comprises 72 pentamers of the major capsid protein VP1 forming loop structures on the outer surface contributing to host cell receptor binding. By inter- and intra- pentameric disulfide bonds and calcium cations these pentamers are stabilized [118, 119].

The life cycle of BKV infection begins with the binding of capsid protein VP1 to cellular receptors to promote internalization [120]. The gangliosides GD1b and GT1b, both containing a terminal α2,8-linked sialic acid residue, are proposed to serve as host cell receptors for BKV [85]. In addition, an N-linked glycoprotein with an α2,3-linked sialic acid residue was suggested to act as a co-receptor for BKV [121]. However, the presence of sialic acids alone appears insufficient for BKV attachment [119]. Following initial attachment to the cell surface, BKV is internalized by caveola-mediated endocytosis [85]. Contrarily, a study showed that BKV can enter the cells additionally through a caveolin and clathrin independent mechanism [122]. After entry, BKV passes through an acidic compartment and the caveosome, and then traffics via caveolae particles to the endoplasmic reticulum (ER), while bypassing the Golgi system [38] along the microtubule network [85, 123, 124], where it arrives approximately eight hours post infection [125]. This process is suggested to be independent of the activity of motor protein dynein [38]. Among DNA viruses, trafficking through ER as a crucial step is unique for PyVs, indicating necessary modifications of PyVs by the environment of the ER. However, for BKV the detailed process of virus uncoating remains elusive. For MuPyV and SV40, it is suggested that the initial disassembly site is in the ER compartment, which contains chaperones,

disulfide isomerases and reductases required for virus uncoating process. Interactions with ER protein disulfide isomerases causes conformational changes in VP1 resulting in membrane penetration or virions disassembly [32, 85]. Additionally, proteins included in the ER associated protein degradation (ERAD) are involved in PyVs trafficking suggesting that PyVs escape from the ER prior to nuclear entry by hijacking the ERAD machinery [125]. After transport to the ER, capsid uncoating in the ER lumen, egress from the ER via the ERAD pathway and entering the cytosol, BKV is hypothesized to translocate into the nucleus, where the uncoated genome have access to the replication machinery of the host cell [117]. Since BKV is dependent on host cell nuclear processes in order to start viral DNA replication, the BKV genome must reach the inner of the nucleus [111]. However, the nuclear entry pathway of BKV is elusive. It was suggested that the virus may use a canonical nuclear import pathway through the nuclear pore complex, while being partially disassembled. Additionally, a nuclear localization signal (NLS) is situated on each of the capsid protein and studies show that the NLS on VP3 may be crucial for nuclear entry [32]. Furthermore, the α/β importin pathway seems to play an pivotal role during nuclear entry of BKV [122].

The entry of the viral genome into the nucleus enables transcription of early viral genes, the T-Ags, to initiate viral DNA replication [85]. By inactivating the cell cycle control proteins Retinoblastoma protein (Rb) and p53, LT-Ag coerces cells to enter S phase and thereby the production of components of the required cellular DNA synthetic machinery [111]. Viral DNA replication is initiated by LT-Ag assembling into multimeric complexes and binding to GRGGC motifs at the ori [126], followed by unwinding of the viral DNA via its helicase-ATPase domain and recruitment of cellular DNA polymerase α-primase complex [111]. Concomitant with initiating of viral replication, LT-Ag represses early gene transcription and activates late promoter to start expression of the structural viral proteins [92]. The capsid proteins VP1, VP2 and VP3 are produced in the cytoplasm and harbor an NLS, promoting their import into the nucleus for virion assembly. During this process progeny virus particles are built around newly synthetized genomes [32], but empty particles without encapsidated nucleic acid may occur [127]. Progeny virions are able to leave the cell and infect new cells [107]. The detailed mechanisms concerning the egress of viral particles is unknown [117]. It was suggested that excessive accumulation of progeny virions within the nucleus induces obstruction and burden on the nuclear envelope resulting in cell lysis [128]. However, the archetype strain of BKV was found to establish a lifelong persistence in its host cells, apparently by very low level of viral replication [117]. The miRNA of BKV is proposed to be involved in sustaining a persistent state by restricting early transcripts and corresponding viral DNA replication [109].

The viral life cycle of BKV in human RPTEC, which are the natural host cells of BKV, takes at least 24 – 48 hours to complete, revealing a slow BKV course of infection [38]. The different steps of BKV life cycle are illustrated in Figure 5.
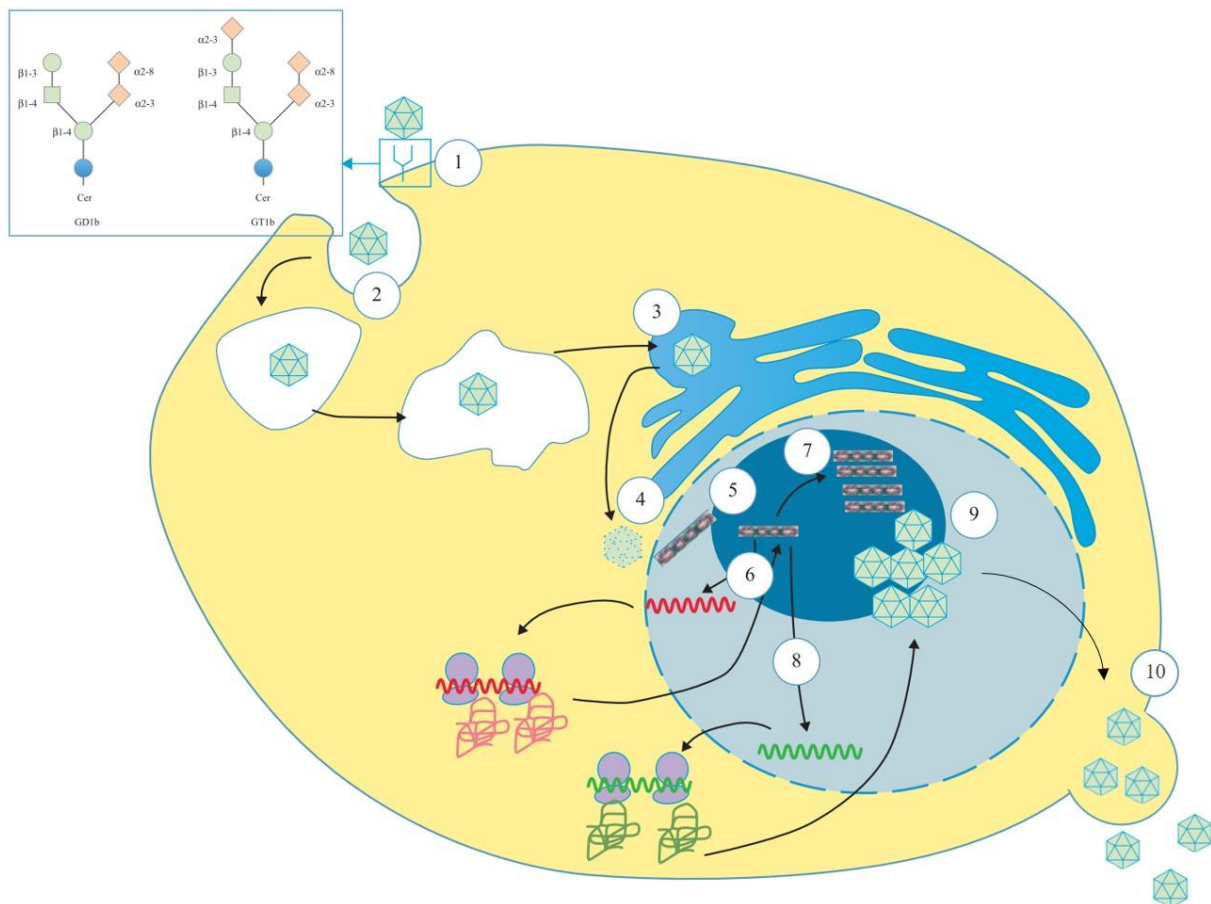
Figure 5: BKV life cycle
The viral life cycle of BKV can be divided into ten different steps: 1. Viral attachment through VP1 to host cell receptors, 2. Internalization by endocytose, 3. Intracellular trafficking to the ER, 4. Virus uncoating and retrograde transport from ER to cytoplasm, 5. Nuclear entry of virus genomes, 6. Transcription of early viral genes, 7. Viral DNA replication, 8. Transcription of late viral genes, 9. Virion assembly around newly synthesized copies of viral genome, 10. Viral egress. Modified from Mazalrey et al. [93].

1.10 Experimental models to study BKV infection

To understand the viral life cycle of BKV, *in vitro* and *in vivo* models are indispensable. By using recombinant proteins, virus-like particles (VLPs), pseudovirions (PsVs) and cell culture-derived infectious virus, the life cycle of BKV can be conflated. Furthermore, with these tools the prevalence of virus specific antibodies can be examined and inhibitors targeting aspects of viral life cycle can be identified. In addition, for assessment of pathological mechanisms underlying BKV associated diseases in transplant patients and for preclinical trials of antiviral drugs, animal models are inevitable and powerful [117].

1.10.1 Different types of BKV

Models for the propagation of human PyVs in cell culture systems have been described for MCPyV [129], JCV [130] and BKV [131]. Productive propagation of archetype and rearranged variants of BKV can be conducted in HEK293TT cells [132]. However, to study certain aspects of viral life cycle and

especially the interaction between BKV and host cells, cell culture-derived infectious BKV together with its physiologically relevant primary cell culture models are used. Since cultivation of archetype BKV is only feasible in HEK293TT cells, only the rearranged BKV variants are currently used to study BKV infection in biological relevant host cells, with the Dunlop strain presenting the common laboratory used BKV type [92]. Additionally, due to the lack of fluorescent labelled recombinant BKV, the implementation of BKV models in routine drug screenings is restricted. Hitherto, antiviral screens with cell culture-derived infectious BKV depend on detection of BKV infection either by immunofluorescence staining or real-time quantitative PCR, presenting labor intensive and time consuming methods [117].

PsVs and VLPs consist of self-assembled capsid proteins without viral DNA. They are produced by transfecting the embryonic-derived cell line HEK293TT, which stably expresses SV40 LT-Ag, with expression vectors encoding BKV capsid proteins VP1, 2 and 3 [117]. PsVs and VLPs present a valuable instrument to investigate early steps of viral life cycle, such as viral attachment and entry. Although they enable the investigation of virus interactions with cell surface receptors, they are not suitable to detect cellular factors that are important for virus replication and assembly in host cells [133].

1.10.2 Cell types for *in vitro* assays

Generally, PyVs are characterized by a narrow host tropism for both the species and cell type, which efficiently supports their replication [134]. While BKV replicates, especially under pathological conditions, in the urinary system, the site of persistence remains unknown. However, several studies suggest a wide spectrum of BKV permissive tissues and cell types [87]. Rearranged BKV was shown to replicate *in vitro* in a wide range of different cell types such as monkey kidney cell lines like CV-1 and Vero, human ovarian, brain and melanoma cancer cell lines, human salivary gland cells [117], primary human endothelial, epithelial cells and fibroblasts [87].

Although, HEK293TT cells, which constitutively express SV40 LT-Ag, support propagation of archetype as well as rearranged variants of BKV [109], these cells are not suitable to study various processes of BKV viral life cycle in the natural host cell type [117]. For instance, bladder and renal tubular epithelial cells present the major sites for BKV replication in BKV associated diseases. Hence, primary human RPTEC present a valuable and state-of-the-art *in vitro* model to apprehend BKV infection [29, 135]. Primary human RPTEC sustain productive infection of BKV and many aspects of viral life cycle have been addressed using this system. Furthermore, following infection BKV induces the release of progeny virions resulting in loss of cell monolayer viability with corresponding cytopathic effect (CPE) [87]. However, in RPTEC no evocation of efficient immune response against BKV infection was observed, and transcriptome profiling studies revealed a lack of proinflammatory responses upon BKV infection

[136–138]. Additionally, RPTEC exhibit replicative senescence, which limits their proliferative potential and experimental design [117].

1.10.3 Animal models

Animal models recapitulating the life cycle of human PyV are essential to investigate toxicity and pharmacokinetics of antiviral drugs and to understand infection with PyVs *in vivo*. However, the development of such *in vivo* models is impeded due to the narrow host and cell specificity of PyVs. Hitherto, available animal models for BKV infection comprise MuPyV infection in mice and Syrian golden hamsters or rhesus macaque infected with SV40 [117].

Similar to BKV, MuPyV infection in outbred mice causes an acute inapparent infection with virus spreading observed in numerous organs, including brain and kidney [139]. Additionally, MuPyV consolidate an asymptomatically lifelong persistent infection in natural populations of mice [140]. MuPyV can be reactivated upon corticosteroid treatment or pregnancy and viral loads can be detected in the urine of infected mice [141].

As mentioned before, the PyV SV40, whose natural host is the rhesus macaque (*Macaca mulatta*), is closely related to BKV and shares more than 80% sequence homology [142]. Due to the high sequence homology of these viruses and their similar pathology in natural hosts, SV40 infection in rhesus macaque serves as a potential *in vivo* model. However, Syrian golden hamsters (*Mesocricetus auratus*) are the commonly used small animal model to study SV40 infection *in vivo*, as they share comparable infectious mechanisms and pathogenicity [143].

2. Aim of the study

Despite the highly prevalence of human PyV infections in the healthy population, solely four of the 13 hitherto known human PyVs, namely MCPyV, TSPyV, JCV and BKV, are associated to cause severe diseases under immunosuppression [9]. While TSPyV and MCPyV can cause rare skin diseases, JCV and BKV reactivation provoke major clinical complications in transplant patients receiving immunosuppressive agents [4]. In particular, uncontrolled BKV replication causes two major diseases, PVAN in 1 – 10% of renal transplant patients and HC after BMT in 5 – 15% of allogenic hematopoietic stem cell transplant patients [144]. Although BKV was discovered decades ago, no specific antiviral drugs are identified that can restrict BKV replication efficiently *in vivo.* Hitherto, the main treatment option of BKV associates diseases is reduction of immunosuppression at the expense of increased risk of graft rejection [32]. Thus, the clinical demand for novel antiviral agents is rising.

The aim of this study was to identify and subsequently characterize novel small molecule inhibitors that are active against human PyV infections with the focus on BKV infection. At first, a cell-based reporter screen suitable for a high throughput screen (HTS) was to be established. The development of such an HTS bears substantial challenges due to restricted *in vitro* culture systems and the small genome size of PyVs. Next, to identify novel inhibitors active against infection with the PyV class including BKV, JCV and SV40, a cell-based HTS of a library consisting of approximately 28,000 small molecule compounds was to be performed. Additionally, inhibitors identified for their activity against BKV infection were to be tested for possible broad range activity against JCV and MuPyV. While an *in vitro* and *in vivo* replication system for MuPyV is already established, the *in vitro* replication system for JCV was to be established in this study. Furthermore, the inhibitory concentration 50% (IC50) and cytotoxicity concentration 50% (CC50) of selected hit compounds were to be determined concerning BKV infection in primary human RPTEC. Moreover, the inhibitory activity against BKV infection of the most promising compound was to be investigated in more detail by pinpointing the different steps during viral life cycle in order to narrow down the target. Therefore, different assays were to be established to enable characterization of the individual steps of the viral life cycle independently from virus infection, such as viral entry and viral DNA genome replication. Finally, the identification of highly promising compounds for the clinical development of a pre-lead structure was to be expected.

3. Material and Methods

3.1 Material

3.1.1 Software

For data analysis, evaluation and visualization the tools listed in Table 1 were used.

Table 1: Software

Name	Manufacturer
Adobe Illustrator CS6	Adobe Systems Inc.
Adobe Photoshop CS6	Adobe Systems Inc.
Avogadro	open source molecular editor
BioAnalyze 2.67.06	Biometra
CLC Main Workbench 7.9.1	Qiagen
FACSDiva™ 8.0.1	BD Biosciences
Fiji	open source platform for biological-image analysis
FlowJo	LLC
Gen5 Image+ 2.09	BioTek
Magellan™	Tecan
Micro-Manager 1.4	open source microscopy software
NIS-Elements AR 4.5.1.01	Nikon
Prism 5.03	GraphPad
RStudio	open source software for R
Rotor Gene Q Series Software 2.0.2	Qiagen
StepOnePlus™ 2.2.2	Applied Biosystems

3.1.2 Instruments and equipment

The Instruments and equipment from following manufacturers were used: Andor, Amersham, BD Biosciences, Biometra, Bio-Rad Laboratories, BioTek, Eppendorf, Eurofins, GE Inspection Technologies, Fujifilm, Hartenstein, Heraeus, Ibidi, Kodak, Leica, Mettler Toledo, Nikon, Okolab, Roche, Tecan, Thermo Fischer Scientific, Qiagen.

3.1.3 Chemicals and consumables

All chemicals were purchased from Merck and Carl Roth. The library comprising approximately 28,000 small molecule compounds was kindly provided by Thomas Schulz from the Institute of Virology at the Medical School Hannover, Germany. Reordered compounds were purchased from Enamine, ChemDiv or MolPort.

All consumables were purchased from Abcam, Addgene, Agilent Technologies, Ambion, Applied Biosystems, Beckman Coulter, Biochrom, BD Biosciences, Bioline, Bio Rad, Carl Roth, Corning Life Sciences, Eppendorf, GE Healthcare, Greiner Bio One, Hartenstein A., Heraeus, Lonza, LTF Labortechnik GmbH, Lucigen, Macherey-Nagel, Merck, New England Biolabs (NEB), PeqLab, Polysciences Inc., Promega, PromoCell, Qiagen, Quanta Bio, Roche, Santa Cruz, Sarstedt, Stemcell, Thermo Fischer Scientific, VWR, Vectorlabs, Whatman and Zymo Research.

3.1.4 Commercial systems

The commercial systems used in this study are summarized in Table 2.

Table 2: Commercial systems

Name	Manufacturer
Alexa Fluor 488 Protein Labeling Kit	Thermo Fischer Scientific
CellTiter-Glo® Luminescent Cell Viability Assay	Promega
DNA Clean & Concentrator™	Zymo Research
DNA-free™ Kit	Thermo Fischer Scientific
Lipofectamine™ 2000 Transfection Reagent	Thermo Fischer Scientific
LookOut® Mycoplasma PCR Detection Kit	Merck
MagNA Pure 96 DNA and Viral Nucleic Acid Small Volume Kit	Roche
NucleoSpin® Tissue XS Kit	Macherey-Nagel
peqGOLD Plasmid Miniprep Kit	peqLab
TC-FlAsH™ II In-Cell Tetracysteine Tag Detection Kit	Thermo Fischer Scientific
TransfeX™ Transfection Reagent (ACS-4005™)	LGC Standards GmbH
QIAamp 96 DNA QIAcube HT Kit	Qiagen
QIAamp DNA Mini Kit	Qiagen
QIAcube HT Plasticware	Qiagen
QIAGEN Plasmid Midi and Maxi Kit	Qiagen
QuantiFast Pathogen +IC Kit	Qiagen
Qubit™ Protein Assay Kit	Thermo Fischer Scientific
PerfeCTa SYBR® Green FastMix	Quanta Bio
RNA Bee	Ambion
Roti®-Quant Bradford assay	Carl Roth
Rotor-Gene Multiplex PCR Kit	Qiagen
SensiMix™ SYBR® Hi-ROX Kit	Bioline
SuperScript™ III Reverse Transcriptase	Thermo Fischer Scientific
Zymoclean™ Gel DNA Recovery Kit	Zymo Research
ZR Viral DNA/RNA Kit	Zymo Research

3.1.5 Plasmids

The plasmids, which were used or generated in this study, are listed in Table 3.

Table 3: Plasmids

Plasmid name	Backbone	Insert
pSV40	psV	SV40 (proviral clone)
pBKV_dun	pBR322	BKV Dunlop strain
pBKV_gard	pCR2.1	BKV Gardner strain
pJCV_Mad1	pBR322	JCV Mad-1 strain
pBluescript-sk+PTA	pBluescript-sk	MuPyV
pUC18	pUC18	no insert
pCDNA-miRB1	pCDNA3.1	BKV miRB1
pmCherry	pmCherry-N1(+)	mCherry
pWB2b	pGwf	BKV VP1, VP2
pWB3b	pGwf	BKV VP1, VP3
pVP1_TC	pBR322	BKV Dunlop strain, TC tag
pTC_VP2	pBR322	BKV Dunlop strain, TC tag
pTC_LT	pBR322	BKV Dunlop strain, TC tag
Lenti gag-pol	phCMV	gag-pol
Lenti rev	phCMV	rev
VSV env	phCMV	VSV env
lentiCas9-Blast	pFUGW	EFS-promoter
LeGO-RFP_modified	LeGO	Neomycin, RFP
LeGO-GFP_modified	LeGO	Neomycin, eGFP
LeGO-iC2	LeGO	IRES-mCherry
LeGO-iC2-miRB1	LeGO-iC2	BKV miRB1
LeGO-EFS-RFP	LeGO-RFP_modified	EFS-promoter
LeGO-miRNA-GFP	LeGO-GFP_modified	16 BKV miRNA target sites

3.1.6 Oligonucleotides

Oligonucleotides used in this study were purchased purified and salt free from Eurofins Genomics. Probes for Taqman qPCR were purified with HPLC. The sequences of primers and probes are summarized in the Tables 4 – 11.

Table 4: Primers used for cloning pCDNA-miRB1

Name	Sequence 5`-3`
miRB1_F	AATAAGGATCCTATTTTGGGGGTGGTGTT
miRB1_R	GGGGCGAATTCGATTCTGAGATAAGTATGTA
miRB1_col_F	GTGGTGTTTTAGGCCTTTTAAAACAC
vector_col_R	GACAATGCGATGCAATTTCCTCA

Table 5: Primers used for cloning recombinant BKV with TC tag

Name	Sequence 5`-3`	Application
Vec_overhang_VP1_R	TGTTGCCCCGGGTGCTGTTAAACAGGTGCTTTTATTGTACATATAC	VP1::TC
Vec_VP1_F	AAGCATTTTGGTTTGCAA	VP1::TC
Col_VP1_R	ATGCTTTGTTGCCCCGGG	Colony VP1::TC
Col_Seq_VP1_F	CCAATCACAATGCTCTTCCC	Colony VP1::TC
Col_Seq_LT-Ag_F	ATGTCTGTCATGCACTTTCC	Colony TC::LT-Ag
Col_Seq_LT-Ag_R	CTTTATCACAGCACCCGG	Colony TC::LT-Ag
Vec_overhang_LT_R	CACAGCACCCGGGGCAACACATTTTTGCAAAAATTGC	TC::LT-Ag
Vec_LT_F	GATAAAGTTCTTAACAGGGAAG	TC::LT-Ag
Vec_VP2_F	ACAGCACCCGGGGCAACACATGAACCTGGAAATACAAAAAAAAAG	TC::VP2
Vec_VP2_R	GGTGCTGCTCTAGCACTTTTG	TC::VP2

Table 6: Primers used for cloning LeGO-miRNA-GFP

Name	Sequence 5`-3`
BK_miRNA_Eco_fw	TTAGAATTCGAACCATGCTCTTCCCAAGTCTCAGATGAACGGATGGCACCGAACCATGCTCTT CCCAAGTCTCAGATGAACGGATGGCACCGTGCaCATCCGTAGCAGAGAGGAGACCAC
BK_miRNA_Eco_rev	ATAGAATTCCTCGAGGGTGCCATCCGTTCATCTGAGACTTGGGAAGAGCATGGTTCATTGGG TGCTTGATCCATGTCCAGAGTCTTGGTGGTCTCCTCTCTGCTACGGATGt
Legotre_1_fw	CGGCATGGACGAGCTGA
Legotre_1_rev	CGCTGCCCATCTTGTTCAGCTCGTCCATGCCG
Legotre_2_F	CACTGGGACTGCCCTGTACACCTTGGATCGATC
Legotre_2_R	GATCGATCCAAGGTGTACAGGGCAGTCCCAGTG
Lenticas_1_fw	GCTAGCTAGGTCTTGTACAAGGAGTGGGAATTG
Lenticas_1_rev	CAATTCCCACTCCTTGTACAAGACCTAGCTAGC
Lenticas_2_fw	GAACACAGGACCGGTTGTACAGCGCTGCCACCATGG
Lenticas_2_rev	CCATGGTGGCAGCGCTGTACAACCGGTCCTGTGTTC
ColonyCas9_fw	GAATTGGCTCCGGTGCCCGTC
mi_target_F	GACAAGGTACCCACGCTCTAGACA
mi_target_R	CGGTGACTAGTGTTCATCTGAGACTTGG

Table 7: Primers used for cloning LeGO-iC2-miRB1

Name	Sequence 5`-3`
miRB1_F	AAATTAGCGGCCGCTATTTTGGGGGTGGT
miRB1_R	AGCCCGGGGAATTCGATTCTGAGATAAGTATG
colony_F	CAATCAGCCTGCTTCTCGCTT
colony_R	CAAGAGAAGAGGATTCAGAAACTGAAG

Table 8: Primers used for cloning pBKV_gard

Name	Sequence 5`-3`
BKV_gardner_fw	CAATTCTGCAGGCGGTATCAGCTCACTCAAAG
BKV_gardner_rev	CACTACTGCAGCACTTTTCGGGGAAATGTG

Table 9: Primers used for cloning LeGO-EFS-RFP

Name	Sequence 5`-3`
Legotre_1_F	CGGCATGGACGAGCTGAACAAGATGGGCAGCG
Legotre_1_R	CGCTGCCCATCTTGTTCAGCTCGTCCATGCCG
Legotre_2_R	CACTGGGACTGCCCTGTACACCTTGGATCGATC
Legotre_2_R	GATCGATCCAAGGTGTACAGGGCAGTCCCAGTG
Lenticas_1_F	GCTAGCTAGGTCTTGTACAAGGAGTGGGAATTG
Lenticas_1_R	CAATTCCCACTCCTTGTACAAGACCTAGCTAGC
Lenticas_2_F	GAACACAGGACCGGTTGTACAGCGCTGCCACCATGG
Lenticas_2_R	CCATGGTGGCAGCGCTGTACAACCGGTCCTGTGTTC
ColonyCas9_F	GAATTGGCTCCGGTGCCCGTC
ColTre2_R	CTTCACGGTGTTGTGGCCCTC

Table 10: Primers used for Sanger sequencing

Name	Sequence 5`-3`	Application
iC2_seq_F	CAGTCCTCCGATTGACTGAG	LeGO-iC2-miRB1
iC2_seq_R	CTAGGAATGCTCGTCAAGAAGAC	LeGO-iC2-miRB1
SeqCas9	GAAGGTGGAGAGAGAGACAG	LeGO-EFS-RFP
SeqTre1	CAACAGCCACAACGTCTATATC	LeGO-EFS-RFP
SeqTre2	CTTCACGGTGTTGTGGCCCTC	LeGO-EFS-RFP
TetKrab_Seq	CCTTCAAGGATGTATTTGTGGAC	LeGO-miRNA-GFP
Seq2_Gardner_F	CTTTCACCAGCGTTTCTGGGTGAGC	BKV Gardner strain
Seq2_Gardner_R	CTTGAAAGAGCTGCCTGGGGAAATC	BKV Gardner strain
BKV_NCCR_F	AGCAGCAGCCTCAGATACAC	NCCR BKV
BKV_NCCR_R	GATTTCCCCAGGCAGCTCTT	NCCR BKV
Col_Seq_LT-Ag_F	ATGTCTGTCATGCACTTTCC	TC::LT-Ag
Col_Seq_VP1_F	CCAATCACAATGCTCTTCCC	VP1::TC
Seq_n-term_VP2	CCAGGAGCACCAGCAATTAC	TC::VP2
SeqCas9	GAAGGTGGAGAGAGAGACAG	LeGO-miRNA-GFP
SeqTre1	CAACAGCCACAACGTCTATATC	LeGO-miRNA-GFP
SeqTre2	CTTCACGGTGTTGTGGCCCTC	LeGO-miRNA-GFP
SeqTre_fw	CAGATACCAGGATATCGCCCTGGC	LeGO-miRNA-GFP
Seq_EFS	AACATCATGGTGGAGAACGG	LeGO-miRNA-GFP
Seq_long_R	GACATCACTTTCCCAGTTTAC	LeGO-miRNA-GFP

Table 11: Primers used for qPCR and RT-PCR

Name	Sequence	Application
Taqman_GAPDH_F	TGTGTCCCTCAATATGGTCCTGTC	qPCR genome copies
Taqman_GAPDH_R	ATGGTGGTGAAGACGCCAGTG	qPCR genome copies
Taqman_probe_GAPDH	HEX-GTGGCGCTGAGTACGTCGTGGAGTC-BHQ1	qPCR genome copies
Taqman_BK-VP1_F	TGATAGCCCAGAGAGAAAAATGC	qPCR genome copies
Taqman_BK-VP1_R	TCCACAGGTTAGGTCCTCATTTAAA	qPCR genome copies

25

Name	Sequence	Application
Taqman_probe_BKV	Fam-TTACAGCACAGCAAGAATTCCCCT-BHQ1	qPCR genome copies
Taqman_SV40-LT_F	GGGTCTTCTACCTTTCTCTTCTTT	qPCR genome copies
Taqman_SV40-LT_R	GCAGTGGTGGAATGCCTTT	qPCR genome copies
Taqman_probe_SV40	Fam-ACCTGTTTTGCTCAGAAGAAATGCCA-BHQ1	qPCR genome copies
Taqman_JCV-LT_F	TTAGTGGTATACACAGCAAAAGAAG CA	qPCR genome copies
Taqman_JCV-LT_F	AAAACACAGGATCCCAACACTC TAC	qPCR genome copies
Taqman_probe_JCV	FAM-TC CTGTAGATCTGCATGCA-BHQ1	qPCR genome copies
SYBR_LT_F	AGTAGCTCAGAGGTGCCAA	qPCR transcripts
SYBR_LT_R	AGTGTTGAGAATCTGCTGTTGC	qPCR transcripts
SYBR_VP1_F	GCTGTAGGTGGAGAACCCTT	qPCR transcripts
SYBR_VP1_R	GATCAGGTACCCAGCACTCA	qPCR transcripts
SYBR_GAPDH_F	GGTCGGAGTCAACGGATTTG	qPCR transcripts / miRNA
SYBR_GAPDH_R	ATGGTGGTGAAGACGCCAGT	qPCR transcripts / miRNA, stem-loop cDNA-synthesis
Universal_R	GTGCAGGGTCCGAGGT	qPCR BKV-miR-B1
BK_miR_5p_fw	GCCTCGATCTGAGACTTGGGAA	qPCR BKV-miR-B1
BKV-miR-B1_5p_SL	GTCGTATCCAGTGCAGGGTCCGAGGTATTCGC ACTGGATACGACATGCTC	stem-loop cDNA-synthesis
Mice_GAPDH_gDNA_F	GCCTGTAGGAAAAGGGAAGTTTA	qPCR genome copies
Mice_GAPDH_gDNA_R	ACCAAGCACACATACTGAGGTTT	qPCR genome copies
PTA _F	GATGAGCTGGGGTACTTGT	qPCR genome copies
PTA _R	TGTATCCAGAAA GCGACCAAG	qPCR genome copies

3.1.7 Antibodies

The antibodies applied in Western Blot technique (WB), Immunofluorescence analysis (IF) or life cell imaging are listed in Table 12 and 13.

Table 12: Primary antibodies

Name	Application	Description	Dilution	Manufacturer and Catalog #
PAB416	WB, IF	Mouse monoclonal to T-Ag	1:50	Abcam, ab16879
SV40-VP1	WB, IF	Rabbit polyclonal	1:5000	Abcam, ab53977
α-Tubulin	WB	Rabbit polyclonal	1:1000	Abcam, ab4074
I58	IF	rabbit polyclonal anti MuPyV VP1	1:5000	kindly provided by Chris Sullivan, UT Austin

Table 13: Secondary antibodies

Name	Application	Dilution	Manufacturer
α-mouse HRP	WB	1:5000	Santa Cruz
α-rabbit HRP	WB	1:5000	Santa Cruz
Alexa Fluor 488	IF	1:1000	Thermo Fischer Scientific

Name	Application	Dilution	Manufacturer
Alexa Fluor 555	IF	1:1000	Thermo Fischer Scientific
Alexa Fluor 647	IF	1:1000	Thermo Fischer Scientific
WGA, Alexa Fluor™ 488 Conjugate	Life cell imaging	1:1000	Thermo Fischer Scientific

3.2. DNA techniques

3.2.1 Bacteria

For amplification of plasmid DNA *Escherichia coli* (*E. coli*) DH5α cells were used.

Table 14: Bacterial strain

Name	Genotype	Manufacturer
Escherichia coli DH5α	F– Φ80*lac*ZΔM15 Δ(*lac*ZYA-*arg*F) U169 *rec*A1 *end*A1 *hsd*R17 (rK–, mK+) *pho*A *sup*E44 λ– *thi*-1 *gyr*A96 *rel*A1	Thermo Fischer Scientific

3.2.1.1 Culture of *E. coli*

Bacteria were cultured at 37 °C in liquid culture containing Lysogeny Broth (LB) medium under constant shaking at 220 rpm in a shaking incubator or on LB agar plates. For lentiviral plasmids bacteria were cultured at 30 °C. LB medium was sterilized by autoclaving and supplemented with 1 µg/mL ampicillin.

3.2.1.2 Glycerol stocks

For long-term storage, bacterial glycerol stocks were created. Single colonies were picked from agar plates and grown overnight in liquid culture. After bacterial growth, 0.5 mL of the overnight culture were added to 0.5 mL of 50% sterile glycerol, mixed and stored at – 80 °C.

3.2.1.3 Generation of chemically competent *E. coli*

Chemically competent *E. coli* cells were generated using the rubidium-chloride-method. Bacteria were inoculated in LB medium and grown over night at 37 °C under constant agitation. The overnight culture was diluted 1:100 in LB+ medium (Table 15) and continuously grown until an optical density $(OD)_{600}$ of 0.3 – 0.5 was reached. Subsequently, cells were chilled for 15 min on ice and pelleted by centrifugation (300 g, 4 °C, 5 min). While the supernatant was discarded, the cell pellet was resuspended in 150 mL ice cold TFP1 buffer (Table 16) and incubated for 90 min on ice. After renewed centrifugation the TFB1 buffer was removed, cells were resuspended in 25 mL ice cold TFB2 buffer (Table 17) and immediately aliquots of 200 µL were frozen in liquid nitrogen and stored at – 80 °C.

Table 15: LB+ medium

Components	Concentration
LB medium	500 mL
Magnesium sulfate	8 mM
Potassium chloride	10 mM

Table 16: TFB1 buffer

Components	Concentration
Rubidium chloride	100 mM
Potassium acetate	30 mM
Calcium chloride	10 mM
Mangan (II) chloride	50 mM
Glycerol	15% (v/v)
Acetic Acid	to pH 5.8

Table 17: TFB2 buffer

Components	Concentration
Rubidium chloride	10 mM
MOPS	10 mM
Calcium chloride	75 mM
Glycerol	15% (v/v)

3.2.1.4 Transformation of chemically competent *E. coli*

Chemically competent *E. coli* cells were slowly thawed on ice. 100 µL competent cells were added to 0.1 - 1 µg plasmid DNA or 20 µL ligated DNA, gently mixed by flicking the tube and incubated for 5 min on ice. Subsequently, a heat shock was performed in a water bath at 42 °C for 30 sec and cells were immediately incubated on ice for further 5 min. 800 µL of LB medium were added and cells were incubated for 60 min at 37 °C under constantly shaking. Afterwards, cells were pelleted by centrifugation (4000 g, 4 min, RT) and resuspended in 100 µL LB medium.

For screening of different clones after transformation with ligated DNA, bacteria were plated onto LB agar plates supplemented with antibiotics and incubated over night at 37 °C. For amplification of a single plasmid, cells were diluted in 60 mL LB medium supplemented with antibiotics and cultured over night at 37 °C in a shaking incubator.

3.2.1.5 Preparation of plasmid DNA from *E. coli*

Transformed *E. coli* were grown for at least 6 h under selective conditions prior to extraction of plasmid DNA. Small amounts of plasmid DNA were isolated from 3 mL bacterial cultures using the peqGOLD Plasmid Miniprep Kit (Peqlab) as described by the manufacturer. However, larger amounts of plasmid

DNA were isolated from 50 mL bacterial cultures with the Qiagen Plasmid Midi Kit according to the manufacturer's instruction.

3.2.2 Determination of DNA concentration and purity

Concentration of DNA samples was measured with a spectrophotometer (Nanodrop-1000, Thermo Scientific) at a wavelength of 260 nm. The purity of DNA samples was determined by calculating the ratios of 260/280 nm and 260/230 nm with ratios between 1.8 and 2.0 indicating pure DNA without contaminations through proteins or organic compounds.

3.2.3 Enzymatic digestion of DNA

Sequence specific digestion of DNA was achieved with Fast Digest endonucleases (NEB) according to the manufacturer`s instructions. To prevent self-ligation vector plasmids were dephosphorylated with 1 U of Calf Intestine Phosphatase (CIP, NEB).

3.2.4 Ligation of DNA fragments

DNA fragments were ligated into linearized plasmids using T4 DNA Ligase (Thermo Fischer Scientific). The composition of a ligation reaction is shown in Table 18. Reactions were incubated for 40 min at 22 °C or overnight at 16 °C.

Table 18: Ligase reaction mixture

Component	Amount
Linear vector DNA	10 - 100 ng
Insert DNA	3:1 molar ratio over vector
10x T4 DNA Ligase buffer	2 µL
T4 DNA Ligase	0.2 µL
DEPC treated water	to 20 µL

3.2.5 KLD reaction

To combine efficient phosphorylation, ligation and template removal in one single step, a KLD (kinase, ligase, DpnI) reaction was performed. The mixture of the reaction components is specified in Table 19 and the recipe for the KLD buffer is described in Table 20. KLD reaction mix was incubated for 30 min at RT.

Table 19: KLD reaction mixture

Component	Amount
2x KLD buffer	5 µL
Unpurified PCR product	4.1 µL
Fast Digest DpnI	0.3 µL
T4 PNK	0.3 µL
T4 DNA Ligase	0.3 µL

Table 20: KLD buffer

Component	Amount
10x Fast Digest Buffer (NEB)	80 µL
24% PEG 6000 (Sigma)	167 µL
1 M DTT	8 µL
10 mM ATP	80 µL
DEPC treated water	65 µL

3.2.6 Purification of DNA

To purify DNA after enzymatic reaction or PCR products from substances like salts, primers and enzymes that might interfere with subsequent reactions, the Clean and Concentrator Kit (Zymo Research) was used according to the manufacturer`s instructions.

To isolate DNA fragments from Ethidium Bromide containing agarose gels, DNA bounds were visualized under UV light and excised with a scalpel. DNA was extracted using the Gel DNA recovery kit (Zymo Research) as described by the supplier.

3.2.7 Agarose gel electrophoresis

Gel electrophoresis with agarose as a matrix was used to separate DNA fragments according to their size in an electric field. Different agarose concentrations were used dependent on the size of DNA fragments (Table 21).

Table 21: Agarose concentration depending on size of DNA fragments

Agarose concentration	Size of DNA fragment
0.8%	> 5 kb
1.0%	1 kb - 5 kb
1.2% - 2%	0.1 kb - 1 kb

To prepare gels the desired amount of agarose was dissolved in 50 - 150 mL 1x TAE buffer (Table 22) by boiling. Thereafter, 10 mg/mL Ethidium Bromide were added, and the gel was poured into a gel tray with a comb of appropriate size depending on the sample volume. After completed polymerization the gel was transferred to an electrophoresis chamber containing 1x TAE buffer.

Table 22: 10x TAE buffer

Component	Amount
Tris acetate	400 mM
EDTA	20 mM
Acetic acid	Adjust to pH 8.5

DNA samples were mixed with 6x DNA loading dye (Thermo Fischer Scientific) and loaded into the pockets of the gel. To determine the size of DNA fragments a DNA ladder was used (Quick-Load Purple DNA Ladder, NEB). The gel was run at 5-10 V/cm until the desired separation of DNA fragments was accomplished. Since Ethidium Bromide intercalates with DNA, DNA bands were visualized under UV light. To prevent DNA damages, preparative gels were visualized on a UV-transilluminator with longer wave length (365 nm) and specific DNA bands were excised with a scalpel for isolation of the DNA. Analytical gels were documented using the BioDoc Analyze (Biometra) with the corresponding software.

3.2.8 Sanger sequencing

Sequence analysis of PCR products and plasmids was conducted by Eurofins Genomics. Sequencing results were analyzed with CLC Main Workbench (Qiagen).

3.2.9 Isolation of genomic DNA

For manual isolation of genomic DNA (gDNA) from 10^4 - 10^6 cells, cells were harvested and washed once with DPBS. Pelleted cells were used for isolation of gDNA with the NucleoSpin® Tissue XS (Macherey-Nagel) according to the manufacturer`s instructions.

To determine viral titer, viral supernatant was first filtered through 0.22 μm syringe filter units (Merck) to gain a cell free supernatant. Then, gDNA was isolated manually from 0.5 mL filtered supernatant using ZR viral DNA/RNA Kit (Zymo Research) as described by the supplier.

In secondary screening with BKV (see chapter 3.5.17.3), gDNA from cells or supernatant was isolated as described in the following. 150 μL viral supernatant was filtered via 96-Well Filter Plates (Merck) by centrifugation (3000 g, 3 min, RT) to obtain a cell free supernatant. Cells were harvested, washed once with DPBS and resuspended in 100 μL DPBS supplemented with 0.5% FBS. In 96-Deep Well Plates (VWR) 189 μL of DPBS supplemented with 0.5% FBS were mixed with 21 μL of either resuspended cells or filtered supernatant to maintain 210 μL end volume prior to automated gDNA isolation. An automated high throughput isolation of gDNA from cells and viral supernatant was performed on the MagNA Pure 96 Symphony Instrument (Roche) using the MagNA Pure 96 DNA and Viral Nucleic Acid Small Volume Kit (Roche). The Internal Control RNA from the QuantiFast Pathogen +IC Kit (Qiagen) was added to the extraction procedure as an internal control for subsequent qPCR analysis.

To characterize the inhibitory effect of a small amount of small molecule compounds against BKV or JCV, cells were first harvested, washed once with DPBS and resuspended in 100 μL DPBS supplemented with 0.5% FBS. 150 μL viral supernatant was filtered via 96-Well Filter Plates (Merck) by centrifugation (3000 g, 3 min, RT) to obtain a cell free supernatant. 100 μL supernatant and 100 μL resuspended cells were added to 100 μL DPBS to maintain 200 μL end volume. For automated high throughput isolation, gDNA was extracted by the QiaCube (Qiagen) using QIAamp 96 DNA QIAcube HT Kit (Qiagen).

To determine the inhibitory effect of a small amount of small molecule compounds against MuPyV, cells were harvested, washed once with PBS and resuspended in 210 μL DPBS. Cell free viral supernatant was sustained by centrifugation. With the QiaAmp DNA Mini Kit (Qiagen) gDNA from both cell suspension and cell free supernatant was extracted according to the manufacturer´s instructions.

3.2.10 Polymerase chain reaction (PCR)

Mullis et al. [145] originally described the polymerase chain reaction (PCR) as an *in vitro* technique for amplification of specific DNA sequences. PCR typically consists of a cycling progression of three individual steps: Denaturation of ds DNA, annealing of specific primers to the target DNA region and elongation of the complementary strand by polymerases, resulting in multiple copies of a specific DNA region. Amplification of short DNA fragments and analytical screening of bacterial colonies was performed with a Taq polymerase (DreamTaq DNA polymerase, Thermo Fischer Scientific). However, to reduce the error rate amplicons for cloning, specific mutagenesis and sequencing, a proofreading polymerase (PfuUltra II HS DNA polymerase, Agilent) was used. Amplification of DNA was carried out in a thermocycler (Eppendorf).

3.2.10.1 Site directed mutagenesis

To establish the lentiviral constructs LeGO-EFS-RFP, which was used for the primary an HTS, and LeGO-miRNA-GFP, which was applied for miRNA-based reporter screen, the generation of point mutations by site directed mutagenesis was required. For site directed mutagenesis the primer design is a critical step. Primers should have a length of 25 – 45 bp with the mutated sequence located in the middle. The melting temperature should be above 78 °C. To estimate the melting temperature the following formula adapted from Agilent was used:

$$T_m = 81.5 + 0.41 \times (\%GC) - (675 \div \text{primer lenght}) - \%\text{mismatch}$$

The mixture of site directed mutagenesis PCR reaction is shown in Table 23 and cycling program is described in Table 24.

Table 23: Site directed mutagenesis PCR components

Components	Amount
10x PCR buffer	4 µL
dNTPS (10 mM)	1 µL
Primer forward (10 µM)	1 µL
Primer reverse (10 µM)	1 µL
Template DNA	50 ng
PfuUltra II HS DNA polymerase	1 µL
DEPC treated water	Add 40 µL

Table 24: Site directed mutagenesis PCR program

Cycles	Temperature [°C]	Time
1	95	5 min
18	95	50 sec
	60	50 sec
	68	9 min
1	68	9 min
1	4	hold

Success of PCR was confirmed by agarose gel electrophoresis. To eliminate the non-mutated template DNA, which is methylated due to amplification in *E. coli*, 1 µL of restriction enzyme DpnI (10 U/µL, NEB) was added to the PCR product and incubated for 1 h at 37 °C. PCR products were purified and transformed in *E. coli*. To confirm successful mutation several bacterial colonies were screened with colony PCR and analyzed by Sanger sequencing.

3.2.10.2 Colony PCR

To verify correct insertion of DNA fragments into a vector or to revise integrated point mutations, bacterial colonies were analyzed by performing a colony PCR. Single colonies were picked from a LB agar plate, resuspended in 10 µL DEPC treated water and were used as template for PCR with the reaction mixture described in Table 25 and the cycling program shown in Table 26. Amplified DNA was analyzed by agarose gel electrophoresis.

Table 25: Colony PCR components

Components	Amount
10x PCR buffer	2.5 µL
dNTPS (10 mM)	0.2 µL
Primer forward (10 µM)	1 µL
Primer reverse (10 µM)	1 µL
Template resuspended colony	1 µL

Components	Amount
DreamTaq DNA polymerase	0.1 µL
DEPC treated water	Add 25 µL

Table 26: Colony PCR program

Cycles	Temperature [°C]	Time
1	95	5 min
30	95	30 sec
	T_m-5	30 sec
	72	60 sec
1	72	3 min
1	4	hold

3.2.10.3 Conventional PCR

Conventional PCR was conducted to amplify small DNA fragments prior to cloning. Additionally, since different BKV rearranged (rr) strains are distinguished by the DNA sequence of their NCCR, the working viral supernatant stock was affirmed by conventional PCR amplifying the NCCR of gDNA isolated from viral supernatant. The integrity of the NCCR was confirmed by sequencing of PCR products. PCR components of conventional PCR are shown in Table 27 and the PCR program is described in Table 28.

Table 27: PCR components

Components	Amount
10x PCR buffer	4 µL
dNTPS (10 mM)	1 µL
Primer forward (10 µM)	1 µL
Primer reverse (10 µM)	1 µL
Template plasmid or gDNA	10 - 50 ng
PfuUltra II HS DNA polymerase	1 µL
DEPC treated water	Add 40 µL

Table 28: PCR program

Cycles	Temperature [°C]	Time
1	95	2 min
30	95	20 sec
	T_m-5	20 sec
	72	15 sec
1	72	3 min
1	4	hold

3.2.11 Rolling circle amplification

For generation of a plasmid containing the genome of the rr-BKV strain Gardner (pBKV_gard), rolling circle amplification was performed to rapidly synthesize multiple copies of circular DNA of viral genome. The illustra TempliPhi Amplification Kit (GE Healthcare) was used according to manufacturer's instructions with 5 µL virus stock as template DNA. To obtain monomeric Gardner genome, 1 µL of rolling circle amplification product was digested with BamHI and subsequently analyzed on a 0.8% agarose gel.

3.2.12 Quantitative real-time PCR (qPCR)

Quantitative real-time PCR (qPCR) combines PCR amplification and detection in one single step allowing the monitoring of PCR progress in real time. Quantification of PCR products is achieved by measuring the fluorescence intensity of fluorescence dyes that label PCR products during each cycle. The cycle at which the fluorescent signal exceeds background fluorescence is called cycle threshold (Ct). With higher starting copy number of a nucleic acid target a significant increase in fluorescence is examined at early Ct values. The Ct values allows calculation of the concentration of the input sample based on a given standard value.

In this study two different qPCR methods were performed: Taqman qPCR or SYBR green qPCR. In the following both qPCR methods are explained in detail.

3.2.12.1 Taqman qPCR

The Taqman qPCR method was used to determine genome copy numbers of SV40, BKV, JCV and human GAPDH or Beta-globin, with the last two mentioned serving as housekeeping genes.

The Taqman probe exhibit sequence specificity to a gene of interest and consists of a reporter fluorescent dye at 5´end and a quencher dye at 3´end. Due to fluorescence resonance energy transfer (FRET) the close proximity of the reporter dye to the quencher dye impairs the emission of its fluorescence. Hydrolyzation of the Taqman probe by DNA polymerase leads to separation of the reporter dye from the quencher dye allowing emission of its fluorescence signal, which is proportional to the amount of PCR products.

The detection of multiple genes of interest in one Taqman qPCR (multiplex PCR) was performed by using various Taqman probes with different fluorescence dyes. In this study, two different multiplex PCR were performed as described in the following.

In secondary screening with BKV infection (see chapter 3.5.17.3), antiviral activity of selected compounds was determined by Taqman qPCR using the LightCycler 480 II (Roche) with corresponding software. To provide an internal control for qPCR quality, the QuantiFast Pathogen +IC Kit (Qiagen) was used according to the manufacturer`s instructions. Beta-globin as a housekeeping gene and the

1st WHO international standard for BKV were used as standards for quantification. In all qPCR analyses, one sample of each standard was included as a positive control and DEPC treated water served as a negative control.

To quantify genome copy numbers in all the other remaining assays, Taqman qPCR was performed using the Rotor-Gene Q Realtime machine (Qiagen) with gain optimization at the beginning of the run and analyzed with the Rotor-Gene 600 software (Qiagen). The components of the reaction mixture and cycling parameters are shown in the Tables 29 – 31. In each qPCR analysis, DEPC-H$_2$0 was included as the negative control and viral genome DNA of BKV, JCV or SV40 served as the positive control, while GAPDH was used as the housekeeping gene for normalization.

Table 29: 20x Primer-probe mix for Taqman qPCR

Components	Amount
Reverse primer (100 µM)	2 µL
Forward primer (100 µM)	2 µL
Probe (100 µM)	1 µL
DEPC treated water	Add 50 µL

Table 30: Reaction mixture for Taqman qPCR

Components	Amount
2x Rotor Gene Multiplex PCR Mastermix (Qiagen)	5 µL
20x Primer-probe mix GAPDH	1 µL
20x Primer-probe mix BKV (VP1) / SV40 (LT-Ag) / JCV (LT-Ag)	1 µL
Template gDNA	10 ng
DEPC treated water	Add 10 µL

Table 31: Cycling parameters for Taqman qPCR

Cycles	Temperature [°C]	Time
1	95	10 min
40	95	10 sec
	60	20 sec

A standard curve for GAPDH was performed by serial dilutions of one gDNA sample. The standard curve for BKV, JCV or SV40 genomes was produced by serial dilution of viral genome DNA. Based on the following formula the copy number of a template was calculated, where the length of ds DNA amplicon of SV40 was 5243 bp, of BKV 5153 bp, of JCV 5000 bp and of GAPDH 3x10^9 bp:

$$number\ of\ copies = \frac{amount\ of\ amplicon\ [ng] \times 6.0221 \times 10^{23}\ [\frac{molecules}{mole}]}{lenght\ of\ ds\ DNA\ amplicon\ \times 660\ [\frac{g}{mole}] \times 10^9\ [\frac{ng}{g}]}$$

For quantification of viral genome copy numbers relative to cellular background, the BKV, JCV or SV40 genome copy numbers were normalized to GAPDH copy numbers.

3.2.12.2 SYBR green qPCR

The fluorescent dye SYBR green was used to quantify gene expression levels and to determine genome copy numbers of MuPyV and mouse GAPDH. Binding of SYBR green unspecifically to any ds DNA, increases fluorescence intensities in correspondence to the amount of ds DNA that rises during PCR process.

To determine mRNA expression levels, total RNA was converted into cDNA by reverse transcriptase PCR (RT-PCR) using random hexamer primers, specified in chapter 3.3.2. Primers for qPCR binds specifically to the gene region of LT-Ag, VP1 or GAPDH.

To analyze miRNA expression levels by qPCR, total RNA was synthetized into cDNA with stem-loop primer, described in chapter 3.3.3. For qPCR analyses, a miRNA specific forward primer and a universal reverse primer binding the conserved region of the stem-loop primer sequence were used.

For all primer pairs, standard curves were performed by serial dilutions of a cDNA sample. For each qPCR analysis, one sample of standard curve as a positive control and DEPC treated water as the negative control were included. The composition of a SYBR green qPCR reaction is described in Table 32 and the corresponding cycling parameters are shown in Table 33. For the quantification of expression levels, mRNA or miRNA expression levels were normalized to GAPDH expression levels.

The qPCR was performed using the Rotor-Gene Q Realtime machine (Qiagen) and analyzed with the Rotor-Gene 600 software (Qiagen). At the beginning of a run a gain optimization was performed. After completed qPCR a melting curve was carried out.

Table 32: Reaction mixture for SYBR green qPCR quantifying transcript levels

Components	Amount
2x SensiMix SYBR Hi-Rox Mastermix (Bioline)	5 µL
Primer forward (10 µM)	1 µL
Primer reverse (10 µM)	1 µL
Template cDNA	2 µL
DEPC treated water	Add 10 µL

Table 33: Cycling parameters for SYBR green qPCR quantifying transcript levels

Cycles	Temperature [°C]	Time
1	95	10 min
50	95	10 sec
	60	15 sec
	72	20 sec

For analysis of gDNA extracted from cells infected with MuPyV and corresponding viral supernatant, genome copy numbers and viral load were quantified by SYBR green qPCR using QuantStudio 3 Real-Time PCR System with the StepOnePlus™ 2.2.2 software (Applied Biosystems). For the qPCR reaction, 2 µL gDNA were added to a 18 µL reaction mixture containing 6.40 µL nuclease free water, 0.80 µL of each primer and 10 µL PerfeCTa SYBR® Green FastMix (Quant Bio). Cycling parameters of the qPCR are shown in Table 34. In the final stage a melting curve was performed. All samples were measured in technical duplicates.

Table 34: Cycling parameters for SYBR green qPCR

Cycles	Temperature [°C]	Time
1	95	10 min
40	95	15 sec
	60	30 sec

For each qPCR a freshly prepared standard curve using the plasmid pBluescript-sk+PTA containing the genome of MuPyV was included with concentrations ranging from 10^3 to 10^8 genome copies/µL. To obtain viral genome copies relative to cellular background, viral genome copies of MuPyV were normalized to GAPDH copies.

3.3 RNA techniques

Prior to working with RNA, all pipettes and surfaces were cleaned with RNase-Zap (Ambion) and only RNase free tubes and filter tips were used. Additionally, for all experiments only DEPC treated water was used.

3.3.1 Isolation and Quantification of total RNA from eukaryotic cells

Total RNA from eukaryotic cells was isolated using the RNA Bee (Amsbio) method. First, 10^4 - 10^6 cells were harvested, washed once with DPBS and lysed in 500 µL RNA Bee by vigorous pipetting on ice. 100 µL chloroform were added, samples were mixed for 20 sec and incubated on ice for 10 min. After incubation the samples were centrifuged at 12,000 x g for 15 min at 4 °C to separate organic phase, harboring DNA and proteins, and aqueous phase, containing RNA. The latter one was transferred to a new tube and precipitated by addition of 250 µL isopropanol for 30 min at RT. Afterwards, RNA was pelleted by centrifugation (full speed, 5 min, 4 °C) and washed once with 500 µL 75% ethanol. After centrifugation and removal of residual ethanol, RNA pellet was air dried for 10 min at RT and resuspended in 20 – 50 µL DEPC treated water depending on pellet size. Using a spectrophotometer (Nanodrop-1000, Thermo Scientific) the RNA concentration was examined.

3.3.2 Reverse-transcriptase PCR (RT-PCR)

To investigate mRNA expression by qPCR, isolated RNA was reverse transcribed into cDNA. Prior to RT-PCR, RNA was digested with the DNA-free™ Kit (Thermo Fisher Scientific) according to the manufacturer's instructions to remove residual gDNA. RT-PCR using random hexamer primer was performed with the Superscript III (Thermo Fisher Scientific). The composition of the RT-PCR is described in Table 35.

Table 35: RT-PCR mixture

Components	Amount
RNA	1 µg
dNTPS (10 mM)	1 µL
Random hexamer primer (250 ng)	1 µL
5x First Strand Buffer	4 µL
DTT (0.1 M)	1 µL
RNaseOUT	0.7 µL
SuperScript III	0.3 µL
DEPC treated water	add 20 µL

RNA was diluted in 12 µL DEPC treated water, dNTPS and random hexamer primer were added and incubated for 5 min at 65 °C to break secondary structures, and immediately incubated on ice for 2 min. Then, 5x First Strand Buffer, DTT, RNaseOUT and SuperScript III (all reagents purchased from Thermo Fischer Scientific) were added. A sample lacking SuperScript III was included as a negative control. Annealing of random hexamer primer was proceeded at 25 °C for 5 min with following reverse transcription for 60 min at 50 °C. Eventually, reaction was stopped by incubating at 70 °C for 15 min. Afterwards, by addition of 0.2 µL RNase H (NEB) and incubation for 20 min at 37 °C, remaining RNA was removed, prior to subsequent qPCR analysis.

3.3.3 miRNA stem-loop cDNA-synthesis

Since amplification of mature miRNA is insufficient by standard RT-PCR concerning its small size, a primer with an internal stem-loop structure was used for elongation of miRNA at its 3`end. This primer was appropriated to serve as a scaffold for a universal primer in subsequent qPCR.

1 µg of total RNA was dissolved in DEPC treated water and mixed with dNTPS as well as BKV miRNA specific stem-loop. To break secondary structures and to enable primer binding, the mix was incubated for 5 min at 65 °C with immediately incubation on ice, prior to cDNA-synthesis. The residual components, described in Table 36, were added to the mixture and cDNA-synthesis was accomplished by using a pulsed program specified in Table 37.

Table 36: stem-loop cDNA-synthesis

Components	Amount
RNA	1 µg
dNTPS (10 mM)	1 µL
BKV-miR-B1-5p SL primer (1 µM)	0.5 µL
DEPC treated water	add 13 µL
5 min at 65 °C, 2 min on ice	
5x First Strand Buffer	4 µL
DTT (0.1 M)	1 µL
GAPDH RT rev primer (2 µM)	1 µL
RNaseOUT	0.5 µL
SuperScript III	0.5 µL

Table 37: Pulsed program for miRNA stem-loop cDNA-synthesis

Cycles	Temperature [°C]	Time
1	16	30 min
60	30	30 sec
	42	30 sec
	50	1 sec
1	85	5 min

To degrade remaining RNA, 0.2 µL RNase H (NEB) and 1.8 µL DEPC treated water were added and incubated at 37 °C for 20 min. Subsequently, miRNA was quantified by qPCR.

3.4 Protein Techniques

3.4.1 Isolation of protein from cultured cells

To obtain protein from cultured cells in 6 well-plate, cells were scraped with 1 mL ice cold DPBS, transferred into 1.5 mL Eppendorf tube and pelleted by centrifugation (1200 x g, 5 min, RT). Cell pellets were resuspended in 150 µL ice cold lysis buffer (Table 38). For complete disruption of membranes, lysates were further homogenized by passing through a syringe (0.5 mm). Cell lysates were incubated for 30 min at 4 °C and subsequently centrifuged at 25,000 x g for 20 min. Supernatants containing whole cell extracts were transferred into new 1.5 mL Eppendorf tubes and placed on ice or stored at -20 °C.

Table 38: Lysis buffer

Components	Concentration
Sodium chloride	150 mM
NP40	1%
Sodium deoxycholate	0.5%
SDS	0.1%
Tris hydrochloride, pH 8.0	50 mM
EDTA	5 mM
Protease inhibitor cocktail (Roche)	1 tablet per 10 mL lysis buffer

3.4.2 Determination of protein yield

For Western Blot analysis, protein concentration was determined photometrically with the Roti®-Quant Bradford assay (Carl Roth) according to the manufacturer`s instructions. This assay is suitable for quantifying protein concentrations in the range of 0 – 2 mg/mL.

To quantify protein yield for VLP labelling, the Qubit™ Protein Assay Kit (Thermo Fischer Scientific) was accomplished according to the manufacturer`s instructions, allowing quantification of proteins ranging from 12.5 μg/mL – 5 mg/mL.

3.4.3 Concentration of proteins

For higher protein yields, protein samples were concentrated with Amicon® Ultra Centrifugal Filters (Sigma) according to the manufacturer`s instructions. Briefly, 500 μL of protein solution were centrifugated for 10 min at 14,000 x g to collect filtrate. By further centrifugation at 1,000 x g for 2 min protein samples were recovered.

3.4.4 Protein purification method using iodixanol (Optiprep)-based density gradient

To isolate and purify mature capsids, an iodixanol (Optiprep)-based density gradient was accomplished. Optiprep is a trade name for 60% (wt/vol) iodixanol solution. For preparation of Optiprep gradients, 46% (wt/vol) iodixanol solution was diluted to 27%, 33% and 39% using DPBS supplemented with 0.8 M NaCl. Optiprep gradients were poured in thin wall polyallomer 5 mL tubes (Beckman Coulter) by underlaying 1.3 mL of 27% solution, then 33% solution and then 39% solution using syringe fitted with a long needle. The gradients diffused for 2 h at 4 °C. Afterwards, 400 μL of clarified cell lysates were layered onto the Optiprep gradient and centrifugated for 4 h at 16 °C at 42,000 rpm in an SW60Ti swinging bucket ultracentrifuge rotor (Beckmann) while acceleration and deceleration were set to slow. After ultracentrifugation, gradient fractions were collected by puncturing the bottom of the tube slightly off center without rocking, using a syringe needle (0.2 mm). Into 1.5 mL protein low bind tubes (Eppendorf) fractions were dripped. The first 750 μL were collected

as fraction one, then further fractions were collected every 300 µL, while the top 2 mL of the gradient were discarded.

3.4.5 SDS-polyacrylamide gel electrophoresis (PAGE)

To separate proteins by electrophoresis, proteins were dissolved in 3x sample buffer (Table 39) and boiled for 5 min. By SDS-PAGE proteins were separated in an electric field, using a 10% polyacrylamide gel for subsequent analysis by Western blot, or using a 12% polyacrylamide gel for detection of proteins with silver staining (Table 40 – 42) and 1x electrophoresis buffer (Table 43) as running buffer. At a voltage of 80 V gel runs were initiated for 10 min and continued at 120 V until the bromo phenol blue reached the end of the gel. To estimate the molecular weight the standard Spectra™ Multicolor Broad Range Protein Ladder (Thermo Fischer Scientific) was used.

Table 39: 3x sample buffer

Components	Concentration
SDS	1.2 g
Glycerol	4.65 mL
Tris hydrochloride, pH 7.0	200 mM
Bromo phenol blue	0.4 g
β-Mercaptoethanol	0.5 mL
Distilled water	Add 10 mL

Table 40: Polyacrylamide stacking gel

Components	Amount
30% Acrylamide (Roti30)	670 µL
1.0 M Tris hydrochloride, pH 6.8	500 µL
10% SDS	40 µL
10% APS	100 µL
TEMED	10 µL
Distilled water	2.7 mL

Table 41: 10% Polyacrylamide running gel

Components	Amount
30% Acrylamide (Roti30)	3.3 mL
1.5 M Tris hydrochloride, pH 8.8	2.5 mL
10% SDS	100 µL
10% APS	100 µL
TEMED	8 µL
Distilled water	4.1 mL

Table 42: 12% Polyacrylamide running gel

Components	Amount
30% Acrylamide (Roti30)	4.0 mL
1.5 M Tris hydrochloride, pH 8.8	2.5 mL
10% SDS	100 µL
10% APS	100 µL
TEMED	8 µL
Distilled water	3.4 mL

Table 43: 10x electrophoresis buffer

Components	Concentration
Tris base	30.3 g
Glycine	144.0 g
SDS	10.0 g
Distilled water	Add 1.0 L
pH 8.3	

3.4.6 Western Blot analysis

To investigate protein expression by Western Blot analysis, 12 µg protein were used. After completed electrophoresis, proteins were blotted on a 0.45 µm PVDF membrane (Carl Roth) by semi-dry transfer. The electrophoretic transfer was performed in blotting buffer (Table 44) at 115 mA for 75 min.

Table 44: 1x Blotting buffer

Components	Concentration
Tris base	25 mM
Glycine	192 mM
SDS	0.01%
Methanol	20%

The membrane was incubated for 1 h in 5% milk-TBST (Table 45) at RT and subsequently incubated with primary antibody diluted in 5% milk-TBST over night at 4 °C. To detect LT-Ag the primary mouse antibody PAb416 (ab16879, Abcam) was diluted 1:50 and for detection of VP1 the primary rabbit antibody ab53977 (Abcam) was diluted 1:5000 in 5% milk-TBST. The membrane was washed three times for 15 min in TBST and incubated for 1 h at RT with HRP-coupled secondary antibody diluted in 1:5000 in 5% milk-TBST. Prior to detection the membrane was washed again three times in TBST for 15 min and twice in 1x TBS for 5 min. Using the Western Blotting Luminol Reagent (Santa Cruz) according to manufacturer`s instructions, proteins on the membrane were detected on an X-ray film (Fujifilm Super RX, Hartenstein A.).

Table 45: 1x TBST

Components	Concentration
Tris base	20 mM
Sodium chloride	150 mM
Tween-20	0.1%
pH 7.5	

3.4.7 Silver staining of proteins in polyacrylamide gels

To detect proteins in the low nanogram range, silver staining was performed. 20 µL protein sample were mixed with 10 µL of 3x sample buffer (Table 39), boiled for 10 min and proteins were separated by electrophoresis, as described in chapter 3.4.5. Generally, all steps for silver staining were performed at RT while gentle shaking the gel. Solutions used for staining are described in Table 46. After cutting of the stacking gel, the running gel was fixed for 30 min with gentle shaking. Then, gel was washed two times for 20 min using wash solution, and further washed with distillated water two times for 30 sec each time. Afterwards, gel was incubated with sensitizer solution for 1 min and washed again two times with distillated water for 30 sec. Gel was incubated in silver staining solution for 30 min and subsequently washed tree times with distillated water for 15 sec. Finally, gel was incubated with developer solution for 5 to 10 min. Stop solution was added before protein bands were getting too dark stained and the gel was stored with 5% acetic acid.

Table 46: Solutions for silver staining

Solution	Components	Concentration
Fixation solution	Ethanol	40%
	Acetic acid	10%
Wash solution	Ethanol	30%
Sensitizer solution	Sodium thiosulfate	0.02%
Staining solution	Silver nitrate	0.1%
	Formaldehyde	0.02%
Developer solution	Sodium carbonate	2%
	Formaldehyde	0.04%
Stop solution	Acetic acid	96%

3.4.8 Indirect Immunofluorescence analysis

3.4.8.1 Detection of SV40 and BKV gene expression using immunostaining

Cells were seeded on coverslips and infected with BKV or SV40 as described in chapter 3.5.13. To determine the titer of virus stocks by fluorescent focus assay (FFA) or to examine infection rates, 3 days post infection (p.i.) medium was changed, and cells were incubated for further 48 h. However, to investigate the inhibitory effect of small molecule compounds, cells were infected with BKV and simultaneously treated with a compound as described in chapter 3.5.14. Without changing the medium immunofluorescence analysis were performed 2 or 5 days p.i..

First, cells were washed once with DPBS and fixed for 20 min with 4% paraformaldehyde (PFA). Then, cells were washed twice with DPBS for 10 min, permeabilized for 10 min with permeabilization buffer (Table 47) and washed again with DPBS. Afterwards, cells were blocked by addition of blocking buffer (Table 48) for 30 min. To detect LT-Ag the primary mouse antibody PAb416 (ab16879, Abcam) was diluted 1:50 and for detection of VP1 the primary rabbit antibody ab53977 (Abcam) was diluted 1:1000 in blocking buffer. Primary antibodies were added to the cells for 2 h. After incubation coverslips were washed three times for 15 min with DPBS. To detect primary antibodies, secondary α-mouse or α-rabbit antibodies labelled with Alexa Fluor® 488 or 555 dye (Thermo Fisher Scientific) were diluted 1:1000 in blocking buffer and added to the cells for 1 h in the dark. After incubation cells were washed three times for 15 min with DPBS and coverslips were mounted with DAPI containing vectashield mounting medium (Vectorlabs). All steps were performed at RT. Cells were observed under a laser scanning confocal microscope with a 100er magnification (Nikon). Using the software NIS-Elements AR 4.5.1.01 (Nikon) images from 25 adjacent fields were captured and stitched together, resulting in a large image. Using the software Fiji, from 12 large images the number of total cells (DAPI stained) and infected cells (LT-Ag or VP1 stained) were counted, and the average was calculated.

Table 47: Permeabilization buffer

Components	Concentration
DPBS	1x
Triton X-100	1%
Trisodium citrate	0.1%

Table 48: Blocking buffer

Components	Concentration
DPBS	1x
Triton X-100	1%
Tween20	0.5%
BSA	3%

3.4.8.2 Detection of MuPyV using immunostaining

With a fluorescent focus assay (FFA) as specified in chapter 3.5.12, the titer of MuPyV viral stocks was determined using NMuMG cells. 40h p.i. medium was aspirated, cells were washed with DPBS, fixated with 4% PFA and incubated for 20 min at RT. All following steps were performed at RT with gently rocking. Cells were washed three times with DPBS. Using 0.1% Triton-X-100 cells were permeabilized for 5 min and subsequently washed again three times with DPBS. For blocking cells were incubated for 1 h with blocking solution (5% goat serum). Blocking solution was removed, 100 µL of I58 antibody (rabbit polyclonal anti MuPyV VP1) diluted at 1:5000 in 5% goat serum was added to the cells and incubate for 1 h. Afterwards, cells were washed again three times with DPBS and incubated with 100 µL of goat anti-rabbit IgG-Alexa Fluor 488 (Thermo Fischer Scientific) diluted at 1:250 for 1 h in the dark. After incubation, cells were washed three times with DPBS. Cells were stored at 4 °C till microscopic analysis was performed using an inverted fluorescence microscope (Leica) to quantify the numbers of total and stained cells per field.

3.5 Cell biological methods

The eukaryotic cell lines, which were used in this study, are described in Table 49.

Table 49: Eukaryotic cell lines

Name	Cell type	Supplier and Catalog #
RPTEC	Human, renal proximal tubule epithelial cells	Lonza, CC-2553
RPTEC/TERT1	Human, renal proximal tubule epithelial cells, immortalized with pLXSN-hTERT retroviral transfection	ATCC® LGC Standards, CRL-4031™
WI-38	Human, lung fibroblast cells	ATCC® LGC Standards, CCL-75™
NMuMG	Mouse, mammary gland epithelial	ATCC® LGC Standards, CRL-1636™
CV-1	African green monkey, kidney fibroblast cells	ATCC® LGC Standards, CCL-70™
COS-7	African green monkey, derived from the CV-1 with constitutive expression of SV40 LT-Ag	ATCC® LGC Standards, CRL-1651™
Lenti-X293T	Human, clone selected HEK293 with constitutive expression of SV40 LT-Ag	ClonTech, 632180
HEK293A	Human, clone selected HEK293 with relatively flat morphology	kindly provided by Wolfram Brune, Heinrich-Pette-Institute, Hamburg
HEK293TT	Human, clone selected HEK293 engineered to express high levels of SV40 LT-Ag	kindly provided by Nicole Fischer, UKE, Hamburg

3.5.1 Culture of eukaryotic cell lines

In general, all cells were cultured in polystyrene cell culture flasks or dishes at 37 °C in a 5% CO_2 atmosphere with a relative humidity of 95%. The cell lines NMuMG, WI-38, Lenti-X293T, HEK293A, HEK293TT, CV-1 and COS-7 were grown in DMEM medium (Thermo Fisher Scientific) supplemented with 10% fetal bovine serum (FBS, Biochrom) and 1% Penicillin/Streptomycin (Thermo Fisher Scientific). RPTEC/TERT1 cells were cultured in hormonally defined medium consisting of a 1:1 mixture of DMEM and Ham`s F-12 nutrient mix supplemented with 2 mM Glutamax, 1x Insulin-Transferrin-Selenium solution, 1% P/S, 10 ng/mL epithelial growth factor (EGF, Thermo Fisher Scientific), 36 ng/mL Hydrocortisone (Stemcell), 0.1 mg/mL G418 and 2% FBS (Biochrom). Cells were splitted, when they reach 90% density in a ratio of 1:10, 1:3 in the case of WI-38 or 1:5 in the case of NMuMG. Cells were splitted or harvested by washing once with DPBS (Merck) and incubated with 0.25% Trpysin/EDTA (Thermo Fischer Scientific) for 1 – 5 min at 37 °C until cell detachment. Subsequently, cells were resuspended in DMEM and 1/10 or 1/3 of cells were reseeded in fresh growth medium. However, primary human RPTEC were grown in REBM medium (Promocell) supplemented with 2% FSC and 1x Gentamicin/Amphotericin B Solution (Thermo Fisher Scientific). Cells were splitted or harvested by washing once with DPBS (Merck) and incubated with a solution containing 0.025% trypsin and 0.01% EDTA (Thermo Fisher Scientific) for 5 – 10 min at 37 °C. Trypsin was neutralized with DPBS supplemented with 0.5% FBS. Cells were centrifuged at 220 x g for 5 min, resuspended in 3 mL growth medium and 1/5 of cells were re-seeded in fresh medium.

3.5.2 Storage of eukaryotic cells

For long-term storage, cells were centrifuged at 220 x g for 5 min at RT, resuspended in growth medium supplemented with 10% dimethyl sulfoxide (DMSO, Merck) in the case of RPTEC/TERT1, WI-38, Lenti-X293T, HEK293A, HEK293TT, CV-1 and COS-7, and divided into CryoPure tubes. However, pelleted NMuMG and RPTEC were resuspended in growth medium supplemented with 5% DMSO. Cells were slowly frozen to – 80 °C in an isopropanol bath to avoid formation of ice crystals and after 24 h transferred to liquid nitrogen.

To culture frozen cells, an aliquot of cells was thawed at 37 °C in a water bath for 5 min. Cells were resuspended in 5 mL growth medium and centrifuged for 3 min at 220 x g. Then, cell pellets were resuspended in 10 mL growth medium and seeded in an appropriate cell culture dish or flask.

3.5.3 Cell seeding for transfection, transduction or infection experiments

Cells were seeded one day prior to transfection, transduction or infection. For infection cell density reached 25 – 40%, for transfection and transduction it was 60 – 80%. First, cells were trypsinized and resuspended in medium. 10 µL of cell suspension were mixed with 10 µL of trypan blue to exclude

death cells. Using a Neubauer counting chamber viable cells were counted under the light microscope (Leica) and cell number was determined using the following formula.

$$cell\ number = \frac{amount\ of\ cells\ (counted\ in\ 4\ large\ quares)}{4} \times 10^4$$

The number of cells that were seeded in different cell culture vessels is demonstrated in Table 50.

Table 50: Number of seeded cells

Cell culture vessel	Number of cells per well or dish
384-well plate	$4x10^2$
96-well plate	$1\text{-}5x10^3$
24-well plate	$1x10^4$
12-well plate	$3x10^4$
6 well-plate	$1\text{-}3x10^5$
10 cm-dish	$5x10^6$

3.5.4 Transient transfection

To transiently introduce DNA in eukaryotic cells different transfection reagents were used in dependence on cell type and transfection efficiency, which are described in detail in the following.

3.5.4.1 Transfection with Lipofectamine

HEK293TT were transfected with Lipofectamine™ 2000 Transfection Reagent (Thermo Fischer Scientific) to produce VLPs, further described in chapter 3.5.19.

3.5.4.2 Transfection with PEI

Lenti-X293T, CV-1, COS-7 or WI-38 cells were transfected with PEI. To generate working stocks, Polyethyleneimine (PEI, Polysciences Inc.) was dissolved in sterile H_2O at a concentration of 1 mg/mL, neutralized by addition of HCl to a pH 7.2 and sterilized by filtration using 0.22 µm syringe filter units (Merck). Aliquots of PEI working stocks were stored at – 80 °C.

Lenti-X293T cells were transfected to produce lentiviral particles, described in chapter 3.5.5. However, WI-38, CV-1 or COS-7 cells were transfected to propagate BKV, SV40 or JCV viral supernatants, further explained in detail in chapter 3.5.9.

3.5.4.3 Transfection with TransfeX

Transfection of primary RPTEC was required to investigate viral DNA replication with BKV replication assay described in chapter 3.5.15. RPTEC were transfected using TransfeX™ Transfection Reagent (LGC Standards GmbH) according to manufacturer`s instructions.

3.5.5 Production of lentiviral particles

For establishment of a phenotypic primary HTS, the modified lentiviral vector LeGO-EFS-RFP was used to generate an RFP positive stable cell line using CV-1 cells. However, for the miRNA-based reporter screen the modified lentiviral vector LeGO-miRNA-GFP was used in order to generate RPTEC/TERT1 or HEK293A reporter cells with stable GFP expression. Furthermore, using the modified lentiviral vector LeGO-iC2-miRB1, in RPTEC/TERT1 cells the expression of BKV miRNA driven by a CMV promoter was accomplished.

Lentiviral particles were produced by co-transfection of vector plasmid with packaging plasmids into Lenti-X293T cells. Prior to transfection, growth medium was replaced with 6 mL serum-free OptiMEM (Thermo Fischer Scientific) per 10 cm-dish. The composition of the transfection reaction mixture is described in Table 51. Vector plasmid (LeGO-EFS-RFP, LeGO-miRNA-GFP or LeGO-iC2-miRB1) and packaging plasmids (gag-pol, rev, VSV env) were added to 1 mL OptiMEM. 270 µL PEI were added to the solution and mixed by vortexing. After 30 min incubation at RT the transfection mixture was added dropwise to the cells and incubated for 4-6 h at 37 °C. Then, medium was replaced with fresh growth medium supplemented with 10% FBS, 1% P/S and 20 mM HEPES.

Table 51: Transfection mixture lentiviral particles

Components	Amount per 10 cm-dish
Vector plasmid	10 µg
Lenti gag-pol	10 µg
Lenti rev	5 µg
VSV env	2 µg
OptiMEM	1 mL
PEI	270 µL

24 h post transfection medium was changed. 48 h post transfection the first supernatant containing viral particles was harvested, sterile filtered using 0.22 µm syringe filter units (Merck), divided into 1 mL aliquots and stored at -80 °C. Fresh growth medium was added to the cells. After further 24 h the second viral supernatant was harvested as described previously.

3.5.6 Transduction with lentiviral particles

One day prior to transduction, CV-1, HEK293A or RPTEC/TERT1 cells were seeded in 6-well plates. Growth medium was removed and 3 mL of viral supernatant per well were added. To facilitate virus attachment, 8 µg/mL polybrene were added and plates were spinoculated at 800 x g and 37 °C for 1 h. After 24 h of incubation, growth medium was replaced, and cells were further incubated until selection with G418 started (see chapter 3.5.7).

To obtain comparable transduction efficiencies, the titer of supernatant containing lentivirus was examined by titration. In 24-well plates, Lenti-X293T cells were seeded. After cell attachment, growth medium was aspirated, 500 µL of lentiviral supernatant, at different ratios diluted in growth medium, and 8 µg/mL polybrene were added to the cells. After spinoculation and 24 h of incubation under standard culture conditions, growth medium was replaced and cells were further incubated. After 48 h of incubation, flow cytometry analysis was conducted to evaluate transduction efficiency. Using the following formula, the titer of lentiviral supernatant was calculated:

$$T = \frac{N \times P}{V}$$

T = titer in FFU/mL, N = number of cells, P = percent of positive cells, V = volume of viral supernatant

3.5.7 Generation of stable cell lines

CV-1 reporter cells with a stable RFP expression were needed to perform a phenotypic primary HTS, while HEK293A and RPTEC/TERT1 cells with stable GFP expression were required for the miRNA-based reporter screen. Therefore, lentiviral particles using the modified lentiviral vectors, LeGO-EFS-RFP or LeGO-miRNA-GFP, were produced as described in chapter 3.5.5. Using these particles CV-1 or HEK293A and RPTEC/TERT1 cells were transduced. Since inserted vector DNA leads to the expression of neomycin resistance gene resulting in positive cells with neomycin resistance, 48h after transduction RFP positive CV-1 cells and GFP positive HEK293A cells were selected with G418 at a concentration of 1 mg/mL. After 2 weeks of selection, > 90% of cells were RFP or GFP positive. These polyclonal reporter cells were sorted by FACS into single cell colonies as described in chapter 3.5.8. To generate CV-1 reporter cells for HTS, three different single colonies were pooled. In the case of miRNA-based reporter screen, one GFP positive cell colony was used as the reporter cell line for further experiments.

3.5.8 Flow cytometry and Fluorescence Activated Cell Sorting (FACS)

Using flow cytometry, the number of GFP or RFP positive reporter cells was determined. However, fluorescence activated cell sorting (FACS) was used to selectively collect RFP or GFP positive cells and sort single colonies after transduction and G418 selection. Prior to sorting or flow cytometry analysis, cells were trypsinized, washed once with DPBS and resuspended in 200 µL FACS buffer (Table 52). Cell suspension was pipetted through a cell strainer cap into round-bottom FACS tubes.

Table 52: FACS buffer

Components	Concentration
DPBS	1x
FBS	1%
EDTA	5 mM
HEPES	25 mM

Sorting was performed on FACSAria (BD Bioscienes) and flow cytometry on LSRFortessa™ (BD Biosciences) using the channels PE for RFP positive cells or FITC for GFP positive cells. Data were analyzed with the software FACSDiva™ 8.0.1 (BD) and FlowJo® (LLC).

3.5.9 Generation of SV40, JCV and BKV viral supernatants from DNA

The plasmid pSV40 containing the genome of SV40, the plasmid pBKV_dun harboring the genome of BKV strain Dunlop and the plasmid pJCV_Mad1 comprising the genome of JCV strain Mad-1 were digested with the Fast Digest endonucleases BamHI (NEB) for 1 h at 37 °C, and immediately heat inactivated for 5 min at 80 °C. The plasmid pBKV_gard harboring the genome of BKV strain Gardner was digested with the Fast Digest endonucleases PstI (NEB).

Using agarose gel electrophoresis, the viral genome with the size of approximately 5 kb was separated from bacterial backbone, excised and purified prior to ligation that was incubated at 16 ° C overnight to re-circularize viral genomes. After ligation genomes were purified again.

For production of SV40 viral supernatants CV-1 cells were used, while for the production of JCV viral supernatant COS-7 cells were used and for the production of BKV viral supernatants WI-38 cells were used. In a 6 well-plate, viral supernatants were produced by co-transfection of genome DNA and the empty plasmid pUC. Prior to transfection, growth medium was replaced with 1 mL fresh growth medium per well. First, DNA of re-ligated viral genomes and pUC18 were mixed in serum-free OptiMEM. PEI was added and the mixture was vortexed. After incubation for 30 min at RT, the whole transfection mixture was added dropwise to the cells and incubated for 8 h at 37 °C. After incubation, medium was removed and replaced with fresh growth medium. The composition of the transfection reaction mixture is presented in Table 53.

Table 53: Transfection mixture for production of viral SV40, JCV or BKV viral supernatant

Components	Amount per 10 cm-dish
Re-ligated genome	200 ng
pUC18	500 ng
OptiMEM	100 µL
PEI	7 µL

Four days in the case of SV40 or in the case of JCV and BKV after seven days post transfection, cells were harvested by scraping and supernatant containing viral particles was collected. Then, collected supernatants were frozen at – 80 °C and thawed at 37 °C three times, centrifuged at 1960 x g and 4 °C for 15 min, sterile filtered using 0.22 μm syringe filter units (Merck) and divided into 100 μL aliquots that were stored at – 80 °C. To determine viral titers of virus stocks, gDNA was isolated using the ZR viral DNA/RNA Kit (Zymo Research) as described in chapter 3.2.9. Viral load was quantified by Taqman qPCR as defined in chapter 3.2.12.1 and viral titer was indicated in Geq/mL.

In the case of JCV, this virus stock was used for further experiments. However, in the case of SV40 or BKV viral stocks were propagated as described in chapter 3.5.10.

3.5.10 Propagation and Storage of BKV or SV40 stocks

One day prior to infection, CV-1 cells in the case of SV40 or WI-38 cells in the case of BKV were seeded in a 10 cm-dish. Per one dish 3 mL growth medium with supernatant containing virus at a multiplicity of infection (MOI) of 0.01 Geq/mL were prepared. Growth medium on cells was removed, medium containing virus was added to the cells and incubated for 3 h at 37 °C. After incubation, 7 mL growth medium was added to the cells and further incubated.

In the case of SV40 7d p.i. the CPE induced by SV40 infection was almost completed. Remaining cells were harvested by scraping and supernatant containing viral particles was collected. However, in the case of BKV 7d p.i. a CPE induced by BKV infection indeed was visible, but the CPE was completed not until 4 weeks p.i.. Every week growth medium was changed, supernatant was collected and centrifuged at 4 °C and 15 min for 1000 x g. Pellet was resuspended in 3 mL growth medium and stored at – 80 °C. The collected supernatant contained detached cells resulting from CPE caused by BKV. 4 weeks p.i. cells were harvested by scraping, supernatant was collected and combined with the supernatants of previous weeks.

Viral supernatant was frozen at – 80 °C and thawed at 37 °C three times, centrifuged at 1960 x g and 4 °C for 15 min, sterile filtered using 0.22 μm syringe filter units (Merck) and divided into 100 μL aliquots that were stored at – 80 °C. These viral stocks were used for further experiments. To determine viral titers of virus stocks, a viral titration using the fluorescence focus assay (FFA) was performed as described in chapter 3.5.12.

3.5.11 Propagation and Storage of MuPyV stocks

One day prior to infection, NMuMG cells were seeded in a 10 cm dish to reach 25% confluency. For infection, media was changed to 1 mL growth media and 10 μL of virus was added to get 1:100 dilution. Cells were incubated for 1.5 h at 37 °C with rocking every 15 min. After incubation, 9 mL growth media were added, and cells were incubated for further 5 – 8 days until total CPE was visible. Cells were

harvested by scraping, media was collected and centrifuged for 20 min at 7000 rpm in a Sorvall centrifuge. Supernatant was discarded, pellet was resuspended in 1 mL growth medium and frozen/ thawed three times. Next, supernatant was incubated for 30 min at 42 °C and centrifuged at 7000 rpm for 20 min. Afterwards, supernatant was collected, aliquoted and stored at – 80 °C. By FFA the titer of viral supernatant was examined as described in chapter 3.5.12.

3.5.12 Titration of virus stock using the fluorescent focus assay

For quantification of SV40 or BKV stocks using a fluorescent focus assay (FFA), CV-1 cells in the case of SV40 or RPTEC in the case of BKV were seeded in 24-well plate one day prior to infection. On the next day, growth medium was removed, and cells were incubated with 10-fold serial dilutions of prepared virus stocks for 72 h at 37 °C. 3d p.i. medium was changed and cells were incubated for further 48 h. The number of infected cells was detected by antibody against LT-Ag in indirect immunofluorescence analysis described in chapter 3.4.8. 5d p.i. cells were analyzed with a laser scanning confocal microscope (Nikon). At a magnification of 100x, images from 9 adjacent fields were captured and stitched together, resulting in a large image. With the software Fiji the number of infected cells from 5 large images were counted and the average was calculated. Then, the number of infected cells in the whole well was calculated from the average of the number of infected cells in each field, subsequently multiplied with the reciprocal of the volume of sample added to the well and finally multiplied by the reciprocal of the dilution factor. Viral titer was indicated in fluorescence forming units per mL (FFU/mL).

To examine the titer of MuPyV viral stocks by fluorescent focus assay (FFA), in 24 well-plates $6x10^5$ of NMuMG cells were seeded 16 h prior to infection. Virus was diluted at 1:10 and 1:100 in cold DMEM without supplements. Medium was aspirated from cells, and either 100 µL of virus dilution or DMEM without supplements were added to the cells in duplicates. Cells were incubated for 1 h at 37 °C with gently rocking the plate every 15 min. After incubation, virus suspension was removed and 500 µL of growth medium was added to the cells and incubated for further 40 h at 37 °C. The number of infected cells was quantified by staining against VP1 in indirect immunofluorescence analysis, further described in chapter 3.4.8. Based on indirect immunofluorescence analysis infectious titers were determined (FFU/ml).

3.5.13 Infection with SV40 or BKV

About 50 - 80% confluent cells were infected with SV40 or BKV at a MOIs indicated in the respective experiments. If not stated otherwise, virus stocks were diluted in the appropriate growth medium in 1/3 volume of the considered volume and added to the cells. After 3h of incubation at 37 °C, fresh growth medium was added to the cells to reach final volume.

3.5.14 Compound treatment

If not stated otherwise, cells were treated with small molecule compounds or control inhibitors together with infection. Tested compounds and control inhibitors were dissolved to 10 mM in dimethyl sulfoxide (DMSO) to generate stock solutions. If not stated otherwise, prior to treatment and infection all compounds were freshly diluted to 10 µM in growth medium supplemented with virus inoculum or without virus in the case of uninfected cells.

3.5.15 BKV replication Assay

In a 12 well-plate RPTEC (p5) were seeded one day prior to transfection. The transfection mixture for one well was prepared as described in Table 54 and the components were added to 1.5 mL tubes in the indicated order. The transfection mixture was mixed by vortexing and incubated for 30 min at RT. Prior to transfection, growth medium was replaced with 1 mL fresh growth medium per well. The transfection mixture was added dropwise to the cells. After 24h of incubation, supernatant and cells were harvested as described before. Briefly, supernatant was aspirated and sterile filtered through a 0.22 µm syringe filter unit (Merck). Cells were washed once with PBS, detached with Trypsin and cell suspension was divided into cell pellets for DNA and RNA isolation. Samples harvested 24h post transfection (p.t.) were used as input for subsequent qPCR analysis.

Table 54: Transfection mixture for BKV replication assay

Components	Amount per 12 well
OptiMEM	100 µL
Plasmid DNA pBKV_dun	1 µg
TransfeX	2 µL

For compound treatment, 24h p.t. growth medium was aspirated, and cells were treated with DMSO or compound C1 at 10 µM. After 2d, 4d and 7d of incubation, viral supernatant and cells were harvested as described above. Genomic DNA from viral supernatant and cell suspension was isolated with the QiaCube (Qiagen) as described in chapter 3.2.9. Total cell RNA was isolated with RNA Bee (Amsbio) as shown in chapter 3.3.1. Using qPCR analysis DNA replication and mRNA expression levels were examined.

3.5.16 Establishment of cell-based assays suitable for HTS

3.5.16.1 Tetracysteine-based fluorescent tag system

To generate viral supernatant of recombinant BKV, WI-38 cells were transfected with re-ligated genome DNA of wild type (WT) or recombinant BKV (VP1::TC, TC::VP2, TC::LT-Ag) or pUC DNA, serving

as a negative control, as described in chapter 3.5.4. After 7d of incubation, cells and supernatant were harvested as specified in chapter 3.2.9, and BKV load was examined with Taqman qPCR.

To test detection of TC tagged proteins by non-fluorescent biarsenical labeling reagent (FlAsh-EDT$_2$), in 96-well plates using REBM without supplements, RPTEC (p4) were either uninfected or infected with viral supernatants, which were harvested 7d post transfection, of WT BKV or recombinant BKV (VP1::TC, TC::VP2, TC::LT-Ag) at a MOI of 10. After 5d of incubation, labelling solution was prepared by diluting FlAsh-EDT$_2$ stock solution (2 mM, Thermo Fischer Scientific) to 20 µM using HBSS (Sigma). 10 µL of diluted labelling solution were added to the cells and incubated for 30 min at 37 °C in the dark. Green fluorescent signal was detected with a microplate photometer (Tecan) at excitation 508 nm and emission 528 nm.

For detection of green fluorescent signal upon binding of FlAsh-EDT$_2$ to TC tagged BKV proteins using confocal microscopy, in 8-well chamber slides (Ibidi) using REBM without supplements RPTEC (p4) were either uninfected or infected with viral supernatants, which were harvested 7d post transfection, of WT BKV and TC::VP2, VP1::TC, TC::LT-Ag at a MOI of 10. After 5d of incubation, FlAsh-EDT$_2$ was added to the cells at 2 µM and incubated for 30 min in the dark at 37 °C. After incubation, medium was aspirated, and cells were washed two times with 100 µL 1x BAL wash buffer (Thermo Fischer Scientific) diluted in REBM without supplements. Then, cells were fixed with 4% PFA for 20 min at RT and washed twice with DPBS for 10 min. Afterwards, cells were incubated in 100 µL Dapi solution (Abcam) diluted 1:100 in DPBS. Using Spinning Disk confocal microscope with a Nikon Ti2 frame with 100x magnification, images of 48 areas were captured. With the software NIS-Elements AR 4.5.1.01 images were analyzed.

3.5.16.2 BKV miRNA based GFP reporter system

In 12-well plates, HEK293A cells were infected with rr-BKV strain either Dunlop or Gardner at a MOI of 0.1. After 3d and 6d of incubation, cell pellets were harvested, gDNA and total cell RNA were isolated as described in the chapters 3.2.9 and 3.3.1. BKV load in cells was examined by Taqman qPCR. BKV miRNA expression and GAPDH expression levels were obtained by RT-PCR and subsequent SYBR green qPCR.

To determine BKV miRNA expression levels under the regulation of a CMV promoter, HEK293A cells were transfected with 0.5 µg pCDNA-miRB1 and total cell RNA was harvested after 1d, 3d and 6d of incubation, while the 1d samples served as input. With RT-PCR and subsequent SYBR green qPCR the BKV miRNA expression levels based on 5p-miRB1 expression and mRNA expression levels of GAPDH were analyzed.

To examine GFP expression levels, in 24-well plates HEK293A reporter cells were either transfected with 0.5 µg pCDNA-miRB1 or infected with BKV at a MOI of 10. After 3d and 6d of incubation, flow cytometry analysis was performed as described in chapter 3.5.8.

In 12-well plates HEK293A were seeded on coated glass cover slides and infected with BKV at a MOI of 10. After 5d of incubation, immunofluorescence analysis was performed as described in chapter 3.4.8.

In 6-well plates, RPTEC/TERT1 cells were either infected with BKV at a MOIs ranging between 0.01 and 10 or transduced with LeGO-iC2-miRB1 at a MOI of 1. After 3d and 6d of incubation, cell pellets were harvested, and RNA as wells as gDNA were isolated as described in the chapters 3.3.1 and 3.2.9. With Taqman qPCR BKV cellular load was determined and using RT-PCR with following SYBR green qPCR, miRNA expression and GAPDH expression levels were examined.

In 24-well plates, reporter cells were either transduced with LeGO-iC2-miRB1 at a MOI of 1, infected with BKV at a MOI of 10 or mock infected. After 3d and 6d of incubation, flow cytometry analysis was performed to determine GFP expression levels.

In 12-well plates RPTEC/TERT1 were seeded on glass cover slides and 24h p.i. cells were either infected with BKV at a MOI of 10 or mock infected. After 3d of incubation, immunofluorescence analysis was performed as described in chapter 3.4.8.1.

3.5.16.3 Phenotypic cell-based assay using SV40

To examine the required MOI and incubation time for a visible CPE induced by SV40, in 24-well or 96-well plates CV-1 reporter cells were infected with SV40 at a MOIs of 1 – 100, and further incubated for 4 or 6 days under standard culture conditions. After incubation, cells were washed once with DPBS and the cell number as a measurement for CPE was investigated by using a fluorescence microscope (Leica) with 10x or 20x objective. Additionally, with a microplate photometer (Tecan) the RFP intensity levels were measured. To verify the complete cell death induced by SV40 infection, in 96-well plates CV-1 reporter cells were either uninfected or infected with SV40 at a MOI of 50 and either not treated or treated with Staurosporine at concentrations between 1 nM and 100 µM, and further incubated under standard culture conditions for a period of 6 days. After 4h or 1, 2, 4 and 6d of incubation, cells were washed once with DPBS. Using a microplate photometer (Tecan) the RFP intensity levels were measured and MTT assays were performed, described in chapter 3.5.18.1.

To determine the inhibitory effect of known control inhibitors against SV40 infection, in 96-well plates CV-1 reporter cells were either uninfected or infected with SV40 at a MOI of 50 and treated either with Cidofovir (CDF), Hexachlorophene (HXC) or DMSO and further incubated under standard culture conditions. After 6d of incubation, cells were washed once with DPBS, RFP intensity levels were measured with a microplate photometer (Tecan) and MTT assays were performed as described in chapter 3.5.18.1.

3.5.17 Cell-based assays to screen for small molecule inhibitors active against PyV infection

3.5.17.1 Primary HTS with SV40

To identify novel inhibitors against PyV infection, a library consisting of approximately 28,000 small molecule compounds was used for primary HTS. This library, provided by Thomas Schulz from the Institute of Virology at the Medical School Hannover, Germany, was created by using four different compound libraries bought from the companies Enamine or ChemDiv, and comprises novel small molecule compounds, which were not screened for antiviral activity against PyV infection beforehand. The primary HTS was conducted in the Institute of Virology at the Medical School Hannover, Germany by using a robotic, BSL-2 compatible, high throughput system. In 384-well plates CV-1 reporter cells were either uninfected or infected with SV40 at a MOI of 50 in the presence of 10 µM compound, DMSO or HXC, and further incubated under standard culture conditions. 6d p.i. culture medium was removed, and cells were washed two times with DPBS. With the Cytation™ 5 Cell Imaging Multi-Mode Reader (BioTek) fluorescence intensity (FI) of RFP was measured. Additionally, using a 4x objective, images from two fields per well were taken representing the overall culture well. Subsequently, the mean fluorescence intensity (MFI) was calculated using the software Gen5 Image+2.09 (BioTek). Furthermore, to determine the cytotoxic effect of tested compound, MTT assays with uninfected cells treated with the compound library as wells as DMSO or HXC were performed, further described in chapter 3.5.18.1.

As a positive control uninfected cells were used, as a negative control infected cells treated with DMSO and as a reference inhibitor control infected cells treated with HXC. Overall, 243 different plates were analyzed. Per each plate uninfected cells were present in 52 replicates, infected cells treated with DMSO in 20 replicates, infected cells treated with HXC in 12 replicates and infected cells treated with 114 new putative compounds were explored in duplicates.

3.5.17.2 Confirmatory screen with SV40

Selected hit compounds were re-ordered by Enamine or ChemDiv to confirm their inhibitory effect against SV40 in a higher number of biological replicates. The experimental set-up was identical to the primary HTS described in chapter 3.5.17.1 with the exception that the hit compounds were analyzed on 6 different plates with two compound replicates per plate. The reference inhibitor control HXC was added in 20 replicates per plate, the negative control in 36 replicates per plate and the positive control in 60 replicates per plate. Since the readout of the screen was the inhibition of the CPE, highly cytotoxic compounds (false positives) were not expected and no MTT assay was performed.

3.5.17.3 Secondary screen with BKV

In 96-well plates, primary RPTEC at passage 4 were either uninfected or infected with BKV at a MOI of 5 and treated with either DMSO, HXC, CDF or selected hit compounds. 6d p.i. gDNA from cells and viral supernatant was isolated using the MagNA Pure 96 Symphony Instrument (Roche), and viral load was determined by Taqman qPCR analysis as described in chapter 3.2.12.1.

3.5.17.4 JCV Screen

In 96-well plates, COS-7 cells were either uninfected or infected with JCV at a MOI of 3 and treated with either DMSO, HXC, CDF or selected hit compounds. 6d p.i. gDNA from cells and viral supernatant was isolated using a QiaCube (Qiagen), and viral load was determined by Taqman qPCR analysis as described in chapter 3.2.12.1.

3.5.17.5 MuPyV Screen

In 24-well plates, NMuMG cells at passage 5 – 8 were either uninfected or infected with MuPyV at a MOI of 0.5. Infected cells were treated with either DMSO, HXC, CDF or selected hit compounds. 6d p.i. gDNA from cells and cell free viral supernatant was isolated with QiaAmp DNA Mini Kit (Qiagen). MuPyV load was quantified by SBYR green qPCR as described in chapter 3.2.12.2.

3.5.18 Cytotoxicity studies

To determine cytotoxic effects of a compound on viable cells, MTT assay and ATP assay were performed as described in the following. Additionally, MTT assay was used to determine the number of living cells after SV40 infection with attendant CPE.

3.5.18.1 MTT assay

MTT assay is based on the reduction of the tetrazolium dye MTT (3-(4,5-dimethylthiazol-2-yl)-2,5-diphenyltetrazolium bromide) by living cells to insoluble formazan crystals. By measuring the amount of formazan crystals, which are related to mitochondrial activity, the number of viable cells can be estimated. Proliferating and viable cells with an active metabolism show higher rates of MTT converting reaction, while dead cells or slow growing cells manifest lower levels.

For preparation of a working MTT solution, MTT powder (Merck) was dissolved in DPBS to 5 mg/mL, sterile filtered through a 0.22 µm syringe filter unit (Merck) into light protected tubes and stored at 4 °C for frequent use. In 384-well plate or 96-well plates, cells were seeded one day prior to infection and compound treatment, and incubated under standard culture conditions for desired period of exposure indicated in the corresponding experiments. After incubation, 10 µL MTT solution were added per well and cells were incubated for 4 h at 37 °C. Then, cell culture supernatant was removed,

100 µL isopropanol complemented with 0.04 M HCl were added to each well and mixed thoroughly to solubilize formazan crystals. At a wavelength of 570 nm and reference of 630 nm the absorbance was measured in a microplate photometer (Tecan or BioTek).

3.5.18.2 ATP assay

ATP assay is based on the reaction of cellular Adenosine 5´-triphospahte (ATP), produced in mitochondria of living cells, and exogenously added luciferin, which is turned into oxy-luciferin by luciferase enzymes resulting in strong fluorescent light. Monitoring ATP levels with a bioluminescent detection leads to the determination of cytotoxic effects, as the amount of luminescence light is directly proportional to the viability of cells.

To investigate ATP levels, the CellTiter-Glo® Luminescent Cell Viability Assay (Promega) was used according to manufacturer`s instructions. Luminescence was measured in a microplate photometer (Tecan).

3.5.19 Production of fluorescent labelled virus like particles (VLPs)

To produce VLPs *in vitro*, 1×10^7 HEK293TT cells were seeded in a 10 cm dish 16 h prior to transfection to reach a cell density of 40%. For transfection, Lipofectamine™ 2000 Transfection Reagent (Thermo Fischer Scientific) was diluted with 2 mL of OptiMEM. In a separate tube, 12 µg of pmCherry-N1, pWB2b and pWB3b were mixed with 2 mL of OptiMEM. Both mixtures were incubated at RT for 10 min, then combined and further incubated for 20 min. Transfection mixture was added dropwise to pre-plated cells. After 6h of incubation, medium was changed and cells were incubated for 30 h.

Producer cells were collected by trypsinization, resuspended in 10 mL growth medium and transferred to 50 mL tube. Cells were pelleted and supernatant was discarded. Cells were resuspended in 500 µL of DPBS by gently agitating the tube and transferred to 1.5 mL protein low bind tubes (Eppendorf). After further centrifugation, the supernatant was discarded. The cell pellet was resuspended in one pellet volume of DPBS and briefly mixed by vortexing. Neuraminidase V (Sigma) was added to a final concentration of 2 U/mL and incubated for 15 min at 37 °C. Then, Triton X-100 (Carl Roth) was added to a final concentration of 0.5% and incubated at 37 °C for additional 15 min. Afterwards, 0.1% Benzonase (Sigma) and 0.1% ATP-dependent DNase (Lucigen) were added and cell lysate was incubated at 37 °C over night while gently shaking for capsid maturation. After 24 h of incubation, lysate was incubated for 5 min on ice. Then 0.17 volume of 5 M NaCl (Carl Roth) were added and lysate was incubated for 10 min on ice. Afterwards, lysate was clarified by centrifugation at 5,000 x g for 10 min and clarified supernatant was transferred into new 1.5 mL protein low bind tubes (Eppendorf). Protein concentration was determined with Qubit™ Protein Assay Kit (Thermo Fischer Scientific) as specified in chapter 3.4.2, and lysate was diluted to 4 mg/mL with distillated water.

Prior to capsid purification, clarified cell lysate was labelled using the Alexa Fluor 488 protein labelling kit (Thermo Fischer Scientific). 50 µL of 1 M bicarb buffer were added to 500 µL of diluted lysate and transferred into an Alexa Fluor tube while vortexing gently. The mixture was incubated on a stirrer for 1h in the dark. After conjugation reaction, the pH was neutralized by adding 20 µL of 1 M sodium phosphate (pH 6.5). Labelled capsids were purified with Optiprep-gradient described in chapter 3.4.4. Proteins in collected fractions were analyzed with silver staining, specified in chapter 3.4.7. Fraction containing VLPs with the size of about 40 kDa were pooled, concentrated (see chapter 3.4.3) and analyzed again using silver staining.

The infectivity of labelled VLPs was examined with flow cytometry. In 24 well-plate HEK293TT were infected with VLP diluted at 1:100, 1:500 and 1:1000. 48h p.i. flow cytometry was conducted, and the titer was calculated as described in chapter 3.5.8. Labelled VLP were aliquoted and stored at – 80 °C.

3.5.20 Life cell imaging

In an 8-chamber slide (Ibidi), $2x10^4$ of RPTEC (p5) were seeded using 300 µL growth medium. After 16h of incubation, in a 1.5 mL tube a stain solution was prepared by mixing 1 µL of Höchst with 1 µL WGA (Thermo Life Science) in 998 µL growth medium. Medium from cells was exchanged with 298 µL stain solution. Cells were uninfected or infected with 1 µL of fluorescent labelled VLP and either treated with DMSO or compound C1 at 10 µM. Cells were incubated for 1h at 4 °C under constant shaking. Using Spinning Disk confocal microscope with a Nikon Ti2 frame, cells were incubated for 20 h under live cell conditions. Every hour an image of 5 different areas per well was taken with 100x magnification conducting Z-stacks. Using NIS-Elements AR 4.5.1.01 images were analyzed.

3.5.21 Cell culture test for biological contamination

To exclude contamination by biologicals like Mycoplasma, Acholeplasma, and Ureaplasma in cell cultures, the LookOut® Mycoplasma PCR Detection Kit (Merck) was used according to manufacturer's instructions.

3.6 Data evaluation and statistical analysis

Statistical analysis was performed with the software Prism 5.02 (GraphPad). To evaluate the statistically significance in two independent datasets, the students unpaired t-test was applied. If not stated otherwise, in all figures the mean of at least three biological replicates and the corresponding standard deviation is shown. The IC50 and CC50 values were determined by fitting a dose response curve using the software Prism 5.02 (GraphPad).

The automated data evaluation of the primary HTS and confirmatory screen was performed using the software RStudio with self-written scripts in R.

4. Results

Considering the clinical relevance of BKV the identification of efficient and specific inhibitors against BKV infection is highly desirable. To alleviate the urgent need for antiviral therapies, at first a cell-based reporter screen suitable for HTS was established. Subsequently, to identify novel inhibitors active against BKV infection, a primary HTS of a library consisting of approximately 28,000 small molecule compounds was performed. Inhibitors, identified by primary HTS, were then tested for cross-reactivity against JCV and MuPyV infection. In addition, the antiviral activity of inhibitors, selected upon *in silico* data, was further investigated by determining their IC50 and CC50 values. Finally, the inhibitory activity of one top compound was characterized for its effect on BKV life cycle in more detail by pinpointing its involvement in different steps during viral infection.

4.1 Evaluation of cell-based assays suitable for HTS

To investigate whether compounds from a library comprising approximately 28,000 small molecule compounds are active against BKV infection, a cell-based assay suitable for an HTS was required. The criteria for evaluating the suitability of an HTS are defined as the following. Assays for an HTS require robustness, reproducibility, independency from cell numbers and a high signal to background ratio. Additionally, since in this study the inhibitory activity of compounds against viral infections are visualized by detecting fluorescence intensity, reporter cells with a stable and consistent reporter gene expression are required, as viral infection should be detected by monitoring expression levels of the reporter.

The development of such an HTS bears substantial challenges concerning propagation of BKV and tissue culture systems, which are described in the following in more detail. Firstly, PyVs are species and cell type specific. Consequently, *in vitro* tissue culture systems and animal models are highly restricted. While BKV infects human primary RPTEC *in vitro*, manifestation of a phenotypically mild CPE occurs only after 14d. Therefore, establishing an HTS based on morphological changes induced by BKV infection is unfavorable. Furthermore, since the number of cell population doublings is highly limited, genetic manipulation of primary cells by introducing a fluorescent reporter is not possible.

In addition, PyVs are small non-enveloped viruses with a ds DNA genome of approximately 5 kb. Due to the small genome size, the introduction of a fluorescent protein into the genome of PyVs, without disturbing viral protein expression, is challenging. For example, Husseiny and Lacey reported the development of infectious recombinant BKV by introducing the fluorescent protein GFP into the genome of BKV, but viral protein expression was impaired resulting in production of non-infectious virions [146]. So far, there are no robust cell-based assays known that sufficiently detect fluorescence intensity based on BKV infection. Therefore, in this study, three novel cell-based assays were established and used to investigate detection of PyVs infection by measuring fluorescence intensity.

4.1.1 Tetracysteine-based fluorescent tag system using recombinant BKV

The tetracysteine (TC) biarsenical labelling system was tested in order to detect fluorescent labelled BKV proteins. In general, this system uses a small TC tag with the CCPGCC motif to label proteins and theoretically, TC tagged proteins become fluorescent upon covalent binding of cysteine pairs to a membrane permeable biarsenical reagent [147].

The present study hypothesized that introduction of such a small tag into the genome of BKV should minimize the risk of disrupting the overall structure of the targeted protein and thus, exhibit limited effect on viral gene expression. The following experiments addressed whether the biarsenical TC labelling system is usable to quantify BKV infection by measuring fluorescence intensity levels of TC tagged viral proteins either using a microplate photometer or by microscopic analysis.

The insertion of the small TC tag containing 6 amino acids (aa) into the genome of BKV was designed with regard to increase the probability of generating infectious recombinant BKV, by introducing the TC tag to viral proteins without disrupting the ORF of BKV and the non-coding control sequences. Since the viral protein LT-Ag plays a major role in regulating the replication of PyVs and represents the expression of early proteins, it was selected as a target protein for TC tagging. On the other hand, the late protein VP1 was also selected as a target protein for introduction of the TC tag, since VP1 is important for capsid formation as wells as viral infection and represents the expression of late genes. In addition, the viral protein VP2 was selected as a second late protein as interaction of VP1 with host cell surface receptors during viral entry might be impaired even by minor changes in the viral genome. Therefore, three different TC tagged viral proteins were generated by fusing the TC tag either to the N-terminus of VP2 and LT-Ag, or to the C-terminus of VP1 (Figure 6A).

To assess the consequences of a fused TC tag to BKV proteins on virus infectivity, WI-38 cells were transfected with re-ligated genome of either WT or recombinant BKV. 7d post transfection, viral supernatant was harvested and BKV progeny were detected based on VP1 copy numbers as genome equivalents (Geq) by qPCR analysis, referred to as BKV load in the following. Replication of recombinant BKV was detectable 7d post transfection, but BKV loads measured in the supernatant of recombinant BKV were approximately two orders of magnitude lower compared to the viral loads of WT (Figure 6B). Re-infection using these supernatants showed significant lower virus progeny in the supernatant of cells infected with recombinant VP1 virus (similar for recombinant VP2 and LT virus), as virus progeny, measured by gDNA copy numbers, was significantly lower compared to WT virus (Figure 6C). These results indicate that despite the small size, the insertion of TC tag into the genome of BKV diminished the production of viral progeny.
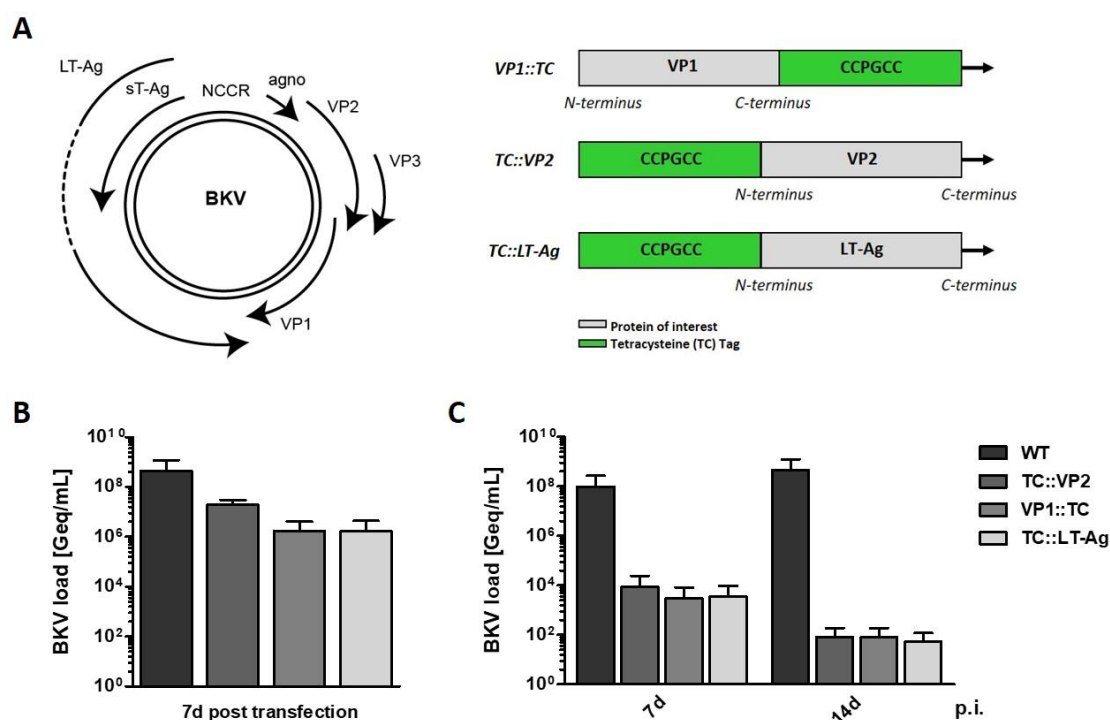
Figure 6: Tetracysteine tagged BKV are less infectious
(A) Left: Schematic illustration of the BKV genome. **Right:** A tetracysteine (TC) tag consisting of 6 aa (CCPGCC) was introduced either to the C-terminus of VP1 or the N-terminus of either VP2 or LT-Ag, generating three different recombinant BKV genomes. **(B)** WI-38 cells were transfected with re-ligated genome of either WT or recombinant BKV. 7d post transfection viral supernatant was harvested and BKV progeny were quantified as Geq per mL by qPCR analysis (n=3), here indicated as BKV load. **(C)** WI-38 cells were infected with the supernatant collected from the previous experiment (B). 7d or 14d p.i. the supernatant was isolated and BKV production was assessed by qPCR analysis, referred to as BKV load (n=3).

To investigate whether TC tagged BKV proteins are successfully fluorescent labelled upon incubation with the membrane permeant fluorogenic biarsenical reagent FlAsh-EDT$_2$, viral supernatants containing WT or recombinant BKV were used to infect RPTEC. These supernatants were collected from WI-38 cells 7d post transfection with re-ligated genome of either WT or recombinant BKV, since replication of recombinant BKV was detectable in the supernatant of these cells (Figure 6B). 5d p.i. RPTEC were incubated with FlAsh-EDT$_2$ reagent to label TC tagged proteins. Expression of TC tagged proteins was quantified by measuring fluorescence intensity at excitation wavelength of 508 nm and emission wavelength of 528 nm using a microplate photometer.

The fluorescence intensity of recombinant BKV was detected in the same range as fluorescence intensity of WT virus or even of uninfected cells indicating a high background (Figure 7A). This result demonstrates that by using a microplate photometer the expression of TC tagged viral protein is not distinguishable from cellular proteins harboring a motif with cysteine pairs, suggesting that infection with recombinant BKV is not enough to overcome the fluorescent signals detected in cellular proteins.
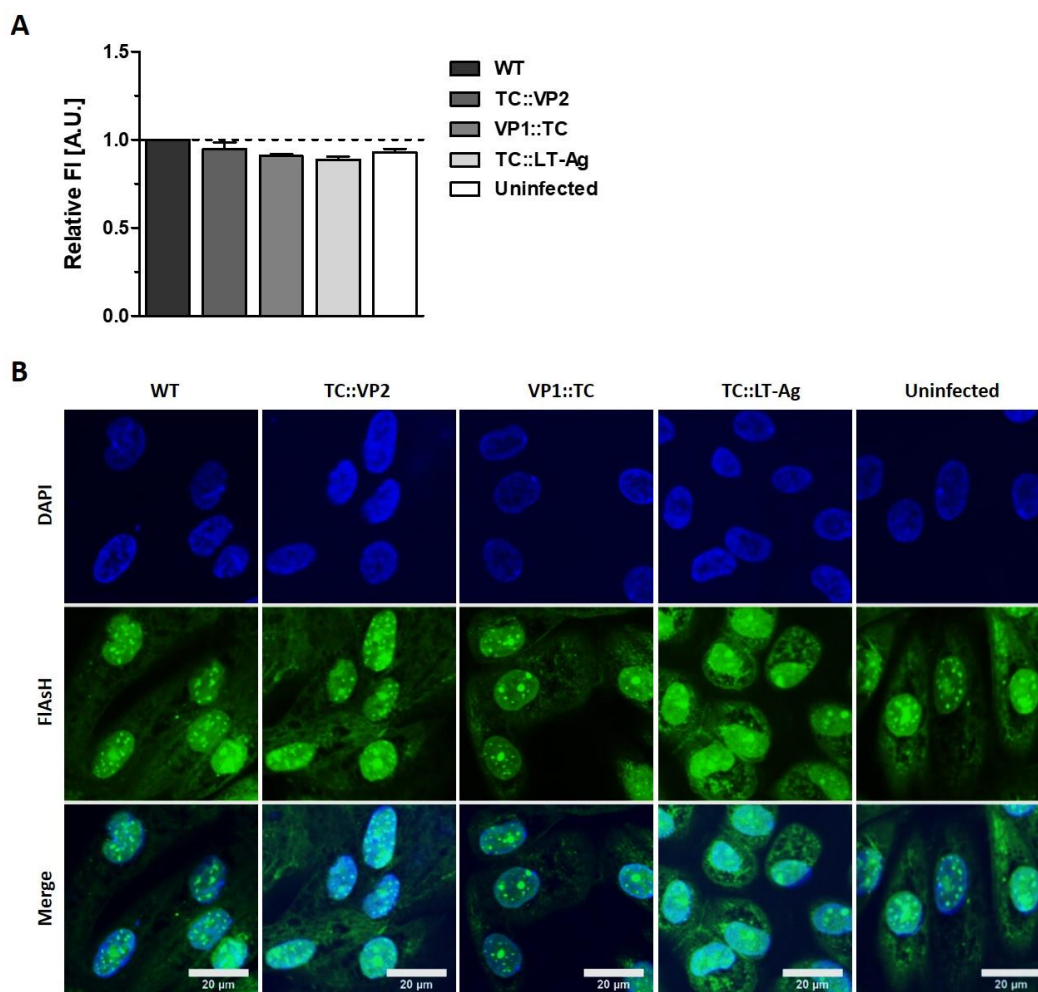
Figure 7: Tetracysteine tagged BKV proteins labelled with fluorogenic biarsenical reagent FlAsh-EDT2 could not be detected

Viral supernatants, which were harvested from WI-38 cells 7d post transfection with re-ligated genome of either WT or recombinant BKV, were used to infect RPTEC. 5d p.i. cells were incubated with FlAsH-EDT$_2$ labelling reagent for 30 min at RT. **(A)** After incubation, fluorescence intensity (FI) of FlAsH binding reagent was detected at excitation wavelength of 508 nm and emission wavelength of 528 nm using a microplate photometer (Tecan). Shown here is the FI of infected cells normalized to uninfected cells, which were set to 1 (n=6). **(B)** After incubation, cells were fixed and nuclei were stained with DAPI. Cells were analyzed by confocal microscopy (Nikon) with 100x lens, and images from 48 different fields were captured (n=1). Shown here are representative images.

However, the detection of fluorescent labelled proteins by fluorescence microscopy is more sensitive in order to discriminate between fluorescence signals from FlAsh-EDT$_2$-labelled TC tagged BKV proteins and fluorescent signals from FlAsh-EDT$_2$-labelled cellular protein containing cysteine pairs. Therefore, RPTEC were infected with WT or recombinant BKV. 5d p.i. RPTEC were incubated with FlAsh-EDT$_2$ reagent to label TC tagged proteins and fluorescence signals were detected by confocal microscopy. As demonstrated in Figure 7B, fluorescent signals detected in recombinant BKV were comparable to signals of WT virus and, unfortunately, to uninfected cells, indicating that FlAsh-EDT$_2$ labelling reagent binds primarily to cysteine pairs found in cellular proteins. One explanation for that could be enormous amounts of cellular proteins harboring motifs with cysteine pairs being expressed by RPTEC. However,

it is more likely that the infection by recombinant BKV failed and therefore labelling of TC tagged viral proteins with the FlAsh-EDT$_2$ reagent is undetectable. As no co-staining of the viral proteins LT-Ag or VP1 was conducted in this experiment, an efficient infection of RPTEC with recombinant BKV or WT virus cannot be affirmed. In addition, since no positive control was available to verify the detection of TC tagged proteins with the fluorogenic biarsenical reagent FlAsh-EDT$_2$, the functionality of the TC biarsenical labelling system in RPTEC cannot be ensured.

Summarized, insertion of a TC tag consisting of 6 aa into the genome of BKV impairs production of viral progeny. Additionally, fluorescence signals of TC tagged proteins detected after labelling with the membrane permeant fluorogenic biarsenical reagent FlAsh-EDT$_2$ were unchanged for viral fusion proteins and cellular proteins, presumably due to insufficient infection of RPTEC using recombinant BKV. Taken these findings together, the detection of BKV infection by using the functional TC-based fluorescent tag system with recombinant BKV was not achieved.

4.1.2 BKV miRNA-based GFP reporter system

Viral miRNAs are known to play a crucial role during infection by posttranscriptionally regulating viral gene expression [109]. BKV is one of only a subset of PyVs known to encode a miRNA targeting LT-Ag mRNA [107]. It was proposed that the miRNA of BKV modulates viral replication by down-regulating early gene expression through binding to LT-Ag transcripts, as one of the major functions of LT-Ag is the regulation of viral DNA replication [111].

Based on that, in this study, a novel cell-based assay was established that takes advantage of the role of BKV miRNA in the regulation of viral gene expression by binding to its target during BKV infection. It was hypothesized that by fusing the target site for BKV miRNA to a gene coding for a green fluorescent protein (GFP), BKV infection impair translation of GFP due to binding of the BKV miRNA to its target sites. Hence, GFP expression levels should be decreased.

Therefore, a lentiviral construct consisting of the reporter gene GFP fused to 16 target sites for BKV miRNA was used to generate reporter cell lines with stable GFP expression by genome integration into the two human cell lines, HEK293A and RPTEC/TERT1. Theoretically, these cells should exhibit decreased GFP fluorescence intensity levels, upon BKV infection and concomitant miRNA expression. On the other hand, an inhibitor against BKV infection should prevent the down-regulation of GFP by BKV miRNA expression, resulting in unchanged GFP fluorescence intensity levels, as described in Figure 8.

A

3p-miRB1 target site

5` TGCTTGATCCATGTCCAGAGTC

5p-miRB1 target site

5` ATCTGAGACTTGGGAAGAGCAT

B
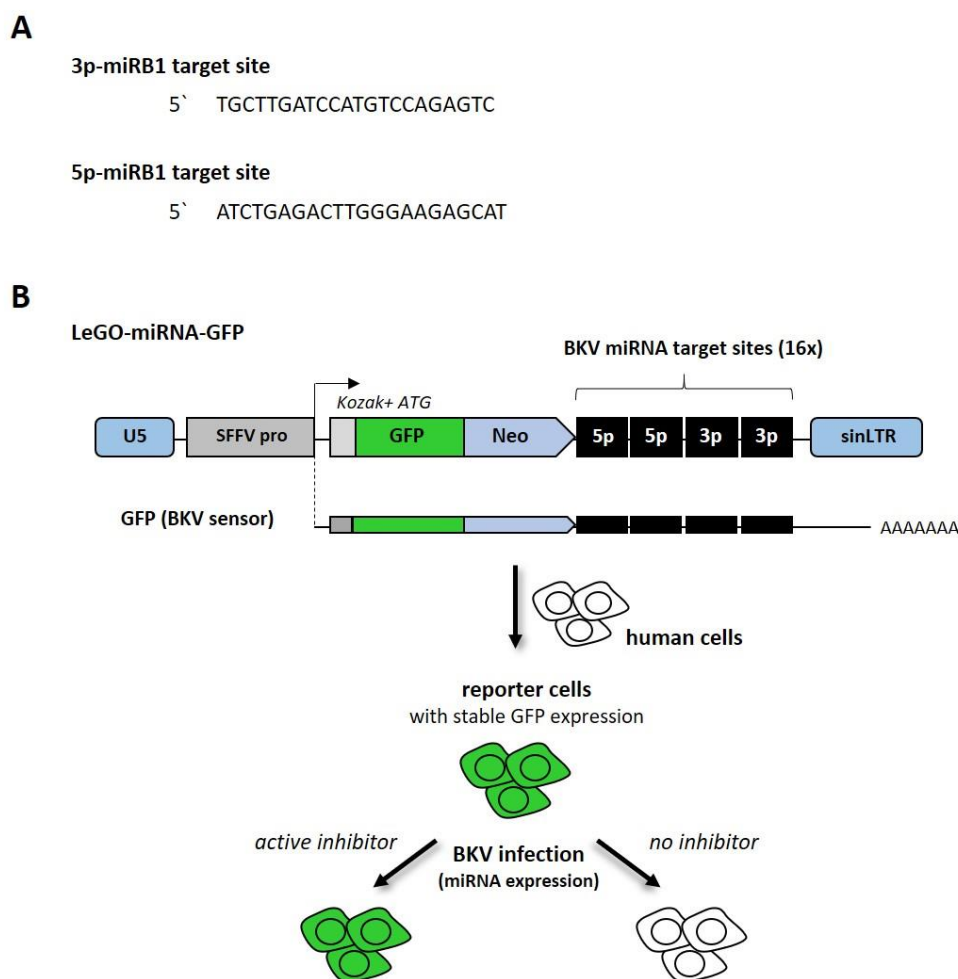
Figure 8: Schematic illustration of BKV miRNA-based GFP reporter system
(A) Sequences of the target sites for BKV miRNAs (3p- and 5p-miRB1). **(B)** The reporter construct LeGO-miRNA-GFP containing 16 BKV miRNA target sites fused to a GFP reporter gene is introduced into two different human cell lines, HEK293A and RPTEC/TERT1 cells, resulting in reporter cells with a stable integrated GFP reporter cassette. In theory, upon BKV infection and concomitant miRNA expression, the BKV miRNA down-regulates GFP expression as a result of binding to its target sites and thus resulting in decreased GFP intensity levels. Contrarily, an active inhibitor against BKV infection should prevent down-regulation of GFP expression upon binding of BKV miRNA to its target sites leading to unchanged GFP intensity levels.

There are two naturally occurring BKV forms, designated archetype and rearranged (rr) strains, which are distinct in the DNA sequence of their NCCR. The archetype form is postulated to be the transmissible form, whereas the rearranged strains were isolated in patients associated with BKV diseases [109]. In general, the NCCR is divided into five sequence blocks: O, P, Q, R and S. While the O sequence block is highly conserved among the rr-BKV strains and contains the ori, the remaining sequence blocks harbor promotor/enhancer elements regulating the expression of early and late genes [93, 95]. The rr-BKV strains are characterized by duplications and deletions of sequence blocks within the NCCR, which alter viral gene expression, replication potency and cytopathology [95].

Since gene expression between rr-BKV strains varies based on the arrangement of the sequence blocks, two different rr-BKV strains, Gardner and Dunlop, were investigated to identify the strain with the

highest miRNA expression levels. The differences in the NCCR sequence of the two rr-BKV strains is presented in Figure 9A. HEK293A cells were infected with either Gardner or Dunlop strain at a MOI of 0.1. 3d and 6d p.i. gDNA was harvested and viral DNA copy numbers were determined based on VP1 as Geq per cell by qPCR analysis, referred to as BKV load. Figure 9B shows that at early and at late time points of infection, the Gardner BKV strain resulted in almost 10-fold higher BKV loads when compared to the Dunlop BKV strain.
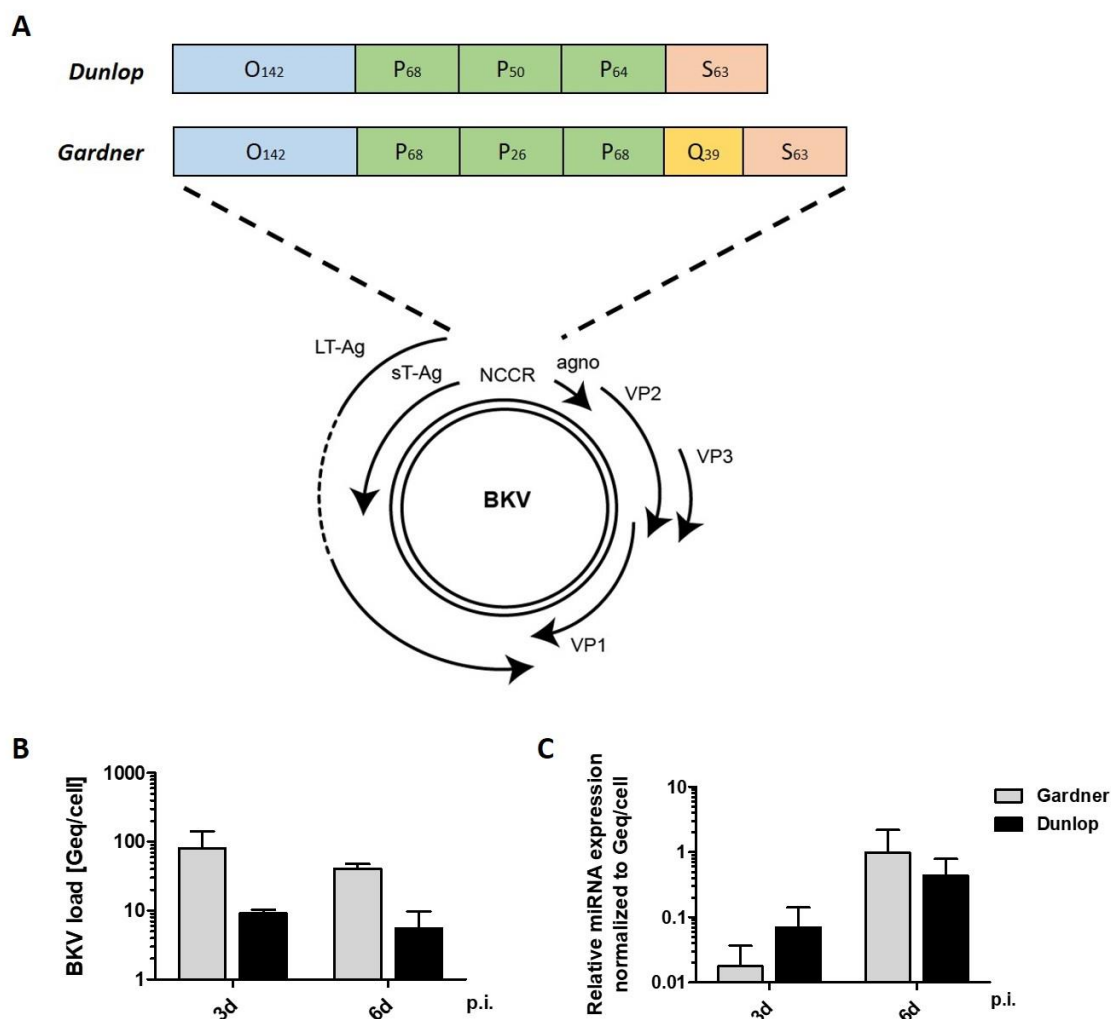
Figure 9: miRNA expression of different rr-BKV strains
(A) Schematic illustration of the BKV genome. The NCCR of the rearranged BKV strains, Gardner and Dunlop, are divided into sequence blocks called O, P, Q, and S. The subscript numerals represent the numbers of base pairs. **(B-C)** Using the two different rearranged BKV strains, Gardner or Dunlop, HEK293A cells were infected at a MOI 0.1. 3d and 6d p.i. gDNA **(B)** or total RNA **(C)** was harvested (n=3). **(B)** Viral DNA copy numbers were quantified by qPCR analysis and normalized to GAPDH. Presented as BKV load in Geq/cell. **(C)** BKV 5p-miRB1 expression was quantified by stem-loop RT-qPCR and normalized to GAPDH. Shown is the miRNA expression per cell relative to BKV load.

Furthermore, 3d and 6d p.i. total RNA was harvested and miRNA expression based on 5p-miRB1 levels, reportedly being the more abundant miRNA of BKV [101], was quantified by stem loop RT-qPCR.

Figure 9C demonstrates that 3d p.i. nearly 10-fold higher miRNA expression levels were detectable using the Dunlop BKV strain compared to Gardner BKV strain, however, overall miRNA expression is hardly detectable in both rr-BKV strains. 6d p.i., both strains exhibited increased miRNA expression levels, albeit miRNA expression still being very low.

This experiment reveals that the miRNA expression was detectable at low levels in both tested rr-BKV strains, with the Dunlop strain exhibiting higher mRNA expression than the Gardner strain at early time points and similar miRNA expression at later time points. Therefore, the Dunlop strain was selected for further infection studies.

To verify the function of the designed miRNA-based GFP reporter system, it was investigated whether binding of BKV miRNA to its target sites down-regulates GFP expression. Therefore, the construct called pcDNA-miRB1, encoding the BKV miRNA (3- and 5p-miRB1) under control of a CMV promoter, was generated to induce BKV miRNA expression independent of BKV replication levels (Figure 10A). Next, it was examined whether transfection of this construct into HEK293A cells results in expression of BKV miRNA. HEK293A cells were transfected with pcDNA-miRB1 and total RNA was harvested 1d, 3d and 6d post transfection (p.t.). Using stem-loop RT-qPCR, BKV miRNA expression based on 5p-miRB1 levels was quantified and miRNA expression levels detected 1d p.t. were used for normalization. Figure 10B shows that transient BKV miRNA expression was detectable at early and late time points, with peaked expression 3d p.t. and 10-fold lower expression 6d p.i. This finding is contrarily to miRNA expression observed in cells upon BKV infection, where miRNA expression increases over time (Figure 9C).
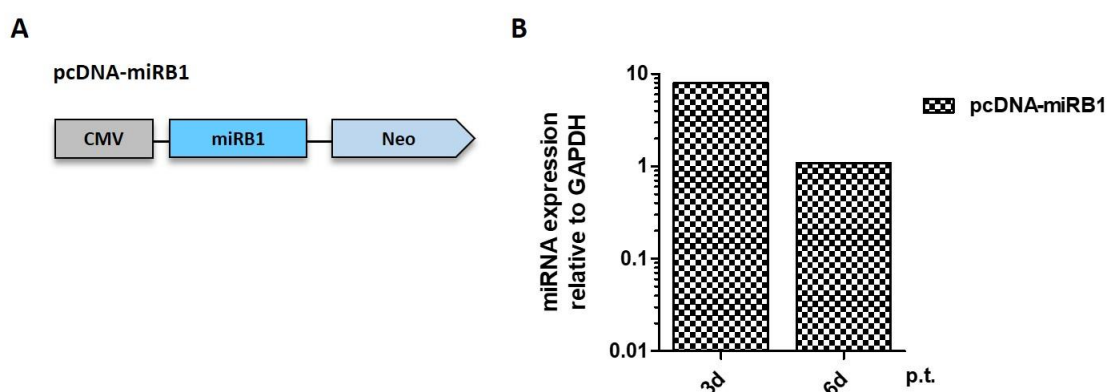
Figure 10: Transient expression of BKV miRNA
(A) Schematic map of the generated construct pcDNA-miRB1 containing the coding sequence of BKV miRNAs (3p- and 5p-miRB1), and a CMV promoter that drives miRNA expression independent of BKV replication. **(B)** HEK293A cells were transfected with pcDNA-miRB1 and total cell RNA was harvested 1d, 3d and 6d p.t. BKV 5p-miRB1 expression was quantified by stem-loop RT-qPCR and normalized to GAPDH. The miRNA expression per cell relative to day 1 is presented (n=2).

To establish a miRNA-based GFP reporter system in HEK293A cells, the generation of HEK293A reporter cells was required. Therefore, a lentiviral construct consisting of the reporter gene GFP fused to 16 target sites for BKV miRNA, was integrated into HEK293A cells resulting in reporter cell lines with stable GFP expression. Since GFP expression observed in the bulk population of these reporter cells was not uniform, one single cell clone, which exhibited medium high GFP intensity levels, was used as HEK293A reporter cells in the subsequent analysis.

In the following, it was investigated whether transient expression of BKV miRNA in HEK293A reporter cells enables binding of BKV miRNA to its target sites and whether this binding results in decreased GFP intensity. Therefore, HEK293A reporter cells were transfected with pcDNA-miRB1 and 3d and 6d p.t. GFP intensity levels were analyzed by flow cytometry. Transient expression of BKV miRNA leads to a 45% reduction of GFP intensity levels 3d p.t. and even a 60% reduction 6d p.t. (Figure 11A, C).

Next, it was analyzed whether infection of HEK293A reporter cells with BKV enables sufficient expression of BKV miRNA to reduce the GFP expression. Therefore, HEK293A reporter cells were infected with BKV Dunlop at a MOI of 10 and 3d and 6d p.i. GFP intensity levels were analyzed by flow cytometry. Figure 11B, C demonstrates that 3d p.i. no reduction of GFP intensity levels was detected. This observation is not surprising, given that BKV miRNA expression upon BKV infection was hardly detectable 3d p.i. (Figure 9C). Strikingly, 6d p.i. GFP intensity levels were decreased by 50% (Figure 11B, C), similar to the reduction of GFP intensity levels observed by transient miRNA expression (Figure 10B).

As GFP intensity levels were only decreased by 50% upon BKV infection, BKV infection of HEK293A reporter cells appears to be inefficient. Therefore, it was investigated whether HEK293A reporter cells are successfully infected by BKV. HEK293A reporter cells were infected with BKV Dunlop at a MOI of 10. 5d p.i. GFP expression and expression of BKV LT-Ag was examined by immunofluorescence analysis using an antigen specific monoclonal antibody combined with DAPI staining of nuclear DNA. Figure 11D demonstrates that approximately 30% of total cells were positive for LT-Ag, indicating low infection efficiency, but in almost all LT-Ag positive cells the signal intensity of GFP was either greatly decreased or not detectable, confirming decreased GFP intensity levels upon BKV infection. These results prove the functionality of the designed miRNA-based GFP reporter system, with decreased GFP intensity levels in the infected reporter cells upon efficient BKV infection and concomitant miRNA expression.
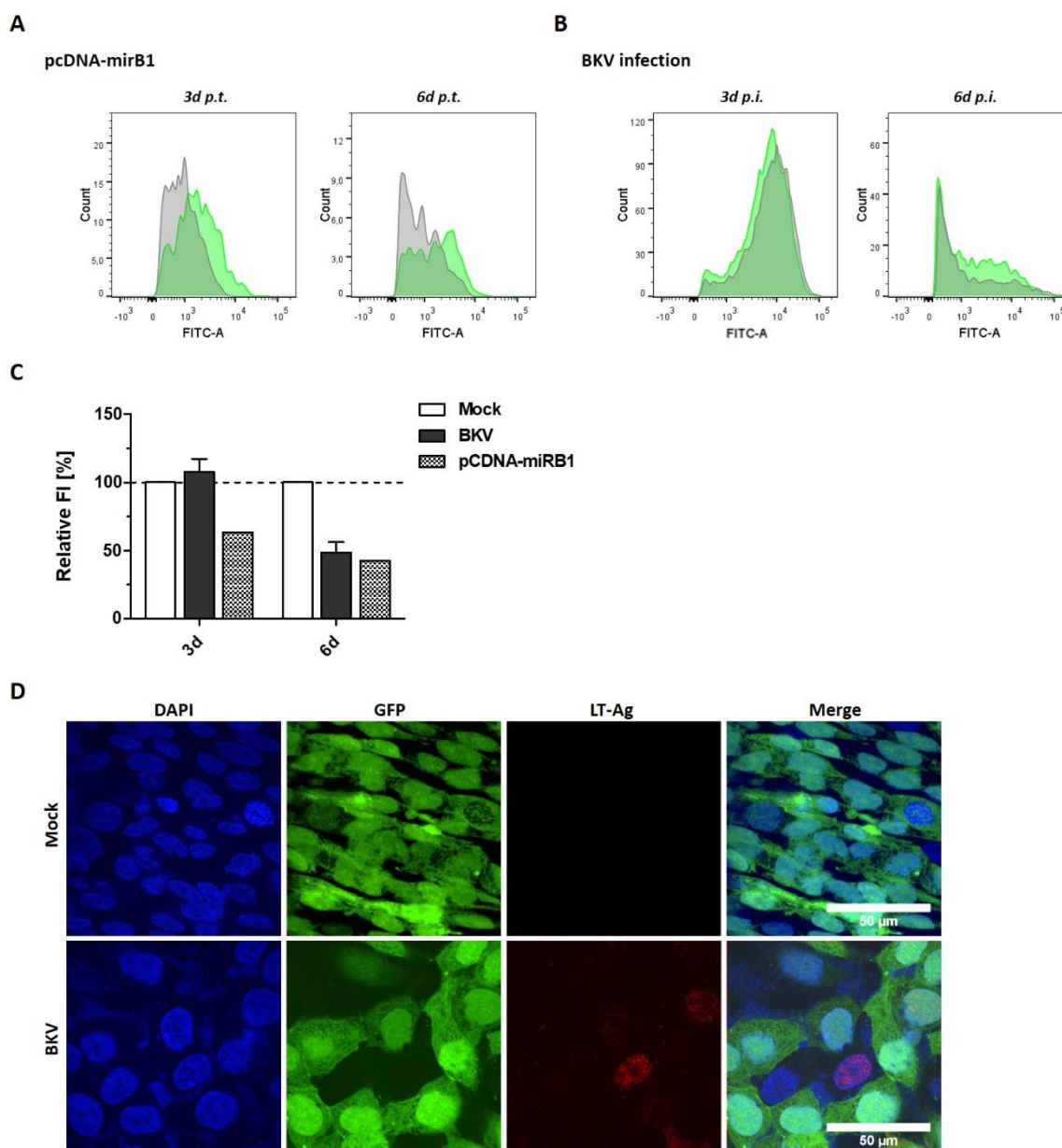
Figure 11: BKV miRNA-based GFP reporter system in HEK293A cells
(A-C) HEK293A reporter cells were either uninfected (Mock, green), infected with BKV Dunlop (grey) at a MOI of 10 (n=3) or transfected with pCDNA-miRB1 (n=1, grey). 3d and 6d p.i. fluorescence intensity (FI) of GFP expression was quantified by flow cytometry. **(C)** Shown is the GFP FI of infected cells normalized to uninfected cells, set to 100%. **(D)** HEK293A reporter cells were uninfected (Mock) or infected with BKV Dunlop at a MOI of 10. 5d p.i. cells were fixed and processed for immunostaining of LT-Ag (red) and DAPI staining of the nuclei (blue). The cells were analyzed by confocal microscopy (Nikon) using a 100x lens and images from 54 different fields were captured (n=1).

The generation of this miRNA-based GFP reporter system was essential in order to establish a cell-based assay that is suitable for an HTS. The criteria for evaluating the suitability of an HTS are mentioned previously. Briefly, a cell-based assay suitable for HTS require consistent expression of a reporter gene, detection of viral infection by measuring fluorescence intensity levels and a high signal to background ratio to distinguish active compounds from non-active compounds. It was shown that

BKV infection of HEK293A reporter cells resulted in an overall decrease of GFP intensity by 50% and microscope analysis indicated that at a single-cell level BKV infection could abolish the GFP signal completely. Although the miRNA-based GFP reporter assay using HEK293A cells fulfilled some criteria for a suitable HTS, performing an HTS of a relatively large compound library at single-cell level is not feasible and the 50% decrease of GFP intensity in the bulk population of reporter cells is probably insufficient to allow a discrimination between active and non-active compounds.

In general, PyVs are characterized by a narrow host tropism regarding both host species and cell type that efficiently promote their replication [134]. Accordingly, viral infections, including steps of viral life cycle like viral entry, gene expression and production of viral progeny, are high diverse between different cell types [32, 87]. While HEK293 cells support propagation and replication of BKV, they are not the host cells of BKV [117] and thus the course of BKV infection, including high infection rates, is not comparable with BKV infection in its natural host cells, which are primary human RPTEC. Since primary cells are not suitable for an HTS due to limited cell numbers and the impossibility of genetic manipulation by introduction of a fluorescent reporter, RPTEC/TERT1 cells were selected as an additional human cell line to establish the miRNA-based GFP reporter system. The RPTEC/TERT1 cell line is derived from RPTEC and has been immortalized using the human telomerase reverse transcriptase (hTert) subunit [148]. Furthermore, it has been reported that the RPTEC/TERT1 cell line overcomes the main disadvantage of primary RPTEC, as they do not experience replicative senescence [149].

In the following experiments, it was investigated whether RPTEC/TERT1 cells are better suited for efficient BKV infection compared to HEK293A cells and whether these cells allow sufficient expression of BKV miRNA to reduce GFP expression in reporter cells.

At first, it was examined whether RPTEC/TERT1 supports efficient BKV infection. Therefore, RPTEC/TERT1 cells were infected with BKV Dunlop using increasing amounts of input virus. 3d and 6d p.i. gDNA was harvested and BKV loads were determined by qPCR analysis. Figure 12A demonstrates that 3d p.i. BKV loads of approximately 5 – 50 Geq/cell (depending on input virus) were detected, with dramatically higher BKV loads 6d p.i. (50 – 5000 Geq/cell), suggesting efficient BKV replication in RPTEC/TERT1 cells at early and late time points of infection. In comparison to the BKV loads observed in HEK293A cells (Figure 9B), the BKV loads detected in RPTEC/TERT1 cells are similar, when using the same MOI of 0.1. However, by infecting RPTEC/TERT1 cells at higher MOIs, e.g. at a MOI of 5 or 10, much higher BKV loads were observed compared to HEK293A cells. The highest BKV load was measured 6d p.i. in RPTEC/TERT1 cells with BKV infection at a MOI of 5.

Furthermore, 3d and 6d p.i. total RNA was isolated and miRNA expression was quantified by RT-qPCR analysis. Figure 12B shows that by infecting RPTEC/TERT1 cells at MOIs of 0.01 – 5 miRNA expression is detectable at similar levels as observed in HEK293A cells 3d p.i. (Figure 9C). This indicates that miRNA

is barely expressed. Interestingly, 6d p.i. the miRNA expression levels detected in HEK293A cells were 10-fold higher compared to levels observed in RPTEC/TERT1 cells. Strikingly, when RPTEC/TERT1 cells were infected at a MOI of 10, 6d p.i. high miRNA expression levels were detectable, indicating that a lot of input virus is required to induce high expression of BKV miRNA in RPTEC/TERT1 cells.
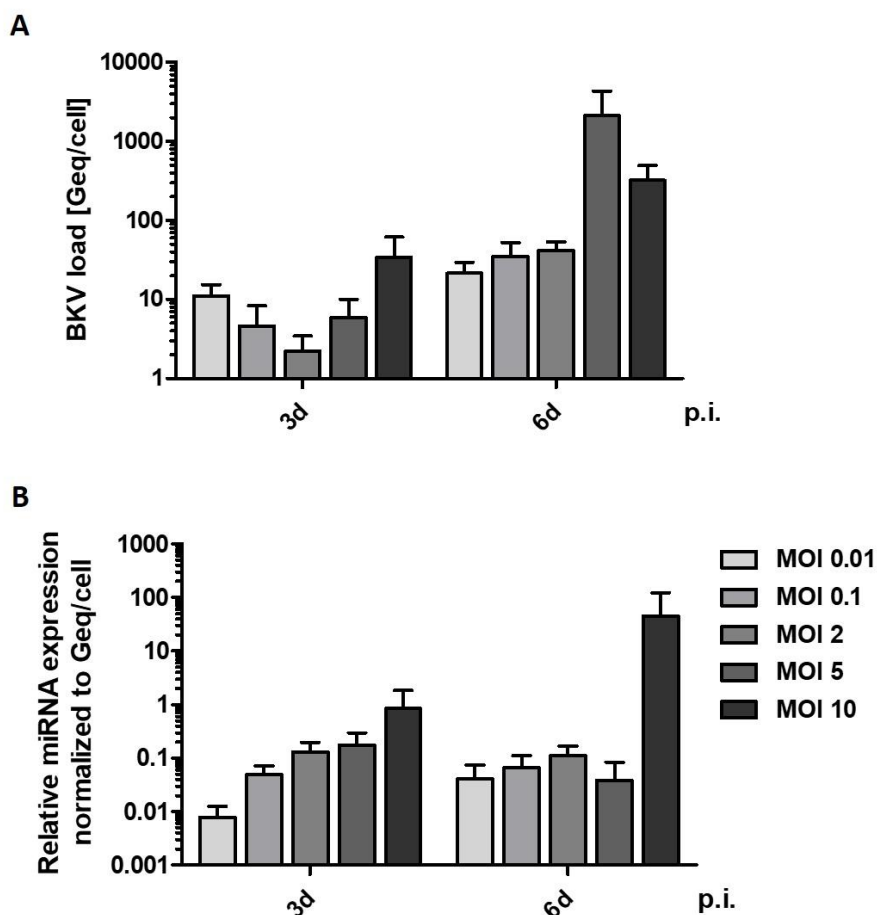

Figure 12: BKV miRNA expression using increasing input virus
RPTEC/TERT1 cells were infected with BKV Dunlop using increasing amounts of input virus. 3d and 6d p.i. gDNA **(A)** or total cell RNA **(B)** were harvested (n=3). **(A)** Viral DNA copy numbers were quantified by qPCR analysis and normalized to GAPDH, shown as BKV load in Geq/cell. **(B)** BKV 5p-miRB1 expression was quantified by stem-loop RT-qPCR and normalized to GAPDH. Shown is the miRNA expression per cell relative to BKV load.

To determine whether the designed miRNA-based GFP reporter system is fully functional in RPTEC/TERT1 cells, it was investigated whether expression of BKV miRNA and subsequent binding to its target sites down-regulates GFP expression. Therefore, a lentiviral construct called LeGO-iC2-miRB1 was generated, allowing expression of BKV miRNAs (3p- and 5p-miRB1) under the regulation of a SFFV promoter, to monitor BKV miRNA expression independent of BKV replication levels (Figure 13A). Subsequently, it was verified whether introduction of this construct into RPTEC/TERT1 cells results in expression of BKV miRNA. RPTEC/TERT1 cells were transduced with LeGO-iC2-miRB1 and total RNA was harvested 1d, 3d and 6d post transduction (p.t.). Using stem-loop RT-qPCR, BKV miRNA expression

based on 5p-miRB1 levels was quantified and miRNA expression levels detected 1d p.i. were used for normalization. Figure 13B shows that high expression of BKV miRNA was detectable at early and late time points at the same levels, indicating that using the construct LeGO-iC2-miRB1 a consistent BKV miRNA expression in RPTEC/TERT1 cells is achieved.
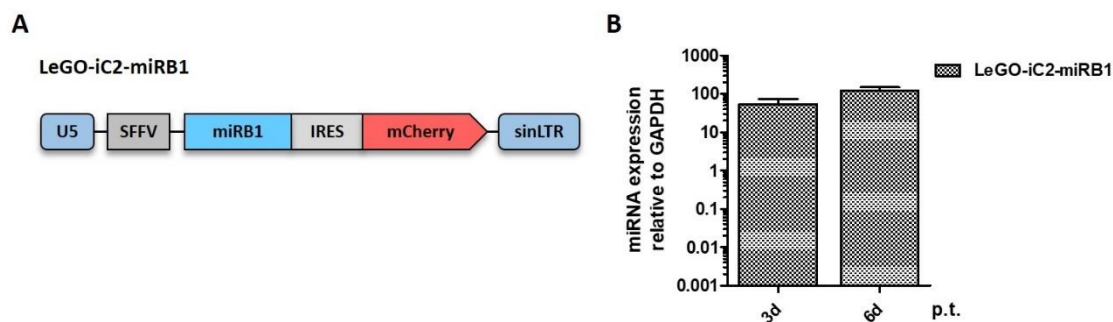
Figure 13: BKV miRNA expression in RPTEC/TERT1 cells
(A) Schematic map of the generated construct LeGO-iC2-miRB1 containing the coding sequence of BKV miRNAs (3p- and 5p-miRB1) fused to an IRES and mCherry reporter gene. A SFFV promoter drives miRNA expression independent of BKV replication. **(B)** RPTEC/TERT1 cells were transduced with LeGO-iC2-miRB1 at a MOI of 1 and total RNA was harvested 1d, 3d and 6d p.t. BKV 5p-miRB1 expression was quantified by stem-loop RT-qPCR and normalized to GAPDH. Shown is the miRNA expression per cell relative to day 1 (n=3).

To establish the miRNA-based GFP reporter system in RPTEC/TERT1 cells, a lentiviral construct consisting of the reporter gene GFP fused to 16 target sites for BKV miRNAs was integrated into RPTEC/TERT1 cells resulting in reporter cell lines with stable GFP expression. Since the GFP expression in the bulk population of these reporter cells was not uniform, one single cell clone expressing GFP at medium high intensity levels was selected and expanded to generate the RPTEC/TERT1 reporter cell line.

In the following experiments, it was examined whether the expression of BKV miRNAs and subsequent binding to its target sites down-regulates GFP expression, assessed in decreased GFP intensity levels. Therefore, RPTEC/TERT1 reporter cells were transduced with the construct LeGO-iC2-miRB1 and GFP intensity levels were detected 3d and 6d p.t. by flow cytometry. In Figure 14A, C it is demonstrated that 3d and 6d p.t. expression of BKV miRNAs in RPTEC/TERT1 reporter cells leads to an 80% reduction of GFP intensity levels further confirming the working principle of this miRNA-based GFP reporter system.

Next, it was investigated whether BKV infection of RPTEC/TERT1 reporter cells allows sufficient expression of BKV miRNAs to induce down-regulation of GFP expression upon miRNA binding to its target sites. Therefore, RPTEC/TERT1 reporter cells were infected with BKV Dunlop at a MOI of 10 and GFP intensity levels were measured 3d and 6d p.i. by flow cytometry. In Figure 14B, C it is shown that 3d p.i. BKV infection results in a merely 15% decrease in GFP intensity levels and 6d p.i.no reduction of

GFP intensity levels was measured. These findings were unexpected, as miRNA expression after transduction with the construct LeGO-iC2-miRB1 resulted in 80% reduced GFP intensity levels (Figure 14C). Additionally, despite the observation of the same miRNA expression levels in HEK293A cells 6d p.i. (Figure 9C) and RPTEC/TERT1 cells 3d p.i. (Figure 12B), the GFP intensity levels in HEK293A reporter cells were decreased by 50% upon BKV infection (Figure 11C), while no decrease of GFP intensity levels was measured in RPTEC/TERT1 reporter cells (Figure 14C).

To determine whether BKV infection of RPTEC/TERT1 reporter cells was inefficient to induce reduction of GFP intensity levels, RPTEC/TERT1 reporter cells were infected with BKV Dunlop at a MOI of 10. 3d p.i. GFP expression and expression of BKV LT-Ag was examined by immunofluorescence analysis using an antigen specific monoclonal antibody and DAPI staining of nuclear DNA. Figure 14D shows that approximately 30% of total cells were positive for LT-Ag, which is similar to the findings in HEK293A reporter cells (Figure 11D), suggesting a low infection rate, but contrarily to the observation in HEK293A reporter cells, GFP intensity in LT-Ag positive RPTEC/TERT1 reporter cells was not decreased. These results show that BKV infection of RPTEC/TERT1 reporter cells does not induce any down-regulation of GFP expression, indicating that these cells are not suitable for establishment of the miRNA-based GFP reporter system.

The generation of this miRNA-based GFP reporter system was essential in order to establish a cell-based assay that is suitable for an HTS of novel inhibitors against BKV infection. The miRNA-based GFP reporter assay using HEK293A cells was not suitable for HTS due to overall low GPF intensity decrease, presumably caused by insufficient BKV infection of reporter cells. Hence, it was hypothesized that by using RPTEC/TERT1 as reporter cells, which were reported to behave similar to primary RPTEC, the poor infection rate could be overcome. However, the findings in this study reveal that BKV infection of RPTEC/TERT1 reporter cells did not induce down-regulation of GFP expression, although high miRNA expression was detectable.

Since the reduction of GFP intensity levels upon BKV infection could not be increased by using RPTEC/TERT1 reporter cells compared to HEK293 reporter cells, it was decided that the established miRNA-based GFP reporter system was not suitable for a primary HTS.
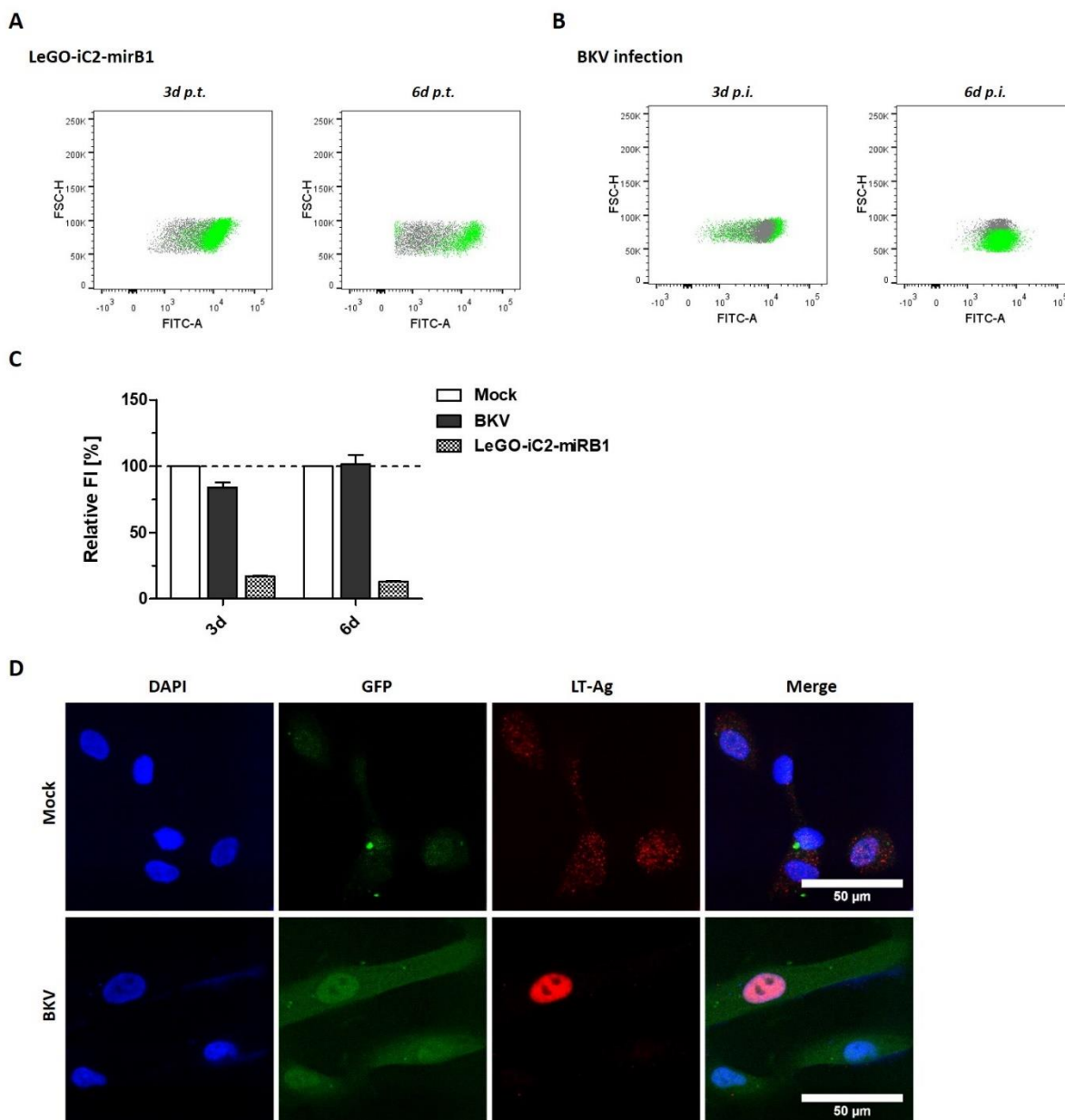
Figure 14: BKV miRNA-based GFP reporter system in RPTEC/TERT1 cells
(A-C) RPTEC/TERT1 reporter cells were either mock infected (green), infected with BKV Dunlop (grey) at a MOI of 10 (n=5) or transduced with LeGO-iC2-miRB1 (grey) at a MOI of 1 (n=3). 3d and 6d p.i. fluorescence intensity (FI) of GFP expression was quantified by flow cytometry. **(C)** GFP FI of infected cells was normalized to mock infected cells, which were set to 100%. **(D)** RPTEC/TERT1 reporter cells were mock infected or infected with BKV at a MOI of 10. 3d p.i. cells were fixed and processed for immunostaining of LT-Ag (red) and DAPI staining of nuclei (blue). The cells were analyzed by confocal microscopy (Nikon) using a 100x lens and images from 125 different fields were captured (n=2).

4.1.3 Phenotypic cell-based assay using SV40

BKV and SV40 are closely related members of the PyV family. They share 70% DNA sequence homology and up to 81% aa homology for the early coding region and 86% aa homology for the late coding region [24]. While BKV infection of human primary RPTEC is characterized by slow viral growth and manifestation of a phenotypically mild CPE arises only after 14d, SV40 exhibits fast and efficient viral

75

growth in the African green monkey cell line CV-1 and induces a CPE 4 to 7d p.i.. Furthermore, using BKV in combination with its natural host cells, primary RPTEC, to establish a cell-based HTS is challenging due to limited number of cell population doublings and inability of genetic manipulation of primary cells by introducing a fluorescence reporter to detect viral infection. On the other hand, SV40 in combination with CV-1 cells overcome the restrictions of *in vitro* cell culture systems experienced with BKV and primary RPTEC, given that CV-1 cells are characterized by rapid cell growth, no restriction in cell numbers and the ability to introduce a fluorescent reporter for stable reporter gene expression.

Considering the benefits of *in vitro* cell culture systems using SV40 and the close relationship of SV40 and BKV, SV40 infection of CV-1 cells was used for the establishment of an HTS to screen for novel inhibitors active against this PyV class. This cell-based assay was designed based on morphological changes induced by the SV40 and by taking advantage of a CPE, occurring in cells efficiently infected with SV40. Sensor cell lines with a stable integrated RFP reporter cassette were generated and RFP intensity levels were utilized as a measure for cell viability. In principle, SV40 infection of these reporter cells induces a CPE that is detectable by greatly decreased RFP intensity levels. An active inhibitor against SV40 should prevent cell death, resulting in RFP intensity levels similar to uninfected cells (Figure 15).
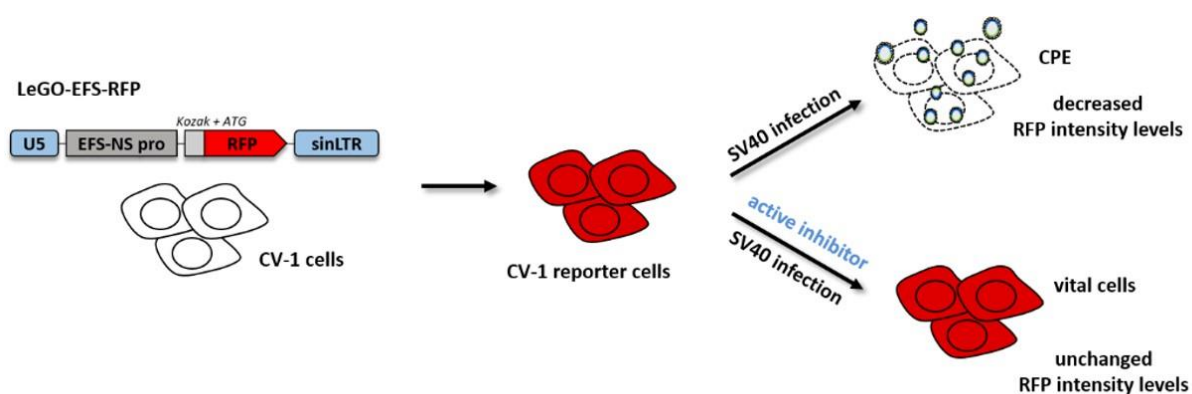
Figure 15: Work flow of the phenotypic cell-based assay using SV40 as a surrogate virus for BKV
The EFS-RFP reporter cassette was transduced into CV-1 cells and cells with integrated RFP reporter were selected by Neomycin. SV40 infection with concomitant CPE leads to decreased RFP expression, while an active inhibitor might prevent cell death resulting in unchanged RFP expression.

To establish a phenotypic cell-based system using SV40 as a surrogate virus for BKV, the generation of CV-1 reporter cells was required. Therefore, a lentiviral construct consisting of the reporter gene RFP was integrated into CV-1 cells resulting in a reporter cell line with stable RFP expression. Since the RFP expression observed in the bulk population of these reporter cells was not uniform, three single cell

clones, which exhibit high RFP intensity at same levels, were combined to generate CV-1 reporter cells that were used in the subsequent analysis.

In the following experiments optimal conditions for an HTS were determined by identifying the MOI required for a visible CPE and the sensitivity of the screen by using known inhibitors against PyV infection.

To explore the MOI required for detection of a CPE induced by SV40 infection, CV-1 reporter cells were infected with increasing amounts of input virus. 4d and 6d p.i. RFP intensity levels were determined by measuring fluorescence intensity at excitation wavelength of 540 nm and emission wavelength of 590 nm using a microplate photometer. Figure 16A demonstrates that 4d p.i. SV40 infection at a MOI of 50 and 100 results in 40 – 60% reduction of RFP intensity levels, while no decrease of RFP intensity levels was observed, when reporter cells were infected at a MOI of 10. Furthermore, 6d p.i. SV40 infection at a MOI of 10 induces 60% decrease of RFP intensity levels and SV40 infection at a MOI of 50 and 100 achieves reduction of RFP intensity levels by 90%. Additionally, morphological changes of the reporter cells upon SV40 infection were observed by microscopic analysis confirming that 6d p.i. SV40 infection at a MOI of 50 results in a complete CPE that is detectable in highly decreased RFP intensity levels (Figure 16B).
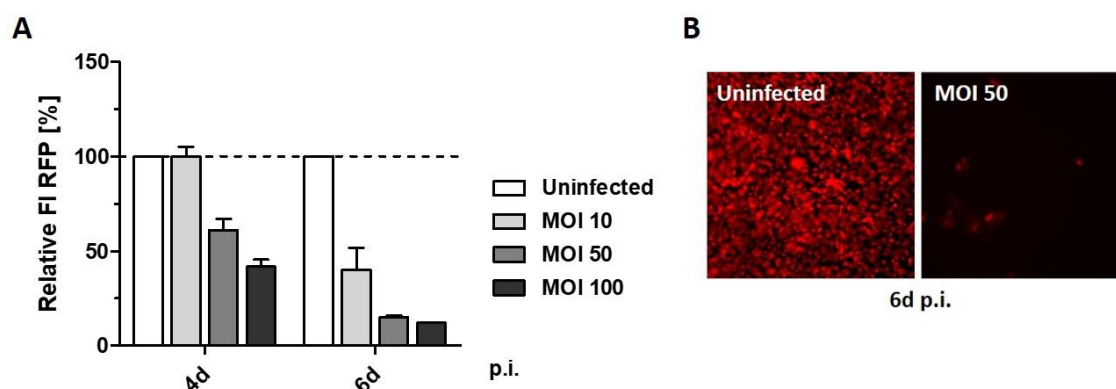
Figure 16: Phenotypic cell-based assay using SV40
(A) SV40 Titration. CV-1 reporter cells were either left uninfected or infected with BKV using increasing amounts of input virus. 4 or 6 days p.i. fluorescence intensity of RFP (FI RFP) was measured with a microplate photometer (Tecan). FI RFP of infected cells were normalized to uninfected cells, which were set to 100%. **(B)** Effect of SV40 infection on cell morphology. CV-1 reporter cells were either uninfected or infected with BKV at a MOI of 50. 6d p.i. cells were analyzed using a microscope (Leica) with a 20x magnification.

In the next experiment it was verified whether cell death of CV-1 reporter cells is detectable by a decrease in RFP intensity levels. Therefore, the protein kinase inhibitor Staurosporine, a cell permeable alkaloid inducing apoptosis [150], was used as a positive control. In order to determine the concentration of Staurosporine required to induce cell death, CV-1 reporter cells were treated with increasing amounts of Staurosporine and cellular viability was determined by MTT assay.

Figure 17A shows that treatment with Staurosporine at 50 and 100 nM led to cell death observed in 95% of CV-1 reporter cells. To compare the influence of Staurosporine treatment to the effect of SV40 infection regarding RFP intensity levels, CV-1 reporter cells were either infected with SV40 at a MOI of 50 or left uninfected and additionally treated with Staurosporine at 50 nM. 6d p.i. RFP intensity levels were determined using a microplate photometer. Figure 17B shows that SV40 infection of untreated CV-1 reporter cells resulted in an 80% decrease of RFP intensity levels, with the same decrease detected in infected CV-1 reporter cells treated with Staurosporine. Consensually, treatment with Staurosporine induced an equal reduction of RFP intensity levels in uninfected CV-1 reporter cells. These results confirm that cell death of CV-1 reporter cells, either induced by SV40 infection or by treatment with Staurosporine, is detectable by greatly decreased RFP intensity levels.
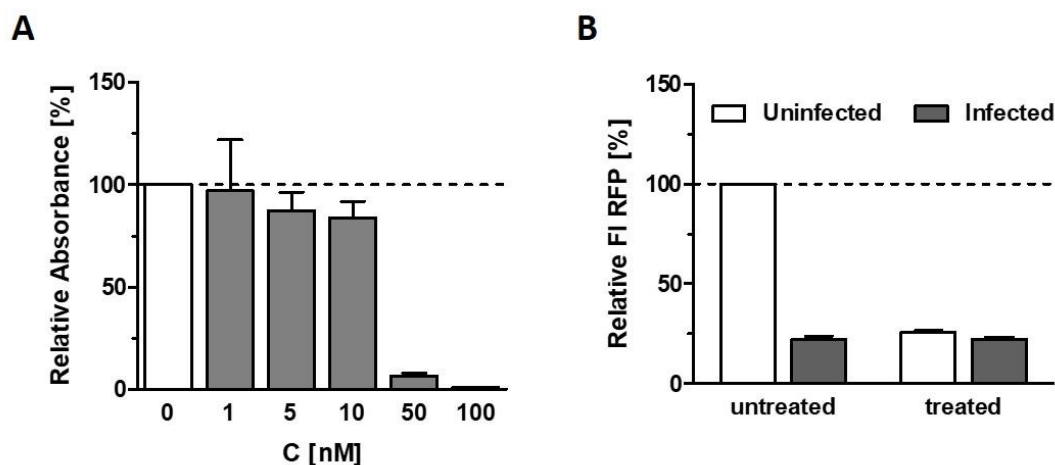
Figure 17: Impact of Staurosporine treatment on CV-1 reporter cells
(A) Effect of Staurosporine titration on cellular viability. CV-1 reporter cells were either left untreated or treated with increasing amounts of Staurosporine, before analysis of cell viability by an MTT assay. **(B)** Influence of Staurosporine treatment on RFP expression. CV-1 reporter cells were either left uninfected or infected with BKV at a MOI of 50, and either left untreated or treated with Staurosporine (50 nM). 6d p.i. FI RFP levels were measured with a microplate photometer (Tecan). FI RFP of uninfected and untreated cells was set to 100%.

Next, it was investigated whether an established inhibitor against SV40 infection can prevent cell death and whether its inhibitory activity can be detected by measuring RFP intensity levels of CV-1 reporter cells. It was hypothesized that RFP intensity levels of infected CV-1 reporter cells, which were treated with an inhibitor active against SV40 infection, should be increased compared to the RFP intensity levels of untreated but infected CV-1 reporter cells. As active inhibitors the known antiviral inhibitors Cidofovir (CDF) and Hexachlorophene (HXC) were analyzed. HXC is reported to inhibit LT-Ag ATPase activity of SV40 and BKV *in vitro* [151]. The nucleoside analogue CDF is licensed for the treatment of CMV retinitis in AIDS patients and *in vitro* studies showed a broad-spectrum antiviral activity against herpes-, papilloma- and polyomaviruses [59]. CDF is effective against herpesviruses by inhibiting the

viral DNA polymerase. However, its inhibitory mechanism against PyVs is unclear as PyVs hijack a cellular DNA polymerase for their replication [60].

To examine whether treatment with CDF or HXC induces cell death, CV-1 reporter cells were treated with either CDF or HXC at 10 µM and after 6d of incubation, cellular viability was determined by MTT assay. Treatment with DMSO was used as vehicle control. Figure 18A shows that HXC treatment resulted in cell death in 20% of CV-1 reporter cells, while CDF treatment induced cell death in 40% of CV-1 reporter cells indicating a more toxic potential of CDF compared to HXC.
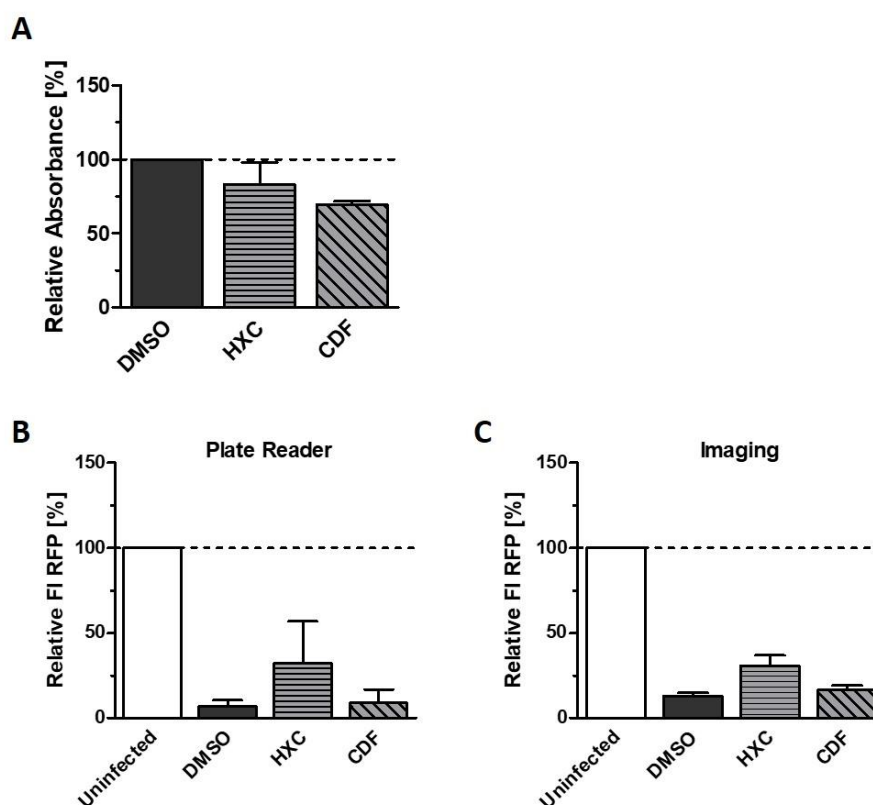
Figure 18: Influence of CDF or HXC treatment on cellular viability and RFP expression
(A) Cell viability was determined by MTT assay after 6d of incubation. Absorbance of uninfected cells treated with HXC or CDF were normalized to uninfected cells treated with DMSO, which were set to 100%. **(B, C)** 6d p.i. FI RFP was measured by multi-mode microplate reading and automated digital wide field microscopy (BioTek). The RFP intensity of infected reporter cells, treated with either DMSO or one of the known inhibitors HXC and CDF, was normalized to uninfected cells, which were set to 100%.

Next, it was investigated whether the reported inhibitory activity of CDF and HXC against SV40 infection is detectable by measuring RFP intensity levels of CV-1 reporter cells. Therefore, CV-1 reporter cells were either left uninfected or infected with SV40 at a MOI of 50 and additionally treated with either CDF or HXC at 10 µM. 6d p.i. RFP intensity levels were determined using a microplate photometer, referred to as plate reader. Figure 18B demonstrates that SV40 infection of DMSO treated CV-1 reporter cells resulted in a 90% decrease of RFP intensity levels. However, treatment with HXC

induced a 60% decrease of RFP intensity levels, while treatment with CDF led to an 80% decrease. Similar results were observed, when RFP fluorescent intensity levels were detected by microscopic analysis, referred to as imaging (Figure 18C). These findings indicate that HXC exhibits a higher inhibitory activity than CDF and the CPE induced by SV40 infection is attenuated by treatment with HXC, but not by treatment with CDF.

These results demonstrate that the established phenotypic cell-based system allows reproducible detection of SV40 infection by measuring RFP intensity levels of CV-1 reporter cells either by using a microplate photometer or by microscopic analysis. Independent experiments show that infection with SV40 decreased RFP intensity levels by $80-90\%$. Additionally, the present findings reveal the detection of viral infection with high sensitivity, enabling detection of compounds exhibiting various inhibitory activity against SV40 infection. Furthermore, it was shown that the known inhibitor HXC hampers cell death induced by SV40 infection, measurable by increased RFP intensity levels. However, RFP intensity levels of CV-1 reporter cells upon treatment with HXC were increased by $10-20\%$ compared to RFP intensity levels of untreated CV-1 reporter cells, indicating that HXC is a weak inhibitor against SV40 infection.

Taken together all the previous findings presented in this study, the phenotypic cell-based system using SV40 as a surrogate virus for BKV has been proven as a suitable primary HTS to screen for novel inhibitors against this PyV class. Despite the weak inhibitory activity of HXC, this inhibitor was chosen as a reference inhibitor control, with the expectation to identify novel inhibitors exhibiting stronger inhibitor activity against PyV infection.

4.2 Identification of novel small molecule inhibitors active against PyV infection

Using the established phenotypic cell-based assay with SV40 as a surrogate virus for BKV, a primary HTS of a library consisting of approximately 28,000 small molecule inhibitors was conducted in order to identify novel inhibitors against this PyV class. This library was created by merging four different compound libraries bought from the companies Enamine or ChemDiv, and comprises novel small molecule compounds, which were not screened before for their antiviral activity. Hence, the primary HTS performed in this study represents a novel non-target-based screening approach.

Compounds identified as active against SV40 infection were further validated for their inhibitory activity against BKV infection in a secondary screen. Additionally, selected hit compounds were analyzed for broad range activity against infection with JCV and MuPyV.

4.2.1 Novel SV40 inhibitors identified in a phenotypic cell-based HTS

By using a robotic, BSL-2 compatible, high throughput system approximately 28,000 small molecule compounds were screened for their inhibitory activity against SV40 infection. CV-1 reporter cells seeded in 384-well plates were either left uninfected or infected with SV40 at a MOI of 50 and treated with DMSO, HXC or test compounds in duplicates at a final concentration of 10 µM. 6d p.i. RFP intensity levels were determined by multi-mode microplate reading (Figure 19A) and automated digital wide field microscopy capturing one image of the whole well (Figure 19B). The fluorescence intensity of RFP (FI RFP) represent the inhibitory activity of each compound. Uninfected cells were used as a positive control (FI RFP = 100%), while DMSO treated cells were used as a negative control (FI RFP = 0%) and HXC served as a reference inhibitor control. For each 384-well plate a total of 114 test compounds were evaluated for their inhibitory effect while normalizing their FI RFP levels to positve and negative controls present on each plate. In Figure 19A-B, the relative FI RFP in percentage of each compound is presented with regard to the corresponding plate number.

The majority of tested compounds exhibited no antiviral effect against SV40 infection (FI ≤ 0%), as depicted in Figure 19A-B. Only for 10 test compounds FI RFP levels over 50% were detected in infected CV-1 reporter cells. However, the reference inhibitor HXC exhibited a high variance in its influence on FI RFP of infected CV-1 reporter cells with FI RFP values varying between 5% and 30%. Furthermore, FI RFP detected with microscopic analysis, referred to as imaging, or microplate photometer, referred to as plate reader, exhibited different signal to noise ratios. Using the plate reader, the background level is narrowly distributed and only compounds inducing great changes of FI RFP in CV-1 reporter cells are clearly detectable (Figure 19A). Otherwise, detecting FI RFP using microscopic analysis revealed broadly distributed background levels but higher sensitivity for differences in FI RFP induced by tested compounds allowing the identification of compounds with weak or strong inhibiory activity against SV40 infection (Figure 19B).

In addition to the measurement of FI RFP, in this primary HTS the toxic potential of each compound was analyzed. Therefore, CV-1 reporter cells seeded in 384-well plates were treated with DMSO, HXC or test compounds in duplicates at a final concentration of 10 µM. After 6d of incubation, cellular viability was determined by MTT assay. Figure 19C demonstrates that treatment with some compounds induced cell death, while other compounds even resulted in cell growth or had no effect on cell viability. Only compounds, which did not result in a great decrease in cell viability (MTT absorbance > 50%) were included in further analyses.

A

B
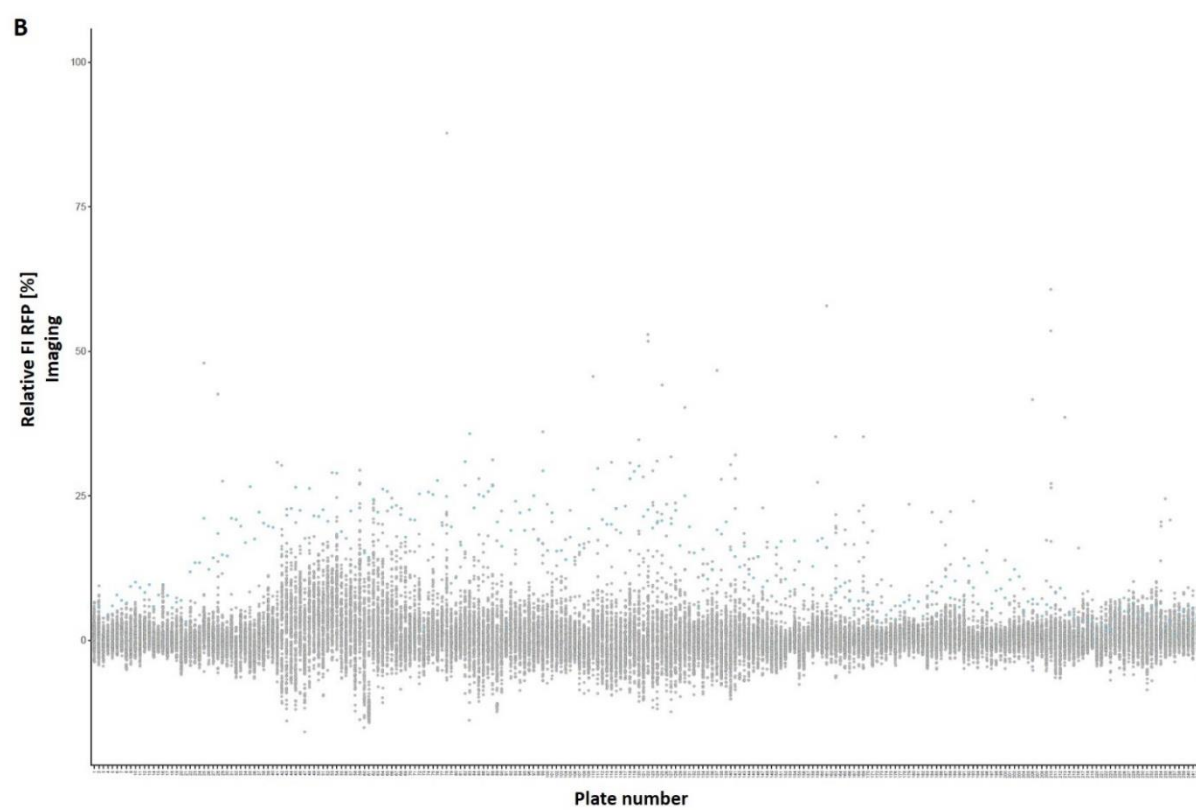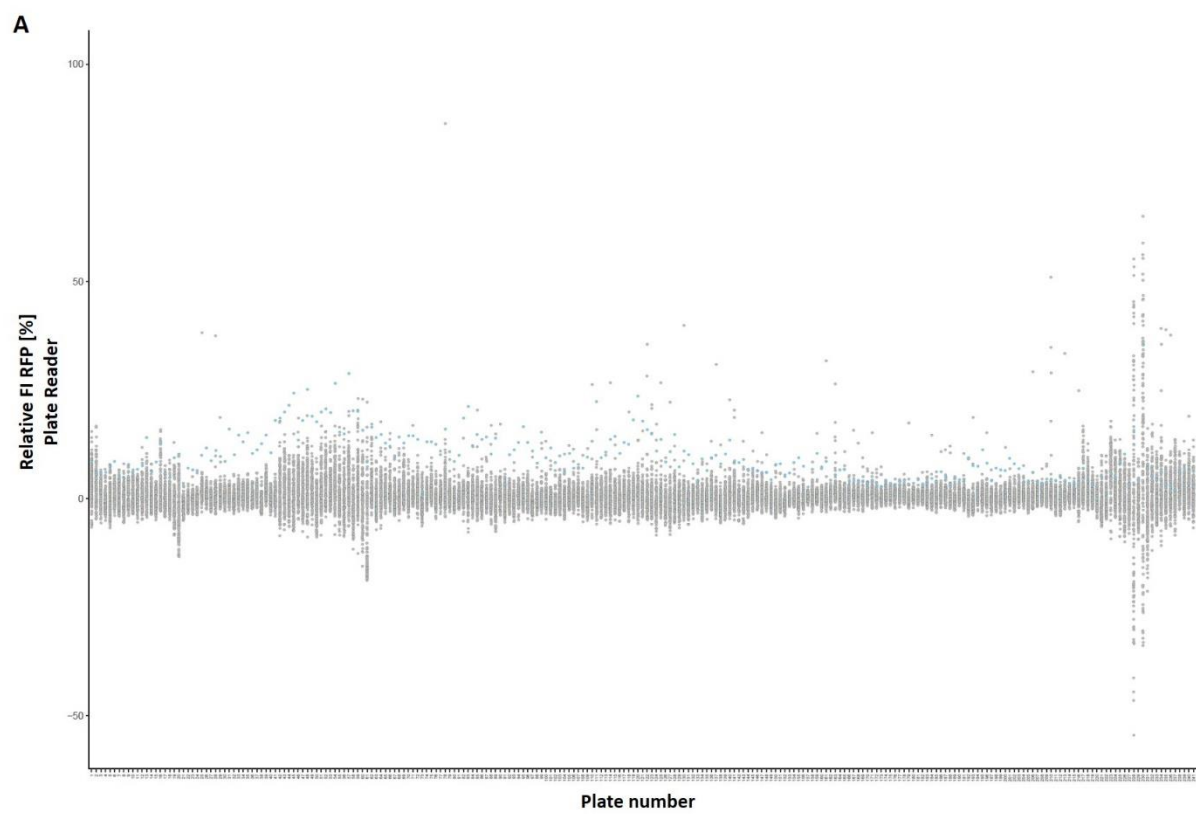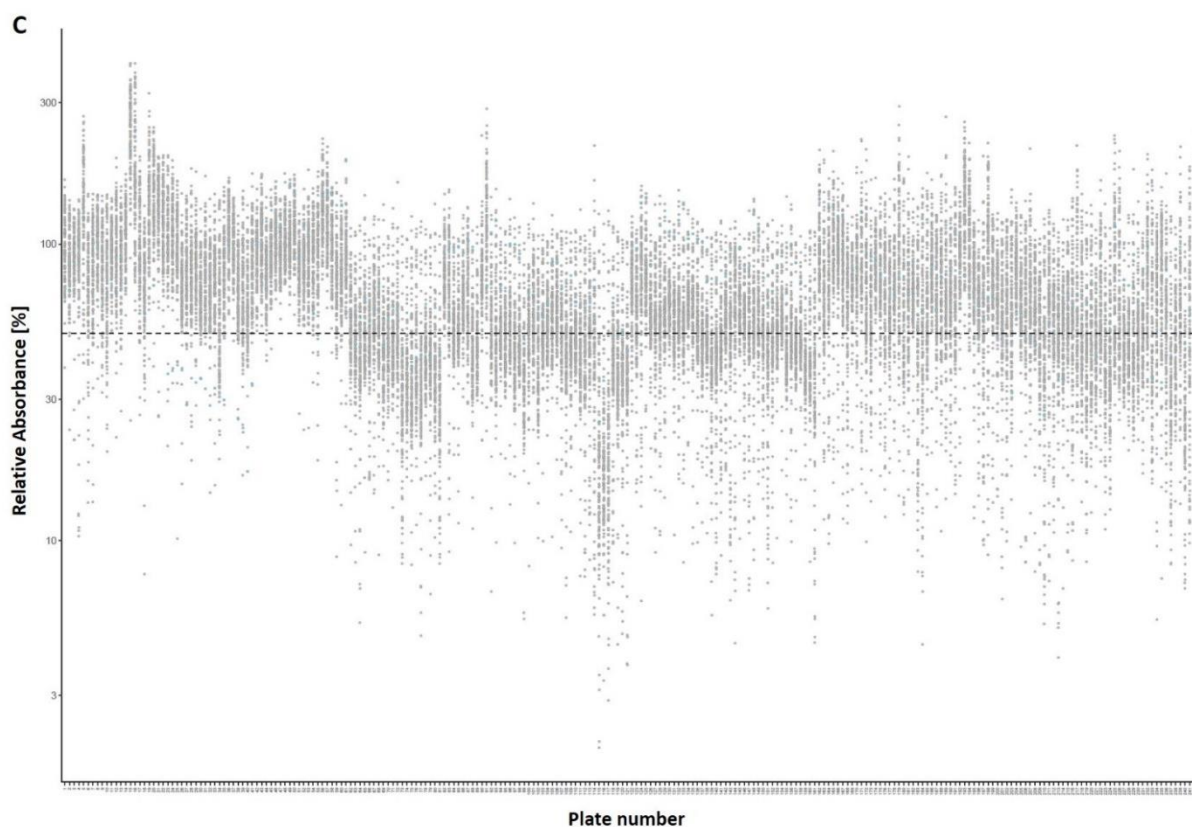
Figure 19: Phenotypic HTS for small molecule inhibitors active against SV40 in CV-1 cells
Compounds from a library consisting of approximately 28,000 small molecule inhibitors were analyzed at a final concentration of 10 µM (grey circles). Cells treated with HXC are shown in blue circles. FI RFP, detected by plate reader **(A)** or imaging **(B)** of uninfected cells were set to 100%, while the FI RFP of infected cells treated with DMSO was set to 0%. FI RFP of infected cells treated with HXC or new putative compounds were normalized to controls. **(C)** Cell viability was determined by MTT assay. Shown is the mean absorbance of uninfected cells treated with HXC or new compounds normalized to the median absorbance of uninfected cells treated with DMSO, which was set to 100%.

Since the FI RFP levels of infected CV-1 reporter cells treated with the reference inhibitor control HXC varied between different plates, evaluation and corresponding selection of compounds that inhibit SV40 infection was performed plate-wise. Evaluation of 243 plates was conducted in total. For hit selection two different cut-offs were set. First, compounds are considered as hits, if their FI RFP, detected by both imaging and plate reader, is greater than or equal to 20%. The second cut-off is based on the fold change of the FI RFP of tested compounds compared to the FI of the reference inhibitor HXC, which was set to 1. Compounds are considered as hits, if their fold change is greater than or equal two. In Figure 20 the hit selection is shown representatively by demonstrating the data evaluation of three different plates. The plate with number 78 shows the selection of hits matching both cut-offs (Figure 20A, D), while the plate with the number 59 depicts the identification of hits, selected only with the first cut-off (Figure 20B, E), and the plate with the number 222 demonstrates the identification of hits, selected only based on the second cut-off (Figure 20C, F).
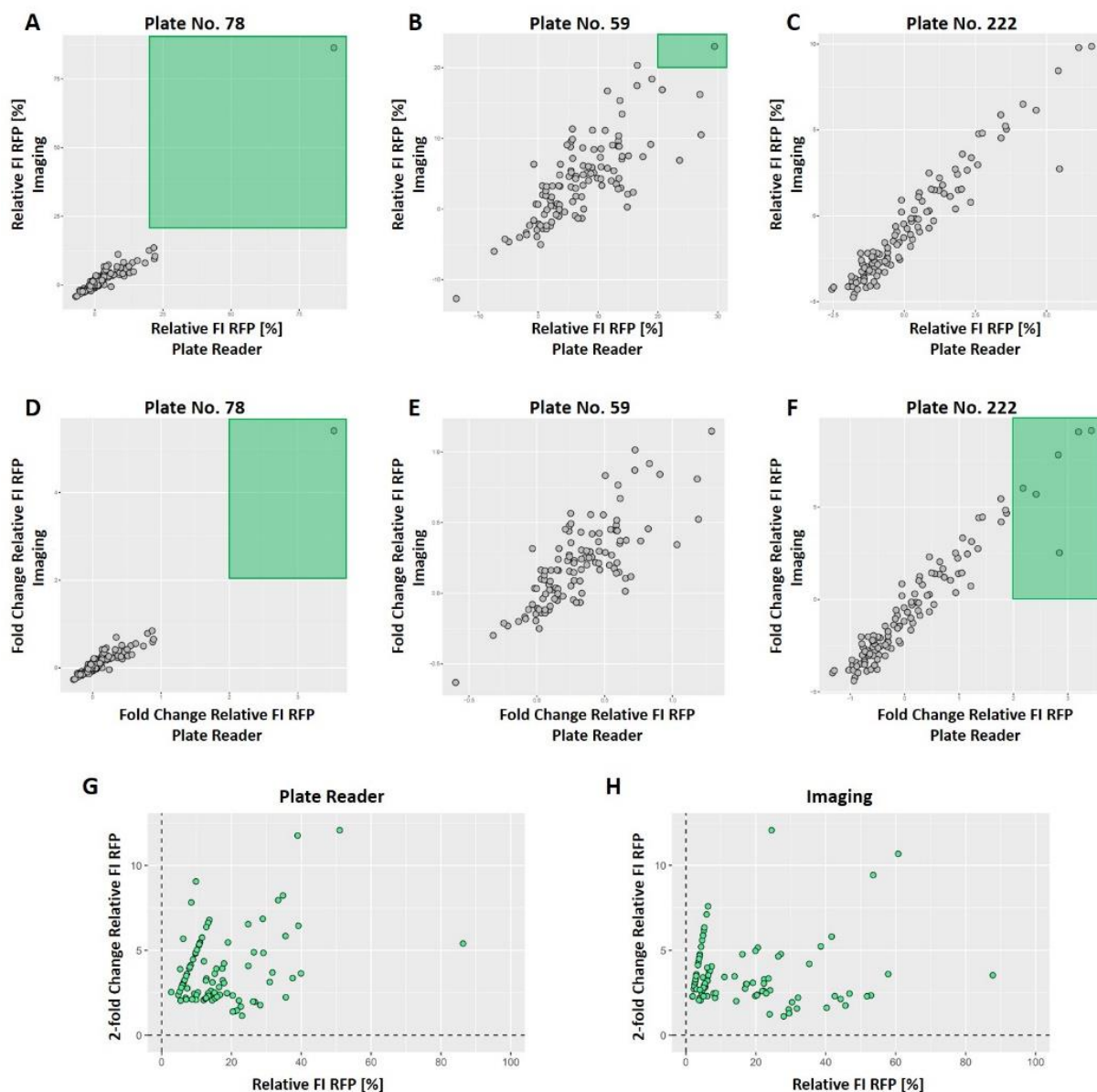
Figure 20: Selection of hit compounds inhibiting SV40 infection in primary HTS
Selection of hit compounds was performed plate-wise by setting two different cut-offs: Relative FI RFP is greater than or equal to 20%, or fold change relative FI RFP is greater than or equal 2. Shown here is representative data evaluation of three different plates. Data sets necessary for hit selection using the first cut-off are presented in A-C. Data sets required for hit selection using the second cut-off are shown in D-F. Relative FI RFP necessary for the first cut-off and 2-fold change relative FI RFP required for the second cut-off of the top 98 selected compounds, detected by plate reader are shown in G, whereas the corresponding data detected by imaging is presented in H.

In the primary HTS, the first cut-off enables selection of 26 compounds, whereas using the second cut-off 84 compounds were selected, resulting in 111 hits in total with 16 compounds matching both cut-offs. Since the companies Enamine and ChemDiv no longer supplied 13 compounds for re-ordering, 98 compounds were chosen as potential inhibitors active against SV40.

As depicted in Figure 20G and 20H, the hit selection by using both cut-offs does not correlate between all evaluated plates. For example, data evaluation of some plates revealed that treatment with a test

compound led to a detection of 80% RFP intensity levels, indicating high inhibitory activity, but exhibited only a 5-fold change compared to the reference inhibitor control HXC. Whereas treatment with other compounds resulted in FI RFP of 10% but a fold change of 10 compared to the reference inhibitor control HXC. Therefore, it was important to use two cut-offs for the hit selection and to verify the inhibitory activity of selected compounds in a subsequent confirmatory screen.

To perform a confirmatory screen of selected hit compounds, CV-1 reporter cells seeded in 384-well plates were either left uninfected or infected with SV40 at a MOI of 50 and treated with DMSO, HXC or the 98 hit compounds in 12 replicates at a final concentration of 10 µM. 6d p.i. similar to primary HTS (Figure 19A, B), FI RFP levels were determined by multi-mode microplate reading (plate reader) and automated digital wide field microscopy (imaging). Figure 21A demonstrates that detecting FI RFP by imaging results in a higher signal to noise ratio compared to FI RFP detected by plate reader, indicating that imaging represents a more sensitive detection method for fluorescence intensity levels. However, Figure 21B shows that fold change levels of FI RFP measured by imaging correlates with fold change levels of FI RFP determined by plate reader, with only a few exceptions. Compounds resulting in fold change values greater than or equal 2 are depicted in red. Compounds with fold change values less than 2 but greater than or equal to 1 are depicted in green. Whereas compounds with fold change values less than 1 but greater than or equal to 0.5 are presented in yellow, and compounds with fold change values less than 0.5 are delineated as grey circles. Overall, 33 compounds were identified with fold change values greater than or equal to 0.5 (yellow, green, red) compared to HXC (blue), indicating diverse inhibitory activity against SV40 infection.

Figure 21C represents the correlation between the fold change FI of 98 hit compounds, identified in the primary HTS, and their fold change FI measured in the confirmatory screen. In the primary HTS approximately 28,000 small molecule inhibitors were analyzed in duplicates and 98 compounds were selected as hits (0.35% of all tested compounds). In a confirmatory screen, these 98 compounds were re-screened in 12 replicates to reduce the false positive rate. Out of these 98 selected hit compounds, 33 compounds were confirmed as truly active inhibitors against SV40 infection (approximately 0.12% of all tested compounds). These 33 compounds were selected for further analysis regarding their inhibitory activity against BKV infection in a secondary screen.
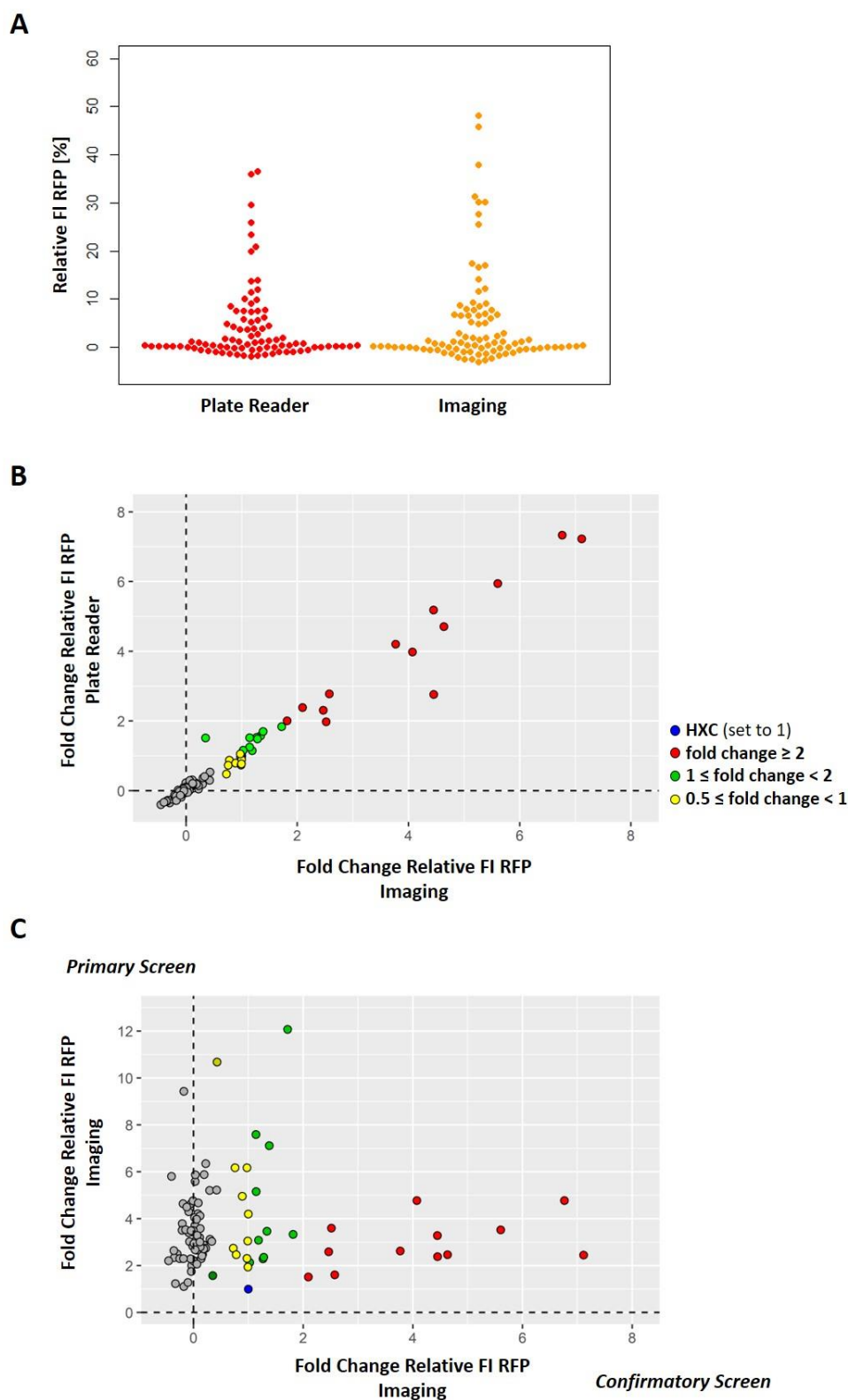
Figure 21: 33 out of 98 compounds were confirmed with high inhibitory activity against SV40 in CV-1 cells
(A) FI RFP, detected by imaging or plate reader, of uninfected cells was set to 100%, while FI RFP of infected cells treated with DMSO were set to 0%. FI RFP of infected cells treated with HXC or new compounds was normalized to the controls. **(B)** FI RFP of infected cells treated with HXC was set to 1, and relative FI RFP of new compounds was normalized to it. Shown here is the fold change expression of RFP intensity, detected by imaging or plate reader, respectively. **(C)** Correlation between fold change relative FI RFP of 98 hit compounds, identified in the primary HTS, and their fold change relative FI RFP examined in the confirmatory screen.

86

4.2.2 Novel BKV inhibitors identified in a secondary screen

In a secondary screen the top 33 compounds, identified in primary screening, were investigated for their inhibitory activity against infection with the human PyV BKV. Therefore, primary human RPTEC were either left uninfected or infected with BKV at a MOI of 5 and treated with 33 hit compounds or DMSO as a negative control and HXC or CDF as reference inhibitor controls. 6d p.i. gDNA from cells and viral supernatant was harvested and viral DNA copy numbers were determined as Geq by qPCR analysis. Geq examined from gDNA isolated from cells are termed intracellular BKV load, whereas Geq examined from gDNA extracted from viral supernatant refer to the extracellular BKV load. Figure 22 shows that treatment with HXC led to 90% decrease in intracellular and extracellular BKV load, whereas treatment with CDF reduced intracellular BKV load by 65% (Figure 22A) and extracellular BKV load by 75% (Figure 22B). While 17 compounds exhibited either no inhibitory activity against BKV infection or an inhibitory activity less than the detected inhibitory activity of CDF, 16 compounds significantly decreased intracellular and extracellular BKV load to a greater extent than CDF, and 9 compounds even induced a lower BKV load compared to HXC.
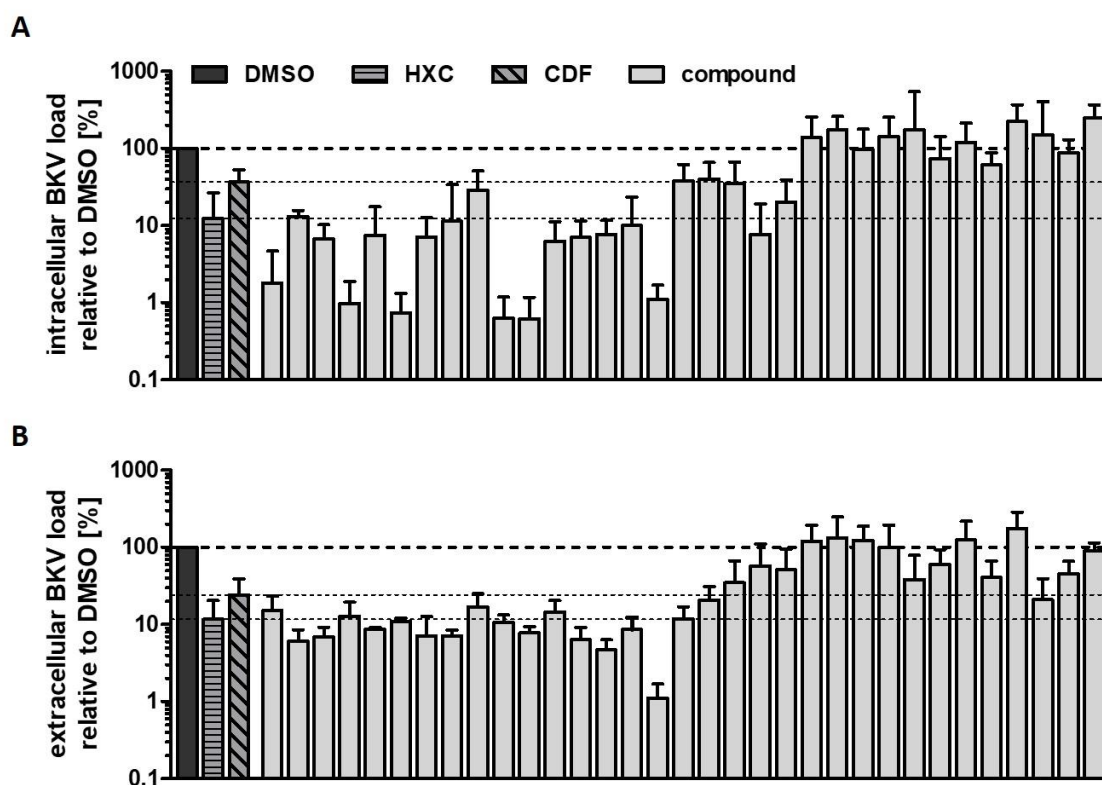
Figure 22: 16 compounds show high inhibitory activity against BKV infection in primary human RPTEC
Primary RPTEC were infected with BKV and treated with either DMSO, HXC, CDF or the 33 compounds, identified in primary screening. 6d p.i. gDNA from cells or viral supernatant was harvested and viral DNA copy numbers were determined as Geq by qPCR analysis (n=6). Geq determined from gDNA isolated from cells were normalized to GAPDH and are depicted as intracellular BKV load **(A)**, whereas Geq examined from gDNA extracted from viral supernatant are termed extracellular BKV load **(B)**. BKV load of infected cells treated with DMSO was set to 100%.

Since CDF is used for treatment against BKV replication in clinical applications, CDF was considered as the more relevant reference inhibitor control in order to select hit compounds for further analysis. Therefore, 16 compounds, which induced a higher BKV load reduction than CDF, were selected for analysis regarding their chemical structure.

Martin Empting from the Helmholtz Institute for Pharmaceutical Research Saarland in Germany performed chemical structure analysis of the top 16 compounds to investigate the compounds with regard to their prospective non-toxic *in vivo* activity and chemical accessibility. Therefore, DEREK (deductive estimate of risk from existing knowledge), Lipinski's rule of five and chemical accessibility were examined. Briefly, DEREK describes a computational method to calculate structural alerts based on molecular substructures in order to indicate possible toxic responses *in vivo* induced by compound treatment [152], whereas Lipinski's rule of five evaluates the chemical properties of a compound in order to estimate the probability of a compound becoming an active therapeutic drug in humans [153]. As shown in Table 55, the top 16 compounds, selected for their inhibitory activity against BKV infection, were ranked from A – D in respect of their chemical accessibility, molecular weight and cLogD value, which is a partition coefficient describing the ratio of water and octanol. In this study, compounds ranked with A or B have a molecular weight less than 450 Da, a cLogD value of less than 4.5 and chemical accessibility comprising 5 – 6 steps or less. Additionally, compounds were ranked high, if no warnings in DEREK analysis were issued.

In general, compounds with rank A – B show the most promising chemical structure properties for approaches *in vivo*. In this study, only the compounds C1 – 4 met all these criteria, while compound C5 showed a slight deviation. But C5 was still ranked relatively high, as no warnings concerning DEREK analysis were issued. Therefore, the five compounds (C1 – C5) were selected for further investigation regarding their inhibitory efficacy against BKV infection in more detail.

Table 55: Chemical structure analysis of 16 compounds being active against BKV in RPTEC
Compounds identified in secondary BKV screen were ranked according their prospective non-toxic *in vivo* activity and chemical accessibility.

Compound	Rank	DEREK Warnings	Physical chemical properties	Lipinski compliance	Chemical accessibility
C1	A	None	MW 307.37 cLogD(pH7.4) 2.95	OK	3 – 4 steps
C2	A	Hepatotoxicity	MW 346.43 cLogD(pH7.4) 3.97	OK	3 – 4 steps
C3	A-B	Hepatotoxicity Teratogenicity	MW 267.29 cLogD(pH7.4) 1.48	OK	2 – 3 steps
C4	B	None	MW 414.48 cLogD(pH7.4) 4.05	OK	3 – 4 steps
C5	B	None	MW 452.5 cLogD(pH7.4) 4.52	OK	5 – 6 steps
C6	B-C	Carcinogenicity	MW 485.38 cLogD(pH7.4) 4.19	OK	3 – 4 steps
C7	B-C	None	MW 449.48 cLogD(pH7.4) 1.07	OK	4 – 5 steps
C8	C	None	MW 521.58 cLogD(pH7.4) 3.27	bad (MW>500)	4 – 5 steps
C9	C	Chromosome damage (*in vitro*) Hepatotoxicity	MW 331.32 cLogD(pH7.4) 4.49	OK	6 – 7 steps
C10	C	Hepatotoxicity HERG inhibition	MW 426.60 cLogD(pH7.4) 2.88	OK	4 – 5 steps
C11	C	None	MW 490.58 cLogD(pH7.4) 3.52	OK	difficult
C12	D	Hepatotoxicity	MW 470.50 cLogD(pH7.4) 4.52	OK	difficult
C13	D	Chromosome damage (*in vitro*) Photoallergenicity	MW 479.98 cLogD(pH7.4) 7.53	bad (lipophilicity)	4 – 5 steps
C14	D	HERG Inhibition	MW 415.50 cLogD(pH7.4) 4.3	OK	difficult
C15	D	Cyanide-type effects teratogenicity	MW 463.53 cLogD(pH7.4) 4.73	OK	difficult
C16	D	Hepatotoxicity	MW 481.59 cLogD(pH7.4) 4.29	OK	difficult

To investigate the inhibitory activity against BKV infection of the compounds C1 – C5 in further detail, RPTEC were infected with BKV at a MOI of 0.5 and treated with HXC, CDF or compounds C1 – 5 at decreasing concentrations. 6d p.i. gDNA from cells and viral supernatant was harvested and BKV loads were determined. To evaluate the inhibitory activity against BKV infection of each compound, the BKV loads of infected cells treated with a compound were normalized to BKV loads of infected cells treated

with DMSO, which were set to 100%. In Figure 23 the relative reduction of BKV loads induced by compound treatment and the corresponding logarithmic inhibition curves are demonstrated. All five compounds (C1 – C5) exhibited dose dependent inhibition of BKV infection with IC50 values ranging from 230 to 930 nM (intracellular BKV load) and from 0.91 to 5.5 µM (extracellular BKV load), respectively. CDF and HXC displayed intracellular IC50 values ranging from 1.0 to 2.5 µM and extracellular IC50 values ranging from 0.58 to 3.4 µM. However, dose dependent inhibition observed in intracellular BKV loads induced by the compounds C2, C4 and C5 are shifted significantly to lower IC50 values compared to dose dependent inhibition of extracellular BKV loads.
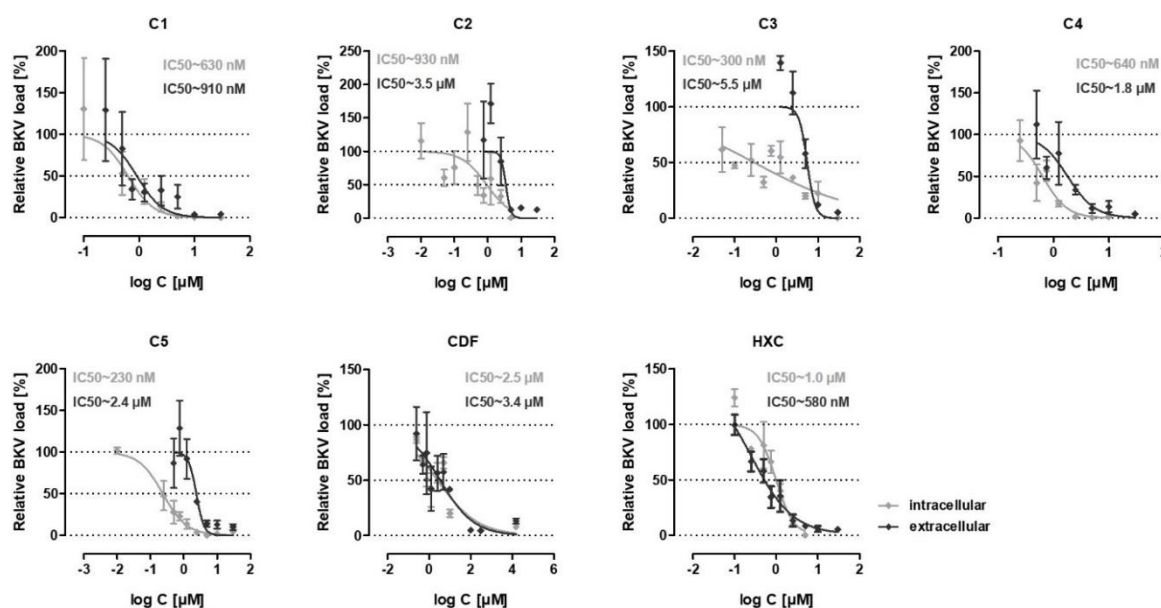
Figure 23: Influence of compound titration on BKV load
Primary RPTEC were infected with BKV at a MOI of 0.5 and treated with increasing concentrations of either HXC, CDF or one of the top compounds C1 – C5. 6d p.i. BKV load in cells (intracellular, light grey) or supernatant (extracellular, black) was determined by qPCR analysis (n=3). BKV load of infected cells treated with DMSO was set to 100%. Logarithmic inhibition curves and approximate IC50 values are shown for each compound.

To further investigate the influence of the selected compounds on primary human RPTEC, the cytotoxicity potential of C1 – C5, HXC and CDF was assessed. RPTEC were treated with HXC, CDF or compounds C1 – C5 at decreasing concentrations. 6d p.i. cell viability was determined by MTT assay and ATP assay. The cytotoxicity relative to DMSO and the logarithmic cytotoxicity curves are depicted in Figure 24. Interestingly, compound C1 exhibited no dose dependent cytotoxicity in RPTEC (CC50 ≥ 93 µM), while CDF treatment resulted in minor cytotoxicity as determined with MTT assay (CC50 ~ 59 µM), which was undetected in the ATP assay (CC50 ~ 102 µM). However, HXC and the remaining four compounds (C2 – C5) revealed dose dependent cytotoxicity with CC50 values ranging from 2.0 to 9.0 µM, indicating a high cytotoxic potential in primary human RPTEC.
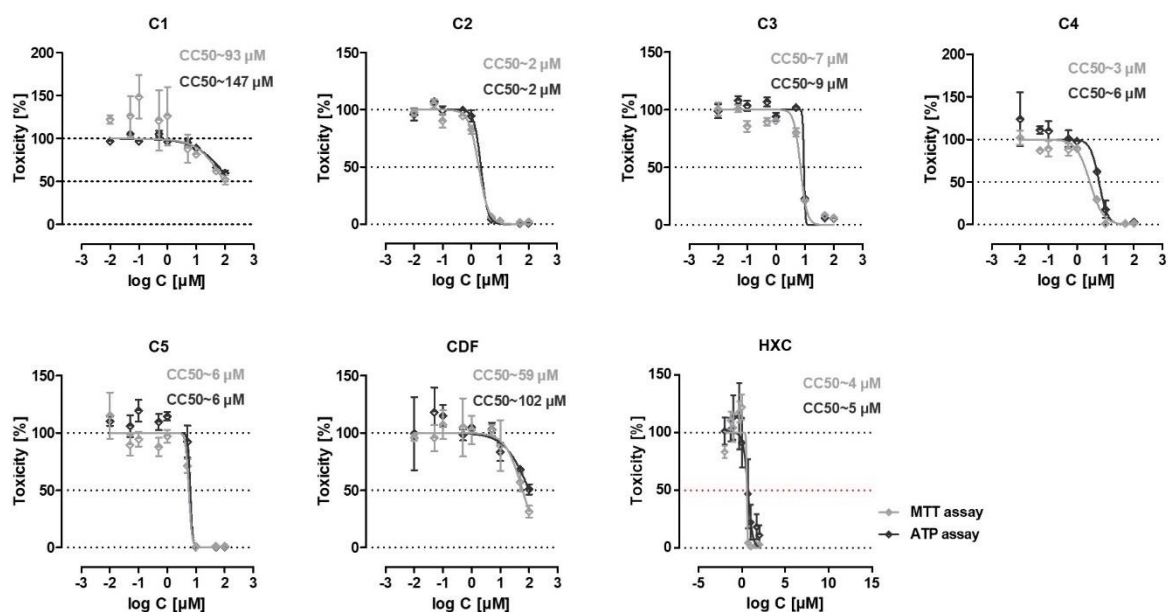
Figure 24: Influence of compound titration on RPTEC cytotoxicity
Primary RPTEC were treated with increasing concentrations of either HXC, CDF or one of the compounds C1 – C5. 6d post treatment, cytotoxicity was examined by MTT (light grey) or ATP assay (black) (n=3). Toxicity of cells treated with DMSO was set to 100%. Logarithmic cytotoxicity curves and approximate CC50 values are shown for each compound.

Table 56 summarizes the inhibitory activity against BKV infection and cytotoxic potential of the top five compounds, CDF and HXC in a dose dependent fashion. The compounds C2 – C5 revealed a high inhibitory activity against BKV at low concentrations, but at the same time seemed to exhibit a high cellular cytotoxicity. However, compound C1 showed no toxic potential even at high concentrations and still displayed a high inhibitory activity against BKV infection.

Table 56: Evaluation of IC50 and CC50 values
Summary of dose dependent inhibitory activity against BKV infection and cytotoxicity of top five compounds as wells as HXC and CDF in primary human RPTEC.

Compound	CC50 [µM] ATP Assay	IC50 [µM] intracellular	IC50 [µM] extracellular	Selectivity Index intracellular	Selectivity Index extracellular
C1	147.0	0.63	0.91	233.33	161.54
C2	2.2	0.93	3.5	2.37	0.63
C3	9.4	0.3	5.0	31.33	1.88
C4	5.9	0.64	1.8	9.22	3.30
C5	6.3	0.23	2.4	27.30	2.63
CDF	102.0	2.5	3.4	40.8	30.00
HXC	4.9	1.0	0.58	4.9	8.45

Furthermore, the selectivity index (SI) of a compound, a widely accepted parameter used to express a compound's *in vitro* efficacy in inhibition of virus replication, is defined as the ratio between CC50 and IC50 [154]. Table 56 shows that only compound C1 had a SI of over 100, suggesting a highly inhibitory selectivity towards BKV and no cellular toxicity towards the host. However, the compounds C3 with a SI of 31 and C5 with a SI of 27 regarding their intracellular inhibition activity, showed only a very low extracellular inhibitory activity with SIs of approximately 2. The other two compounds, C2 and C4 with SI of less than 10, appeared to induce cell death of the host cells rather than efficient BKV infection.

4.2.3 Broad range activity of compounds against PyV infection

The human PyVs JCV and BKV share great sequence homology with about 86% aa homology in the early and late region [24]. While BKV is associated to cause HC and PVAN in transplantation patients, JCV has been linked to PML and hematological diseases [4]. Since both human PyVs are known to cause severe diseases in immunosuppressed patients and to date treatment options for BKV and JCV are limited, the identification of novel inhibitors active not only against BKV but also against JCV is highly desirable. Hence, to expand the specificity of compounds identified by secondary screening, the top five candidates were further investigated for cross-reactivity with the human PyV JCV.

Therefore, COS-7 cells were either left uninfected or infected with JCV at a MOI of 3 and treated with either DMSO, HXC, CDF or one of the top five selected compounds (C1 – C5). 6d p.i. gDNA from cells and viral supernatant was harvested and JCV loads were determined by qPCR analysis. The absolute JCV loads are presented in the supplements, in Figure S2. However, to evaluate the inhibitory activity of each compound against JCV infection, the JCV loads of infected cells treated with a compound were normalized to JCV loads of infected cells treated with DMSO, which were set to 100%.

In Figure 25, the relative reduction of JCV loads induced by compound treatment is depicted. HXC treatment of COS-7 cells infected with JCV resulted in 95% decrease of the extracellular JCV load (Figure 25A), but only in a 45% decrease of the intracellular JCV load (Figure 25B), while CDF exhibited no antiviral activity against JCV in COS-7 cells. Strikingly, the compounds C1, C4 and C5 reduced JCV load by more than 90% indicating high inhibitory activity against JCV. The compounds C2 and C3 decreased extracellular JCV load by 90% but indicating less antiviral activity against intracellular JCV load, with 10% decrease after treatment with C2 and 70% reduction after treatment with C3. However, compared to HXC the reduction of extracellular JCV load induced by all five compounds was similar, but concerning the intracellular JCV load, especially the compounds C1, C4 and C5 demonstrated a greater decrease than HXC.

These findings indicate that all five compounds show inhibitory activity against SV40, BKV and JCV suggesting a high specificity of the five selected compounds against infection by this class of PyVs.
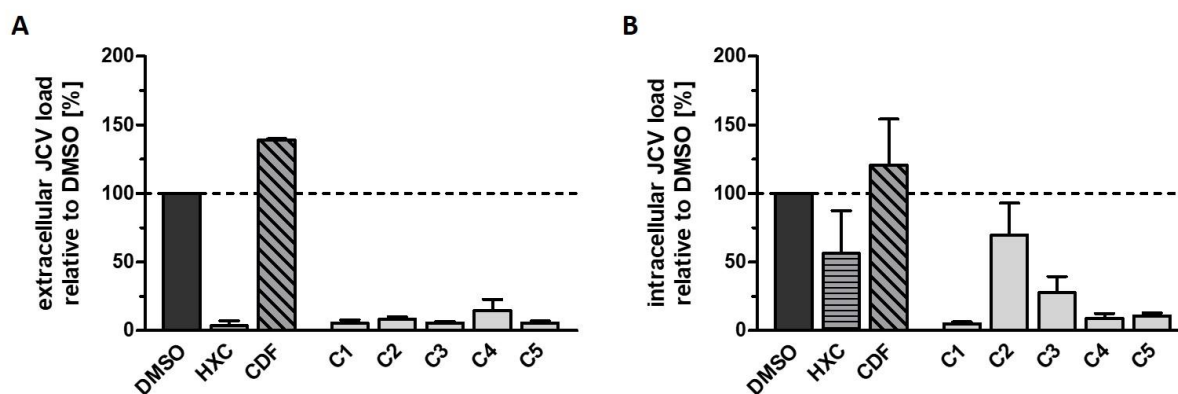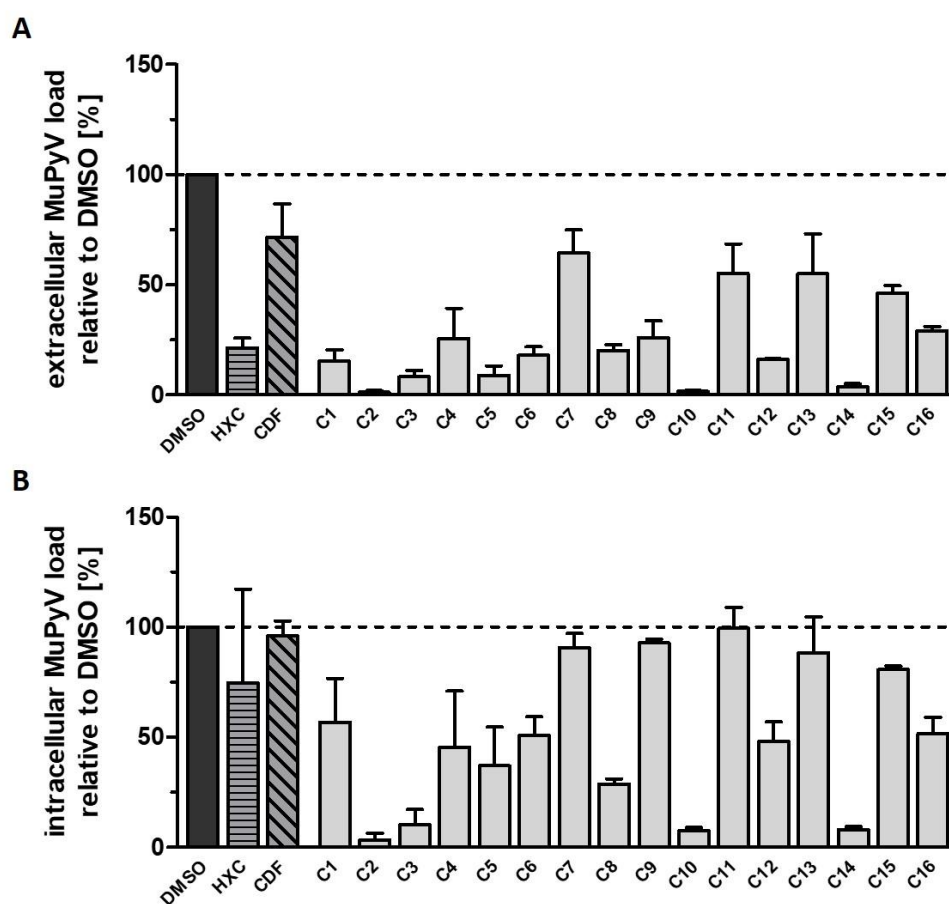
Figure 25: Inhibitory activity of the top five compounds against JCV infection
COS-7 cells were infected with JCV and treated with either DMSO, HXC, CDF or one of the compounds C1 – C5.
6d p.i. JCV load in supernatant **(A)** or within cells **(B)** was determined by qPCR analysis (n=3). JCV load of infected cells treated with DMSO was set to 100%.

In the next experiment, the 16 compounds, which were previously identified based on their inhibitory activity against BKV infection (Figure 22), were further validated for their inhibitory activity against PyV infection in mice, in order to evaluate their antiviral activity in prospective *in vivo* studies. Due to restricted animal models, MuPyV infection in mice is usually used as a surrogate system for BKV infection *in vivo* [117].

NMuMG cells were left uninfected or infected with MuPyV at a MOI of 0.5. Infected cells were either treated with the controls DMSO, HXC, CDF or the selected hit compounds C1 – C16. 6d p.i. gDNA from cells and viral supernatant was harvested and MuPyV loads were determined by qPCR analysis. The absolute MuPyV loads are presented in the supplements, in Figure S3. However, to evaluate the inhibitory activity of each compound against MuPyV infection, the MuPyV loads of infected cells treated with a compound were normalized to MuPyV loads of infected cells treated with DMSO, which were set to 100%.

In Figure 26, the relative reduction of MuPyV loads induced by compound treatment is demonstrated. Treatment with the reference inhibitor HXC led to 80% reduction of extracellular MuPyV load but merely 25% reduction of intracellular MuPyV load compared to DMSO treated cells. Additionally, a high toxic potential of HXC in NMuMG cells was detected by microscopic analysis (data not shown), indicating that the observed inhibitory activity might be due to high cellular toxicity. Treatment with the second reference inhibitor, CDF, induced only a 25% decrease of extracellular MuPyV load and nearly no reduction of intracellular MuPyV, indicating that CDF only exhibits a weak inhibitory function against MuPyV. However, treatment with the compounds C2, C3 and C14 resulted in more than 90% reduction of MuPyV loads, but also induced 80% cell death detected by microscopy (data not shown). These results indicate that the observed high inhibitory activity might be a result of high cellular toxicity, further suggesting that these compounds might not specifically influence viral infection.

Furthermore, the compounds C7, C11, C13 and C15 resulted in less than 50% decrease of extracellular load and merely 10 – 20% decrease of intracellular load, suggesting a very low inhibitory activity against MuPyV infection. The remaining compounds induced a 75 – 90% reduction of extracellular load, but only 50 – 60% reduction of intracellular load. Interestingly, after treatment with compound C9 almost no reduction of intracellular MuPyV load was observed, although extracellular MuPyV was reduced by 75%.

Overall, the majority of the tested compounds only displayed a weak inhibitory activity against MuPyV infection, indicating that these compounds are more specific for the PyV class including SV40, JCV and BKV. Only treatment with compound C10 induced more than 95% inhibition of MuPyV load, measured in both intracellular and extracellular load, indicating a high inhibitory activity against MuPyV infection.

Figure 26: Inhibitory activity of the top 16 compounds against MuPyV infection
NMuMG cells were infected with MuPyV and treated with either DMSO, HXC, CDF or one of the selected compounds C1 – C16. 6d p.i. MuPyV load in supernatant **(A)** or within cells **(B)** was determined by qPCR analysis. MuPyV load of infected cells treated with DMSO was set to 100%.

4.3 Characterization of the inhibitory effect of compound C1 against BKV

All five compounds (C1 – C5) identified after secondary screening exhibited high inhibitory activity against BKV infection even at low concentrations. However, the compounds C2 – C5 showed high cellular toxicity, while no toxicity was found for compound C1 in primary human RPTEC (Figure 23, 24). Furthermore, the SI is a great parameter to evaluate the selectivity of a compound. Only for compound C1 a SI of over 100 was determined (Table 56), indicating that the inhibitory activity of C1 is highly specific for BKV infection. Therefore, compound C1 was selected to further investigate its inhibitory activity against BKV infection in more detail.

4.3.1 Structure activity relationship of compound C1

Structure activity relationship (SAR) is a powerful tool to analyze whether structural characteristics of a compound correlate with its biological activity. SAR is helpful to predict biological effects based on molecular structure using data from similar compounds with comparable physical and biological properties. By analyzing the relationship between the molecular structures and their biological activity, functional groups of a compound important for its activity could be identified and potential biological targets could be predicted [155].

In this study, SAR was used to investigate whether the inhibitory activity of compound C1 against BKV infection was dependent on its structure and if minor alterations of its chemical structure, particularly functional groups, might affect its efficacy. An *in silico* analysis for compound C1 (further on named C1.1) related structures based on Tanimoto distances (≥ 0.81) was performed using the MolPort library, and 14 derivatives (C1.2 – C1.15) were selected for further analysis of their efficacy in inhibiting BKV infection and their influence on cell viability.

To investigate the inhibitory activity of the compounds C1.1 – C1.15 against BKV infection, human primary RPTEC were infected with BKV at a MOI of 0.5 and treated with the indicated compounds at increasing concentrations. 6d p.i. gDNA from viral supernatant was harvested and extracellular BKV load was determined by qPCR analysis. To evaluate the inhibitory activity against BKV infection of each compound, the BKV loads of infected cells treated with a compound were normalized to BKV loads of infected cells treated with DMSO, which were set to 100%. In Figure 27 the relative reduction of BKV load induced by compound treatment and the corresponding logarithmic inhibition curves are illustrated (black).

Additionally, the influence of derivatives on cell viability of primary human RPTEC was determined. Therefore, RPTEC were treated with the compounds C1.1 – C1.15 at decreasing concentrations. 6d p.i. cell viability was determined by MTT assay. The cytotoxicity relative to DMSO and the logarithmic cytotoxicity curves are demonstrated in Figure 27 (grey).
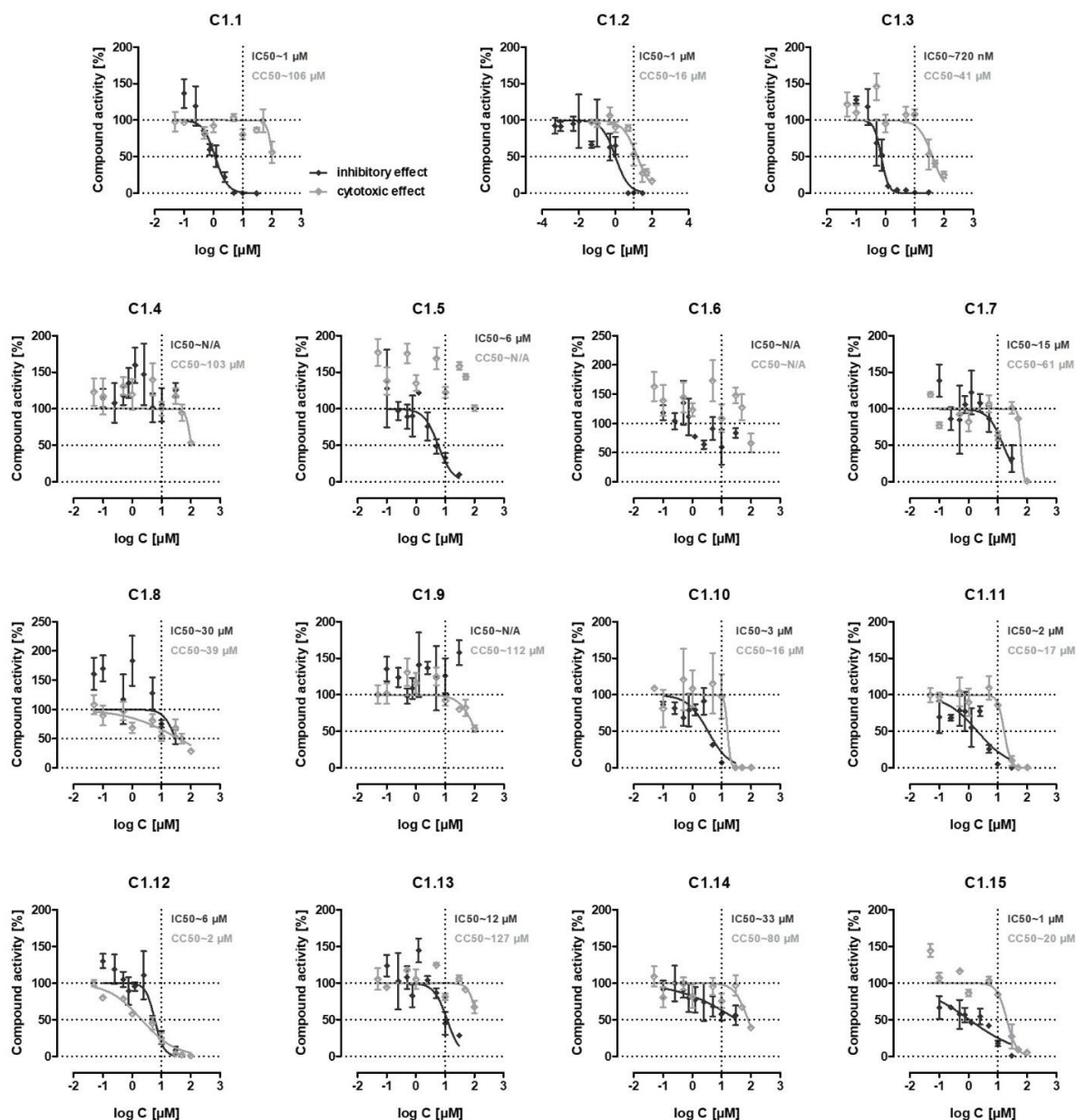
Figure 27: SAR analysis of compound C1

Based on an *in silico* search for compound C1.1 related structure with Tanimoto distances ≥ 0.81, 14 derivatives (C1.2 – C1.15) were analyzed for their inhibitory activity against BKV infection and their cytotoxicity in RPTEC. Inhibitory effect (black) was determined by measuring the BKV load in supernatant by qPCR analysis. Cytotoxicity was examined by performing MTT assay (grey). Cells treated with DMSO were set to 100%. Logarithmic inhibition or cytotoxicity curves and approximate IC50 or CC50 values are shown for each derivative.

It was confirmed that treatment with compound C1.1 continuously showed no cellular toxicity (CC50 ~ 106 µM), while still exhibiting high inhibitory activity against BKV (IC50 ~ 1 µM). Out of the 14 derivatives, three compounds showed no inhibitory activity against BKV infection and no toxic potential (C1.4, C1.6 and C1.9). Five compounds demonstrated slightly less antiviral activity compared to C1.1 with IC50 values ranging from 2 to 6 µM (C1.5, C1.10, C1.11, C1.12 and C1.15), with the latter four also showing relatively high toxicity with CC50 values ranging from 2 to 20 µM. Furthermore, four

compounds showed notably less inhibitory activity against BKV infection with IC50 values ranging from 15 to 33 μM with none or low cytotoxicity at all (C1.7, C1.8, C.13 and C1.14). Additionally, two compounds inhibited BKV infection similar to compound C1.1, but at the same time exhibited a high toxic potential with CC50 values ranging from 16 to 41 μM (C1.2 and C1.3).

Summarized, almost all derivatives, except C1.4, C1.6 and C1.9, exhibited high inhibitory activity against BKV infection in a dose dependent fashion with three compounds (C1.5, C1.13 and C1.14) even showing no toxic potential.

In Table 57 the influence of compound C1 derivatives on BKV infection and cell viability are summarized, including calculated selectivity indices (SI) as a parameter for a compound's *in vitro* efficacy. Beside compound C1.1, only derivative C1.3 revealed a high SI of over 50. The derivatives C1.2, C1.13 and C1.15 resulted in SI values ranging from 10 to 20 and the remaining compounds only demonstrate low SI values. These findings indicate that the chemical structure of compound C1 is highly crucial for its inhibitory activity against BKV. Additionally, these SAR analyses suggest that minor changes in chemical structure of compound C1 affect its inhibitory activity against BKV infection and increase the risk of cytotoxicity in primary human RPTEC.

Table 57: Evaluation of IC50 and CC50 values of compound C1 derivatives
Summary of dose dependent inhibitory activity against BKV infection and cytotoxicity in primary human RPTEC of C1 like compounds.

Compound	MW	Similarity Index	CC50 [μM]	IC50 [μM]	Selectivity Index
C1.1	307.37	1	106	1	106
C1.2	312.4	0.89	16	1	16
C1.3	319.39	0.87	41	0.72	56.94
C1.4	355.42	0.86	103	N/A	N/A
C1.5	294.38	0.86	N/A	6	N/A
C1.6	329.42	0.85	N/A	N/A	N/A
C1.7	352.47	0.85	61	15	4.07
C1.8	230.29	0.84	39	30	0.3
C1.9	341.48	0.84	112	N/A	N/A
C1.10	431.37	0.84	16	3	5.33
C1.11	386.92	0.83	17	2	8.50
C1.12	404.49	0.82	2	6	0.33
C1.13	280.35	0.81	127	12	10.58
C1.14	407.54	0.81	80	33	2.42
C1.15	360.45	0.81	20	1	20

4.3.2 Combination of Cidofovir and compound C1 treatment against BKV infection

The nucleoside analogue CDF, which is approved for the treatment of AIDS related CMV retinitis, is reported to exhibit inhibitory activity against BKV infection in *in vitro* studies [156]. Since the clinical demand for treatments of BKV associated diseases is rising and hitherto no antiviral drug with a proven efficacy against BKV infection has been approved by the FDA, CDF has been used in small clinical studies to treat PVAN in renal transplant patients and HC in allogeneic hematopoietic stem cell transplant patients [43]. Due to the lack of alternatives to CDF and its low efficacy, it is crucial to investigate whether a combined treatment of CDF and compound C1 leads to a greater decrease of BKV replication.

Therefore, primary human RPTEC were infected with BKV at a MOI of 1 and treated with both compounds combined at 10 µM, and only C1 or CDF, respectively. 6d p.i. BKV load was determined in cells (intracellular) or supernatant (extracellular) by qPCR analysis. Corresponding results are expressed as Geq in Figure 28. Both CDF and compound C1 led to a highly significant decrease in BKV loads, but compound C1 inhibited BKV replication significantly greater than CDF. However, the combination of compound C1 and CDF was not significantly different from the antiviral effect of compound C1 alone, suggesting that the ability of CDF and compound C1 to inhibit BKV infection is not synergistic.
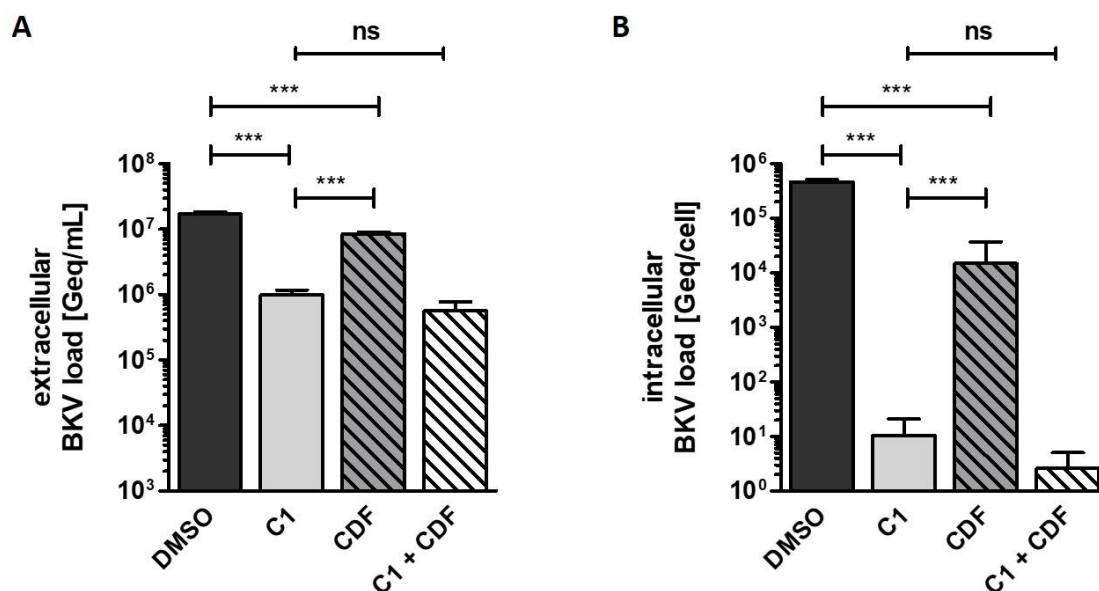
Figure 28: Combination of CDF and compound C1 does not further inhibit BKV infection
Primary human RPTEC were infected with BKV at a MOI of 1 and treated with both compounds combined at 10 µM, and only C1 or CDF, respectively. 6d p.i. BKV loads in supernatant **(A)** or cells **(B)** were determined by qPCR analysis (n=3).

4.3.3 Influence of compound C1 on the time course of BKV infection

To analyze whether the antiviral effect of compound C1 was dependent on the levels of input virus, RPTEC were infected with decreasing MOIs of BKV and treated with compound C1 at 10 µM or DMSO. 6d p.i. BKV load was detected in cells (intracellular) and supernatant (extracellular) by qPCR analysis (Figure 29). Considering the extracellular BKV load, expressed as Geq/mL in Figure 29A, compound C1 treatment did not reduce BKV load at a MOI of 100. However, dependent on the levels of input virus, BKV load was significantly decreased over 1.1 orders of magnitude using a MOI of 10, 1.2 orders of magnitude with a MOI of 1 and 1.6 orders of magnitude with a MOI of 0.1. Furthermore, regarding the intracellular BKV load, described as Geq/cell in Figure 29B, treatment with compound C1 considerably influenced BKV infection, even at high levels of input virus. Using a MOI of 1 – 100 treatment with compound C1 reduced intracellular BKV load over 2.2 to 3.5 orders of magnitude, but at a MOI of 0.1 nearly no BKV infection in RPTEC was able to be detected, resulting in a decrease of BKV load of over 5 orders of magnitude. These findings reveal that the inhibitory activity of compound C1 against BKV infection is dependent on the amount of input virus, strongly influencing the final extracellular and intracellular BKV load. Furthermore, while using a MOI of 0.1 treatment with compound C1 resulted in the highest impact on BKV infection with almost no detectable BKV load left in cells (0.006 Geq/cells).
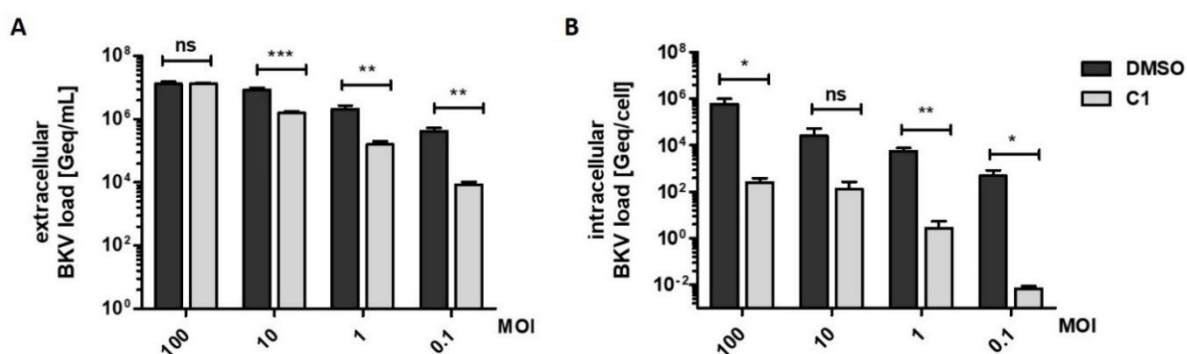
Figure 29: Inhibitory effect of compound C1 is dependent on levels of input virus
RPTEC were infected with decreasing amount of BKV and treated with either DMSO or compound C1. 6d p.i. BKV load in supernatant **(A)** or cells **(B)** was examined by qPCR analysis (n=3).

To investigate whether the inhibitory activity of compound C1 on BKV infection could be enhanced, primary human RPTEC, infected with BKV at a MOI of 0.1, were either treated with compound C1 at 10 µM once (singular), or repeatably every 24h. 6d p.i., BKV load was quantified in cells (intracellular) or supernatant (extracellular) by qPCR analysis. Figure 30 shows that daily treatment with compound C1 did not result in greater decrease of BKV infection neither in the extracellular BKV load nor in the intracellular BKV load, suggesting that compound C1 inhibits early stages of BKV infection.
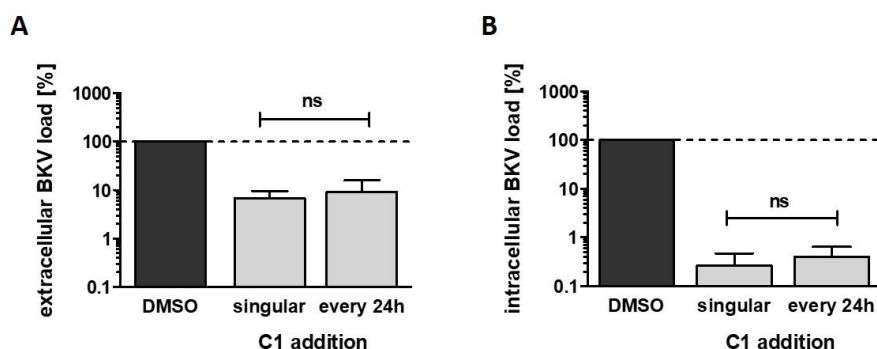
Figure 30: Daily treatment with compound C1 does not further inhibit BKV infection
RPTEC were either treated together with BKV infection (singular) or every 24h while replacing the media with new media containing DMSO or compound C1 at 10 µM. 6d p.i., BKV load in supernatant **(A)** or cells **(B)** was monitored by qPCR analysis (n=3). BKV load of cells treated with DMSO was set to 100%.

To examine whether BKV inhibition of compound C1 was equally effective throughout the entire viral replication cycle, primary human RPTEC, infected with BKV at a MOI of 0.1, were treated with 10 µM compound C1 at the indicated time points p.i. (Figure 31). 6d p.i. BKV load was measured in cells (intracellular) or supernatant (extracellular) by qPCR analysis (Figure 31). When compound C1 was added in the first 0 to 12h p.i., inhibition of BKV replication was most pronounced detected in extracellular BKV load and addition of compound C1 from 24h p.i. onwards resulted in a diminished decrease of the extracellular BKV load (Figure 31A). However, regarding the intracellular BKV load, treatment with compound C1 added from 0 to 24h p.i. resulted in noticeable impaired BKV infection, which was not apparent when C1 was added at later time points (Figure 31B). These findings suggest that BKV inhibition by compound C1 is time dependent. Furthermore, compound C1 seems to interfere particularly with early stages of BKV infection, as its inhibitory activity against BKV infection persists only during the time of early gene expression up to 24h p.i. but not at later stages.
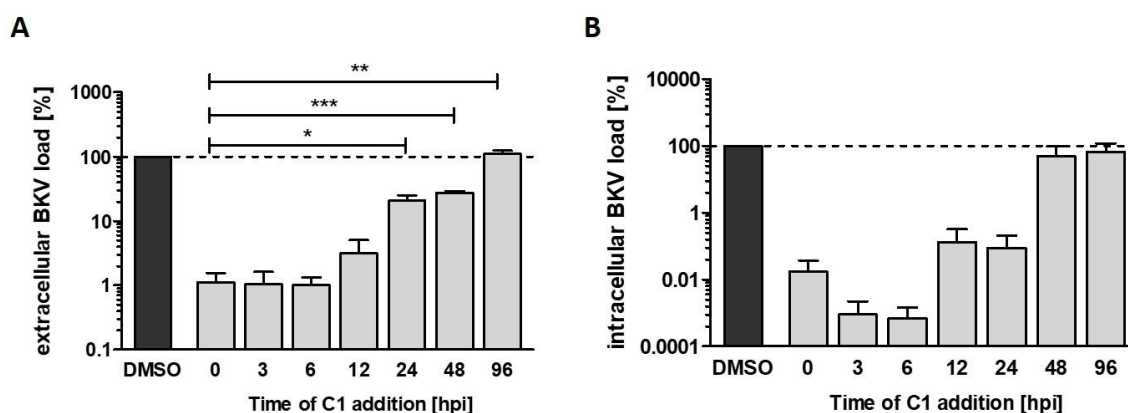
Figure 31: Compound C1 inhibition is time dependent
Infected RPTEC were treated with 10 µM of compound C1 at indicated time points p.i.. 6d p.i. BKV load in supernatant **(A)** or cells **(B)** was determined by qPCR analysis and expressed as percentage relative to BKV load of cells treated with DMSO, which was set to 100% (n=3).

100

The findings in this study suggest that compound C1 inhibits BKV infection by hampering early steps of viral infection. The early steps include receptor binding, intracellular trafficking, virus uncoating, nuclear entry and the initiation of replication [32]. In addition, the results shown in Figure 29 indicate that inhibitory activity of compound C1 against BKV infection is dependent on the initial virus burden.

In the next experiments, it was investigated whether compound C1 interacts with cellular factors in the absence of BKV infection and whether compound C1 blocks host cell surface receptor preventing BKV entry.

Therefore, at first, uninfected RPTEC were treated with compound C1 prior to infection for the indicated time points. After incubation, the supernatant from these cells was used to treat fresh RPTEC, which were infected with BKV at a MOI of 0.1. 6d p.i. BKV load was quantified in cells (intracellular) or supernatant (extracellular) by qPCR analysis. Figure 32A demonstrates that treatment with compound C1, which was pre-incubated 3h prior to infection, resulted in a significantly lower decrease of extracellular BKV load than treatment with compound C1, which was not pre-incubated on RPTEC prior to that (indicated at 0h). These results suggest that the inhibitory activity of compound C1 is attenuated within the first 3h, implying an interaction of compound C1 with cellular factors. Unexpectedly, incubation of compound C1 for longer time periods (6 – 24h) did not result in any diminished decrease of BKV load compared to the reduction in BKV load detected when compound C1 was not pre-incubated, indicating that within the first 3h compound C1 might interact with cellular factors, albeit this interaction appears to be presumably weak and compound C1 is released or reactivated. Alternatively, reasons for this unexpected behavior could be either that binding of compound C1 to cellular factors is not stable over time or that compound C1 is degraded over time. In contrast, Figure 32B shows that no significant decrease of intracellular BKV load upon treatment with pre-incubated compound C1 was observed compared to the decrease of intracellular BKV load upon treatment with compound C1, which was not pre-incubated (indicated as 0h).
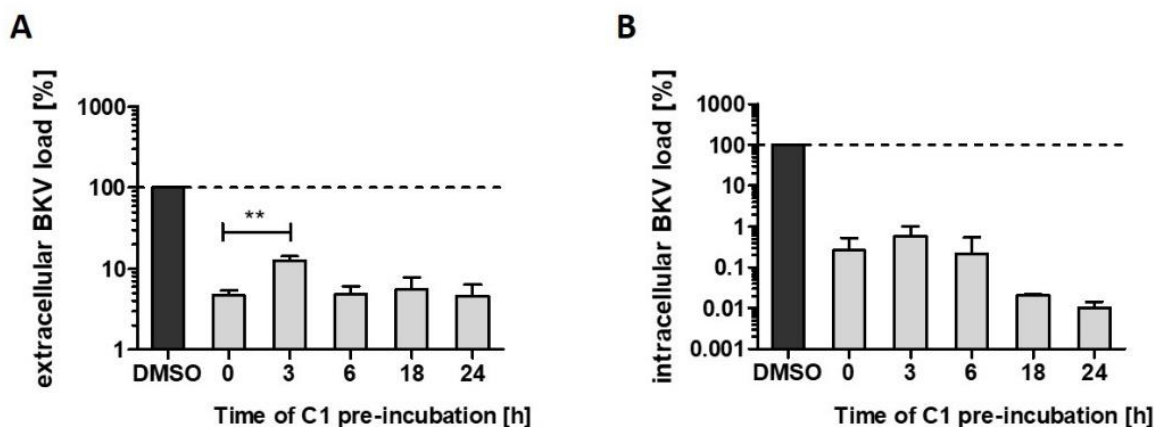
Figure 32: Effect of compound C1 inhibition after pre-incubation on uninfected RPTEC
Prior to infection, compound C1 was pre-incubated on uninfected RPTEC for indicated time points. Supernatant from these cells containing pre-incubated compound C1 was used to treat new RPTEC, which were infected with BKV at a MOI of 0.1. 6d p.i., BKV load in supernatant **(A)** or cells **(B)** was examined by qPCR analysis and expressed as percentage relative to BKV load of cells treated with DMSO, which was set to 100% (n=3).

Next, it was investigated whether compound C1 degrades over time when incubated at 37 °C. Therefore, prior to infection compound C1 was incubated at 37 °C for the indicated time points. After incubation, RPTEC were infected with BKV at a MOI of 0.1 and treated with pre-incubated compound C1. 6d p.i. BKV load was detected in cells (intracellular) or supernatant (extracellular) by qPCR analysis. Figure 33A shows that pre-incubation of compound C1 at 37 °C for 3 to 6h resulted in significant lower decrease of extracellular BKV load compared to treatment with compound C1, which was not pre-incubated (indicated at 0h). These findings suggest that compound C1 becomes inactivated within 3 – 6h. In contrast, pre-incubation of compound C1 for 24h at 37 °C resulted in a significant decrease of extracellular BKV load compared to the decrease in BKV loads of infected cells treated with compound C1, which was not pre-incubated on RPTEC prior to that (indicated at 0h), suggesting that the inhibitory activity of compound C1 is restored and even enhanced after 24 hours of incubation at 37 °C. However, no significant decrease of intracellular BKV load after pre-incubation of compound C1 at 37 °C was detected (Figure 33B).
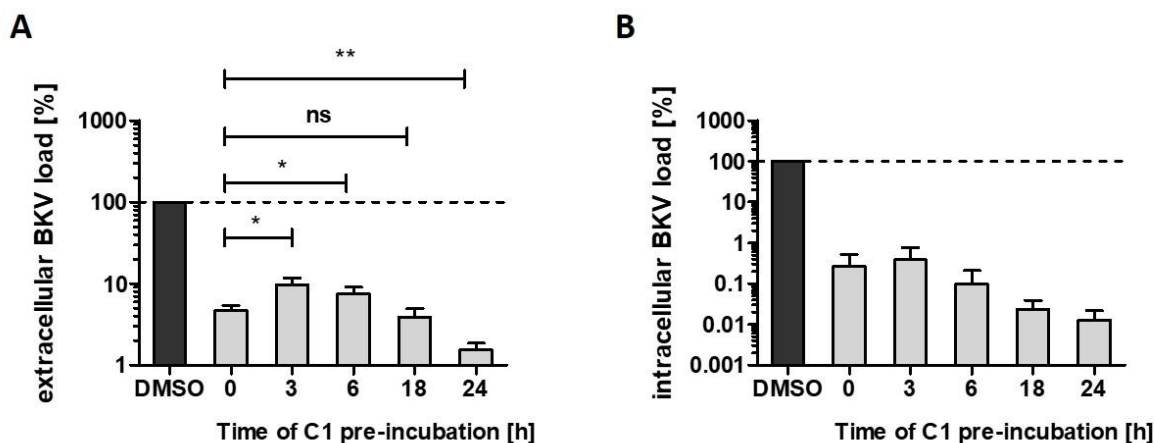
Figure 33: Effect of compound C1 inhibition after pre-incubation at 37 °C
Prior to infection, compound C1 was pre-incubated at 37 °C for indicated time points. Pre-incubated compound C1 was used to treat RPTEC, which were infected with BKV at a MOI of 0.1. 6d p.i., BKV load in supernatant **(A)** or cells **(B)** was examined by qPCR analysis and expressed as percentage relative to BKV load of cells treated with DMSO, which was set to 100% (n=3).

4.3.4 Influence of compound C1 on different steps in BKV life cycle

The influence of compound C1 on BKV life cycle was investigated to pinpoint the affected stages of BKV infection upon treatment with compound C1 and to narrow down its potential target.

To examine compound C1's inhibitory activity against BKV replication and gene expression during viral life cycle, RPTEC were infected with BKV at a MOI of 0.1 and treated with DMSO or compound C1 at 10 µM. At the indicated time points p.i., intracellular BKV load was determined by qPCR analysis (Figure 34A). A significantly reduction of intracellular BKV load was detected upon treatment with compound C1 compared to intracellular load of infected RPTEC treated with DMSO, with approximately 60-fold lower viral genome loads at 2d p.i. in compound C1 treated cells. This difference further increased during viral life cycle with 260-fold lower viral genome loads at 4d p.i. and even 105-fold lower viral genome loads 7d p.i..

Additionally, total RNA was isolated and early mRNA expression was quantified by RT-qPCR quantifying LT-Ag expression levels (Figure 34B), and late mRNA expression was determined by RT-qPCR detecting VP1 expression levels (Figure 34C). Both early and late transcripts were significantly reduced upon compound C1 treatment with further reduction of mRNA transcripts during viral life cycle. 2d p.i. early and late mRNA expression of compound C1 treated cells was decreased up to 20-fold compared to DMSO treated cells. 7d p.i. early mRNA expression was 270-fold lower in compound C1 treated cells than in DMSO treated cells and in the case of late mRNA expression level, even 10^4 lower late mRNA transcripts were observed after compound C1 treatment.

These findings indicate that inhibition of BKV by C1 was persistent during the viral life cycle. However, compound C1 blocks BKV infection significantly but not completely, since some residual intracellular BKV loads and mRNA transcripts could be observed.
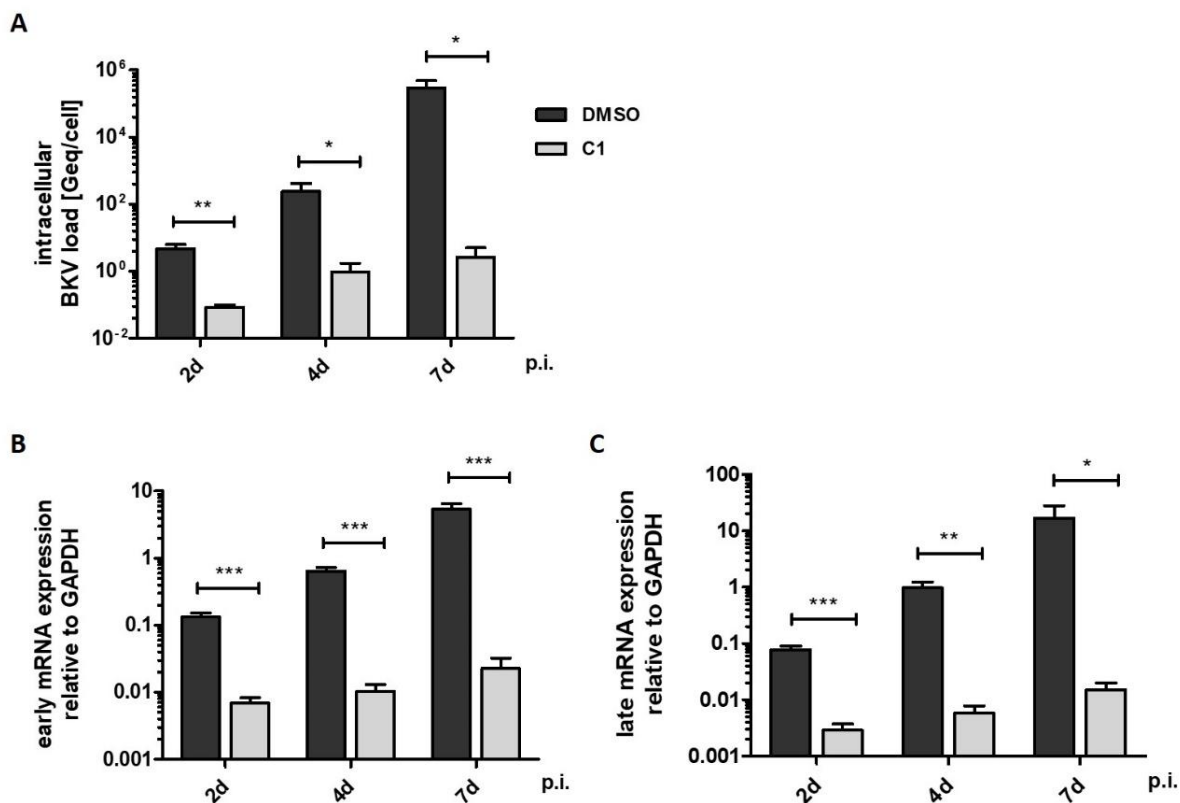
Figure 34: Characterization of the life cycle
RPTEC were infected with BKV at a MOI of 0.1 and treated with DMSO or compound C1 at 10 µM. Either gDNA **(A)** or total RNA **(B, C)** was extracted at indicated time points. **(A)** Intracellular BKV loads were measured by qPCR analysis and normalized for cellular DNA using GAPDH qPCR analysis. **(B)** LT-Ag expression or **(C)** VP1 expression was measured by RT-qPCR and normalized to GAPDH transcripts.

In the next experiment, morphological examination of BKV early and late gene expression upon compound C1 treatment was accomplished at the single-cell level. RPTEC were infected with BKV at a MOI of 0.1 and treated with DMSO or compound C1 at 10 µM. 2d and 5d p.i. the expression of BKV LT-Ag as well as VP1 expression was examined by confocal microcopy using antigen-specific monoclonal antibodies combined with DAPI staining of nuclear DNA, as shown in Figure 35A (blue: nucleus, red: LT-Ag, green: VP1). 2d p.i. a 2-fold decrease in LT-Ag (Figure 35B) and VP1 (Figure 35C) positive cells was observed, while 5d p.i. a 25-fold reduction in LT-Ag positive cells and 10-fold decrease in VP1 positive cells was observed. Quantification of LT-Ag positive and VP1 positive cells reveal that the overall inhibition of compound C1 on BKV early and late proteins is also detectable at the single-cell level.
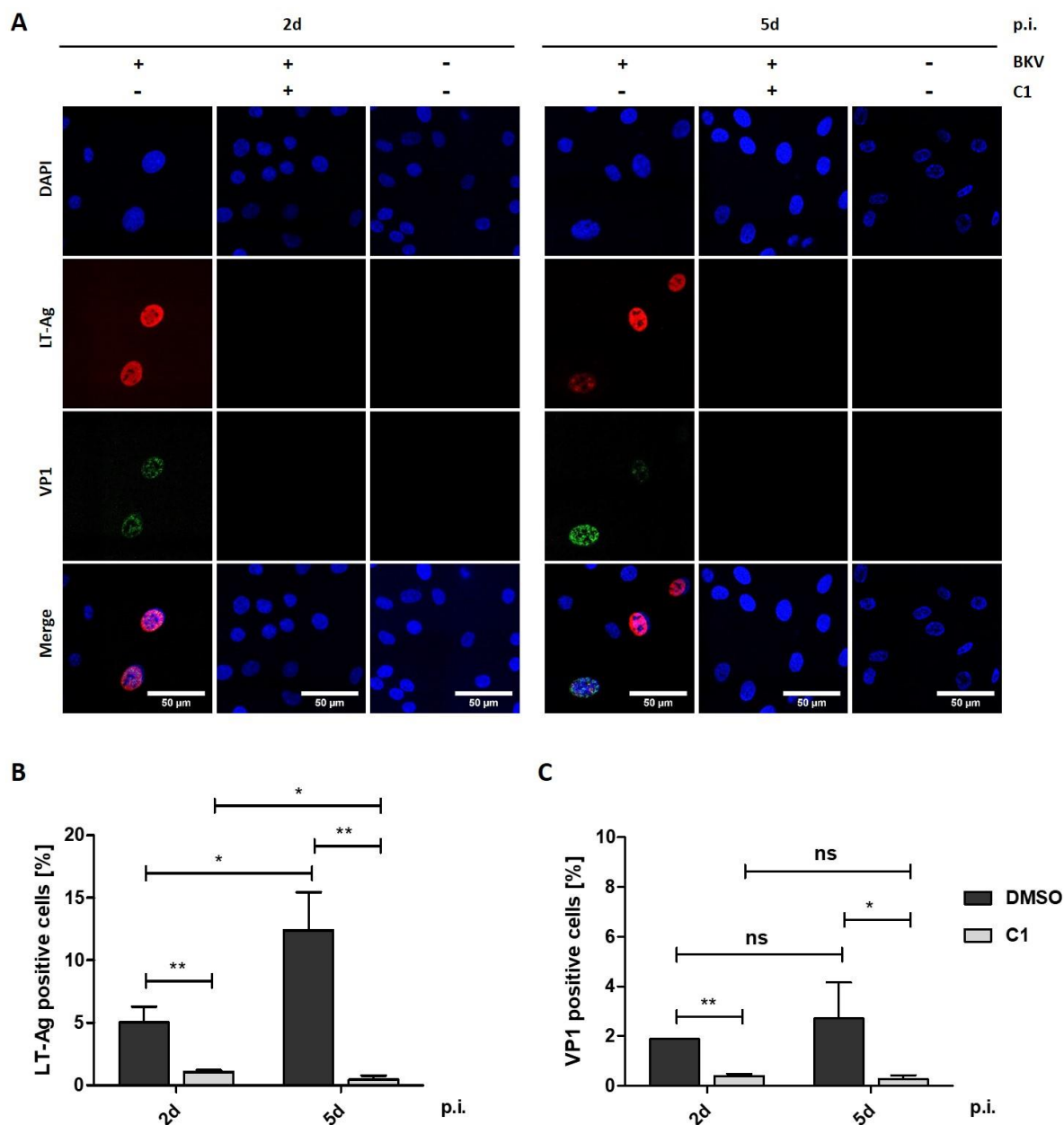
Figure 35: Indirect immunofluorescence staining
RPTEC were infected with BKV at a MOI of 0.1 and treated with compound C1 at 10 µM or DMSO. 2d and 5d p.i. cells were fixed and processed for immunostaining of LT-Ag (red), VP1 (green) and DAPI staining of nuclei (blue). The cells were analyzed by confocal microscopy (Nikon) with a 100x lens and images from 50 different fields were captured (n=3). **(A)**. LT-Ag positive cells **(B)** and VP1 positive cells **(C)** were quantified by counting and normalized to total cell count (DAPI-positive cells).

To further investigate the influence of compound C1 treatment on BKV protein expression during viral life cycle, Western immunoblot analysis was performed. RPTEC were infected with BKV at a MOI of 0.1 and treated with DMSO or compound C1 at 10 µM. Cell extracts were prepared at different time points p.i. and analyzed for the indicated viral and host cell proteins (Figure 36).

4d p.i. in DMSO treated RPTEC, LT-Ag with a protein band at approximately 80 kDa and VP1 with a protein band at approximately 40 kDa were detected. As the infection progressed over time, the

intensity of viral protein bands increased greatly and in addition to the full-length VP1 band, two to three distinct faster migrating protein bands became apparent, indicating proteolytic cleavage of VP1, possibly during the disulfide bond rearrangement process.

However, in infected RPTEC treated with compound C1 no LT-Ag expression and only low VP1 protein expression was detectable at 6d p.i. with increased, but still greatly, reduced VP1 protein expression at 8d p.i. These results suggest that although compound C1 greatly decreases BKV infection and also expression of the viral proteins LT-Ag and VP1, its inhibitory activity is not permanent throughout the entire life cycle, indicating that treatment with compound C1 delays BKV infection and subsequent BKV protein expression.
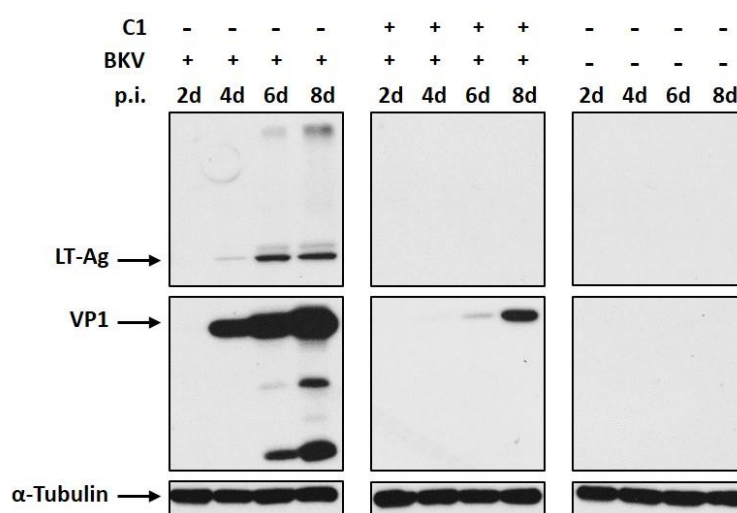
Figure 36: Compound C1 treatment delays and reduces BKV protein expression
Western immunoblot analysis of cell extracts from DMSO treated and compound C1 treated BKV infected and uninfected RPTEC at indicated time points was performed with antibodies detecting LT-Ag, VP1 and α-Tubulin as a loading control.

So far, the findings presented in this study indicate that although compound C1 inhibits BKV infection, it does not block the expression of viral proteins to full extent, but rather leads to a delay in viral protein expression. Additionally, these results suggest that compound C1 is involved in inhibiting early steps of BKV life cycle occurring within 24h p.i. such as receptor binding, viral entry, trafficking and genome replication, including initial LT-Ag transcription and expression.

The next goal was to narrow down the step during the early stages of viral life cycle, which is affected by compound C1. First, a replication assay was performed to investigate whether genome replication and concomitant gene expression were affected by compound C1 without effecting the precedent viral entry mechanism. RPTEC were transfected with a plasmid containing the genome of BKV and 1d p.t. the cells were treated with DMSO or compound C1 at 10 µM. At the indicated time points p.t., intracellular and extracellular BKV loads were determined by qPCR analysis. Figure 37 shows that

during the entire viral life cycle, no significant inhibition of either extracellular (Figure 37A) or intracellular BKV load (Figure 37B) was detected indicating that compound C1 does not affect BKV genome replication itself. Interestingly, 3d p.t. the intracellular BKV load of RPTEC treated with compound C1 was increased by almost 50-fold compared to intracellular BKV load of DMSO treated RPTEC.

Additionally, at the indicated time points p.t. total RNA was isolated and early mRNA expression (Figure 37C) and late mRNA expression (Figure 37D) were determined by RT-qPCR. Treatment with compound C1 did not influence significantly early gene expression or late gene expression at later time points (5d or 8d p.t.). However, 3d p.t. the late gene expression upon treatment with compound C1 was significantly decreased compared to late gene expression of DMSO treated RPTEC, and early gene expression of compound C1 treated cells was decreased by 10-fold compared to early gene expression of DMSO treated cells.
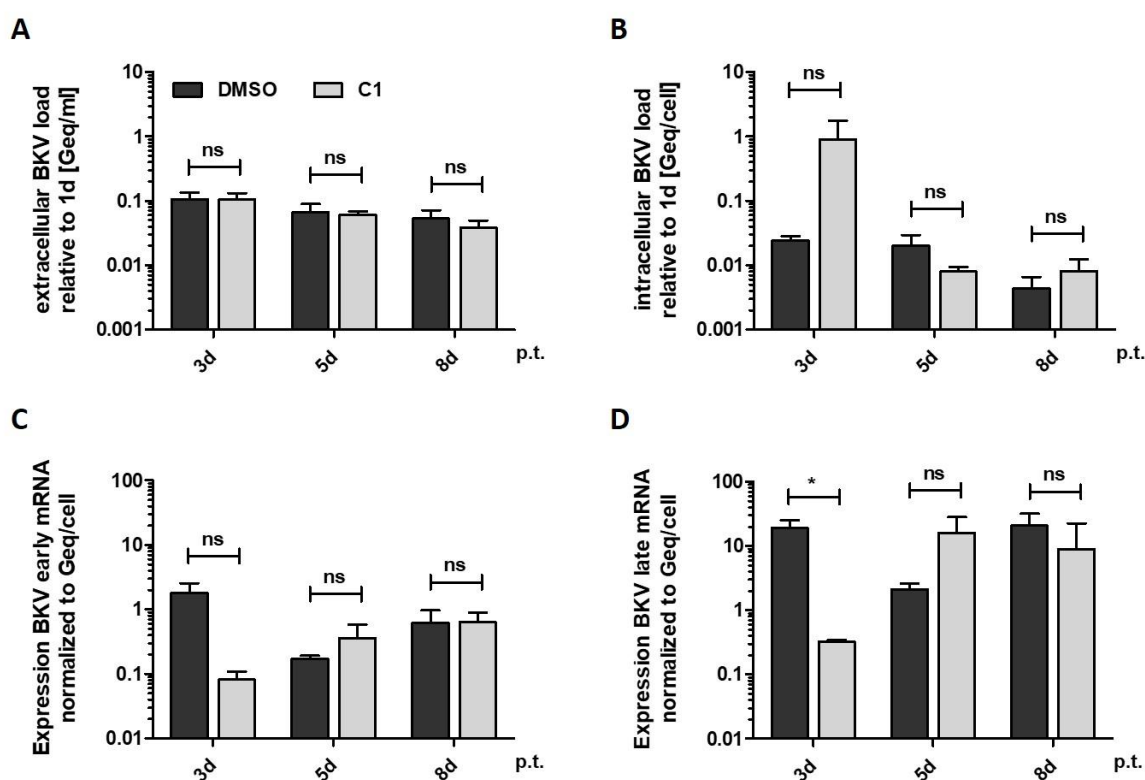
Figure 37: Compound C1 treatment does not influence BKV replication levels
RPTEC were transfected with a plasmid containing BKV genome DNA and treated with compound C1 or DMSO. 1d, 3d, 5d and 8d p.t. viral supernatant, DNA and total RNA were harvested. Extracellular **(A)** and intracellular BKV **(B)** were quantified by qPCR analysis and normalized to BKV load detected at day 1. LT-Ag expression **(C)** or VP1 expression **(D)** were measured by RT-qPCR and normalized to GAPDH transcripts. Corresponding data is presented as mRNA expression levels normalized to intracellular BKV load.

These findings indicate that compound C1 does not influence viral genome replication at later time points, but at early time points compound C1 treatment induces increased intracellular BKV load and highly decreased early and late gene expression suggesting an inhibitory activity of compound C1 during early steps of infection.

In the next experiment, it was investigated whether compound C1 impairs viral entry, including processes like receptor binding, internalization or trafficking to the nucleus. In order to verify the interaction of compound C1 with components involved in the entry steps of BKV infection, life cell imaging using VLPs labelled with Alexa Fluor 488 dye was performed. RPTEC were infected with labelled VLPs and treated with DMSO or compound C1 at 10 µM. As shown in Figure 38, nuclei were stained with Höchst (blue) and the plasma membrane was stained with WGA (red).
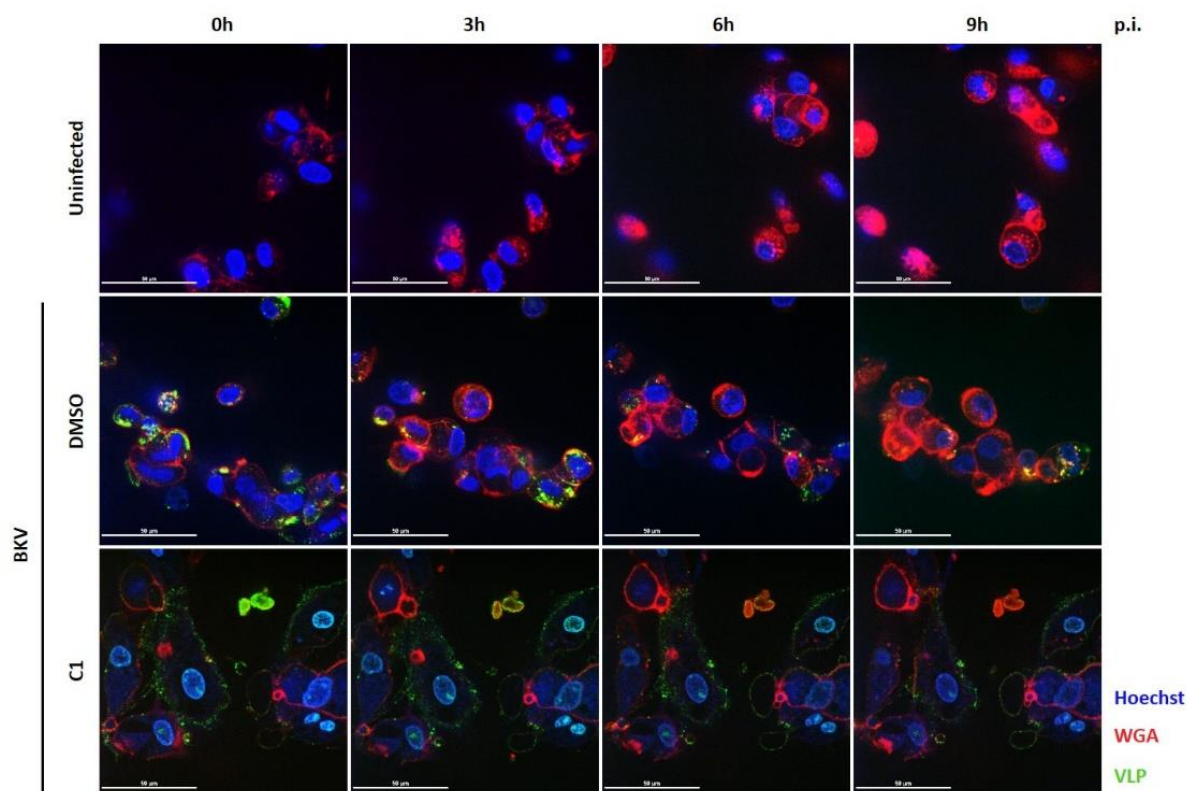
Figure 38: Compound C1 blocks BKV entry
RPTEC were infected with labelled VLPs and treated with DMSO or compound C1. BKV VLPs were labelled with Alexa Fluor 488 dye (green), nuclei with Hoechst (blue) and plasma membrane with WGA (red). Cells were observed by confocal microscopy (Nikon) using 100x lens at the indicated time points (n=1). For a period of 24h, every 60 min images from 5 different areas were captured. Presented are images of the cells 0h, 3h, 6h and 9h p.i.. Scale bars present 50 µm.

For a period of 24h, images of the RPTEC were captured every 60 min. Within a few hours p.i. in infected and DMSO treated RPTEC labelled VLPs were detected to be attached to the cell membrane and in the cells as small green dots and as aggregates. 9h p.i. almost no VLPs were detectable in these cells. However, in infected RPTEC treated with compound C1 labelled VLPs were detected as small single dots attached to the outer cell membrane, but no accumulation of labelled VLPs inside the cells was visible. Furthermore, treatment of compound C1 resulted in lower detection levels of WGA compared to the DMSO treated RPTEC, in which the WGA signal was not impaired, indicating that compound C1 affects binding of WGA to the cell membrane.

Overall, the findings presented in this study indicate that compound C1 greatly inhibits the entry steps of BKV during infection. However, further analyses are required to determine the exact mechanism of its inhibitory activity and the identification of its target.

5. Discussion

Despite the identification of BKV decades ago, no specific antiviral inhibitors are available and treatment of BKV associated diseases is restricted to the reduction of immunosuppressive regimen resulting in highly increased risk of graft rejection [32]. To fill this gap, the aim of this study was to identify and characterize novel small molecule inhibitors active against human PyV infection with the main focus on BKV infection.

5.1 Evaluation of cell-based assays suitable for HTS

In order to perform an HTS for the identification of novel small molecule compounds, a robust cell-based system had to be established. Since in general PyVs, including BKV, are species and cell type specific, the *in vitro* cell culture systems are highly restricted [87, 134]. Although primary human RPTEC support BKV replication involving the production of infectious progeny [87, 135], manifestation of a phenotypically mild CPE is visible only 14d p.i.. Additionally, donor variability, general costs of RPTE cell culturing and development of replicative senescence following passaging of RPTEC, make these cells unsuitable for primary HTS. Furthermore, usually fluorescent labelled recombinant viruses are used for an HTS of novel small molecule compounds. Due to the small size of BKV genome the introduction of fluorescent tags including GFP impairs protein expression leading to production of non-infectious virions [117]. In this study, three novel cell-based assays were established and evaluated for their suitability in primary HTS.

Firstly, the biarsenical TC labelling system was used to generate recombinant BKV. A small TC tag comprising six amino acids forming a CCPGCC motif was fused in frame to the C-terminus of VP1 or the N-terminus of either VP2 or LT-Ag of BKV. Since viral genome copies of recombinant BKV were measurable 7d p.t. (Figure 6B), the introduction of this small tag seemed to be compatible with propagation of new infectious BKV virions. However, the generated recombinant BKV were highly unstable during further infection rounds. Within two rounds of infection, no BKV was detectable in the supernatant of cells infected with recombinant BKV 14d p.i. (Figure 6C), while in cells infected with WT BKV a clear CPE was observed at this time point. These results reveal that even the introduction of a small tag consisting of six amino acids into the genome of BKV impairs effective production of viral progeny.

The reasons for the impaired production of viral progeny of recombinant BKV could be a result of the crucial function of these viral proteins being impaired by the tag: e.g. impaired DNA replication in the case of LT-Ag or the formation of instable capsids in the case of the capsid proteins VP1 and VP2. LT-Ag plays an important role in regulating viral DNA replication and the activation of late gene expression, which is essential for virion assembly [92, 126]. In this study it was shown that viral titers generated from the first round of infection were already notably decreased 7d p.i. of recombinant BKV compared

to WT virus (Figure 6B) suggesting that expression of viral proteins was diminished. However, the expression levels of viral proteins during the viral life cycle could be verified by performing a Western Blot detecting LT-Ag or VP1. Furthermore, the structure of BKV capsid is formed by the major structural protein VP1 and the minor capsid proteins VP2 and VP3. The capsid consists of 360 copies of VP1 forming 72 pentons, which form the basic building block of the capsid. Each pentameric structure comprises a ring of five β-barrel-containing VP1 monomers forming a T = 7d lattice, which encompass an invading arm containing the C termini of each VP1 able to interact with adjacent pentameric structures to stabilize the capsid shell [157]. It is likely that introduction of a tag to the C terminus of VP1 affects the interacting of VP1 with adjacent pentons resulting in destabilized capsid shells. Additionally, the minor capsid protein VP2 binds within the cavity on the internal face of each VP1 penton [157]. The fusion of a tag to VP2 could hamper binding of VP2 to VP1 and therefore virion assembly, resulting in a highly impaired infectivity of recombinant BKV. By performing electron microscopy changes in virus morphology and formation of virus capsids could be elucidated. Moreover, in agreement to the results obtained in this study, Husseiny and Lacey showed that fusion of extraneous polypeptides to BKV proteins results in highly unstable recombinant BKV particles, even when the self-processing 2A peptide was used [146]. On the other hand, fusion of a TC tag to the non-structural Agnoprotein could have resulted in stable recombinant BKV as it has been suggested that Agnoprotein is not involved in the formation of BKV capsids [99].

Despite the stability issues, the TC labelling system revealed further concerns regarding its specificity. Theoretically, upon covalent binding of cysteine pairs to membrane permeable biarsenical reagent FlAsh-EDT$_2$, the TC labelled protein should become fluorescent [147]. In this study the fluorescence intensity of recombinant BKV was not notable higher compared to WT BKV or even uninfected cells (Figure 7A), indicating the detection of unspecific signals. Additionally, microscopic analysis revealed that the biarsenical reagent FlAsh-EDT$_2$ binds unspecifically to other cell proteins (Figure 7B). In contrast, Li et al. demonstrated that this TC labelling system can be applied in Influenza virus to visualize viral NS1 protein in living cells without the detection of unspecific signals [158]. The results in this study suggest that TC binding biarsenical fluorophores interact unspecifically with endogenous cysteine-rich proteins resulting in high background are in agreement with the results of a study by Crivat et al. [159]. Treatment with wash buffer BAL (2, 3 dimercaptopropanol; British anti-Lewisite), which supposedly eliminates unspecific binding (Crivat et al.), did not significantly improve the fluorescence signal (Figure S1). The degree of unspecific interaction of biarsenical fluorophores with endogenous cysteine-rich proteins could be dependent on the expression level of these proteins in different cell lines. Overall, the instability of recombinant BKV and high fluorescent background in human RPTEC rendered this assay inadequate for a primary HTS.

As a second approach for a cell-based assay suitable for an HTS, a miRNA-based GFP reporter system was established. In general, the miRNAs of PyVs, including BKV, show complete sequence complementarity to the LT-Ag transcript. Hence, the miRNA targets LT transcripts for Ago2-dependent degradation by RISC resulting in decreased LT protein translation and down-regulation of early gene expression [111]. In this study, a lentiviral construct containing a GFP reporter cassette fused to 16 target sites for BKV miRNA was integrated into human cells, HEK293A and RPTEC/TERT1 cells, generating reporter cells with stable GFP expression. It was hypothesized that by fusing the target site for BKV miRNA to a GFP reporter cassette, BKV infection with concomitant miRNA expression attenuates translation of GFP, as reported for LT-Ag, leading to reduced GFP expression and fluorescence intensity levels.

As in this system reduction of GFP expression is dependent on a high miRNA expression, two different rearranged BKV strains, Dunlop and Gardner strain, were analyzed regarding their miRNA expression levels. The Dunlop strain exhibits higher miRNA expression at early time points of infection and, as a consequence, lower viral replication compared to the Gardner strain supporting previous work by Broekema and Imperiale who showed that miRNA expression regulates viral replication [109]. In addition, others suggested that BKV miRNA plays a role in the escape from the hosts immune response and establishment of persistence, as miRNA expression is upregulated in the archetype BKV strain, which is the transmissible BKV form, found in both healthy and diseased patients [100, 109, 111, 112]. However, the miRNA expression determined in this study was low at a ratio of 0.1 miRNA/gDNA (Figure 9C). The low miRNA expression is presumably attributed to the fact that the rearranged BKV strains, contrarily to the archetype strain, are known to exhibit a rather high replication capacity with increased early gene expression compared to archetype virus and the ability to produce infectious progeny while inducing cell death in host cells [112]. Therefore, high miRNA expression levels resulting in the down-regulation of early gene expression is unfavorable for efficient viral reproduction by concomitant CPE.

As rearranged BKV strains do not show high miRNA expression levels, a cell-based assay relying on high miRNA expression to down-regulate GFP expression could present an insufficient reduction of GFP expression. Nevertheless, a miRNA-based GFP reporter system was established by initially using HEK293A cells to generate reporter cells with stable GFP expression. BKV infection induced an overall GFP decrease of 50% and, in addition, microscope analysis indicated that at a single-cell level BKV infection led to a complete absence of GFP signal (Figure 11C, D), confirming the working hypothesize that binding of BKV miRNA to its target sites results in down-regulated GFP expression. However, confocal microscopy unveiled a low infection rate of the reporter cells by BKV, providing an explanation for the modest GFP reduction upon BKV infection. Although HEK293 cells are found to support

propagation and replication of BKV [117], these cells appear inadequate to visualize processes of BKV infection as HEK293 cells are not the natural host cells of BKV.

Since BKV exhibits a narrow host tropism for both the host species and cell type that supports BKV replication [134], it is important to use appropriate cell culture models like primary human RPTEC, which are unfortunately not suitable for HTS due to their primary characteristics. However, the RPTEC/TERT1 cell line, which is derived from RPTEC and has been immortalized using the human telomerase reverse transcriptase (hTert) subunit, provide a novel *in vitro* model for drug screening and toxicology studies [148]. The RPTEC/TERT1 cell line is reported to overcome the limitations of primary RPTEC such as replicative senescence [149]. In this study it was found that although RPTEC/TERT1 cells supported efficient BKV replication and exhibited 10-fold higher miRNA expression than HEK293A cells (Figure 12), the GFP expression was not decreased upon BKV infection (Figure 14C, D). A reason for the observed differences in GFP reduction levels between these two cell lines could be explained by different mechanism regulating the early gene expression after miRNA expression upon BKV infection. In agreement, different studies have shown that viral gene expression and stages of the viral life cycle of BKV vary between different cell types [32, 87].

Due to the low overall GFP decrease in HEK293A reporter cells, this system was deemed not suitable for a primary HTS. However, the miRNA-based system GFP reporter assay in HEK293A reporter cells could be applied for screening a limited number of compounds by microscopic evaluation of infected cells at single-cell level.

As a final approach for the establishment of a cell-based assay suitable for an HTS, SV40 was used as a surrogate virus for BKV. The human PyV BKV and the primate PyV SV40 are closely related members of the family of PyVs sharing about 70% DNA sequence homology and up to 81% aa homology in the early coding region and 86% aa homology in the late coding region [24]. Most of the knowledge about PyVs regarding the different steps of viral life cycle and viral genes was obtained from studies on SV40 [111].

Moreover, SV40 was frequently used to screen for novel inhibitors active against BKV infection. One of the first studies screening for an inhibitor against PyV infection used microscopically monitoring of SV40 induced CPE in combination with counting of cell numbers to determine antiviral activity of 13 compounds [160]. Another study investigated SV40 infection by using a BrdU cell proliferation assay to detect antiviral activity of 960 compounds [161]. The majority of the reported HTS use the helicase-activity of SV40 LT-Ag as a readout to classify the antiviral activity of large compound libraries by performing an ATP assay [151, 162, 163]. In contrast, only one study used BKV infection to screen for inhibitors and 19 compounds in total were tested by direct measurement of BKV replication by performing a real time PCR assay over seven days [164].

In this study SV40 infection of CV-1 cells was used to establish a phenotypic reporter screen based on morphological changes induced by the virus. This screen takes advantage of a CPE occurring in cells efficiently infected by SV40 within seven days. Sensor cell lines with a stable integrated RFP reporter cassette were generated and thus RFP intensity levels were used as a measure for cell viability. It was successfully demonstrated that SV40 infection of CV-1 cells at a high MOI resulted in a complete CPE, which is reflected in the RFP intensity levels measured either using a microplate photometer or by performing microscopic analysis (Figure 16). To determine whether an antiviral compound could prevent CPE after SV40 infection, the known inhibitors CDF and HXC were included in the screen.

Sequin et al. identified the compound HXC as the most potent LT-Ag inhibitor in their HTS that hampers LT-Ag ATPase activity resulting in highly attenuated replication of SV40 and BKV [151]. Indeed, in this study it was confirmed that Hexachlorophene was active against SV40 infection and showed almost no toxic potential in CV-1 cells. However, the inhibitory activity observed for HXC in this study was much lower than expected, indicating that either HXC is not very active against SV40 infection as reported previously or that the proposed phenotypic system is not adequate for the identification of inhibitors against LT-Ag.

Furthermore, the nucleoside analogue CDF, which is licensed for the treatment of CMV retinitis in AIDS patients [59], is also reported to inhibit viral growth of SV40 [160]. In this study, CDF was observed to reduce levels of SV40 infection by merely 10%. Different reports state that CDF shows a broad spectrum antiviral activity against different DNA viruses by inhibiting the viral DNA polymerase, however PyVs hijack the cellular DNA polymerases for its replication and thus, the exact antiviral mechanism of CDF against PyVs is unknown [63]. It is generally assumed that the inhibitory activity of CDF against PyVs is due to its toxicity. Since the presented phenotypic assay is based on cell death upon SV40 infection, this system probably only allows identification of compounds that show no toxic potential to CV-1 cells. Therefore, the reason for the modest inhibitory activity determined for CDF against SV40 infection could be its contribution to the cell death induced by SV40 infection rather than an inhibitory activity against SV40 infection.

Overall, using SV40 in a phenotypic cell-based assay as a surrogate virus for BKV to screen for inhibitors against this PyV class also has some disadvantages. Although, SV40 and BKV are sharing great sequence homology, they differ in their NCCR sequence, miRNA expression and some steps during the viral life cycle. Therefore, it is possible that compounds that would be active against targets regulated by the NCCR or miRNA, or inhibit specific steps in the viral life cycle, which differ between these viruses, will not be identified by this screening system. Additionally, since CV-1 cells respond in a different way to viral infection than RPTEC [125], it is possible to identify compounds that show antiviral activity in CV-1 cells but not in the primary host cells of BKV, or vice versa. Generally, a high false positive rate is expected when using this system as the primary HTS. Furthermore, this system bears the risk of

identifying only compounds with an exceptionally high antiviral activity as the compounds must prevent a complete CPE. Additionally, since this assay is based on cell death induced by SV40 infection, compounds with high cell cytotoxicity but also potential antiviral activity, will not be identified.

However, due to the lack of fluorescent labelled BKV and the limitations of *in vitro* cell culture systems of BKV, this phenotypic cell-based system using SV40 as a surrogate virus for BKV has several advantages. Since SV40 replicates fast in CV-1 cells, the generation of virus stocks is not limited, therefore allowing infection at a high MOI in order to obtain a complete CPE. Additionally, CV-1 cells do not show replicative senescence, which enables numerous cell doublings without cell alterations as well as the generation of the reporter assay in the first place. Furthermore, compounds identified in this screen will most likely not only inhibit BKV infection but also infection by JCV, as all three viruses share great sequence homology.

5.2 HTS using a cell-based assay

An HTS was performed to identify novel inhibitors active against PyV infection. For this purpose, a chemical library consisting of approximately 28,000 small molecule compounds was used. The compounds of this library were not pre-screened for their potential antiviral activity, resulting in a non-focused or non-knowledge-based screen.

Commonly, two different HTS approaches are used to screen for novel compounds, which are either cell-based or target-based [165]. While cell-based assays utilize living cells for screening, target-based assays make use of purified protein targets and membrane preparations involving both binding and functional assays [166]. When applying a target-based assay approach, the target is selected before the HTS and compounds are picked according to their chemical structure predicted to bind the target with a high affinity [167]. In the case of BKV, JCV and SV40, LT-Ag is a frequently used target for the identification of novel inhibitors as it initiates genome replication and features an ATPase activity [151, 163, 168–170]. While target-based assays provide reasonable information about a compounds effect on target activity, they often simply measure the affinity of the test compound for its target, without considering target diversity and without yielding crucial information about the compounds activity in a cellular environment. Therefore, compounds identified in target-based assays often demonstrate high toxic potential in cells [165]. Contrarily, using cell-based assays less is known about a compounds specificity, selectivity and mechanism of activity, but the identification of compounds effective against a range of targets is possible, which can be either cellular or viral. Additionally, compound activity against its target is assessed within the cellular environment [166].

Cell-based assays can either use reporter genes such as luminescent proteins, e.g. luciferase, under control of a specific gene promotor, or cell proliferation assays that measure changes in the growth rates of cells. Another option are phenotypic assays monitoring changes in cell morphology [167].

However, the read-out in most cell-based assays presents a functional consequence of the compound activity against its target [167].

In this study, the activity of tested compounds in inhibiting SV40 infection was determined by measuring RFP intensity levels by microplate photometer (plate reader) or microscopic analysis (imaging). The signal to noise ratio was different between the two measurement methods. Measurement of fluorescence intensity levels by plate reader resulted in high background levels only permitting the identification of compounds with particularly high inhibitory activity (Figure 19A). On the other hand, using fluorescence microscopy for the detection of the inhibitory activity appeared to be more sensitive and also allowed the identification of compounds with lower inhibitory activity (Figure 19A). However, both techniques reveal a considerable spread of measured fluorescence intensity levels, which is typically observed in cell-based inhibitor screens as a result of assay interference and compound activity [165].

The quality and robustness of an HTS is usually assessed by two parameters, the Z` factor and choice of controls [165]. The latter one is important to predefine limits for the signal window. For the primary HTS uninfected cells were used as a positive control simulating 100% inhibition activity, while infected cells treated with DMSO act as negative control with 0% inhibition activity. DMSO is a commonly used negative control as compounds of chemical libraries are typically stored in DMSO [165]. In this study, HXC served as a reference inhibitor control showing 40% inhibitory activity in initial studies, but in the primary HTS the antiviral activity of HXC exhibited high variability (5 – 30% inhibitory activity), indicating that either the assay lacks robustness or HXC is an unsuitable reference inhibitor control for this screen. The Z` factor is a statistical parameter that considers signal window and variance between high and low signals in an assay [171], but does not monitor positional effects or any other variability in sample wells. In addition, this parameter does not necessarily correlate with the hit confirmation rates of an assay [172, 173]. Due to the variations observed in the inhibitory activity of HXC between different plates, the data evaluation was performed plate-wise applying two different cut-offs: the relative FI RFP is greater than or equal to 20%, or fold change relative FI RFP is greater than or equal 2 (Figure 20).

Generally, an HTS is prone to produce both false negative and false positive results. Thus, credible controls are crucial in the primary screening and secondary screens are compulsory [165]. Out of approximately 28,000 small molecule compounds that were screened for their inhibitory activity against SV40 infection, 33 compounds were ultimately identified by the primary screening with SV40 (Figure 21), resulting in a hit rate of 0.12%. Typically, a hit rate of ≤ 1% is expected for an HTS using diverse libraries [165], indicating that the hit rate of the screen performed in this study is quite low but still within expectations.

5.3 Identification of small molecule compounds active against BKV infection

The 33 compounds identified as hits in the primary screen with SV40 were further analyzed for their inhibitory activity against BKV infection in a secondary screen using primary human RPTEC, the natural host cells of BKV. This secondary screen identified 16 compounds with a higher inhibitory activity against BKV infection than the clinical control CDF, demonstrating that 50% of compounds identified in the primary screen with SV40 are also highly effective against BKV. Although, BKV and SV40 are closely related members of the PyV family with DNA and aa sequence homology of about 80%, they differ greatly regarding the sequences of miRNA and NCCR [24, 107]. In addition, several processes during viral life cycle e.g. gene regulation and viral entry, are different among these viruses [174].

Conclusively, 16 compounds out of approximately 28,000 small molecule compounds were highly active against BKV resulting in a hit rate of 0.06%, which is considered quite low but may indicate a high specificity of these compounds for BKV infection.

The 16 hit compounds were evaluated for their prospective *in vivo* toxicity and chemical accessibility by DEREK and Lipinski's rule of five analysis. DEREK, short for deductive estimate of risk from existing knowledge, presents a computational method providing a series of structural alerts based on molecular substructures, such as alkylation reagents and acid or halogen-containing molecules, to indicate whether a specific toxic response, such as mutagenicity, carcinogenicity or skin irritation, may be anticipated [152]. In general, the premise of DEREK as stated by its originators is "if a chemical structure feature is present then specific toxic action is a possibility" [175], suggesting that the rules used in DEREK analysis serve as broad generalizations, rather than being specific for tested compounds. However, Lipinski's rule of five is traditionally used to evaluate the chemical properties of a compound in order to determine the probability of a compound becoming an active therapeutic drug in humans, but the pharmacologically activity of a compound is not predicted. According to Lipinski, therapeutics have to meet the following criteria: molecular mass less than 500 Da, no more than five hydrogen bond donors, no more than ten hydrogen bond acceptors, and an octanol-water partition coefficient LogP (cLogP) not greater than five [153]. The majority of clinically accepted drugs have a molecular weight of less than 350 Da and a cLogP of less than 3 [165]. In this study, only the compounds C1 – 4 met all these criteria, while compound C5 showed a slight deviation (Table 55). But C5 was still ranked relatively high, as no warnings concerning DEREK analysis were issued. Overall, the 16 hit compounds were ranked according to their chemical properties and their probability of being effective in *in vivo* studies, but not according to their actual inhibitory activity against BKV infection and putative toxicity in primary human RPTEC.

Based on the *in silico* data and to facilitate in-depth analysis, only the compounds C1 – C5 were selected for further investigations regarding their inhibitory activity against BKV in a dose response manner. The IC50 value describes the concentration of the compound that is required to achieve 50% of

maximal inhibition and is used to assess the efficacy of an inhibitor [165]. All five compounds identified in this study showed a high antiviral activity against BKV with IC50 values in the range 230 nM to 5 µM (Figure 23). In comparison, inhibitors active against LT-Ag found in several other studies provided IC50 values ranging from 15 – 100 µM against SV40 infection [162, 163, 170], while an IC50 of 2 µM was determined for HXC [151]. In addition, another study identified Ellagic and Spiperone as the best inhibitors against early phase of SV40 with an IC50 of 5 µM, respectively [161]. Typically, compounds with an IC50 ≥ 10 µM are considered as weak inhibitors, while compounds with an IC50 ≤ 10 µM are classified as strong inhibitors. However, there is no definite classification for IC50 values, since compound activity is strongly dependent on its targets protein family and the assay used to determine the IC50. For instance, when using a biochemical assay, the IC50 value should be in low nanomolar affinity, while using cell-based assays the IC50 of the same compound can be in the low micromolar range.

Furthermore, the influence of the compounds C1 – C5 on cell viability was evaluated. The CC50 value describes the concentration of the compound that is required to kill 50% of uninfected cells [154]. To estimate the CC50 value of these compounds, two different cell viability assays, MTT and ATP assay, were performed in human primary RPTEC. Both assays revealed that the compounds C4 – C5 showed high toxicity potency with CC50 values in the range 2.0 to 9.0 µM, while only compound C1 had no influence on cell viability with CC50 value over 100 µM (Figure 24). In general, one major challenge in small molecule screens is a high toxicity induced by the identified compounds as small molecules compounds are able to induce cell death *in vivo* even at low concentrations [167].

In addition, the SI of a compound is a widely accepted parameter to assess efficacy of a compound in inhibiting a virus. This parameter is described as the ratio between cytotoxicity (CC50) and antiviral activity (IC50). Compounds with high SI ratio are predicted to be more effective and safer in *in vivo* treatments [154]. In this study, only for the compound C1 a high SI of over 100 was calculated, indicating a high chance for this compound to be suitable for *in vivo* studies. However, for the compounds C3 and C5 a SI of over 10 was estimated, while for the other two compounds, C2 and C4, a SI of less than 10 was calculated (Table 56), indicating that treatment with these inhibitors might induce cell death of the host cells before BKV infection is effectively inhibited. However, by screening derivatives of the identified compounds their antiviral activity could be improved while reducing their cytotoxicity. In general, compounds with a SI of over 10 are preferable for clinical development [164]. Therefore, this study emphasizes the unique identification of three novel small molecule inhibitors that are promising candidates for further optimization with regard to clinical development of an anti BKV drug.

5.4 Identification of broad range activity of compounds against JCV and MuPyV

The human PyV JCV was first isolated in brain tissue from a patient with PML [8]. Typically, the human fetal glial cell line SVG, which express SV40 LT-Ag, has been used to study JCV infection as cells of neural origin are desired. However, a study revealed that SVG cells from ATCC are contaminated with BKV [176] rendering these cells unusable for the testing of compounds for antiviral activity against JCV infection. Therefore, in this study COS-7 cells were used. The fibroblast-like cell line COS-7 is derived from CV-1 cells by transformation with an origin defective SV40 mutant encoding for LT-Ag and is therefore suitable for viruses requiring stable expression of SV40 LT-Ag, which is the case for JCV [177]. The compounds C1 – C5 were tested for their broad range activity against JCV. It was discovered that four of the five compounds tested (C1, C3, C4 and C5) exhibited similar antiviral activity against JCV infection as observed for BKV, while the compound C2 was unable to highly reduce the intracellular JCV load (Figure 25). As JCV and BKV share a high amino acid sequence homology of about 86% in the early and late region [24], a high broad range activity of identified compounds was expected. Additionally, the compound C2 seems to inhibit BKV infection by a specific pathway, which is not present in JCV infection.

In order to investigate BKV or JCV infection *in vivo*, hitherto, small animal models are restricted to the use of surrogates like MuPyV infection in mice or SV40 infection in Syrian golden hamsters [117]. With regard to *in vivo* studies of promising inhibitors identified against BKV and JCV infection, the 16 compounds identified in the secondary screen using BKV were investigated for their inhibitory activity against MuPyV infection *in vitro*. The majority of compounds tested only exhibited a weak antiviral activity against MuPyV infection (Figure 26), suggesting that identified inhibitors are highly specific against the PyV class including SV40, JCV and BKV. On the other hand, four (C2, C3, C10, C14) of the 16 compounds inhibited MuPyV infection by more than 90%, but for three (C2, C3 and C14) of these compounds cell death was observed by microscopy, suggesting that the high antiviral activity might be a result of high cytotoxicity. As the compounds C2 and C3 also showed high cytotoxicity in human RPTEC (Figure 24), their activity against PyV infections could be rather a result of their cytotoxicity than actual specificity against PyVs. However, the compound C10 seems to exhibit a broad range activity against infection with PyVs.

The compound C1 was identified as the most promising compound for clinical drug development as compound C1 inhibited BKV infection at low concentrations without exhibiting cytotoxicity as represented by a SI of over 100 (Table 56). Since the compound C1 does not show a high antiviral activity against MuPyV infection *in vitro*, the evaluation of its efficacy *in vivo* using MuPyV infection in mice is unsuitable. Therefore, SV40 infection in Syrian golden hamsters could be used as an alternative model to study antiviral activity of compound C1 *in vivo*. On the other hand, recent advances in stem cell research enable the growth of human organ-like structures such as kidneys *in vitro* [178–181].

These kidney organoids derive from human pluripotent stem cells and form three-dimensional (3D) epithelial structures resembling the function, cellular composition and architecture of the organ [178, 182]. 3D-kidney organoids present a powerful tool for disease modelling and to study the antiviral activity of potential drugs. Recently, a study demonstrated that infection of primary kidney tubular epithelial organoids with BKV greatly reflects *in vivo* aspects [178]. Therefore, the establishment of a 3D-kidney organoid system originating from induced pluripotent stem cells (iPSC) as a surrogate tissue model for BKV infection should be considered.

5.5 Characterization of compound C1 inhibitory effect against BKV infection

Since compound C1 displays a high inhibitory activity against BKV infection in primary human RPTEC even at a low concentration and without inducing cell toxicity, its exact mechanism to achieve this antiviral activity was investigated in greater detail.

Compound C1 significantly impaired BKV infection including early and late gene expression (Figure 34). However, immunocytochemistry and Western blot analyses revealed that the inhibitory effect of compound C1, when added at the time of infection, resulted in a delay of the viral life cycle (Figure 35 and 36). It is possible that compound C1 might be instable or is degraded resulting in insufficient compound C1 concentrations over time.

Additionally, the antiviral activity of compound C1 is not equally effective through the entire viral life cycle. Detailed studies of BKVs life cycle revealed that compound C1 induced inhibition is most pronounced, when added at the time of infection or during the early stage of BKV replication up to 12h p.i., while addition during the late stage of infection does not significantly reduce BKV progeny (Figure 31). Since LT-Ag expression is usually observed 24h p.i., the data gathered in this study indicate that compound C1 inhibits the entry phase of BKV infection. The entry phase of BKV involves receptor binding, intracellular trafficking, virus uncoating, nuclear entry of virus genomes and initiation of replication [32]. Data gathered from replication assays reveal that compound C1 does not appear to block viral DNA replication but suggest that early and late gene transcription are affected at early time points (Figure 37). Therefore, the influence of compound C1 on the early time points needs to be investigated in further detail. In addition, pre-liminary data gathered from life cell imaging with labelled VLPs (Figure 38) indicate that compound C1 impairs the binding of capsid protein VP1 to the surface of host cells and thus prevents internalization of the virus suggesting an influence of compound C1 on the entry phase of infection.

Daily treatment with compound C1 does not further decrease the intracellular BKV load (Figure 30) verifying that compound C1 appears to be stable over time and indicates that compound C1 hampers new rounds of host cell infection. These findings are in agreement with results shown before that the viral life cycle of BKV is delayed and thus takes longer than 24h to complete. In addition, these results

suggest that compound C1 either blocks the entry receptor or alternatively that compound C1 interacts with the viral capsids and thereby prevents BKV to attach to the host cells.

The inhibitory effect of compound C1 against BKV infection at a constant compound concentration decreases in response to higher levels of input virus (Figure 29) indicating that compound C1 is indeed specific against this class of PyV including BKV, suggesting that the target of compound C1 is either a viral protein or a host cell protein controlled by or necessary for infection.

In addition to the analyses addressing the consequences of compound C1 on BKV infection and viral life cycle, SAR analysis of compound C1 was performed. SAR is an important tool to acquire additional information about potential targets of inhibitors and the on-target efficacy of a novel inhibitor. In this study, the influence of 14 derivatives of compound C1 on BKV infection and on cell viability of human primary RPTEC was examined (Figure 27). The results reveal that even minor alterations of the structure of compound C1 lead to a high decrease of the antiviral activity and increased cytotoxicity suggesting that its structure has a great impact on host cells survival and BKV infection.

With respect to the combined application of compound C1 and known antiviral drugs, this study showed that compound C1 at 10 µM causes 95% reduction of BKV infection, while a ten times higher concentration of the clinically approved drug, CDF, was required to obtain the same inhibitory activity (Figure S4). Furthermore, compound C1 treatment in combination with CDF, both at 10 µM, did not show any synergistic effect, which proposes a significantly higher inhibitory activity of compound C1 compared to CDF.

The identification of compound C1 as a highly active inhibitor of BKV infection raises the question, whether a 95% inhibition of BKV infection *in vitro* is sufficient to clear virus in diseased individuals. Patients with PVAN or HC exhibit high-level BKV replication of $10^7 - 10^{10}$ copies/mL. In studies of mathematical modeling of BKV replication in urothelial and renal tubular epithelial cells was suggested that a decrease of more than 80% of BKV replication must be maintained for up to ten weeks to achieve a clearance of BKV loads in plasma and urine [183]. Thus, a long-term inhibition of BKV by compound C1 is required. Although compound C1 results in a significant inhibition of BKV infection, viral protein expression is not blocked to full extent but rather delayed. For the development of treatment strategies concerning *in vivo* studies, the application of compound C1 at multiple times should be considered in order to maintain clearance of BKV loads.

In conclusion, in the current study compound C1 was identified as an antiviral small molecule inhibitor highly active against BKV and JCV infection. Different experimental setups showed that compound C1 could impair early entry steps during BKV infection. In a study done by Randhawa et all. several FDA approved entry inhibitors were analyzed for their inhibitory activity against BKV infection *in vitro* [164]. Their report demonstrated that of all tested entry inhibitors, Chloroquine, which neutralizes lysosomal acidification [184], exhibited the highest SI with a value of approximately 5 [164]. However, in general,

for clinical development compounds with a SI of over 10 are required. In this study it was shown that compound C1 has a SI of over 100 indicating that compound C1 presents a promising compound with a novel structure for clinical development of drugs against entry steps of human PyV infections.

5.6 Proposed model for activity mechanism of compound C1

In order to narrow down the putative target of compound C1, several experiments were performed to identify the exact step in BKV life cycle that is targeted by compound C1. Briefly, the viral life cycle of BKV comprises viral attachment to host cells through binding of VP1 to the cellular receptors gangliosides GD1b and GT1b, followed by internalization by endocytosis, viral trafficking via caveolae particles through ER and nuclear entry of the virus genomes initiating viral DNA replication [38, 85, 120, 125]. Subsequently, infectious progeny are processed leading to an egress of viral particles and the infection of new host cells [32, 107, 117, 127, 128].

Initial findings indicate that compound C1 interferes with early steps of viral infection including attachment, entry trafficking, nuclear entry of viral genomes and/or initiation of the viral replication. However, the target that is involved in this inhibition process could be either a viral protein of BKV or a host cell protein important for BKV infection.

In general, the first step during viral infection is the binding of a virus to its cell surface receptor [86]. For cellular entry, each virus depends on an interaction with a specific host receptor, which determines the virus' host and tissue tropism [25, 86]. Several studies have shown that BKV attaches to the cell surface through an interaction between VP1 and host cell surface receptors gangliosides GD1b and GT1b [25, 85, 174]. Further studies reveal that an N-linked glycoprotein with α-2,3-linked or α-2,8-linked sialic acid is also required to mediate infection by acting as a putative co-receptor [120, 121]. Contrarily, JCV relies on an α-2,6-linked sialic acid, which is associated with the serotonin 5HT2A receptor in order to attach to its host cells [25, 174]. On the other hand, SV40 uses the ganglioside GM1 and a MHC class I receptor to attach to the host cells during infection [185]. Furthermore, MuPyV can bind to cell surface gangliosides GD1a and GT1b, α-2,3-linked or α-2,8-linked sialic acid receptors or α4-integrin receptor [186, 187]. Therefore, as the sialic acid independent virus SV40 does not share receptor specificity with BKV or JCV and in addition, BKV and JCV require different surface receptors to attach to host cells, it is highly unlikely that compound C1 blocks surface receptors to prevent viral entry.

Following the premise that compound C1 affects attachment of BKV during viral entry, the results showing that the antiviral activity of compound C1 is dependent on the levels of input virus encourage the presumption that compound C1 targets either a viral protein or a cellular protein that is regulated upon infection with BKV during the early entry steps. The major capsid protein VP1 is the only viral protein of PyVs that is involved in binding the host cells to initiate viral entry [85]. Crystal structures of

SV40, JCV and MuPyV revealed that VP1 interacts with cell surface receptors via loop structures on the outer surface of the capsid ensuring receptor specificity. Interestingly, these loops are the only part of VP1 that are not conserved among PyVs [118]. It is possible that compound C1 binds VP1 indiscriminately and thus masks the loop region. Contrarily, it is more likely that compound C1 does not target VP1 directly in order to block viral entry, but rather interacts with a cellular target that is regulated upon infection.

Another possible activity mechanism of compound C1 could be the inhibition of virus internalization. Viral attachment to host cell surface receptor is followed by internalization of the virus [32]. Generally, PyVs enter the cell through endocytosis [25]. Different studies have shown that BKV enter human RPTEC through caveosomes [93, 164, 174]. In contrast, one study demonstrated that BKV can enter RPTEC via a caveolin- and clathrin-independent pathway [122]. In addition to BKV, the PyVs SV40 and MuPyV also have been found to be internalized by caveolae-mediated endocytosis [25, 122, 185]. However, JCV enters host cells through clathrin-mediated endocytosis [93, 122]. In the present study it was shown that compound C1 treatment inhibited infection of JCV and BKV to 90%, but MuPyV infection was merely reduced by 50% upon treatment with compound C1. As the internalization mechanism differs between JCV and BKV, but not between BKV and MuPyV, these results suggest that compound C1 does not target directly the internalization of PyVs upon infection. Nevertheless, it is possible that compound C1 interacts with an unknown cellular protein that regulates internalization of PyVs.

Overall, the present findings allow for speculation that compound C1 impairs the early entry steps of BKV infection by targeting a cellular protein that is regulated depending on BKV infection. This cellular target presumably is involved in viral attachment processes or internalization. A potential model of the putative antiviral activity mechanism of compound C1 is proposed in Figure 39, but the precise mechanism of compound C1 inhibiting BKV infection requires further analysis in order to identify the target and the exact inhibitory pathway of compound C1.

A possible target of compound C1 could be a cellular protein such as tyrosine kinase. Studies have shown that Abl family tyrosine kinases are necessary for replication of PyVs including BKV, and more importantly, that they seem to be involved in the entry step of PyVs [188, 189]. Others demonstrated that the unspecific inhibitor Genistein, which is known to inhibit multiple tyrosine kinases, inhibits the entry of SV40, JCV and BKV [190–192]. However, little is known about tyrosine kinases mediated entry of PyV infections. Compound C1 could inhibit BKV infection by interacting with tyrosine kinases or other cellular factors that mediate receptor binding of BKV or subsequent internalization. Hitherto, the exact mechanisms required for PyVs entry are poorly understood and little information is available concerning cellular factors that are involved in the entry of PyVs. Further analyses are required to

characterize cellular factors that are crucial for PyVs entry in order to identify the target of compound C1.
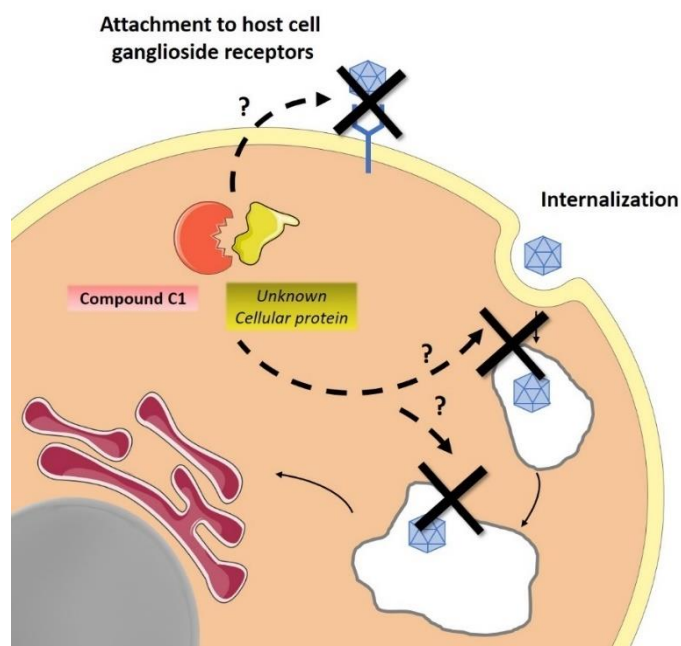
Figure 39: Proposed model for the antiviral mechanism of compound C1 against BKV infection
Compound C1 inhibits BKV infection by impairing entry steps during infection, which constitute either of the attachment of BKV to host cell ganglioside receptor or the internalization of capsids by endocytosis. A possible inhibitory mechanism is that compound C1 interacts with an unknown cellular factor resulting in alterations of the cell surface receptor preventing BKV binding to the host cells. Another possibility is that compound C1 forms a complex with an unknown cellular factor impairing the internalization of BKV capsids.

5.7 Conclusions and Outlook

In this study five major goals were achieved. Firstly, a novel phenotypic cell-based HTS to identify inhibitors active against SV40 as a surrogate virus for BKV was successfully designed. This assay was suitable for screening in 384-well plates allowing the use of a large and diverse chemical library. Secondly, by performing an HTS of a library consisting of approximately 28,000 small molecule compounds, 33 compounds were identified to effectively inhibit SV40 infection. Thirdly, in a secondary screen using BKV and its natural host cells, 16 of the 33 novel inhibitors were identified as highly active against BKV infection. Five of these inhibitors effectively inhibit BKV infection at very low concentrations with intracellular IC50 values of less than 1 µM. Additionally, these inhibitors, selected based on their *in silico* estimated physical and chemical properties, also revealed a high antiviral activity against JCV infection but not against MuPyV infection. Finally, convincing evidences indicate that compound C1 is a strong inhibitor against entry steps during BKV infection with a SI of over 100. Therefore, compound C1 was identified as a promising candidate for clinical development of a drug against human PyV infections.

Overall, the present study does not only provide novel strategies to identify highly active and specific PyV inhibitors, but also identified in total 16 small molecule inhibitors against PyV infections consisting of novel and diverse chemical structures suggesting antiviral activity against various targets. However, further research is required to obtain additional information about the specificity, selectivity and activity mechanism of these compounds. Therefore, target identification of selected inhibitors will be accomplished by generating improved derivatives of these compounds for the use in structure-based lead optimization. Using affinity purification of proteins from infected or uninfected cells, potential targets will be isolated and subsequently identified by mass spectrometry. In addition, functional assays will help to verify mechanistic targets of selected compounds. Furthermore, with the use of siRNAs mediating translational knockdowns, the importance of any identified cellular genes will be assessed, while mutagenesis of viral DNA sequences with subsequent viral replication assays will evaluate the role of viral proteins as potential targets.

Since the main purpose of an HTS is not to identify an actual drug, but rather the characterization of lead compounds and presentation of directions for their optimization, inhibitors that demonstrated toxic potential in this study will be re-formulated and tested for their antiviral activity against BKV infection *in vitro*. In addition, ADME-Tox studies will be performed to characterize these inhibitors based on their physicochemical properties and to predict their *in vivo* efficacy. Information regarding the pharmacokinetics, metabolism and toxicity of selected inhibitors will be collected in order to verify the effectivity and safety of use of the compounds in respect to clinical drug development.

Before the selected and optimized compounds will enter preclinical development, the first step will be the performance of pharmacokinetic and toxicity studies in mice followed by compound activity analysis in established small animal models for PyVs infection, which most precisely reflect the life cycle of human PyVs. So far, small animal models to investigate BKV or JCV infections are restricted to MuPyV infection in mice or SV40 infection in Syrian golden hamsters. Since the majority of selected compounds lack sufficient antiviral activity against MuPyV, Syrian golden hamsters will be considered to serve as a small animal model for SV40 infection to test *in vivo* activity of selected compounds.

Additionally, the establishment of a 3D-kidney organoid system derived from iPSC as a surrogate tissue model for BKV infection is currently in process. Since 3D-kindey organoids represent the function, cellular components and architecture of target organ, they represent a powerful system for modelling BKV associated diseases and screening of nephrotoxicity and antiviral activity of inhibitors against BKV infection accurately reflecting *in vivo* aspects.

6. References

1.   Johne R, Buck CB, Allander T, et al (2011) **Taxonomical developments in the family Polyomaviridae Reimar**. *Arch Virol* 156:1627–1634.

2.   Gross L (1953) **A Filterable Agent, Recovered From Ak Leukemic Extracts, Causing Salivary Gland Carcinomas in C3H Mice**. *Proc Soc Exp Biol Med* 83:21–414.

3.   Sweet BH, Hillemann MR (1960) **The vacuolating virus, S.V. 40**. *Proc Soc Exp Biol Med* 105:420–427.

4.   Dalianis T, Hirsch HH (2013) **Human polyomaviruses in disease and cancer**. *Virology* 437:63–72.

5.   Eddy BE, Borman GS, Grubbs GE, Young RD (1962) **Identification of the oncogenic substance in rhesus monkey kidney cell cultures as simian virus 40**. *Virology* 17:65–75.

6.   Cheng J, DeCaprio JA, Fluck MM, Schaffhausen BS (2010) **Cellular Transformation by Simian Virus 40 and Murine Polyoma Virus T antigens**. *Semin Cancer Biol* 19:218–228.

7.   Gardner S, Field A, Coleman D, Hulme B (1971) **New Human Papovavirus (B.K.) Isolated From Urine After Renal Transplantation**. *Lancet* 297:1253–1257.

8.   Spencer ES, Andersen HK, Padgett BL, et al (1971) **Cultivation of Papova-like virus from human brain with Progressive Multifocal Leukoencephalopathy**. *Lancet* 66:725–258.

9.   Ajuh ET, Wu Z, Kraus E, et al (2018) **Novel Human Polyomavirus Noncoding Control Regions Differ in Bidirectional Gene Expression according to Host Cell, Large T-Antigen Expression, and Clinically Occurring Rearrangements**. *J Virol* 92:1–20.

10.   Mishra N, Pereira M, Rhodes RH, et al (2014) **Identification of a novel Polyomavirus in a pancreatic transplant recipient with retinal blindness and Vasculitic Myopathy**. *J Infect Dis* 210:1595–1599.

11.   Lim ES, Reyes A, Antonio M, et al (2013) **Discovery of STL polyomavirus, a polyomavirus of ancestral recombinant origin that encodes a unique T antigen by alternative splicing**. *Virology* 436:295–303.

12.   Siebrasse EA, Reyes A, Lim ES, et al (2012) **Identification of MW Polyomavirus, a Novel Polyomavirus in Human Stool**. *J Virol* 86:10321–10326.

13.   Bialasiewicz S, Whiley DM, Lambert SB, et al (2007) **A newly reported human polyomavirus,**

KI virus, is present in the respiratory tract of Australian children. *J Clin Virol* 40:15–18.

14. Gaynor AM, Nissen MD, Whiley DM, et al (2007) **Identification of a novel polyomavirus from patients with acute respiratory tract infections**. *PLoS Pathog* 3:0595–0604.

15. Scuda N, Hofmann J, Calvignac-Spencer S, et al (2011) **A Novel Human Polyomavirus Closely Related to the African Green Monkey-Derived Lymphotropic Polyomavirus**. *J Virol* 85:4586–4590.

16. Buck CB, Phan GQ, Raiji MT, et al (2012) **Complete Genome Sequence of a Tenth Human Polyomavirus**. *J Virol* 86:10887–10887.

17. Schowalter RM, Pastrana D V., Pumphrey KA, et al (2010) **Merkel cell polyomavirus and two previously unknown polyomaviruses are chronically shed from human skin**. *Cell Host Microbe* 7:509–515.

18. Korup S, Rietscher J, Calvignac-Spencer S, et al (2013) **Identification of a Novel Human Polyomavirus in Organs of the Gastrointestinal Tract**. *PLoS One* 8:1–7.

19. Feng H, Shuda M, Chang Y, Moore PS (2008) **Clonal Integration of a Polyomavirus in Human Merkel Cell Carcinoma**. *Science* 319:1096–1100.

20. van der Meijden E, Janssens RWA, Lauber C, et al (2010) **Discovery of a new human polyomavirus associated with Trichodysplasia Spinulosa in an immunocompromized patient**. *PLoS Pathog* 6:1–10.

21. Gheit T, Dutta S, Oliver J, et al (2017) **Isolation and characterization of a novel putative human polyomavirus**. *Virology* 506:45–54.

22. Kamminga S, Van Der Meijden E, Feltkamp MCW, Zaaijer HL (2018) **Seroprevalence of fourteen human polyomaviruses determined in blood donors**. *PLoS One* 13:1–11.

23. Imperiale MJ (2001) **The Human Polyomaviruses: An Overview**. *Hum Polyomaviruses* 7:53–71.

24. Barbanti-Brodano G, Sabbioni S, Martini F, et al (2000) **BK virus, JC virus and Simian Virus 40 Infection in Humans, and Association with Human Tumors**. *Adv Exp Med Biol* 40:1–44100.

25. Boothpur R, Brennan DC (2010) **Human polyoma viruses and disease with emphasis on clinical BK and JC**. *J Clin Virol* 47:306–312.

26. Grundhoff A, Fischer N (2015) **Merkel cell polyomavirus, a highly prevalent virus with tumorigenic potential**. *Curr Opin Virol* 14:129–137.

27.   Reuwer AQ, Heron M, van der Dussen D, et al (2017) **The clinical utility of JC virus antibody index measurements in the context of progressive multifocal leukoencephalopathy**. *Acta Neurol Scand* 136:37–44.

28.   Egli A, Infanti L, Dumoulin A, et al (2009) **Prevalence of Polyomavirus BK and JC Infection and Replication in 400 Healthy Blood Donors**. *J Infect Dis* 199:837–846.

29.   Li R, Sharma BN, Linder S, et al (2013) **Characteristics of polyomavirus BK (BKPyV) infection in primary human urothelial cells**. *Virology* 440:41–50.

30.   Jiang M, Abend JR, Johnson SF, Imperiale MJ (2009) **The role of polyomaviruses in human disease**. *Virology* 384:266–273.

31.   Zhao L, Imperiale MJ (2017) **Identification of Rab18 as an Essential Host Factor for BK Polyomavirus Infection Using a Whole-Genome RNA Interference Screen**. *Am Soc Microbiol* 2:e00291-17.

32.   Bennett SM, Broekema NM, Imperiale MJ (2012) **BK polyomavirus: Emerging pathogen**. *Microbes Infect* 14:672–683.

33.   Ramos E, Drachenberg CB, Wali R, Hirsch HH (2009) **The decade of polyomavirus BK-associated nephropathy: State of affairs**. *Transplantation* 87:621–630.

34.   Feng S, Buell JF, Cherikh WS, et al (2002) **Organ donors with positive viral serology or malignancy: Risk of disease transmission by transplantation**. *Transplantation* 74:1657–1663.

35.   Trydzenskaya H, Juerchott K, Lachmann N, et al (2013) **The genetic predisposition of natural killer cell to BK virus-associated nephropathy in renal transplant patients**. *Kidney Int* 84:359–365.

36.   Nickeleit V, Hirsch HH, Binet IF, et al (1999) **Polyomavirus infection of renal allograft recipients: from latent infection to manifest disease.** *J Am Soc Nephrol* 10:1080–1089.

37.   Hirsch HH, Brennan DC, Drachenberg CB, et al (2005) **Polyomavirus-associated nephropathy in renal transplantation: Interdisciplinary analyses and recommendations**. *Transplantation* 79:1277–1286.

38.   Mbianda C, El-Meanawy A, Sorokin A (2015) **Mechanisms of BK virus infection of renal cells and therapeutic implications**. *J Clin Virol* 344:1173–1178.

39.   Fogazzi GB (2010) **Urinalysis**. In: Floege J, Johnson RJ, Feehally J (eds) Comprehensive Clinical Nephrology, 4th ed. pp 39–55

40. Hariharan S (2006) **BK virus nephritis after renal transplantation**. *Kidney Int* 69:655–662.

41. Satyanarayana G, Marty FM, Tan CS (2014) **The polyomavirus puzzle: Is host immune response beneficial in controlling BK virus after adult hematopoietic cell transplantion?** *Transpl Infect Dis* 16:521–531.

42. Lunde LE, Dasaraju S, Cao Q, et al (2015) **Hemorrhagic cystitis after allogeneic hematopoietic cell transplantation: Risk factors, graft source, and survival**. *Bone Marrow Transplant* 50:1432–1437.

43. Dropulic L, Jones R (2008) **Polyomavirus BK infection in blood and marrow transplant recipients**. *Bone Marrow Transplant* 41:11–18.

44. Droller MJ, Saral R, Santos G (1982) **Prevention of cyclophosphamide-induced hemorrhagic cystitis**. *Urology* 20:256–258.

45. Wong ASY, Chan K-H, Cheng VCC, et al (2007) **Relationship of Pretransplantation Polyoma BK Virus Serologic Findings and BK Viral Reactivation after Hematopoietic Stem Cell Transplantation**. *Clin Infect Dis* 44:830–837.

46. Zhou W, Sharma M, Martinez J, et al (2007) **Functional Characterization of BK Virus-Specific CD4 + T Cells with Cytotoxic Potential in Seropositive Adults** . *Viral Immunol* 20:379–388.

47. Schachtner T, Mü ller K, Stein M, et al (2011) **BK virus-specific immunity kinetics: A predictor of recovery from polyomavirus BK-associated nephropathy**. *Am J Transplant* 11:2443–2452.

48. Comoli P, Cioni M, Basso S, et al (2013) **Immunity to Polyomavirus BK Infection: Immune Monitoring to Regulate the Balance between Risk of BKV Nephropathy and Induction of Alloimmunity**. *Clin Dev Immunol* 2013:1–6.

49. Weist BJD, Schmueck M, Fuehrer H, et al (2014) **The role of CD4+T cells in BKV-specific T cell immunity**. *Med Microbiol Immunol* 203:395–408.

50. Babel N, Volk H-D, Reinke P (2011) **BK polyomavirus infection and nephropathy: the virus–immune system interplay**. *Nat Rev Nephrol* 7:399–406.

51. Chiesa M Della, Sivori S, Carlomagno S, et al (2015) **Activating KIRs and NKG2C in viral infections: Toward NK cell memory?** *Front Immunol* 6:1–8.

52. Jiang M, Entezami P, Gamez M, et al (2011) **Functional Reorganization of Promyelocytic Leukemia Nuclear Bodies During BK Virus Infection**. *MBio* 2:1–10.

53. Jiang M, Zhao L, Gamez M, Imperiale MJ (2012) **Roles of ATM and ATR-Mediated DNA**

Damage Responses during Lytic BK Polyomavirus Infection. *PLoS Pathog* 8:e1002898.

54. Smith JM, McDonald RA, Finn LS, et al (2004) **Polyomavirus nephropathy in pediatric kidney transplant recipients**. *Am J Transplant* 4:2109–2117.

55. Ginevri F, De Santis R, Comoli P, et al (2003) **Polyomavirus BK infection in pediatric kidney-allograft recipients: A single-center analysis of incidence, risk factors, and novel therapeutic approaches**. *Transplantation* 75:1266–1270.

56. Ginevri F, Azzi A, Hirsch HH, et al (2007) **Prospective monitoring of polyomavirus BK replication and impact of pre-emptive intervention in pediatric kidney recipients**. *Am J Transplant* 7:2727–2735.

57. Sawinski D, Goral S (2015) **BK virus infection: An update on diagnosis and treatment**. *Nephrol Dial Transplant* 30:209–217.

58. Santeusanio AD, Lukens BE, Eun J (2017) **Antiviral treatment of BK virus viremia after kidney transplantation**. *Am J Heal Pharm* 74:2037–2045.

59. De Clercq E (2003) **Clinical Potential of the Acyclic Nucleoside Phosphonates Cidofovir, Adefovir, and Tenofovir in Treatment of DNA Virus and Retrovirus Infections**. *Clin Microbiol Rev* 16:569–596.

60. Lamoth F, Pascual M, Erard V, et al (2008) **Low-dose cidofovir for the treatment of polyomavirus-associated nephropathy: Two case reports and review of the literature**. *Antivir Ther* 13:1001–1009.

61. Savona MR, Newton D, Frame D, et al (2007) **Low-dose cidofovir treatment of BK virus-associated hemorrhagic cystitis in recipients of hematopoietic stem cell transplant**. *Bone Marrow Transplant* 39:783–787.

62. Tylden GD, Hirsch HH, Rinaldo CH (2015) **Brincidofovir (CMX001) Inhibits BK Polyomavirus Replication in Primary Human Urothelial Cells**. *Antimicrob Agents Chemother* 59:3306–3316.

63. Rinaldo CH, Gosert R, Bernhoff E, et al (2010) **1-O-hexadecyloxypropyl cidofovir (CMX001) effectively inhibits polyomavirus BK replication in primary human renal tubular epithelial cells**. *Antimicrob Agents Chemother* 54:4714–4722.

64. Chimerix (2018) **Chimerix Presents Preclinical Data Demonstrating Antiviral Activity of Brincidofovir Against Polyomavirus at Kidney**. https://www.globenewswire.com/news-release/2018/10/27/1637949/0/en/Chimerix-Presents-Preclinical-Data-Demonstrating-Antiviral-Activity-of-Brincidofovir-Against-Polyomavirus-at-Kidney-Week-2018.html. Accessed

24 Apr 2019

65. Farasati NA, Shapiro R, Vats A, Randhawa P (2005) **Effect of Leflunomide and Cidofovir on replication of BK virus in an in vitro culture system**. *Transplantation* 79:116–118.

66. Bernhoff E, Tylden GD, Kjerpeseth LJ, et al (2010) **Leflunomide inhibition of BK virus replication in renal tubular epithelial cells.** *J Virol* 84:2150–6.

67. Guasch A, Roy-Chaudhury P, Woodle ES, et al (2010) **Assessment of efficacy and safety of FK778 in comparison with standard care in renal transplant recipients with untreated BK nephropathy**. *Transplantation* 90:891–897.

68. Portolani M, Pietrosemoli P, Cermelli C, et al (1988) **Suppression of BK virus replication and cytopathic effect by inhibitors of prokaryotic DNA gyrase**. *Antiviral Res* 9:205–218.

69. Ali SH, Chandraker A, DeCaprio JA (2007) **Inhibition of Simian virus 40 large T antigen helicase activity by fluoroquinolones**. *Antivir Ther* 12:1–6.

70. Gabardi S, Waikar SS, Martin S, et al (2010) **Evaluation of fluoroquinolones for the prevention of BK viremia after renal transplantation**. *Clin J Am Soc Nephrol* 5:1298–1304.

71. Leung AYH, Chan MTL, Yuen K-Y, et al (2005) **Ciprofloxacin Decreased Polyoma BK Virus Load in Patients Who Underwent Allogeneic Hematopoietic Stem Cell Transplantation**. *Clin Infect Dis* 40:528–537.

72. Rosenbaum JT, George RK, Gordon C (1999) **Intravenous Immunoglobulin**. 545–549.

73. Lindner JM, Cornacchione V, Sathe A, et al (2019) **Human Memory B Cells Harbor Diverse Cross-Neutralizing Antibodies against BK and JC Polyomaviruses**. *Immunity* 50:668–676.

74. Randhawa P, Pastrana D V., Zeng G, et al (2015) **Commercially available immunoglobulins contain virus neutralizing antibodies against all major genotypes of polyomavirus BK**. *Am J Transplant* 15:1014–1020.

75. Pastrana D V., Brennan DC, Çuburu N, et al (2012) **Neutralization serotyping of BK polyomavirus infection in kidney transplant recipients**. *PLoS Pathog* 8:e1002650.

76. Bohl DL, Brennan DC, Ryschkewitsch C, et al (2009) **BK virus antibody titers and intensity of infections after renal transplantation**. 43:184–189.

77. Bohl DL, Storch GA, Ryschkewitsch C, et al (2005) **Donor origin of BK virus in renal transplantation and role of HLA C7 in susceptibility to sustained BK viremia**. *Am J Transplant* 5:2213–2221.

78. Novartis (2018) **Determine the Safety, Tolerability, and Efficacy of MAU868 for the Prevention of BK Virus Infection in Kidney Transplant Recipients**. https://clinicaltrials.gov/ct2/show/NCT03456999. Accessed 24 Apr 2019

79. Hirsch HH, Yakhontova K, Lu M, Manzetti J (2016) **BK Polyomavirus Replication in Renal Tubular Epithelial Cells Is Inhibited by Sirolimus, but Activated by Tacrolimus Through a Pathway Involving FKBP-12**. *Am J Transplant* 16:821–832.

80. Fructuoso AI, Calco N, Perez-Flores I, et al (2011) **Mammalian target of rapamycin signal inhibitors could play a role in the treatment of BK polyomavirusnephritis in renal allograft recipients**. *Transpl Infect Dis* 13:584–591.

81. Araki K, Turner AP, Shaffer VO, et al (2009) **mTOR regulates memory CD8 T cell differentiation**. *Nature* 460:108–112.

82. Hymes LC, Warshaw BL (2011) **Five-year experience using sirolimus-based, calcineurin inhibitor-free immunosuppression in pediatric renal transplantation**. *Pediatr Transplant* 15:437–441.

83. Hirsch HH, Markus M, Klimkait T (2001) **Prospective Monitoring of BK Virus Load after Discontinuing Sirolimus Treatment in a Renal Transplant Patient with BK Virus Nephropathy To**. *J Infect Dis* 184:1494–1495.

84. Knowles WA, Pipkin P, Andrews N, et al (2003) **Population-based study of antibody to the human polyomaviruses BKV and JCV and the simian polyomavirus SV40**. *J Med Virol* 71:115–23.

85. Jiang M, Abend JR, Tsai B, Imperiale MJ (2009) **Early Events during BK Virus Entry and Disassembly**. *J Virol* 83:1350–1358.

86. Ahsan N, Shah K (2006) **Polyomaviruses and human diseases.** In: Advances in Experimental Medicine and Biology. pp 1–18

87. An P, Sáenz Robles MT, Duray AM, et al (2019) **Human polyomavirus BKV infection of endothelial cells results in interferon pathway induction and persistence**. *PLoS Pathog* 15:e1007505.

88. Goudsmit J, Dillen PW, van Strien A, van der Noordaa J (1982) **The role of BK virus in acute respiratory tract disease and the presence of BKV DNA in tonsils**. *J Med Virol* 10:91–99.

89. Bofill-Mas S, Pina S, Girones R (2000) **Documenting the epidemiologic patterns of polyomaviruses in human populations by studying their presence in urban sewage**. *Appl*

Environ Microbiol 66:238–245.

90.   Hirsch HH, Steiger J (2003) **Polyomavirus BK**. *Lancet Infect Dis* 3:611–623.

91.   Bofill-Mas S, Formiga-Cruz M, Clemente-Casares P, et al (2001) **Potential Transmission of Human Polyomaviruses through the Gastrointestinal Tract after Exposure to Virions or Viral DNA**. *J Virol* 75:10290–10299.

92.   Abend JR, Jiang M, Imperiale MJ (2009) **BK Virus and Human Cancer: Innocent until Proven Guilty**. *Semin Cancer Biol* 19:252–260.

93.   Mazalrey S, Mcilroy D, Bressollette-Bodin C (2015) **BK polyomavirus: virus-cell interactions, host immune response, and viral pathogenesis**. *Virologie* 19:8–24.

94.   Martelli F, Wu Z, Delbue S, et al (2018) **BK Polyomavirus MicroRNA Levels in Exosomes Are Modulated by Non-Coding Control Region Activity and Down-Regulate Viral Replication When Delivered to Non-Infected Cells Prior to Infection**. *Viruses* 10:E466.

95.   Bethge T, Hachemi H a., Manzetti J, et al (2015) **Sp1 Sites in the Noncoding Control Region of BK Polyomavirus Are Key Regulators of Bidirectional Viral Early and Late Gene Expression**. *J Virol* 89:3396–3411.

96.   Abend JR, Joseph AE, Das D, et al (2009) **A truncated T antigen expressed from an alternatively spliced BK virus early mRNA**. *J Gen Virol* 90:1238–1245.

97.   Zheng ZM (2010) **Viral oncogenes, noncoding RNAs, and RNA splicing in human tumor viruses**. *Int J Biol Sci* 6:730–755.

98.   Tremolada S, Akan S, Otte J, et al (2010) **Rare subtypes of BK virus are viable and frequently detected in renal transplant recipients with BK virus-associated nephropathy**. *Virology* 404:312–318.

99.   Gerits N, Moens U (2012) **Agnoprotein of mammalian polyomaviruses**. *Virology* 432:316–326.

100.   Sullivan CS, Grundhoff AT, Tevethia S, et al (2005) **SV40-encoded microRNAs regulate viral gene expression and reduce susceptibility to cytotoxic T cells**. *Nature* 435:682–686.

101.   Seo GJ, Fink LHL, O'Hara B, et al (2008) **Evolutionarily Conserved Function of a Viral MicroRNA**. *J Virol* 82:9823–9828.

102.   Chen CJ, Cox JE, Kincaid RP, et al (2013) **Divergent MicroRNA Targetomes of Closely Related Circulating Strains of a Polyomavirus**. *J Virol* 87:11135–11147.

103. Chen CJ, Cox JE, Azarm KD, et al (2014) **Identification of a polyomavirus microRNA highly expressed in tumors**. *Virology* 476:43–53.

104. Seo GJ, Chen CJ, Sullivan CS (2009) **Merkel cell polyomavirus encodes a microRNA with the ability to autoregulate viral gene expression**. *Virology* 383:183–187.

105. Cantalupo P, Doering A, Sullivan CS, et al (2005) **Complete nucleotide sequence of polyomavirus SA12.** *J Virol* 79:13094–104.

106. Sullivan CS, Sung CK, Pack CD, et al (2009) **Murine Polyomavirus encodes a microRNA that cleaves early RNA transcripts but is not essential for experimental infection**. *Virology* 387:157–167.

107. Imperiale MJ (2014) **Polyomavirus miRNAs: The beginning**. *Curr Opin Virol* 7:29–32.

108. Theiss JM, Günther T, Alawi M, et al (2015) **A Comprehensive Analysis of Replicating Merkel Cell Polyomavirus Genomes Delineates the Viral Transcription Program and Suggests a Role for mcv-miR-M1 in Episomal Persistence.** *PLoS Pathog* 11:e1004974.

109. Broekema NM, Imperiale MJ (2013) **miRNA regulation of BK polyomavirus replication during early infection.** *PNAS* 110:8200–8205.

110. Moens U, Johansen T, Traavik TI (1995) **Noncoding control region of naturally occurring BK virus variants: Sequence comparison and functional analysis**. *Virus Genes* 10:261–275.

111. Imperiale MJ, Jiang M (2016) **Polyomavirus Persistence**. *Annu Rev Virol* 3:517–532.

112. Gosert R, Rinaldo CH, Funk GA, et al (2008) **Polyomavirus BK with rearranged noncoding control region emerge in vivo in renal transplant patients and increase viral replication and cytopathology.** *J Exp Med* 205:841–852.

113. Sharma PM, Gupta G, Vats A, et al (2006) **Phylogenetic Analysis of Polyomavirus BK Sequences**. *J Virol* 80:8869–8879.

114. Knowles WA, Gibson PE, Gardner SD (1989) **Serological typing scheme for BK-like isolates of human polyomavirus.** *J Med Virol* 28:118–123.

115. Pastrana D V., Ray U, Magaldi TG, et al (2013) **BK Polyomavirus Genotypes Represent Distinct Serotypes with Distinct Entry Tropism**. *J Virol* 87:10105–10113.

116. Bartel DP (2004) **MicroRNAs: Genomics, Biogenesis, Mechanism, and Function Review**. *Cell* 116:281–297.

117. Barth H, Solis M, Kack-Kack W, et al (2016) **In vitro and in vivo models for the study of human polyomavirus infection**. *Viruses* 8:1–17.

118. Neu U, Allen S ann A, Blaum BS, et al (2013) **A Structure-Guided Mutation in the Major Capsid Protein Retargets BK Polyomavirus**. *PLoS Pathog* 9:e1003688.

119. Dugan AS, Gasparovic ML, Tsomaia N, et al (2007) **Identification of Amino Acid Residues in BK Virus VP1 That Are Critical for Viability and Growth**. *J Virol* 81:11798–11808.

120. Low JA, Magnuson B, Tsai B, Imperiale MJ (2006) **Identification of Gangliosides GD1b and GT1b as Receptors for BK Virus**. *J Virol* 80:1361–1366.

121. Dugan AS, Eash S, Atwood WJ (2005) **An N-Linked Glycoprotein with (2,3)-Linked Sialic Acid Is a Receptor for BK Virus**. *J Virol* 79:14442–14445.

122. Zhao L, Marciano AT, Rivet CR, Imperiale MJ (2016) **Caveolin- and clathrin-independent entry of BKPyV into primary human proximal tubule epithelial cells**. *Virology* 492:66–72.

123. Moriyama T, Marquez JP, Wakatsuki T, Sorokin A (2007) **Caveolar Endocytosis Is Critical for BK Virus Infection of Human Renal Proximal Tubular Epithelial Cells**. *J Virol* 81:8552–8562.

124. Moriyama T, Sorokin A (2008) **Intracellular trafficking pathway of BK Virus in human renal proximal tubular epithelial cells**. *Virology* 371:336–349.

125. Bennett SM, Jiang M, Imperiale MJ (2013) **Role of Cell-Type-Specific Endoplasmic Reticulum-Associated Degradation in Polyomavirus Trafficking**. *J Virol* 87:8843–8852.

126. Sowd GA, Fanning E (2012) **A Wolf in Sheep's Clothing: SV40 Co-opts Host Genome Maintenance Proteins to Replicate Viral DNA**. *PLoS Pathog* 8:e1002994.

127. Li TC, Takeda N, Kato K, et al (2003) **Characterization of self-assembled virus-like particles of human polyomavirus BK generated by recombinant baculoviruses**. *Virology* 311:115–124.

128. Drachenberg CB, Papadimitriou JC, Wali R, et al (2003) **BK Polyoma Virus Allograft Nephropathy: Ultrastructural Features from Viral Cell Entry to Lysis**. *Am J Transplant* 3:1383–1392.

129. Liu W, MacDonals M, You J (2016) **Merkel Cell Polyomavirus Infection and Merkel Cell Carcinoma**. *Curr Opin Virol* 20:20–27.

130. Liu CK, Atwood WJ (2001) **Propagation and assay of the JC virus**. *Methods Mol Biol* 165:9–17.

131. Moriyama T, Sorokin A (2009) **BK virus (BKV): Infection, propagation, quantitation,**

purification, labeling, and analysis of cell entry. *Curr Protoc Cell Biol* 42:26.2.1-26.2.13.

132. Broekema NM, Imperiale MJ (2012) **Efficient propagation of archetype BK and JC polyomaviruses**. *Virology* 422:235–241.

133. Gee G V., O'Hara B, Derdowski A, Atwood WJ (2013) **Pseudovirus mimics cell entry and trafficking of the human polyomavirus JCPyV**. *Virus Res* 178:3831–3840.

134. White MK, Safak M, Khalili K (2009) **Regulation of gene expression in primate polyomaviruses.** *J Virol* 83:10846–10856.

135. Nukuzuma S, Takasaka T, Zheng HY, et al (2006) **Subtype I BK polyomavirus strains grow more efficiently in human renal epithelial cells than subtype IV strains**. *J Gen Virol* 87:1893–1901.

136. de Kort H, Heutinck KM, Ruben J, et al (2017) **Primary Human Renal-Derived Tubular Epithelial Cells Fail to Recognize and Suppress BK Virus Infection.** *Transplantation* 101:1820–1829.

137. Abend JR, Low JA, Imperiale MJ (2010) **Global effects of BKV infection on gene expression in human primary kidney epithelial cells**. *Virology* 397:73–79.

138. Assetta B, De Cecco M, O'Hara B, Atwood WJ (2016) **JC Polyomavirus Infection of Primary Human Renal Epithelial Cells Is Controlled by a Type I IFN-Induced Response**. *MBio* 7:1–11.

139. Burke JM, Bass CR, Kincaid RP, et al (2018) **The Murine Polyomavirus MicroRNA Locus Is Required To Promote Viruria during the Acute Phase of Infection**. *J Virol* 92:1–14.

140. Swimm AI, Dong Y, Wilson JJ, et al (2011) **Gamma Interferon Controls Mouse Polyomavirus Infection In Vivo**. *J Virol* 85:10126–10134.

141. Barthold SW, Griffey SM, Percy DH (2016) **Polyomavirus Infections**. In: Pathology of Laboratory Rodents and Rabbits, 4th ed. pp 19–21

142. Fagrouch Z, Karremans K, Deuzing I, et al (2011) **Molecular analysis of a novel simian virus 40 (SV40) type in rhesus macaques and evidence for double infections with the classical SV40 type**. *J Clin Microbiol* 49:1280–1286.

143. Zhang S, Sroller V, Zanwar P, et al (2014) **Viral MicroRNA Effects on Pathogenesis of Polyomavirus SV40 Infections in Syrian Golden Hamsters**. *PLoS Pathog* 10:e1003912.

144. Rinaldo CH, Tylden GD, Sharma BN (2013) **The human polyomavirus BK (BKPyV): Virological background and clinical implications**. *Apmis* 121:728–745.

145. Mullis K, Faloona F, Scharf S, et al (1986) **Specific enzymatic amplification of DNA in vitro: the polymerase chain reaction**. *Cold Spring Harb Symp Quant Biol* 51:263–73.

146. Husseiny MI, Lacey SF (2011) **Development of infectious recombinant BK virus**. *Virus Res* 161:150–161.

147. Adams SR, Campbell RE, Gross LA, et al (2002) **New Biarsenical Ligands and Tetracysteine Motifs for Protein Labeling in Vitro and in Vivo: Synthesis and Biological Applications**. *J Am Chem Soc* 124:6063–6076.

148. Simon-friedt BR, Wilson MJ, Blake DA, et al (2015) **The RPTEC/TERT1 cell line as an improved tool for in vitro nephrotoxicity assessments**. *Biol Trace Elem Res* 166:66–71.

149. Simon BR, Wilson MJ, Wickliffe JK (2014) **The RPTEC/TERT1 cell line models key renal cell responses to the environmental toxicants, benzo[a]pyrene and cadmium**. *Toxicol Reports* 1:231–242.

150. Belmokhtar CA, Hillion J, Ségal-Bendirdjian E (2001) **Staurosporine induces apoptosis through both caspase-dependent and caspase-independent mechanisms.** *Oncogene* 20:3354–3362.

151. Seguin SP, Ireland AW, Gupta T, et al (2012) **A Screen for Modulators of Large T Antigen's ATPase Activity Uncovers Novel Inhibitors of Simian Virus 40 and BK Virus Replication**. *Antiviral Res* 96:70–81.

152. Cariello NF, Wilson JD, Britt BH, et al (2002) **Comparison of the computer programs DEREK and TOPKAT to predict bacterial mutagenicity**. *Mutagenesis* 17:321–329.

153. Goodwin RJA, Bunch J, McGinnity DF (2017) **Mass Spectrometry Imaging in Oncology Drug Discovery**. *Adv Cancer Res* 134:133–171.

154. Pritchett JC, Naesens L, Montoya J (2014) **Treating HHV-6 Infections: The Laboratory Efficacy and Clinical Use of Anti-HHV-6 Agents**. In: Human Herpesviruses HHV-6A, HHV-6B & HHV-7, 3rd ed. pp 311–331

155. Appendino G, Fontana G, Pollastro F (2010) **Comprehensive Natural Products II**. In: Chemistry and Biology. pp 205–236

156. De Clercq E, Holý A (2005) **Case history: Acyclic nucleoside phosphonates: A key class of antiviral drugs**. *Nat Rev Drug Discov* 4:928–940.

157. Hurdiss DL, Morgan EL, Thompson RF, et al (2016) **New Structural Insights into the Genome and Minor Capsid Proteins of BK Polyomavirus using Cryo-Electron Microscopy**. *Structure*

24:528–536.

158. Li Y, Lu X, Li J, et al (2010) **Genetically Engineered, Biarsenically Labeled Influenza Virus Allows Visualization of Viral NS1 Protein in Living Cells**. *J Virol* 84:7204–7213.

159. Crivat G, Tokumasu F, Sa JM, et al (2011) **Tetracysteine-based fluorescent tags to study protein localization and trafficking in plasmodium falciparum-infected erythrocytes**. *PLoS One* 6:e22975.

160. Andrei G, Snoeck R, Vandeputte M, De Clercq E (1997) **Activities of various compounds against murine and primate polyomaviruses**. *Antimicrob Agents Chemother* 41:587–593.

161. Goodwin EC, Atwood WJ, DiMaio D (2009) **High-Throughput Cell-Based Screen for Chemicals That Inhibit Infection by Simian Virus 40 and Human Polyomaviruses**. *J Virol* 83:5630–5639.

162. Ireland AW, Gobillot TA, Gupta T, et al (2014) **Synthesis and structure-activity relationships of small molecule inhibitors of the simian virus 40 T antigen oncoprotein, an anti-polyomaviral target**. *Bioorganic Med Chem* 22:6490–6502.

163. Wright CM, Seguin SP, Fewell SW, et al (2009) **Inhibition of Simian Virus 40 replication by targeting the molecular chaperone function and ATPase activity of T antigen**. *Virus Res* 141:71–80.

164. Randhawa P, Farasati NA, Huang Y (2007) **BK virus replication in vitro: Limited effect of drugs interfering with viral uptake and intracellular transport**. *Antimicrob Agents Chemother* 51:4492–4494.

165. Hughes JP, Rees SS, Kalindjian SB, Philpott KL (2011) **Principles of early drug discovery**. *Br J Pharmacol* 162:1239–1249.

166. Moore K, Rees S (2001) **Cell-Based Versus Isolated Target Screening: How Lucky do You Feel?** *J Biomol Screen* 6:69–74.

167. Abhay A Shukla (2016) **High Throughput Screening of Small Molecule Library: Procedure, Challenges and Future**. *J Cancer Prev Curr Res* 5:1–3.

168. Shin J, Phelan PJ, Chhum P, et al (2014) **Analysis of JC virus DNA replication using a quantitative and high-throughput assay**. *Virology* 468–470:113–125.

169. Fradet-Turcotte A, Morin G, Lehoux M, et al (2010) **Development of quantitative and high-throughput assays of polyomavirus and papillomavirus DNA replication**. *Virology* 399:65–76.

170. Randhawa P, Zeng G, M. B, et al (2014) **Inhibition of large T antigen ATPase activity as a**

potential strategy to develop anti-polyomavirus JC drugs. *Antiviral Res* 112:113–119.

171. Zhang, Chung, Oldenburg (1999) **A Simple Statistical Parameter for Use in Evaluation and Validation of High Throughput Screening Assays.** J. Biomol. Screen. 4:67–73

172. Gribbon P, Lyons R, Laflin P, et al (2005) **Evaluating Real-Life High-Throughput Screening Data**. *J Biomol Screen* 4:67–72.

173. Coma I, Herranz J, Martin J (2009) **Statistics and decision making in high-throughput screening.** *Methods Mol Biol* 565:69–106.

174. Bhattacharjee S, Chattaraj S (2017) **Entry, infection, replication, and egress of human polyomaviruses: an update**. *Can J Microbiol* 63:193–211.

175. Sanderson DM, Earshaw CG (1991) **Computer prediction of possible toxic action from chemical structure; the DEREK system.** *Hum Exp Toxicol* 10:261–73.

176. Henriksen S, Tylden GD, Dumoulin A, et al (2014) **The Human Fetal Glial Cell Line SVG p12 Contains Infectious BK Polyomavirus**. *J Virol* 88:7556–7568.

177. Nukuzuma S, Nakamichi K, Kameoka M, et al (2010) **Efficient propagation of progressive multifocal leukoencephalopathy-type JC virus in COS-7-derived cell lines stably expressing Tat protein of human immunodeficiency virus type 1**. *Microbiol Immunol* 54:758–762.

178. Schutgens F, Rookmaaker MB, Margaritis T, et al (2019) **Tubuloids derived from human adult kidney and urine for personalized disease modeling**. *Nat Biotechnol* 37:303–313.

179. Takasato M, Er PX, Chiu HS, et al (2015) **Kidney organoids from human iPS cells contain multiple lineages and model human nephrogenesis**. *Nature* 526:564–568.

180. Yamaguchi S, Morizane R, Homma K, et al (2016) **Generation of kidney tubular organoids from human pluripotent stem cells**. *Sci Rep* 6:1–11.

181. Takasato M, Er PX, Chiu HS, Little MH (2016) **Generating kidney organoids from human pluripotent stem cells**. *Nat Protoc* 11:1681–1692.

182. Iakobachvili N, Peters PJ (2017) **Humans in a dish: The potential of organoids in modeling immunity and infectious diseases**. *Front Microbiol* 8:1–7.

183. Bernhoff E, Gutteberg TJ, Sandvik K, et al (2008) **Cidofovir inhibits polyomavirus BK replication in human renal tubular cells downstream of viral early gene expression.** *Am J Transplant* 8:1413–1422.

184. Romero NR, Agostinis P (2014) **Molecular Mechanisms Underlying the Activation of Autophagy Pathways by Reactive Oxygen Species and their Relevance in Cancer Progression and Therapy**. In: Autophagy: Cancer, Other Pathologies, Inflammation, Immunity, Infection, and Aging. pp 159–178

185. Schelhaas M, Malmström J, Pelkmans L, et al (2007) **Simian Virus 40 Depends on ER Protein Folding and Quality Control Factors for Entry into Host Cells**. *Cell* 131:516–529.

186. Ahsan N (2007) **Polyomaviruses and Human diseases**. In: Advances in experimental medicine and biology. pp 1–12

187. Hara SDO, Garcea RL (2016) **Murine Polyomavirus Cell Surface Receptors Activate Distinct Signaling Pathways Required for Infection**. *Am Soc Microbiol* 7:1–11.

188. Randhawa P, Farasati NA, Huang Y, et al (2010) **Viral Drug Sensitivity Testing Using Quantitative PCR Effect of Tyrosine Kinase Inhibitors on Polyomavirus BK Replication**. *Am J Clin Pathol* 134:916–920.

189. Swimm AI, Bornmann W, Jiang M, et al (2010) **Abl Family Tyrosine Kinases Regulate Sialylated Ganglioside Receptors for Polyomavirus**. *J Virol* 84:4243–4251.

190. Pelmans L, Püntener D, Helenius A (2002) **Local Actin Polymerization and Dynamin Recruitment in SV40-Induced Internalization of Caveolae**. *Science (80-)* 296:535–539.

191. Querbes W, Benmerah A, Tosoni D, et al (2003) **A JC Virus-Induced Signal Is Required for Infection of Glial Cells by a Clathrin- and eps15-Dependent Pathway**. *J Virol* 78:250–256.

192. Eash S, Querbes W, Atwood WJ (2004) **Infection of Vero Cells by BK Virus Is Dependent on Caveolae**. *J Virol* 78:11583–11590.

7. Supplementary Materials

7.1 Supplementary Figures
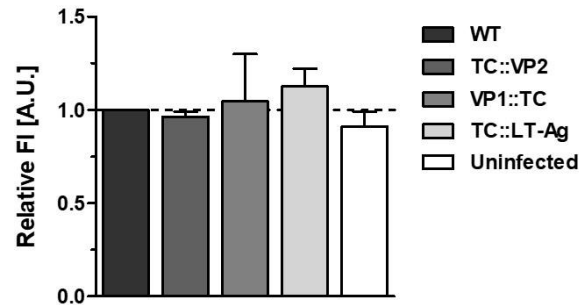
Figure S 1: Tetracysteine tagged BKV proteins labelled with fluorogenic biarsenical reagent FlAsh-EDT2 could not be detected after washing

Viral supernatants, which were harvested from WI-38 cells 7d post their transfection with re-ligated genome of either WT or recombinant BKV, were used to infect RPTEC. 5d p.i. cells were washed with three times with HBSS and afterwards incubated with FlAsH-EDT$_2$ labelling reagent for 30 min at RT. After incubation, cells were washed again with HBSS and fluorescence intensity (FI) of FlAsH binding reagent was detected at excitation wavelength of 508 nm and emission wavelength of 528 nm by a microplate photometer (Tecan). Shown is here the FI of infected cells normalized to uninfected cells, which were set to 1 (n=6).
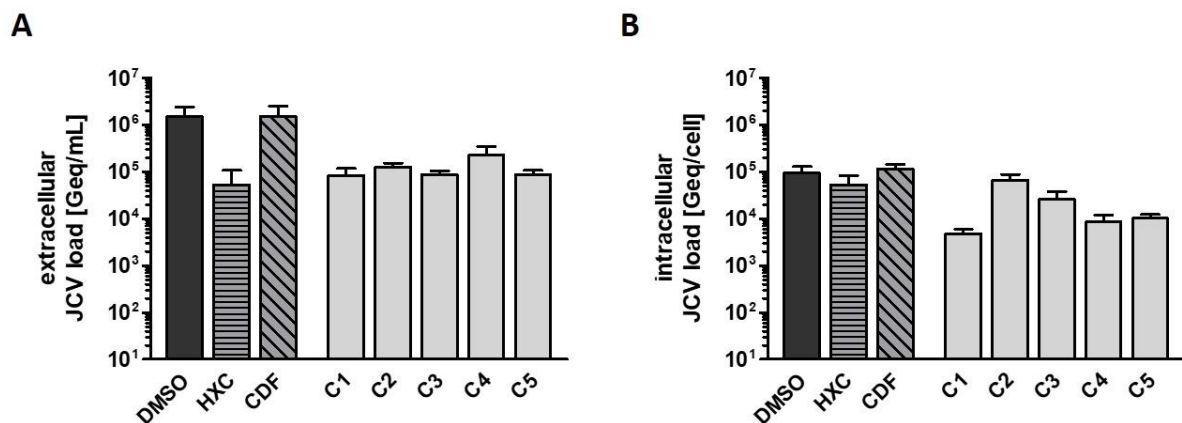
Figure S 2: Absolute inhibitory activity of top 5 compounds against JCV infection

COS-7 cells were infected with JCV and treated with either DMSO, HXC, CDF or one of the compounds C1 − C5. 6d p.i. JCV load in supernatant **(A)** or cells **(B)** was determined by qPCR analysis (n=3).

141
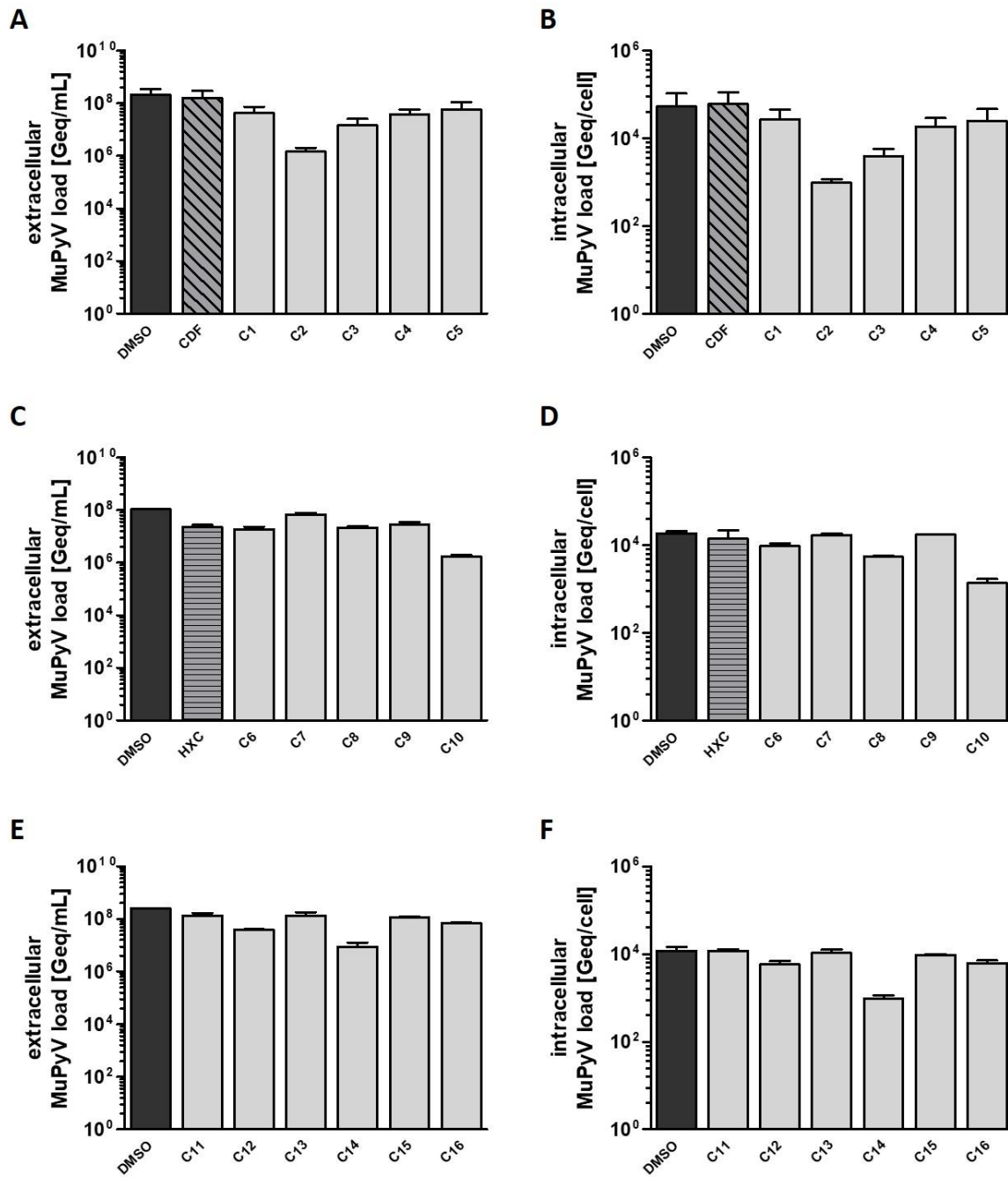
Figure S 3: Absolute inhibitory activity of top 16 compounds against MuPyV infection
NMuMG cells were infected with MuPyV and treated with either DMSO, HXC, CDF or one of the compounds C1 – C16. 6d p.i. MuPyV load in supernatant **(A, C, E)** or cells **(B, D, F)** was determined by SYBR green qPCR analysis. Since this assay was performed in 24-well plates, compounds were divided into three groups for testing.
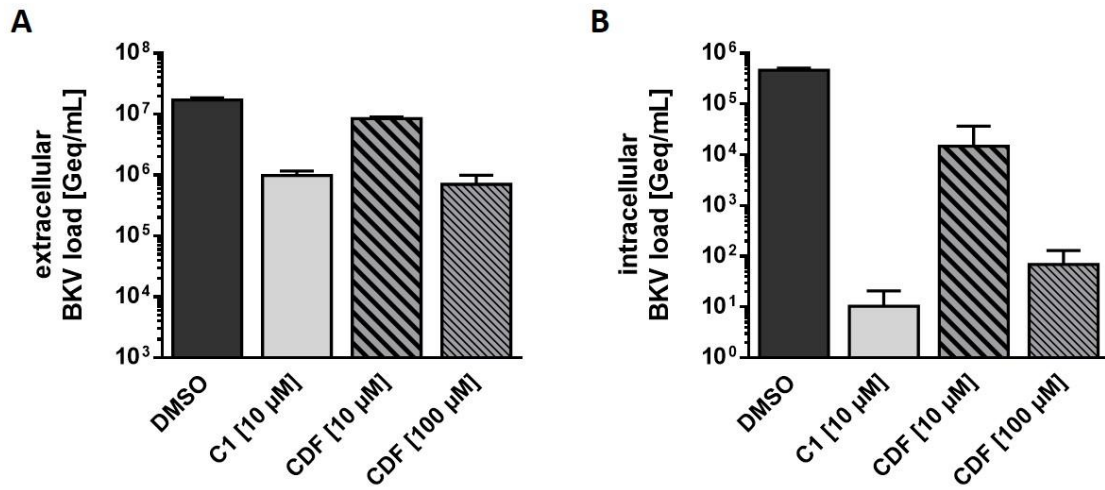
Figure S 4: Antiviral activity of CDF and compound C1
Primary human RPTEC were infected with BKV at a MOI of 1 and treated with compound C1 at 10 µM or CDF at 10 or 100 µM. 6d p.i. BKV loads in supernatant **(A)** or cells **(B)** were determined by qPCR analysis (n=3).

7.2 Hazardous substances according to GHS

Table S 1: Hazardous substances according to GHS

Substance	Hazard pictogram	Hazard statements	Precautionary statements
β-Mercaptoethanol		H227, H301+331, H310, H315, H317, H318, H373, H410	P261, P273, P280, P302+350, P305+351+338, P310, P501
Acetic acid		H226, H314, H402	P210, P233, P240, P241, P242, P243, P260, P264, P273, P280, P301+330+331, P303+361+353
Acrylamide		H301, H312, H315, H317, H319, H332, H340, H350, H361, H372	P201, P280, P301+310, P308+360+313
APS		H272, H302, H315, H317, H319, H334, H335	P280, P302+352, P304+340, P305+351+338, P342+311
Calcium chloride		H319	P264, P280, P305+351+338, P337+313
Cidofovir		H315, H341, H351, H361,	P201, P202, P264, P280,
Chloroform		H302, H315, H319, H331, H351, H361, H372	P201, P202, P260, P264, P270, P271, P280,
DAPI		H315, H317, H335	P264, P280,
DTT		H302, H315, H319, H335	P261, P302+352, P305+351+338, P501
EDTA		H302, H315, H319, H335	P261, P264, P270, P271, P280, P301+330+331, P302+352, P311, P305+351+338, P332+313, P337+313, P362, P403+233
Ethanol		H225, H319	P210, P233, P241, P243, P280, P337+P313, P403+P235
Ethidium bromide		H302, H330, H341	P260, P280, P284, P301+312, P405, P501
Formaldehyde		H226, H302, H314, H317, H318, H331, H350, H401	P201, P202, P210, P233, P240, P241, P242, P243, P260, P264, P270, P271, P272, P273, P280, P301+330+331, P303+361+353, P304+351+338, P308+313, P310, P333+313, P363,

144

Substance	Hazard pictogram	Hazard statements	Precautionary statements
			P370+378, P403+233, P235, P405, P501
Formamide		H360	P201, P202, P308+313
Hexachlorophene		H301, H311, H400, H410	P264, P273, P280
Hydrochloric acid		H290, H301, H314, H330, H334, H335, H370, H372	P260, P280, P301+310, P303+361+353, P304+340, P305+351+338, P308+311, P342+311
Manganese (II) chloride		H302, H341, H360, H372, H401, H412	P201, P202, P260, P264, P270, P273, P281, P301+P312, P308+P313, P314, P330, P405, P501
Magnesium sulfate		H302, H312, H332	P102, P202, P261, P64, P280
Methanol		H225, H301+311+331, H370	P210, P233, P240, P241, P242, P243, P260, P264, P270, P271, P280, P301+310, P303+361+353, P304+340, P330, P361+364, P370+378, P403+235, P404, P501
MOPS		H302, H312, H315, H319, H332, H335	P261, P264, P305+351+338, P302+352
Phenol		H301+H311+H331, H314, H341, H373, H411	P270, P280
Potassium acetate		H302, H315, H319, H335,	P261, P264, P270, P271, P280
Potassium chloride		H412	P273, P501
SDS		H302, H311, H315, H319	P280, P305+351+338, P361, P405, P501
Silver nitrate		H272, H302, H314, H410	P210, P220, P221, P260, P264, P270, P273, P280, P301+330+331, P303+361+353, P304+340, P305+351+338, P310, P363, P391, P405, P501

Substance	Hazard pictogram	Hazard statements	Precautionary statements
Sodium carbonate		H315, H319	P264, P280, P302+352, P305+351+338, P332+313, P362
Sodium chloride		H314	P260, P264, P280, P301+330+331, P303+361+353, P305+351+338, P310, P363, P405, P501
Sodium deoxycholate		H315, H319, H335	P261, P264, P270, P271, P280, P301+P312, P302+P352, P304+P340, P305+P351+P338, P312, P321, P330, P332+P313, P337+P313, P362, P403+P233, P405, P501
Sodium thiosulfate		H315, H319, H332, H335	P261, P264, P271, P280, P302+P352, P304+P312, P304+P340, P305+P351+P338, P312, P321, P332+P313, P337+P313, P362, P403+P233, P405, and P501
Staurosporine		H225, H319, H335, H340, H350	P201, P202, P210, P261, P264, P280
TEMED		H225, H314, H302, H332	P210, P280, P305+351+338, P310
Tris acetate		H315, H319, H335	P261, P305+351+338
Triton X-100		H315, H319	P264, P280, P302+352, P305+351+338, P332+313, P338+313, P362

8. Indices

8.1 Abbreviations

α	Alpha
β	Beta
μL	Mikroliter
μM	Micromolar
≤	Less than or equal to
≥	Greater than or equal to
<	Less than
>	Greater than
%	Percent
°C	Degree Celsius
3D	Three-dimensional
aa	Amino acid
Abl	Abelson murine leukemia viral oncogene homolog 1
Ag	Antigen
Agno	Agno protein
Ago	Argonaute protein
AIDS	Acquired immune deficiency syndrome
ATP	Adenosine triphosphate
BKV	BK virus
BMT	bone marrow transplant
bp	base pair
BrdU	Bromodeoxyuridine
BSA	Bovine serum albumin
C	Cysteine
CC50	Cytotoxicity concentration 50%
CD	Cluster of differentiation
CDF	Cidofovir
cDNA	Complementary DNA
cLog	octanol-water partition coefficient
cm	Centimeter
CMV	Cytomegalovirus

CPE	Cytopathic effect
Ct	Cycle threshold
d	Day(s)
DAPI	4',6-diamidino-2-phenylindole
DDR	DNA damage response
DEPC	Diethylpyrocarbonate
DEREK	Deductive estimate of risk from existing knowledge
DMEM	Dulbecco's
DMSO	Dimethyl sulfoxide
DNA	Deoxyribonucleic acid
dNTP	Deoxyribonucleotide triphosphate
ds	Double stranded
DTT	Dithiothreitol
E. coli	*Escherichia coli*
EDTA	Ethylenediaminetetraacetic acid
EFS	Elongation factor 1α short
e.g.	Exempli gratia
ER	Endoplasmic reticulum
ERAD	ER associated protein degradation
et al.	Et alteri
FACS	Fluorescence activated cell sorting
FCS	Fetal calf serum
FDA	Food and Drug Administration
FFA	Fluorescent focus assay
FI RFP	Fluorescence intensity of RFP
FlAsh-EDT$_2$	Fluorescin arsenical hairpin binder-ethanedithiol
g	Gram
g	Gravity
G	Glycine
GAPDH	Glyceraldehyde 3-phosphate dehydrogenase
gDNA	Genomic DNA
Geq	Genome equivalents
GFP	Green fluorescent protein
GHS	Globally Harmonized System
GM1	Monosialotetrahexosylganglioside

GVHD	graft-versus-host disease
h	Hour(s)
H	Histone
HC	Hemorrhagic cystitis
HEK	Human embryonic kidney
HEPES	4-(2-Hydroxyethyl)-1-piperazineethanesulfonic acid
HIV	Human immunodeficiency virus infection
HLA	Human leukocyte antigen
HPyV	Human polyomavirus
hTert	Human telomerase reverse transcriptase
HTS	High throughput screen
HXC	Hexachlorophene
IC50	Inhibitory concentration 50%
IF	Immunofluorescence
Ig	Immunoglobulin
IL	Interleukin
iPSC	induced pluripotent stem cells
IRES	Internal ribosome entry site
IVIG	Intravenous immunoglobulin
JCV	JC virus
kb	Kilobases
kDa	Kilo Dalton
KIPyV	Karolinska Institute polyomavirus
KIR	Killer cell immunoglobulin-like receptors
KLD	Kinase Ligase DpnI
L	Liter
LB	Lysogeny broth
LIPyV	Lyon IARC polyomavirus
LT-Ag	Large Tumor-Antigen
M	Molar
MCPyV	Merkel cell polyomavirus
MHC	Major histocompatibility complex
min	Minute
miRNA	microRNA
mL	Milliliter

mM	Millimolar
MOI	Multiplicity of infection
MOPS	4-Morpholinepropanesulfonic acid
mTOR	mammalian target of rapamycin
MuPyV	Murine polyomavirus
mRNA	Messenger RNA
MTT	3-(4,5-dimethylthiazol-2-yl)-2,5-diphenyltetrazolium bromide
MW	Molecular weight
MWPyV	Malawi polyomavirus
N	Number of cells
NCCR	Non-coding control region
ng	Nanogram
NJPyV	New Jersey polyomavirus
NK	Natural killer
NLS	nuclear localization signal
nM	Nanomolar
nm	Nanometer
NMuMG	Murine mammary epithelial
nt	nucleotide
OD	Optical density
ORF	Open reading frame
ori	origin of replication
p	Prime
P	Proline
p.i.	Post infection
p.t.	Post transduction
p.t.	Post transfection
PAGE	Polyacrylamide gel electrophoresis
PBS	Phosphate buffered saline
PCR	Polymerase chain reaction
PEG	Polyethylene glycol
PEI	Polyethyleneimine
P/S	Penicillin/Streptomycin
PFA	Paraformaldehyde
pH	Potential hydrogen

PML	Progressive multifocal leukoencephalopathy
PML-NBs	Promyelocytic leukemia nuclear bodies
PNK	Polynucleotide kinase
pol	Polymerase
polyA	Poly adenylation
pre-miRNA	Precursor miRNA
pri-miRNA	Primary miRNA
PsV	Pseudovirions
PVAN	Polyomavirus associated nephropathy
PyV	Polyomavirus
q	quantitative
Rb	Retinoblastoma protein
RCA	Rolling circle amplification
RFP	Red fluorescent protein
RISC	RNA induced silencing complex
RNA	Ribonucleic acid
rpm	Rounds per minute
RPTEC	Renal proximal tubule epithelial cells
rr	rearranged
RT	Reverse transcription
RT	Room temperature
sec	Second(s)
SAR	Structure activity relationship
SDS	Sodium dodecyl sulfate
SFFV	Silencing-prone spleen focus forming virus
SI	Selectivity index
siRNA	Small interfering RNA
sT-Ag	Small Tumor-Antigen
STLPyV	St Louis polyomavirus
SV40	Simian virus 40
T	Temperature
T	Titer
TBS	Tris buffered saline
TEMED	Tetramethylethylenediamine
Tm	Primer melting temperature

T-Ag	Tumor-Antigen
TC	Tetracysteine
TSPyV	Trichodysplasia Spinulosa associated polyomavirus
U	Unit
UV	Ultraviolet
V	Volt
v	Volume
VLP	Virus like particles
VP	Viral protein
WB	Western Blot
WGA	Wheat Germ Agglutinin
WI-38	Wistar Institute-38
WT	Wild type
wt	weight
WUPyV	Washington University polyomavirus

8.2 Figures

8.3 Tables

9. Publications and Presentations

Publication:

Ajuh ET, Wu Z, Kraus E, Weissbach FH, Bethge T, Gosert R, Fischer N, Hirsch HH. (2018). Novel Human Polyomavirus non-coding control regions differ in bi-directional gene expression according to host cell, large T-antigen expression, and clinically occurring rearrangements. *J Virol*. 92(7): e02231-17

Poster Presentations:

Kraus E, Luetgehetmann M, Rückert J, Spohn M, Beauclair G, Schulz T, Fischer N, Grundhoff A
Identification of small molecule inhibitors of clinically relevant human polyomavirus infections
Annual Meeting of the Society for Virology (GfV) 2018, Würzburg

Kraus E, Rückert J, Beauclair G, Schulz T, Fischer N, Grundhoff A
Identification of small molecule inhibitors of clinically relevant human polyomavirus infections
Annual Meeting of German Center for Infection Research (DZIF) 2017, Hamburg

Kraus E, Fischer N, Grundhoff A
High throughput reporter screen to identify inhibitors of clinically relevant human polyomavirus infections
Annual Meeting of the Society for Virology (GfV) 2017, Marburg

Kraus E, Theiss J, Fischer N, Grundhoff A
Mutagenization of the MCPyV non coding control Region (NCCR) to improve late gene expression
European Congress of Virology (ECV) 2016, Hamburg

10. Acknowledgments

157

In addition, I would like to thank Prof. Dr. Chris Sullivan for giving me the opportunity to join his lab for a remarkable research stay. Thank you for your encouraging guidance, your enthusiasm and for making my stay in Austin unforgettable. I also want to thank the Sullivan lab members for their support.

I would like to acknowledge Dr. Kristina Kraus, Steven Schulz and Jacqueline Fröhlich for reading and correcting parts of this thesis. Thank you for your time and encouraging comments.

This work was funded by the German Center for Infection Research (DZIF), giving me the opportunity to conduct my doctoral thesis in an interdisciplinary and inspiring environment.

Finally, I am grateful to my mother for her trust and encouragement and for teaching me pursuing my ambitions. I would like to thank my brothers and my sisters for their great support and encouraging words. I wish to express my sincere thanks to Steven Schulz who provided me with indispensable support in scientific related matters and for being always on my side.

11. Eidesstattliche Versicherung

Hiermit versichere ich an Eides statt, die vorliegende Dissertation selbst verfasst und keine anderen als die angegebenen Hilfsmittel benutzt zu haben. Die eingereichte schriftliche Fassung entspricht der auf dem elektronischen Speichermedium. Ich versichere, dass diese Dissertation nicht in einem früheren Promotionsverfahren eingereicht wurde.

Hamburg, den 26.04.2019

Emma Kraus